MONASH University

Modelling glioblastoma initiating cells and investigation of potential anti-cancer agents

By

Yi Zhang

BSc, BPharmSc(Hons)

A thesis submitted for the degree of Doctor of Philosophy at

Drug Discovery Biology

Monash Institute of Pharmaceutical Sciences

Monash University in 2017

Table of contents

Abstract

Glioblastoma multiforme (GBM) is the most common and malignant primary brain tumor within the Central Nervous System (CNS). Published research has identified a restricted cell population, glioblastoma initiating cells (GICs), within the sub-ventricular zone of the CNS. These cells possess features similar to neural stem cells and are able to differentiate into the various cell types typically found in GBM, propagating the growth of GBM in response to oncogenic cues. Thus, GBM can be regarded as a cancer stem cell disease. Regulation of the activity of GICs and investigation of new targets to specifically modulate GICs is an emerging area of GBM research and therapy.

There is ample evidence that GICs are related to healthy neural stem cells. A comparison of normal neural stem cells with mutant neural stem cells was considered to be an excellent starting point for such a study, and appeared to be a novel idea to explore. To achieve this comparison, neural stem cells were isolated from wild type (control cells in this case) and Cre-mediated transgenic *Pik3ca*^{H1047R}/*PTEN*$^{del/del}$ mice, and control and mutant cell lines were compared in relation to their cellular morphology, proliferation rate, self-renewal ability as well as their multi-potency properties under defined differentiation media. The study showed that mutant *Pik3ca*^{H1047R}/*PTEN*$^{del/del}$ cells exhibit more tightly packed spheres with more filopodia (microvillus-like structures) at sphere surfaces, have an enhanced proliferation rate, and enhanced sphere-forming potential compared to control Neural progenitor and neural stem cells (NPSCs). Multi-potency during differentiation was observed for both control and mutant cells. In early studies, an attempt was also made to reprogram these cells using contemporary methods to form induced pluripotent cells. The aim was to use iPSCs to generate neural stem cells that could then be activated by exposure to Cre recombinase. The subsequent aim was to model GICs and investigate potential specific targets within the PI3K signaling pathway that may provide the basis for discovery of specific new drugs for GBM therapy. In the event the cells derived from primary neurospheres proved to be refractory to reprogramming using the

methods adopted and instead a study of investigation of the difference in kinase expression levels and phosphorylation levels between primary control and mutant mouse neural stem cells was conducted. Kinome profiling identified at least ten over-expressed kinases, in particular FAK1, NEK1 and ROCK1 that may have potential therapeutic value as targets for GBM drug development. In addition, gene ontology analysis, together with protein interaction network analysis revealed that the proteasome system might be an important target to disrupt the functions of GICs. These studies were described in the first half of the thesis (Chapters 2-4).

The theme of anticancer drug discovery is further developed in two separate studies in the second part of the thesis. A study of inhibition of Hh signaling by 26 novel Smoothed (SMO) inhibitors synthesized at Monash Institute of Pharmaceutical Science (MIPS) forms the basis of chapter 5. The structure activity studies emphasized the importance of the -N–N=CH- linker and the piperazine moiety present in SANT-1 to retain cytotoxic efficacy. These compounds may have utility as leads for further medicinal chemistry in the future and development of agents to modulate GICs.

In addition, it is evident that to treat GBM it will be necessary to reduce the burden of proliferating cells as well as reduce the activity of GICs. Consistent with this philosophy, another component of this study concerns the biological assessment of 63 novel tubulin-binding agents based on noscapine. This work was a collaboration with medicinal chemists at MIPS and is reported in chapter 6. The biological evaluation of novel noscapine analogues and noscapine-like analogues addressed the importance of the structure of the heterocyclic ring systems and substitution of the various rings. Some novel compounds were identified with 50-fold higher cytostatic activity than noscapine.

In conclusion, although the model of GICs was not established, the comparison of control and mutant NPSCs provided new information on upregulation of kinases and complemented the work for identification of potential targets in GICs. In addition, the biological evaluation of novel SMO and noscapine analogues further developed our

understanding of the structure-activity relationships and revealed some promising cues for the next generation of anti-cancer drugs.

Abbreviations and units of measurement

Abbreviations

2D-electrophoresis	Two-dimensional polyacrylamide gel electrophoresis
AKT	Protein kinase B
AP	Alkaline phosphatase
Arg	Arginine
ATCC	American Type Culture Collection
BBB	Blood brain barrier
BBC	Basal cell carcinoma
BCC	Basal cell carcinoma
BCNU	bis-chloroethylnitrosourea
BMI1	B lymphoma Mo-MLV insertion region 1 homolog
BTZ	Brotezomib
CDK	Cyclin dependent kinase
CIS	Cisplatin
CKI	Casein kinase
CNS	Central nervous system
Cre	Cre-recombinase
CSC	Cancer stem cell
CSF	Cerebrospinal fluid
DAVID	Database for Annotation, Visualization, and Integrated Discovery
DG	Dentate gyrus
DMEM	Dulbecco's Modified Eagle Medium
Dox	Doxycycline
DTT	Dithiothreitol
ECM	Extracellular matrix
EDTA	Ethylenediaminetetraacetic acid
EGFR	Epithelial growth factor receptor

EGTA	Ethylene glycol-bis (β-aminoethyl ether)-N,N,N',N'-tetraacetic acid
ELDA	Extreme limiting dilution analysis
ERT2	Estrogen receptor ligand-binding domain
ES	Embryonic stem
ESC	Embryonic stem cell
F-12K	Ham's F-12K Kaighn's
F12	Nutrient Mixture F-12
FA	Formic acid
FACS	Fluorescence-activated cell sorting
FAK1	Focal adhesion kinase 1
FBS	Fetal Bovine Serum
FDA	Food and Drug Administration
Fz	Frizzled
GBL	γ-butyolactone
GBM	Glioblastoma multiforme
GFAP	Glial fibrillary acidic protein
GFP	Green flurecsent protein
GIC	Glioblastoma initiating cell
GLB	Glo Lysis Buffer
Gli	Glioma-associated oncogene
GMEM	Glasgow's Modified Essential Medium
GO	Gene ontology
GPCR	G protein coupled recpetor
GSI	γ-secretase inhibitor
GSK3β	Glycogen synthase kinase 3β
Hh	Hedgehog
HHIP	Hedgehog interacting protein
HSC	Human stem cell
ICAT	Isotope-coded affinity tag
INSR	Insulin receptor

iPSC	Induced pluripotent stem cell
iTRAO	Isobaric tagging for relative and absolute quantitation
JAG1	Jagged 1
KCC1A	Calcium/calmodulin-dependent kinase type-1-like
KKCC1	Calcium/calmodulin-dependent protein kinase kinase 1
KO	Knockout
KSR	Knockout serum replacement
LECAM	Neuronal cell adhension molecule
LEF	Lymphoid enhancer factor
LIF	Leukaemia inhibitory factor
LRP	Low-density-lipoprotein-related protein
MEF	Mouse embryonic fibroblast
MELK	Maternal embryonic leucine-zipper kinase
MEM α	Minimum Essential Medium α
mESC	Mouse embryonic stem cell
MIMR	Monash Institute of Medical Research
MOI	Multiplicity of infection
MP2K	Dual specificity mitogen-activated protein kinase kinase
MS	Mass spectrometry
mTOR	Mammalian target of rapamycin
NaF	Sodium fluoride
NEAA	Non-essential amino acid
NEK1	Neve-in Mitosis A related kinase 1
NOS	Not otherwise specified
NPSCs	Neural progenitor and neural stem cells
NSC	Neural stem cell
NSE	Neuron-specific enolase
NSFU	Neurospheres forming unit
PBS	Phosphate buffer saline
PBS-T	0.3% Triton-X-100 in PBS
PDK	Phosphoinositide dependent kinase

PH	Pleckstrin homology
PI	Propidium iodide
PI3K	Phosphatidylinositol-4,5-bisphosphate 3-kinase
Pik3ca	Phosphatidylinositol-4,5-bisphosphate 3-kinase catalytic subunit alpha
PIP2	Phosphatidylinositol 4,5-bisphosphate
PIP3	Phosphatidylinositol (3,4,5)-trisphosphate
PKA	Protein kinase A
PNPP	para-nitrophenolphosphate
Pro	Proline
Ptch	Patched
PTEN	Phosphatase and tensin homolog
RB	Retinoblastoma
RG	Radial glial
ROCK1	Rho associated coil-coil containing protein kinase 1
RT	Room Temperature
RTK	Receptor tyrosine kinase
SDS	Sodium dodecyl sulfate
SGZ	Subgranular zone
SHH	Sonic hedgenhog
SLIAC	Stable isotope labeling with amino acids in cell culture
Smo	Smoothened
SSEA-1	Stage-specific embryonic antigen
SUFU	Suppressor of Fused
SVZ	Subventricular zoone
TCEP	tris(2-carboxyethyl)phosphine
TCF	T cell factor
TCGA	The cancer genome atlas
TFA	Trifluoroacetic acid
THF	Tetrhydrofuran
THIQ	Tetrahydroisoquinolines

TMZ	Temozolomide
Tuj-1	Neuron-specific class III beta-tubulin
USP	Ubiquitin-specific protease
V-SVZ	Ventricular-subventricular zone
WHO	Wold Health Organization
WT	Wild type

Units of measurements

%	Percent
°C	Degree Celsius
pg	Picogram
ng	Nanogram
µg	Microgram
mg	Milligram
g	Gram
nM	Nanomolar
µM	Micromolar
mM	Millimolar
M	Molar
µm	Micrometer
µL	Microliter
mL	Milliliter
L	Liter

List of figures

Chapter 1

Chapter 2

Chapter 3

Chapter 4

Chapter 5

Chapter 6

List of tables

Chapter 2

Chapter 3

Chapter 4

Chapter 5

Chapter 6

Declaration

I hereby declare that this thesis contains no material which has been accepted for the award of any other degree or diploma at any university or equivalent institution and that, to the best of my knowledge and belief, this thesis contains no material previously published or written by another person, except where due reference is made in the text of the thesis.

Yi Zhang

BSc, BPharmSc(Hons)

Acknowledgements

Throughout my PhD study, I have been encouraged and supported by many people who placed their confidence in me. First of all, I would like to express my sincere gratitude to my main supervisor, Prof. Colin Pouton, who has been a great mentor and friend over the past few years, and who always cheered me up during all the stressful moments. I will always be grateful for all your advice, guidance, patience and understanding. I am also very thankful to my advisory panel members, Dr. John Haynes and Dr. Theo Mantamadiotis, for their continuous support and good advice. Also, I would like to thank all the members from our stem cell group, who shared their knowledge with me, taught me many laboratory techniques and moreover, helped me to become an independent researcher. I would like to thank all the members from Drug Discovery Biology (DDB) theme as well as Drug delivery, disposition and dynamics (D4) theme. I would like to thank all the members from Theo's group in the University of Melbourne, who shared their knowledge in the area of neural stem cells with me. I would like to thank all the members from Roger Daly's group in Monash University (Clayton campus), who helped with the MS running and analysis. It has been a great fun to work with all of you and thanks for all the helpful assistance and enjoyable accompany.

I would like to thank my mum and my dad. Without their endless love and supporting, I could not finish this PhD. Thanks for always standing by my side and supporting me. Especially my mum, she came to my place to take care of me during my illness, very appreciated. Thank you for teaching me how to be a strong person and enable me to achieve my goals. I would also like to thank all my friends here, especially Elva who helped me a lot during the difficult time, in Australia and in China for all their thoughtfulness and for the awesome memories.

Chapter 1

General introduction

1.1 The human brain and central nervous system

1.1.1 Basic anatomical structures and biological functions

The brain is one of the most important and complicated organs in the human body, which plays an essential role as a control center in relation to organization, communication and processing information from external stimuli within the human central nervous system (CNS). Generally speaking, the human brain consists of cerebrum, brainstem and cerebellum (Figure 1-1). Together with spinal cord, they constitute the central nervous system. The brain cerebrum is formed with two symmetrical cerebral hemispheres, which is covered by the cerebral cortex that is made up with grey matter. Each cerebral hemisphere contains a large C-shaped cavity, called the lateral ventricle, each of which is full of cerebrospinal fluid (CSF). The brainstem connects cerebrum with spinal cord, and it contains the midbrain, pons and the medulla oblongata. The cerebellum lies behind the pons and mainly contributes to function related to coordination of movements of body parts. The two major cell groups that constitute the brain are functional neurons and supportive glial cells including astrocytes, oligodendrocytes and ependymal cells. The whole brain is suspended in CSF that serves as cushion for external brain damage, and is further protected by the skull. (Standring S, 2008; Martini et al., 2012)

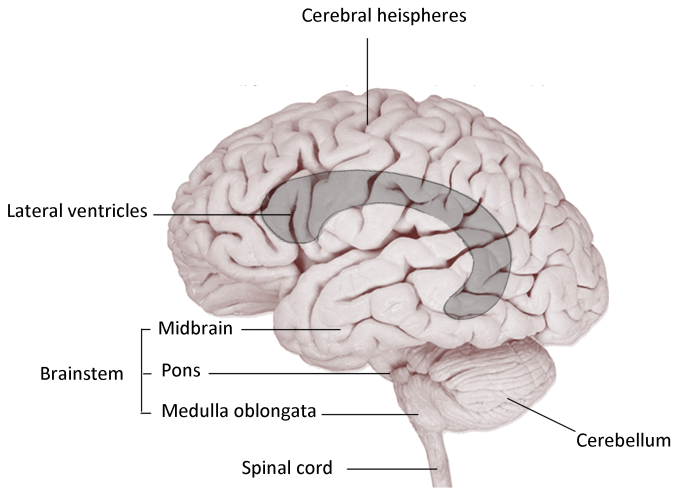

Figure 1-1: Medial view of human central nervous system (redrawn with reference to Martini et al., 2012)

1.1.2 Neurogenesis

Neurogenesis is the process of generation of functional nerve cells from their precursor cells mainly during the embryonic and perinatal period in mammals (Ming and Song, 2005). It is now recognized that this happens continuously even in adult brain, albeit at a slow rate, to produce nerve cells from neural progenitor and neural stem (NPSC) cells throughout the whole life of mammals (Kempermann et al., 1999; Gage FH, 2000). NPSCs are cells that are capable of long-term self-renewal, proliferation and differentiation into neurons and glia cells (Gage FH, 2000).

Mammalian brain development begins with the proliferation of neuroepithelial cells in the neural tube during the embryonic period (Ming and Song, 2005). During the middle stage of brain development, these neuroepithelial cells elongate and convert into radial glial (RG) cells that are capable of dividing into neurons and glia cells. Most of the astrocytes are generated from the RG cells at the later stages of brain development. Some RG cells remain functional as NPSCs in the neonate (Capdevila et al., 2017).

Adult neurogenesis takes place predominantly in two neurogenic niches (Johansson et al., 1999). One is found in the subependymal zone of the lateral ventricles, or the so-called ventricular-subventricular zone (V-SVZ), and another is found in the

subgranular zone (SGZ) within the dentate gyrus (DG) of the hippocampus (Johansson et al., 1999). Neoplastic transformation was previously regarded as the mechanism for generation of glioma cells from astrocytes and oligodendrocytes. However, the identification of NPSCs within the subventricular zone (SVZ) gave rise to a new hypothesis that glioma cells may arise from these NPSCs. (Gage FH, 2000)

1.1.3 Subventricular zone

The SVZ refers to a region (Figure 1-2), under the ependymal layer on the lateral wall of the lateral ventricles, constitutes a large pool of cells that are similar to NPSCs (Mirzadeh et al., 2008). The SVZ is a secondary proliferative zone that does produce nerve cells during the embryonic period (Urban and Guillemot, 2014). However, it plays a more predominant role in the generation of new nerve cells during the adult period (Mirzadeh et al., 2008).

The SVZ is highly regionalized and constitutes three main types of brain cells including neuroblasts (Type A cells), radial glia-like cells (Type B cells) and transient amplifying cells (Type C cells) (Doetsch et al., 1999; Doetsch et al., 2002). Adult neurogenesis in the SVZ starts with the generation of transient amplifying cells from radial glia-like cells, which then convert into neuroblasts (Jackson et al., 2006). These neuroblasts migrate towards the olfactory bulb and finally differentiate into interneurons. (Gage FH, 2002; Ponti et al., 2013)

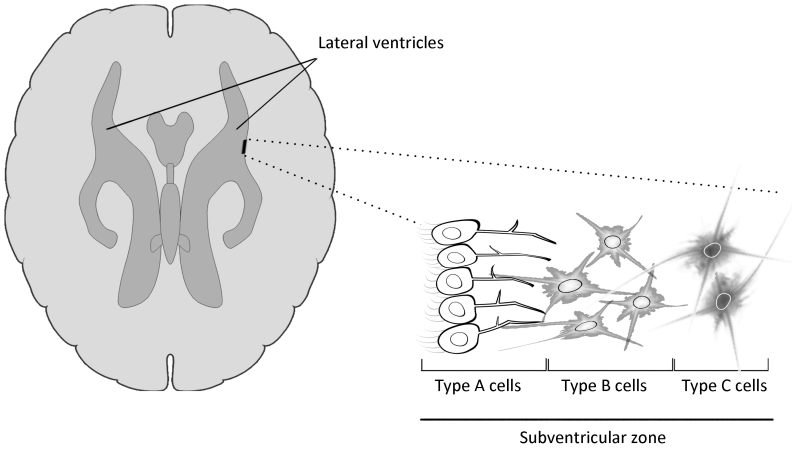

Figure 1-2: The human subventricular zone (redrawn with reference to Arias-Carrion et al., 2008)

1.1.4 Blood brain barrier

The blood brain barrier (BBB) is a semipermeable membrane, where cells are lined and joined by tight junctions lining the blood capillaries in brain. The BBB functions as a barrier allowing the passage of molecules that are crucial to neural function from the circulating blood to brain extracellular fluid in a highly selective manner. The BBB is permeable to water, carbon dioxide, oxygen and most lipid-soluble molecules by passive diffusion, and is less permeable to large and hydrophilic molecules. In addition, the BBB prevents the entry of a wide variety of neurotoxins by means of active efflux transport mechanisms mediated by P-glycoprotein and other efflux transporters. Thus, the BBB is a significant barrier to delivery of drugs to target regions in the brain. (Ballabh et al., 2004; Zlokovic BV, 2008; Daneman R, 2012)

1.2 Tumors, cancer and cancer stem cells

1.2.1 Overview of tumors and cancer

The mammalian body is made up of trillions of cells. If a clump of cells grows out of control, they form either benign (non-cancerous) or malignant (cancerous) tumors. Benign tumors are generally not life threatening. The general features of benign tumors are a slow growth rate and lack of invasion into surrounding tissue. However, benign tumors may disrupt local tissue or organs due to the large size of the tumor. Malignant tumors, generally referred to as cancer, proliferate more rapidly and are capable of invading nearby tissues or organs and can lead to metastases in other parts of the body. (Koten et al., 1993)

According to the statistics published by the GBD 2015 Disease and Injury Incidence and Prevalence Collaborators (2016), deaths from cancer account for around 15.7% of all human deaths, and there is an increasing trend of global cancer incidence (as reported in 2015), with around 18.6 million people suffering from cancer, compared with the estimate published in 2012 (14.1 million). The most common types of cancers are lung cancer (13%), breast cancer (12%), colorectal cancer (9.7%), prostate cancer (7.8%),

stomach cancer (6.8%), liver cancer (5.6%), cervical or uterine cancer (3.8%), esophageal cancer (3.2%) and bladder cancer (3.2%). The specific causes of cancer are still poorly identified, mainly due to the contributions of both environmental factors and inherited genetics.

1.2.2 The origins of cancer

The way tumors develop and are sustained is still the subject of debate. The current accepted leading models of cancer are the clonal evolution model and the hierarchical cancer stem cell model (Figure 1-3). The clonal evolution model hypothesized that normal cells undergo a series of mutations to transform into cancer-like cells, and these cancer-like cells grow and expand spontaneously to finally form tumors. The Hierarchical cancer stem cell model hypothesized that tumors are originated from a specific group of cells, within the tumors, which are capable of self-growing and self-renewing ability. These types of cells can undergo asymmetrical division to form new cancer stem cells (CSCs) and cancer cells. (Visvader JE, 2011; Kreso and Dick, 2014)

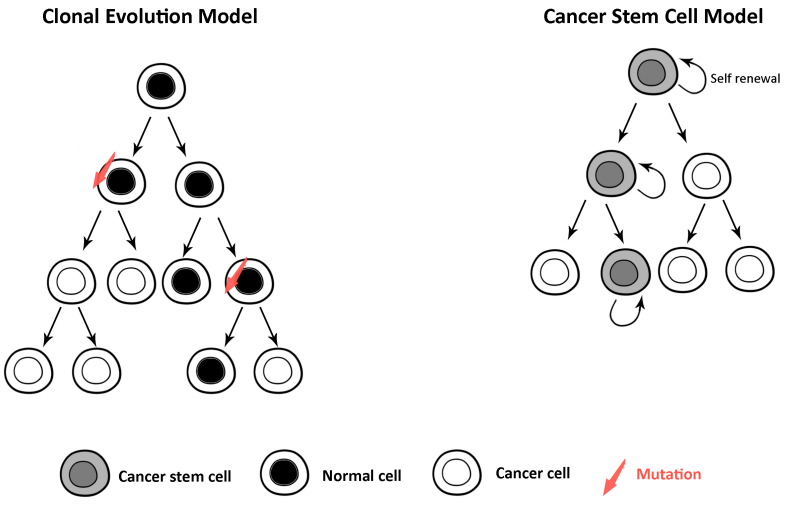

Figure 1-3: The hypothesized models of the origin of cancer (redrawn with reference to Adams and Strasser, 2008)

1.2.3 Cancer stem cells

Cancer stem cells (CSCs) are cells that can self-renew and differentiate to form new cancer cells and a tumor of the same origin. CSCs share characteristics with normal stem cells, and have the capacity to sustain new tumor growth after chemotherapy. Current conventional cancer therapies, in particular cytotoxic drugs and radiotherapy, only target frequently dividing cells, i.e. the bulk of the population of cancer cells, which share common features with transit amplifying cells. Slowly dividing CSCs may resist these conventional therapies and give rise to new primary cancer cells leading to tumor relapse after a period of time. Therefore, the discovery of cancer stem cells implies that effective cancer treatments or therapies may require more focus on inhibiting the growth and function of CSCs. (Reya et al., 2001)

1.3 Brain tumors

Brain tumors account for around 1.8% of all cancer types (Ferlay et al., 2015). Primary brain tumors are generated in the brain but tumors from distant sites can also metastasize to the brain (Singh et al., 2014). According to the recent classification by the World Health Organization (WHO) based on histology and molecular markers, brain tumors can be basically classified as gliomas and non-glioma tumors such as medulloblastomas and meningiomas (Louis et al., 2016). Gliomas are some of the most common types of primary brain tumors (Louis et al., 2016). Based on the WHO grading system, gliomas can be further classified as pilocytic astrocytomas (Grade I), low–grade astrocytomas (Grade II), anaplastic astrocytomas (Grade III) and glioblastoma multiforme (GBM) (Grade IV) (Louis et al., 2016). In this study, we will focus on the most prevalent primary brain tumor, glioblastoma,

1.4 Glioblastoma

1.4.1 The malignance of glioblastoma

Glioblastoma multiforme (GBM) is the most common and malignant primary brain

tumor within the sub-ventricular zone of the CNS, accounting for around 16% of all brain tumors (Thakkar et al., 2014). GBM are predominantly located in the supratentorial region and are mainly diagnosed in male caucasians at a median age of 64 years old (Thakkar et al., 2014). Since this highly aggressive primary brain tumor is resistant to the standard conventional therapies, including surgical interventions, radiation and chemotherapy, the typical survival time for patients after diagnosis of GBM is within the range 12 to 18 months (Stupp et al., 2009). Only 3-5% of GBM patients survive for more than 5 years post diagnosis (Ostrom et al., 2014; Ostrom et al., 2015).

1.4.2 Classification of glioblastoma

Historically and conventionally GBM has been categorized into primary and secondary GBM. Primary GBM develops rapidly *de novo*, without any evidence of a less malignant precursor tumor and represents about 90% of all GBM (Furnari et al., 2007). This type of GBM is genetically associated with overexpression of *EGFR*, mutation of *PTEN* or the deletion of p16INK4a (Furnari et al., 2007). Secondary GBM develops slowly from low-grade or anaplastic astrocytoma, and is characterized by the expression of *TP53* or *RB2* mutations (Furnari et al., 2007).

More recently, based on comprehensive genomic analysis completed in 2011, GBM was divided into four subtypes: classical, mesenchymal, proneural and neural subtypes (Verhaak et al., 2010). The classical subtype accounts for 21% of all GBM cases and typically features amplification of *EGFR* or the loss or mutation of *TP53* (Verhaak et al., 2010). The mesenchymal subtype, which accounts for around 32% of all GBM cases, is distinguished by focal hemizygous deletions of a region of the genome at 17q11.2 which contains the gene *NF1*, or an alternative mechanism resulting in low expression of the *NF1* gene (Verhaak et al., 2010). The high expression of mesenchymal markers including *CHI3L1*, *MET*, *TRADD*, *RELB* and *TNFRSF1A* genes are also the feature within the mesenchymal subtype (Verhaak et al., 2010). The proneural subtype is associated with alterations in the *PDGFRA* gene and point mutations in the *IDH1* gene, and this

accounts for another 31% of cases (Verhaak et al., 2010). The neural subtype, which accounts for the final 16% of GBM core samples, is characterized by the expression of neuron markers like *NEFL*, *GABRA1*, *SYT1* and *SLC12A5* (Verhaak et al., 2010).

According to the recent publication by the World Health Organization (WHO) in 2016, GBM is divided into three types: glioblastoma, IDH-wild type; glioblastoma, IDH-mutant; and glioblastoma, not otherwise specified (NOS), based on both the histopathological and molecular features (Louis et al., 2016). Glioblastoma, IDH-wild type, accounts for around 90% of all cases and predominantly occur in patients over 55 years old. Glioblastoma, IDH-mutant, accounts for the remaining 10% cases, generally characterized as secondary glioblastoma occurring mainly in younger patients.

1.4.3 Genetic abnormalities in glioblastoma

Data collected by The Cancer Genome Atlas (TCGA), together with published molecular studies, have identified genetic abnormalities in glioblastomas that involve four core signalling pathways, including the EGFR pathway, the p53 pathway, the PI3K pathway and the retinoblastoma (RB) tumor suppressor pathway (Rao SK, 2010). In the RB pathway, the *CDKN2A*/*CDKN2B* locus was deleted in 46% of the combined cases. In the EGFR pathway, *EGFR* gene amplification was present in 45% of cases. In the p53 pathway and PI3K pathway, *p53* and *PTEN* gene mutations were each present in around 30% of cases (Rao SK, 2010). Usually, *EGFR* amplifications and *PTEN* mutations occurred more frequently in primary GBM and *p53* mutations occurred more frequently in secondary GBM (Ohgaki H. *et al.*, 2004).

1.4.4 Standard therapies for glioblastoma

Patients with newly diagnosed GBM are commonly offered a multidisciplinary approach including surgical removal followed by concurrent radiation or administration of temozolomide (TMZ) which is an orally active alkylating agent targeting highly proliferating GBM cells to cause DNA damage and cell death. These

combinations of treatments extend the median survival of GBM patients up to 15 months (Stupp et al., 2009). However, prolonged TMZ administration seems unable to lead to any further improvement in the median survival of newly diagnosed GBM patients (Johnson et al., 2015).

Almost 70% GBM patients encountered relapse of GBM within a very short period of time after traditional combination treatments. For those patients with recurrent GBM, the repeated use of these traditional treatments seems to be controversial as evidence suggests that it results in no beneficial effects on median survival rate (Brandes et al., 2013; Franceschi et al., 2015). There are currently no effective therapeutic treatments targeting resistant GBM cells. Thus, there is a clear need for development of new therapeutic treatments for both newly diagnosed GBM patients, but also to treat the resistant GBM cells.

1.5 Glioblastoma initiating cells

1.5.1 Identification of glioblastoma initiating cells

Although the cancer stem cell hypothesis has remained controversial over the last decade, there is increasing evidence showing that GBM is a cancer stem cell disease. In 2012, Parada's group (Chen et al., 2012) pointed out that a restricted cell population, glioblastoma initiating cells (GICs), within the subventricular zone of the CNS, possessed features similar to stem cells and were able to differentiate into GBM cells, propagating the growth of GBM in response to oncogenic cues.

1.5.2 Glioblastoma initiating cell-associated molecular markers

1.5.2.1 CD133

CD133, encoded by the *PROM1* gene, is a glycoprotein that is specifically presented on cell plasma membrane projections (Shmelkov et al., 2005). CD133 has been found not only in human stem cells (HSCs) (Tirino et al., 2008; Schneider et al., 2012; Ren et al.,

2013) but also in neural stem cells (NSCs) (Singh et al., 2004). Thus, it is commonly used as a key marker for identification of GICs. Singh et al. (2003) first pointed out that CD133-positive tumor cells repopulate to form tumors of the same origin at very low cell density, when compared to CD133-negative cells.

However, the use of CD133 as a marker to separate and identify GICs is still the subject of debate, as CD133-negative glioma cells also show potential to give rise to gliomas and to form both CD133-positive and CD133-negative cells in nude rats (Wang et al., 2008). In addition, CSC markers including nestin and GFAP, as well as neuron-specific enolase (NSE) were identified in the CD133-negative GBM cells (Prestegarden et al., 2010), which also suggests that using CD133 as the sole molecular marker for identification of GICs is too simplistic. Although the use of CD133 as GIC marker is controversial, it is still used as an informative marker for identification of GICs (Singh et al., 2004).

1.5.2.2 SSEA-1

The stage-specific embryonic antigen (SSEA-1), or so called CD15, is a carbohydrate adhesion molecule generally expressed in embryonic stem cells (ESCs) during embryonic development and also in adult NPSCs. The expression of SSEA-1 is found in over 95% of GBM cases (Son et al., 2009). SSEA-1 is generally used as one of the adjuvant enrichment markers for identification of GICs. Research by Fine's group (Son et al., 2009) isolated a subpopulation of SSEA-1-positive cells from pre-selected CD133-negative GBM cells and demonstrated that they possessed enhanced tumorigenic capabilities, when compared to SSEA-1 negative cells from same tumor. This may indicate that SSEA-1 could be used alongside CD133 to enrich for GICs from GBM samples. However, based on the research conducted by Watts' group (Kenney-Herbert et al., 2015), both SSEA-1-positive and SSEA-1-negative cells are capable of generating a heterogeneous population that can propagate into GBM cells, which suggests that the use of SSEA-1 as GIC marker is unreliable.

1.5.2.3 Integrin α6

Another candidate for enrichment of GICs is integrin α6, a receptor for the extracellular matrix (ECM) protein laminin, which plays a role in regulation of proliferation and migration of both normal stem cells and cancer stem cells (Gilbertson and Rich, 2007). Integrin α6 was previously found to be over-expressed in embryonic and neural stem cells. A recent study by Rich's group (Lathia et al., 2010) showed evidence of high levels of integrin α6 presented in GICs. With co-expression of CD133, the level of enrichment for GICs was higher than when CD133 was used alone. In addition, targeting of integrin α6 in GICs reduced cell proliferation and tumor formation (Lathia et al., 2010), which suggests that integrin α6 might be a useful therapeutic target in GBM.

1.5.2.4 Other potential markers for glioblastoma initiating cells

Apart from CD133, the neuronal cell adhesion molecule (L1CAM), also known as CD171, is a molecular surface marker that is involved in the regulation of growth, survival and migration of neural cells (Izumoto et al., 1996; Suzuki et al., 2005). L1CAM was frequently reported to be over-expressed in gliomas, especially in some high-grade gliomas including GBM (Bao et al., 2008). Its level of expression has been associated with the aggressiveness of glioma. However, the use of L1CAM is contributory rather than critical in identification and isolation of GICs. CD44, a cell surface glycoprotein, has been reported in the identification of cancer stem cells of several solid cancers (Pietras et al., 2014). However, the evidence for use of CD44 for enrichment of GICs is very limited in the literature. The only publication identified is one study when CD44 was used in combination with Id1 to select the GIC population to allow investigation of the effect of TGF-β receptor inhibition (Anido et al., 2010).

1.6 Major signalling pathways involved in glioblastoma initiating cells

1.6.1 Overview of glioblastoma initiating cell signalling

Although there are several signalling pathways linked to the regulation of cancer stem cells, the major signalling pathways that have been shown to be involved in regulation of GICs are the PI3K pathway, and the Wnt, Hedgehog, Notch, BMI1 and MELK pathways.

1.6.2 PI3K/AKT/mTOR pathway in glioblastoma initiating cells

The phosphatidylinositol-4,5-bisphosphate 3-kinase (PI3K) pathway regulates cell metabolism, cell survival, cell proliferation and cell apoptosis. In many cases of cancer, this pathway is over-activated, which results in reduced apoptosis and increased proliferation (Figure 1-4) (Cantley LC, 2002).

Upon responding to the extracellular stimuli, the PI3K/AKT/mTOR signalling pathway can be activated by binding a ligand, such as insulin or other growth factors, to the high-affinity cell membrane receptor tyrosine kinases (RTKs). Based on the data from The Cancer Genome Atlas (TCGA; Cancer Genome Atlas Research Network, 2008), together with published molecular studies, the epidermal growth factor receptor (EGFR) is found to be frequently amplified in GBM as well as in GICs, which accounts for around 45% of all GBM cases (Rao, S.K., 2010; Szerlip et al., 2012). Inhibition of EGFR suppressed the proliferation of GICs and induced GIC apoptosis (Soeda et al., 2008).

Once PI3K pathway signalling is activated, PI3K catalyzes the phosphorylation of phosphatidylinositol 4,5-bisphosphate (PIP2) to form phosphatidylinositol (3,4,5)-trisphosphate (PIP3), which then regulates the downstream protein kinase B (AKT) by recruiting AKT to the plasma membrane and binding AKT via its pleckstrin homology (PH) domain (Cantley LC, 2002). Activating mutations in the

p110α catalytic subunit of PI3-Kinase, which is encoded by *PIK3CA* gene, have been reported to be present in around 10% of GBM cases (Samuels et al., 2004; Cancer Genome Atlas Research Network, 2008). Unlike p110α, the p85α regulatory subunit of PI3K, which is encoded by *PIK3R1*, has rarely been identified as aberrant in cancers (Cancer Genome Atlas Research Network, 2008).

Formation of PIP3 also regulates the translocation and activation of phosphatidylinositol dependent kinases (PDK), which can phosphorylate AKT at the site of Thr308 in order to fully activate AKT (Cantley LC, 2002). PDK2 as well as the TORC2 complex of the mammalian target of rapamycin (mTOR) protein also phosphorylate AKT at the site of Ser473, leading to full activation of AKT (Cantley LC, 2002). Although AKT acts at the crossroads of various upstream signalling events, its mutation has not been frequently identified in GBM (Knobbe et al., 2003). However, higher elevation of phosphorylated AKT levels resulting from alterations in upstream events were reported to be correlated with poor prognosis in GBM (Suzuki et al, 2010). Inhibition of AKT activity was also reported to preferentially inhibit the growth and proliferation of GICs (Gallia et al., 2009; Eyler et al., 2008).

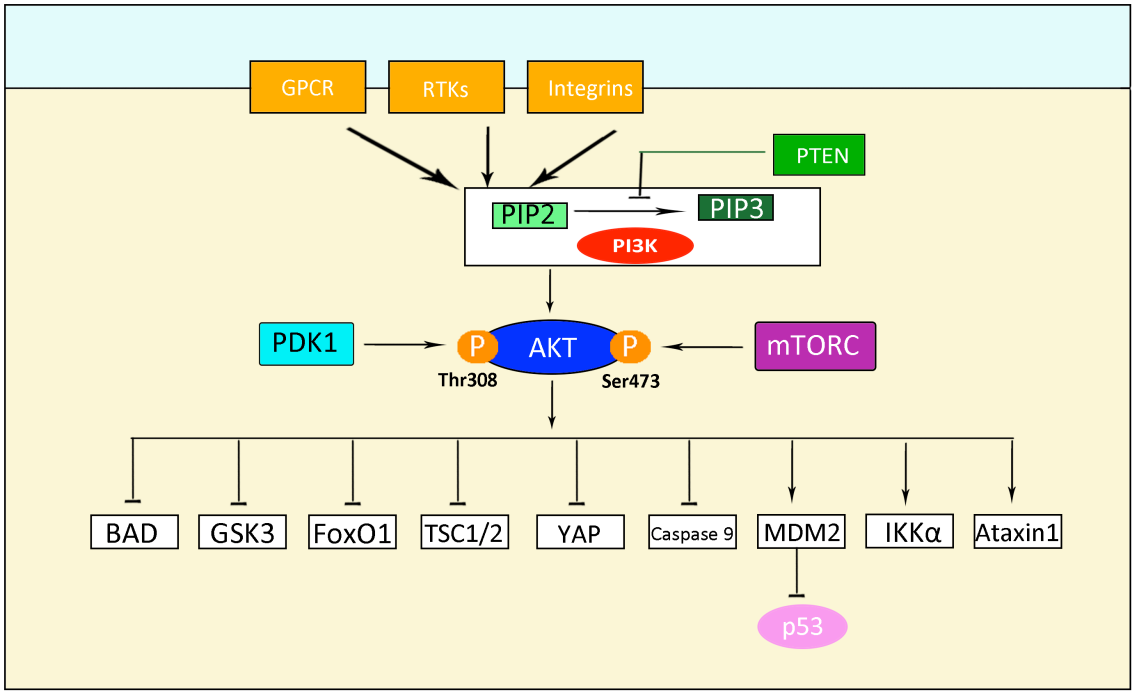

Figure 1-4: Outcomes characteristic of the PI3K pathway (redrawn with reference to Chalhoub and Baker, 2009)

The phosphatase and tensin homolog (PTEN), a tumor suppressor, reverses the phosphorylation activity of PI3K, thus, negatively regulating the PI3K signalling pathway. Zheng et al. (2008) showed that deletion of PTEN, together with loss of p53, promoted neural stem cell self-renewal, proliferation and tumorigenesis. In addition, with the combination of PTEN deletion and inactivation of pRB signalling, astrocytoma progression was found to be accelerated (Xiao et al., 2002).

Thus, targeting these key molecules or proteins of PI3K/AKT/mTOR signalling pathway could provide potential therapeutic targets for the treatment of GBM. This forms the basis for one aspect of the research described in this thesis, which focused on investigation of the PI3K signalling pathway in a novel GIC model, with a view to identifying new targets for the treatment of GBM.

1.6.3 The Wnt pathway in glioblastoma initiating cells

The Wnt signalling pathway is highly conserved in many organisms and can be divided into two different pathways, the canonical pathway and non-canonical pathway. The non-canonical pathway is involved in the regulation of cell motility, tissue polarity and cell fate determination during embryonic development (MacDonald et al., 2009), and will not be discussed in detail here. The canonical Wnt signalling pathway is involved in the regulation of the cell cycle and tumorigenesis and has been linked with various cancers (Suwala et al., 2016).

The canonical Wnt signalling pathway (Figure 1-5) is activated when Wnt ligands bind to the Frizzled/low-density-lipoprotein-related protein (Fz/LRP) coreceptor complex. LRP is phosphorylated by glycogen synthase kinase 3b (GSK3b) and casein kinase (CKI), resulting in recruitment of axin from the destruction complex. This leads to the stabilization and translocation of β-catenin from cytoplasm to nucleus to bind to the transcription factors of T cell factor/lymphoid enhancer factor (TCF/LEF) family, activating Wnt signalling target genes such as c-Myc, N-myc, c-Jun and cyclin D1, which are responsible for the observed tumorigenesis. (Clevers H, 2006)

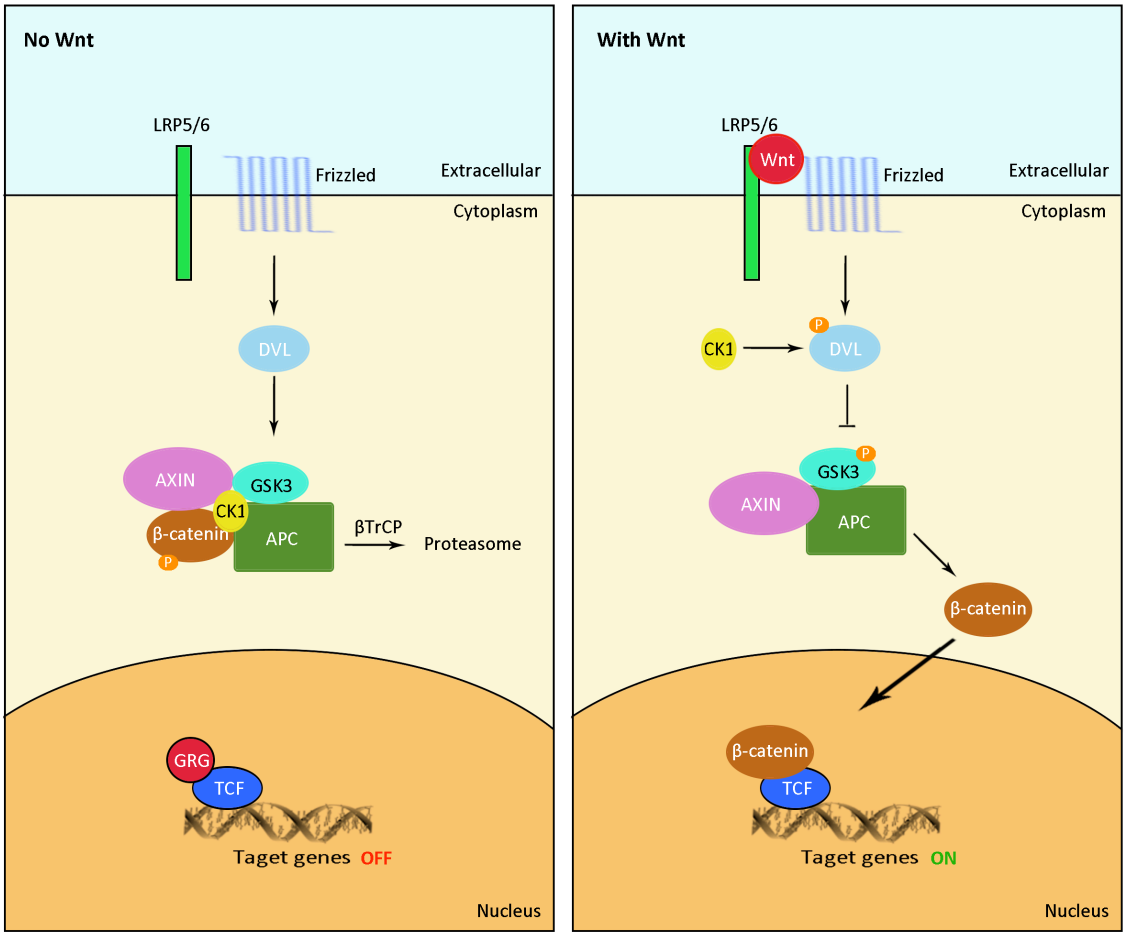

Figure 1-5: The mechanism of canonical Wnt pathway (redrawn with reference to Clevers H, 2006)

Genomic alterations and mutations of several downstream genes of canonical Wnt signalling pathway were found to be associated with many CNS cancers, including medulloblastomas, and astrocytic high-grade gliomas including GBM (Schule et al., 2012; Gong and Huang, 2012; Manoranjan et al., 2013). The over-expression of Wnt3a and Wnt1 ligands is found in GICs, promoting tumor progression in GBM (Kaur et al., 2013). The presence of high levels of some Wnt-signalling pathway-associated proteins, including SFPR3, FoxG1, and FoxM1 are correlated with the level of invasive behaviors of high-grade astrocytomas (Pecina-Slaus et al., 2016; Gong and Huang, 2012). As dissembling and translocation of β-catenin is critical within the canonical Wnt pathway, the aberrant expression of β-catenin was found to act as a predictive tool for the tumor malignance behavior in GBM (Rossi et al., 2011). In addition, the Wnt signalling cascade was found to mediate chemoresistance in many glioma types including

medulloblastoma (Flahaut et al., 2009) and GBM (Lan et al., 2015). When combined with PI3K pathway inhibitor and Wnt signalling inhibitors, an increasing inhibitory effect on the proliferation and invasiveness of TMZ-treated GICs has been reported (Shi et al., 2015).

1.6.4 The hedgehog pathway in glioblastoma initiating cells

Hedgehog (Hh) signalling is essential in cell proliferation, cell differentiation and the regulation of organ patterning during embryonic development. In adult tissue, hedgehog signalling has been reported to be involved in the regulation of neural stem cells. (Briscoe and Therond, 2013)

Hh signalling takes place in the primary cilium (Figure 1-6), where in the absence of Hh ligands, Patched (PTCH) negatively regulates Smoothened (SMO), resulting in reduced activation of SMO (Scales and de Sauvage, 2009). This enables the glioma-associated oncogene 2/3 (Gli2/3) complex to undergo cleavage, resulting in failure of transcription of Hh target genes (Scales and de Sauvage, 2009). When Hh binds to PTCH, the PTCH repression of SMO is relieved, allowing SMO to translocate to the membrane (Scales and de Sauvage, 2009). At this time, the Hh pathway is activated and the Gli complex enters the nucleus and binds to the target gene promoter, initiating the expression of target genes (Scales and de Sauvage, 2009; Briscoe and Therond, 2013). However, the detailed mechanism by which the SMO activation is regulated is still unclear at present.

The hedgehog signalling pathway has been implicated as a major factor in some forms of cancer, including basal cell carcinoma (BCC), medulloblastoma and glioma (Peukert S and Miller-Moslin K, 2010). These tumors frequently show abnormal activation or mutation of components of the Hh pathway. The involvement of Hh signalling cascades has been best characterized in medulloblastoma in the last few years (Shahi et al., 2008). Recent investigation in GBM indicates increasing evidence that hedgehog signalling participates in GBM tumorigenesis. Hh signalling activities are shown to be

consistently expressed and over-activated in some gliomas, including GBM (Dahmane et al., 2001; Shahi et al., 2008). Blockade of Hh signalling cascades following the standard radiation treatment for GBM suppressed the growth and formation of radio-resistant gliomas (Bar et al., 2007)

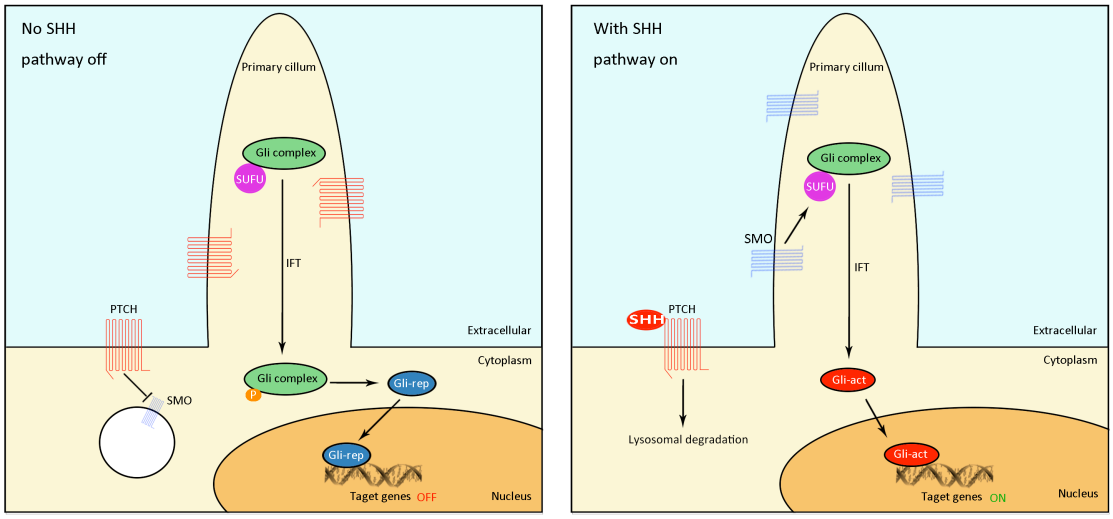

Figure 1-6: The mechanism of Hedgehog signalling pathway in mammalian cells (redrawn with reference to Briscoe and Therond, 2013)

Thus, antagonists targeting components of the Hh pathway, especially SMO, have considerable potential in cancer therapy, especially as drug therapy for GBM. Thus, one of the components of this thesis (described in chapter 5) involves assessment of some novel SMO inhibitors using appropriate cell culture models.

1.6.5 The Notch pathway in glioblastoma initiating cells

The Notch pathway plays an important role in cell proliferation, cell migration and angiogenesis and has been associated with progression of tumorigenesis. The receptor, Notch-1, and its ligands, Jagged 1 (JAG1) and delta-like-1, have been reported to be over-expressed in GBM (Purow et al., 2005; Sarkar et al., 2017). The blockade of Notch signalling in GICs, by γ–secretase inhibitors (GSI) promoted the sensitivity of traditional standard therapies including radiation and temozolomide, as well as attenuated the cell proliferation and clonogenic survival of GBM cells (Fan et al., 2010; Gilbert et al., 2010; Chu et al., 2013). A recent publication suggested that the combination of

clinically approved Notch pathway inhibitor, RO4929097, with radiation and temozolomide, delayed the clonogenicity of GICs (Yahyanejad et al., 2016).

1.6.6 BMI1 signalling pathway in glioblastoma initiating cells

B lymphoma Mo-MLV insertion region 1 homolog (BMI1) signalling functions in regulation of cell cycle, since BMI1 can bind to p14INKa and p16ARF to inhibit the activation of signalling cascades leading to cell cycle disruption (Park et al., 2004). BMI1 signalling was shown to participate in self-renewal of hematopoietic stem cells, and also adult neural stem cells (Abdouh et al., 2009). Bernier's group reported the overexpression of BMI1 in human GBM tumors, especially in CD133+ labeled GICs, and suggested that BMI1 was required for tumor cell growth (Abdouh et al., 2009). This may suggest an important role of BMI1 in GBM cell proliferation, especially for GICs.

1.6.7 MELK pathway in glioblastoma initiating cells

The Maternal embryonic leucine-zipper kinase (MELK), a serine/threonine kinase, was found to be over-expressed in many organ-specific tumor-initiating cells (Hebbard et al., 2010). The expression of MELK was identified as one of the key regulators of the proliferation of GICs, as MELK is expressed at low levels in normal human astrocytes (Nakano et al., 2008). The knockdown of MELK-mediated signalling is demonstrated to be most effective in transformed NPSCs rather than normal NPSCs (Nakano et al., 2008), which suggests a higher tumor-initiating potential of MELK-expressed cells and indicates the potential of MELK as a therapeutic target. A recent study by Nakano's group (Gu et al., 2013) provide the first evidence of the protein complex formed by MELK with the oncoprotein c-JUN (c-JUN/MELK complex) in GICs, and showed that its regulation is mediated by the FGF2/JNK pathway in a p53-dependent manner. However, MELK is currently poorly characterized and its role in regulation of GICs is still to be investigated.

1.7 Aims and scope of the research included in this thesis

Targeting the proteins described above to regulate the activity of GICs is an emerging area of GBM research and therapy. However there is still a need to investigate new targets for modulating GICs. With this in mind one of the aims of this study was to develop a model of GICs to facilitate investigation of potential specific targets within the PI3K signalling pathway that may provide the basis for discovery of specific new drugs for glioblastoma therapy. As described above there is ample evidence that GICs are related to healthy neural stem cells. This suggested that a comparison of neural stem cells with mutant neural stem cells would be an excellent starting point for such a study, and this appeared to be a novel idea to explore. To achieve this comparison, neural stem cells were isolated from wild type and transgenic mice. In early studies, an attempt was made to reprogram these cells using contemporary methods to form induced pluripotent cells. In the event the cells proved to be refractory to reprogramming using the methods adopted and instead a study of primary wild type and mutant mouse neural stem cells was conducted. These studies are described in the first half of the thesis (Chapters 2-4).

The theme of anticancer drug discovery is developed in two separate studies in the second part of the thesis. A study of inhibitors of Hh signalling including some novel SMO inhibitors synthesized at Monash Institute of Pharmaceutical Science (MIPS) forms the basis of Chapter 5. These compounds may have utility as leads for further medicinal chemistry in the future and development of agents to modulate GICs as discussed above.

It is evident that to treat GBM it will be necessary to reduce the burden of proliferating cells as well as reduce the activity of GICs. Consistent with this philosophy, another component of this study concerns the biological assessment of novel tubulin binding agents based on noscapine. This work was collaboration with medicinal chemists at MIPS and is reported in Chapter 6.

In summary, the thesis is comprised of the following chapters: Chapter 1 provides a general introduction to GBM, GICs and potential targets for drug discovery; Chapter 2 describes the characterization of the primary cells used to model healthy and mutant neural stem cells; Chapter 3 describes the work conducted to generate a model of GICs using iPS cell technology; Chapter 4 describes a proteomic study of the two neural stem cell phenotypes using biological mass spectroscopy; Chapter 5 describes an investigation of inhibitors of Hh signalling that could have potential for inhibition of repopulating GICs; Chapter 6 describes structure-activity studies of noscapine derivatives as cell cycle arrest agents; Chapter 7 is a concluding discussion of the findings of the thesis and suggestions for future work.

Chapter 2

Characterization of Cre-mediated mouse transgenic *Pik3ca*^{H1047R}/*PTEN*$^{del/del}$ neurospheres

2.1 Background

Transgenic mouse models can be engineered to give rise to tumors spontaneously, providing more realistic models of cancer than models that rely on transplantation of tumor cells. Such transgenic models offer the opportunity to examine the perturbation of cell functions that are introduced by the mutations introduced. In this study, neural stem cells were extracted from the brains of transgenic mice to provide a model of glioblastoma stem cells. The neural stem cells had aberrant Phosphoinositide 3-kinase (PI3K) signalling as a result of introduced mutations and this allowed a direct comparison with wild-type cells on an identical genetic background to the mutant cells.

A transgenic *Pik3ca*^{H1047R}/*PTEN*$^{lox/lox}$ mouse was generated by researchers from Peter MacCallum Cancer Centre (Kinross et al., 2012) by crossing a mouse containing a knock-in of the *Pik3ca*^{H1047R} mutation, with a mouse containing a Cre-inducible knockout of the *PTEN* gene. To achieve this, the team first generated a mouse that contains a conditional knock out and replacement of exon 20 introducing the H1047R mutation into the *Pik3ca* gene. The phosphatidylinositol-4,5-bisphosphate 3-kinase catalytic subunit alpha (Pik3ca) gene is a gene that encodes the p110α catalytic subunit of PI3K (Kinross et al., 2012). When Cre-recombinase (Cre) was added, the *Pik3ca*^{H1047R} mutation was activated by replacing the wild type (WT) exon 20 with the mutant exon 20 that encodes the p110α–H1047R protein. By also introducing loxP sites flanking the

PTEN gene it was possible to simultaneously induce deletion of *PTEN* on expression of Cre.

The animals used in this project were further modified by Mantamadiotis' group at The University of Melbourne, by crossing a third mouse which enabled Tamoxifen-inducible expression of Cre only in nestin-positive cells. This was achieved using a nestin promoter/enhancer expressing a fusion protein encoding Cre recombinase coupled to the modified estrogen receptor ligand-binding domain (ERT2). Thus, animals were essentially the same as wild type until treated with 4-OH-tamoxifen, when the Pik3ca mutation and the loss of PTEN could be activated simultaneously but only in neural tissues. It was hypothesized that the production of the tamoxifen inducible mouse line would allow extraction of 'wild-type' neural stem cells and subsequent introduction of a glioblastoma-like phenotype by treating the cells with tamoxifen. To our knowledge, data relating to this type of triple transgenic mouse cell line was very limited in the literature. Thus, it was considered worthwhile to investigate and compare the basic properties of these WT (control cells) and mutant *Pik3ca*^{H1047R}*/PTEN*$^{del/del}$ neural stem cell lines.

In this chapter, control cells and mutant *Pik3ca*^{H1047R}*/PTEN*$^{del/del}$ cells are investigated and compared in terms of their proliferation rate, self-renewal ability, as well as their multi-potency properties under defined differentiation media. Due to the lack of information on this novel transgenic cell line in the literature, a preliminary characterization of its properties was undertaken to provide first-hand information on the differences induced by over-activation of the PI3K pathway in neurospheres. It was hypothesized that the mutant *Pik3ca*^{H1047R}*/PTEN*$^{del/del}$ cells would have a faster proliferation rate than the control cells. In addition, as neurospheres are a mixture of cell types, knowledge of self-renewal activity and multi-potency properties under defined differentiation media could help in estimating the percentage of stem cell-like cells in these cell lines, as well as their likely fates on differentiation. In addition this information would help with preparation of the cells for modeling studies and analysis of protein phosphorylation.

2.2 Materials and Methods

2.2.1 Cell culture

2.2.1.1 Maintenance and propagation via three-dimensional (3-D) cell culture

Mouse *Pik3ca*^{H1047R}*/PTEN*$^{del/del}$ neurospheres extracted from transgenic mice were obtained from Dr. Theo Mantamadiotis' Lab at The University of Melbourne. These cells were cultured in *Pik3ca*^{H1047R}*/PTEN*$^{del/del}$ culturing medium, a chemically defined serum-free medium which consisted of Dulbecco's Modified Eagle Medium/Nutrient Mixture F-12 (DMEM/F12; Invitrogen, Australia), B-27® supplement minus vitamin A (Thermo Fisher Scientific, Australia), 1000U/mL penicillin G and streptomycin sulfate (Life Technologies, Australia), 20ng/mL EGF (Invitrogen, Australia) and FGF2 (Invitrogen, Australia) in ultra-low attachment multi-well plates (Sigma-Aldrich, Australia). These neurospheres were dissociated as single cells and passaged once the spheres reached 100µm in size. In this case, a dark area within the centre of each neurosphere marked the time point of propagation, usually about 7 to 10 days. The propagation of neurosphere suspension was done by spinning down the cell pellet at 200g for 5 minutes, dissociating neurospheres into single cells by use of StemPro® Accutase® cell dissociation reagent (Life Technologies, Australia), and then re-suspending dissociated single cells into *Pik3ca*^{H1047R}*/PTEN*$^{del/del}$ culturing medium for splitting. Cultures were all maintained at 37 ^{o}C in a 5% CO_2 incubator. Neurospheres passaged beyond twenty-five passages were discarded in order to keep the minimum variation from prolonged propagation.

2.2.1.2 Adherent monolayer cell culture

Mouse transgenic *Pik3ca*^{H1047R}*/PTEN*$^{del/del}$ neurospheres were dissociated, re-plated and cultured as monolayers for cell differentiation assays and cell reprogramming. These cells were cultured in *Pik3ca*^{H1047R}*/PTEN*$^{del/del}$ culturing medium, as described above in 2.1.1.1, but were propagated using 0.1 % (v/v) gelatin-coated culture plates

for monolayer culture. Cultures were maintained at 37 ^{o}C in a 5% CO_2 incubator and passaged once the culture reached about 80% to 90% confluence. The dissociated neurospheres were cultured for three passages to get rid of clump-liked aggregations and to create an even spread of cell adhesion. Neurospheres propagated after five passages were discarded in order to prevent differentiation resulting from prolonged propagation as monolayers.

2.2.2 Cell proliferation assay

Mouse transgenic *Pik3ca^{H1047R}/PTEN$^{del/del}$* neurospheres were dissociated with StemPro® Accutase® cell dissociation reagent (Life technologies, Australia) and were seeded at 1X10^{6} cells/well in ultra-low attachment plates. Cells were then stained using Click-iT® EdU Alexa Fluor® 488 flow cytometry assay kit (Invitrogen, Australia) according to the manufacturer's instructions. Briefly, EdU was added directly into the cell culture medium at the final concentration of 10μM, and incubated at 37 ^{o}C in a 5% CO_2 incubator for 2 hours. Cell suspensions were centrifuged and the pellet was washed with 1% BSA in PBS. Then, Click-iT® fixative was added to fix the cells and cells were incubated for 15 minutes at room temperature, followed by a wash with 1%BSA in PBS. Next, Click-iT® saponin-based permeabilization and wash reagent was added and the cells were incubated for another 15 minutes at room temperature. Click-iT® reaction cocktail was then added into cell suspensions followed by 30 minutes incubation at room temperature. Cells were then washed with Click-iT® saponin-based permeabilization and wash reagent prior to the analysis on a flow cytometer.

2.2.3 Clonal growth assay

2.2.3.1 Cell preparation

Mouse transgenic *Pik3ca^{H1047R}/PTEN$^{del/del}$* neurospheres were seeded at 1 x 10^{5} cells/mL, 2ml/well, as 3-D cell cultures in 6-well ultra-low attachment plates. Cells were cultured in *Pik3ca^{H1047R}/PTEN$^{del/del}$* culturing medium supplemented with 20ng/mL recombinant human epidermal growth factor (EGF; Invitrogen, Australia) and

recombinant human fibroblast growth factor (FGF2; Invitrogen, Australia) for 4 days. Neurospheres were then collected in a 15mL Falcon conical tube and were centrifuged at 200g for 5 minutes at room temperature. The supernatant was aspirated and discarded. The cell pellets were suspended in 500µL StemPro® Accutase® Cell Dissociation Reagent (Life Technology, Australia) at room temperature for 10 minutes to allow the neurospheres to dissociate into single cells. The separated spheroid was further mixed by gently pipetting it up and down several times to dissociate remaining small cell clumps into single cells. The single cell suspension was then neutralized with 2mL *Pik3ca*^{H1047R}*/PTEN*$^{del/del}$ culturing medium and centrifuged at 200g for 5 minutes at room temperature. The supernatant was aspirated and discarded. The cell pellets were resuspended in 1mL *Pik3ca*^{H1047R}*/PTEN*$^{del/del}$ culturing medium with 20ng/mL EGF and 20ng/mL FGF2 and filtered through a 40µm filter prior to the analysis.

2.2.3.2 Fluorescence-activated cell sorting (FACS)

Dissociated single cells were first stained with propidium iodide (PI; Sigma-Aldrich, Australia) to select live cells. Live cells were then sorted into different concentrations, ranging from 1 cell/well to 300 cells/well into 96-well ultra-low attachment plates. Cells were incubated at 37 ^{o}C in a 5% CO_2 incubator for 14 days, with one top-up of *Pik3ca*^{H1047R}*/PTEN*$^{del/del}$ culturing medium supplemented with corresponding EGF and FGF2 at day 8. Spheroid formation was observed and examined under the microscope at day 14. Data was analysed by extreme limiting dilution analysis (ELDA) software (Hu and Smyth, 2009).

2.2.3.3 Extreme limiting dilution assay (ELDA)

Sample cells were sorted into different concentrations, ranging from 1cell/well to 300cells/well, in the 96-well ultra-low attachment plates (Sigma-Aldrich, Australia). Cells were cultured in 100µL *Pik3ca*^{H1047R}*/PTEN*$^{del/del}$ culturing media with 20ng/mL EGF and 20ng/mL FGF2 for 14 days at 37 ^{o}C in a 5% CO_2 incubator. Cells were topped up with 100µL fresh *Pik3ca*^{H1047R}*/PTEN*$^{del/del}$ culturing media with 20ng/mL EGF and 20ng/mL FGF2 at day 8. Clonal formation was observed and examined under the

microscope at the end of day 14.

Pik3ca^{H1047R}*/PTEN*$^{del/del}$ cells were also seeded as 1 cell/well into the 96-well ultra-low attachment plates (Sigma-Aldrich) in 100µL *Pik3ca*^{H1047R}*/PTEN*$^{del/de}$ culturing media supplemented with different concentrations of EGF and FGF2, ranging from 0ng/mL to 20ng/mL. Either EGF or FGF2 was removed completely in some of the experiments. Cells were all cultured at 37 ^{o}C in a 5% CO_2 incubator for 14 days, with one top-up of growth medium supplemented with the corresponding concentration of growth factors at day 8. Clonal formation was observed and examined under the microscope at the end of day 14.

2.2.4 Cell differentiation assay

2.2.4.1 Cell Preparation

Mouse transgenic *Pik3ca*^{H1047R}*/PTEN*$^{del/del}$ neurospheres were plated as monolayers for three passages onto 0.1% gelatine-coated plates with *Pik3ca*^{H1047R}*/PTEN*$^{del/del}$ culturing media supplemented with 20ng/mL EGF and 20ng/mL FGF2. Cells were replated at $5x10^3$ cells/cm^2 onto laminin-coated plates in *Pik3ca*^{H1047R}*/PTEN*$^{del/del}$ culturing media at 37 ^{o}C in a 5% CO_2 incubator for 24 hours. Adherent cell cultures were then exchanged with N2B27 media which consists of a 1:1 mix of modified DMEM/F12 media and modified Neurobasal media, 1000U/mL penicillin G and streptomycin sulfate for 5 and 10 days respectively. Modified DMEM media consisted of Dulbecco's Modified Eagle Medium/Nutrient Mixture F-12 (DMEM/F12; Invitrogen, Australia), 100X N2 supplement (Invitrogen, Australia), 10mg/mL insulin (Gemini Bioproducts, US) and Bovine Albumin Fraction V solution (Invitrogen, Australia). Modified Neurobasal medium consisted of Neurobasal media (Invitrogen, Australia) and 50X B-27 supplement (Invitrogen, Australia). The differentiation of *Pik3ca*^{H1047R}*/PTEN*$^{del/del}$ adherent cells was then assessed by staining with different neural differentiation markers.

2.2.4.2 Immunocytochemistry

The differentiated cells were washed with phosphate-buffered saline (PBS) and then fixed with 4% paraformaldehyde at room temperature (RT) for 30 minutes. Fixed cells were permeabilized with 0.3% Triton-X-100 (Sigma) in PBS (PBS-T) for 30 minutes at RT, followed by three washes (10 minutes per wash) with PBS. Then, cells were blocked in PBS containing 0.3% Triton-X-100 and 1% BSA (PBS-T-BSA) at RT for 30 minutes followed by three washes with PBS. After two washes with PBS, cells were stained with primary antibody at $4^{o}C$ overnight. The primary antibodies used for investigating the neural differentiation in this case include βIII tubulin antibody, neuron-specific (Tuj-1, 1:1000; Cat.#MAB1195, NOVUS, Australia), Anti-Nestin (1:1000, Cat.#ab11306, Abcam, US), anti-O4 Alexa Fluor® 488 conjugate (Anti-O4, 1:100; Cat.#MAB345A4, Millipore, US) and anti-glial fibrillary acidic protein (Anti-GFAP, 1:1000; Cat.#AB5804, Millipore, US). Following three more washes with PBS, cells were stained with corresponding secondary antibody for 2.5 hours at room temperature. The secondary antibodies used here were donkey anti-mouse Alexa Fluor® 594 (1:1000), donkey anti-rabbit Alexa Fluor® 647 (1:1000) and goat anti-rabbit Alexa Fluor® 647 (1:500). Cells were incubated with a nucleic acid staining marker, DAPI (50ng/mL), at RT for 5 minutes after three more washes with PBS. Then, cells were washed twice again with PBS immediately prior to visualization. Images of cell differentiation at different time points were captured using a Nikon A1-R confocal microscope.

2.2.6 Data analysis

2.2.6.1 Analysis of cell proliferation rate

The cell proliferation rate was analyzed using 488nm excitation with a green emission filter (530/30nm) on a BD FACSCanto™ II flow cytometer (BD Biosciences, US). The cell gating was based on the side and forward scattered-light and non-staining control cells.

2.2.6.2 Analysis of cell clonal ability

The clonal ability of cells was analysed using online Extreme Limiting Dilution Analysis (ELDA) software obtained from the Walter Eliza Hall Institute of Medical Research website (Hu and Smyth, 2009).

2.2.6.3 Quantitative analysis of cell differentiation

The percentage of each cell type during cell differentiation was estimated using the BD FACSCanto™ II.

2.2.6.4 Statistical analysis

All assays were carried out at least three times in triplicate. All data were expressed as mean ±S.E.M and the data were analyzed with ANOVA to determine statistical significance. Results were considered significant when $p<0.05$. All analysis was performed by use of GraphPad Prism, version 5 for Mac.

2.3 Results and Discussion

Upon receiving the aforementioned mouse transgenic cells, it was very important to undertake charaterization of some basic properties of both WT and mutant *Pik3ca*^{H1047R}*/PTEN*$^{del/del}$ cells. Data available for the triple-transgenic cell line was very limited. In this study, the cells were characterized in terms of their cell morphology, cell proliferation rate, stem cell capacity, as well as their multipotency when the growth factors were removed and they were allowed to differentiate.

2.3.1 Mutant neurospheres appear more tightly packed with more microvilli at the sphere surface

It was observed that *Pik3ca*^{H1047R}*/PTEN*$^{del/del}$ cells appeared to be more tightly packed

aggregations, with smaller sphere diameter, compared with the mutant neurospheres. However, packing density and sphere diameter were not determined in detail in this study, but would be worthy of further investigation. In addition, WT neurospheres were observed to show fewer cellular projections at the edge of each sphere, compared with the mutant neurospheres. This may suggest that the mutant *Pik3ca*^{H1047R}*/PTEN*$^{del/del}$ cell line would be a more malignant phenotype. Microvilli-like cellular projections have been identified as a characteristic marker of more invasive and malignant GBM cell lines and serve to protect GBM cells which have survived treatment with cytotoxic drugs (Memmel et al., 2014; Zaguia et al., 2011; Hoa et al., 2010). Moreover, the larger numbers of microvilli-like cellular projections which were observed to be present in the mutant *Pik3ca*^{H1047R}*/PTEN*$^{del/del}$ cell line may contribute to a faster proliferation rate, as these stem-like cells could proliferate not only through cell-cell interactions, but also through microvilli-microvilli interactions in a 3D culture system (Zaguia and Schneider, 2011). Although these observations were not quantified in detail in this study, all the observations were consistent with the observations from the work of Dr. Theo Mantamadiotis Lab in the University of Melbourne. The observations from this laboratory are included in Appendix B.

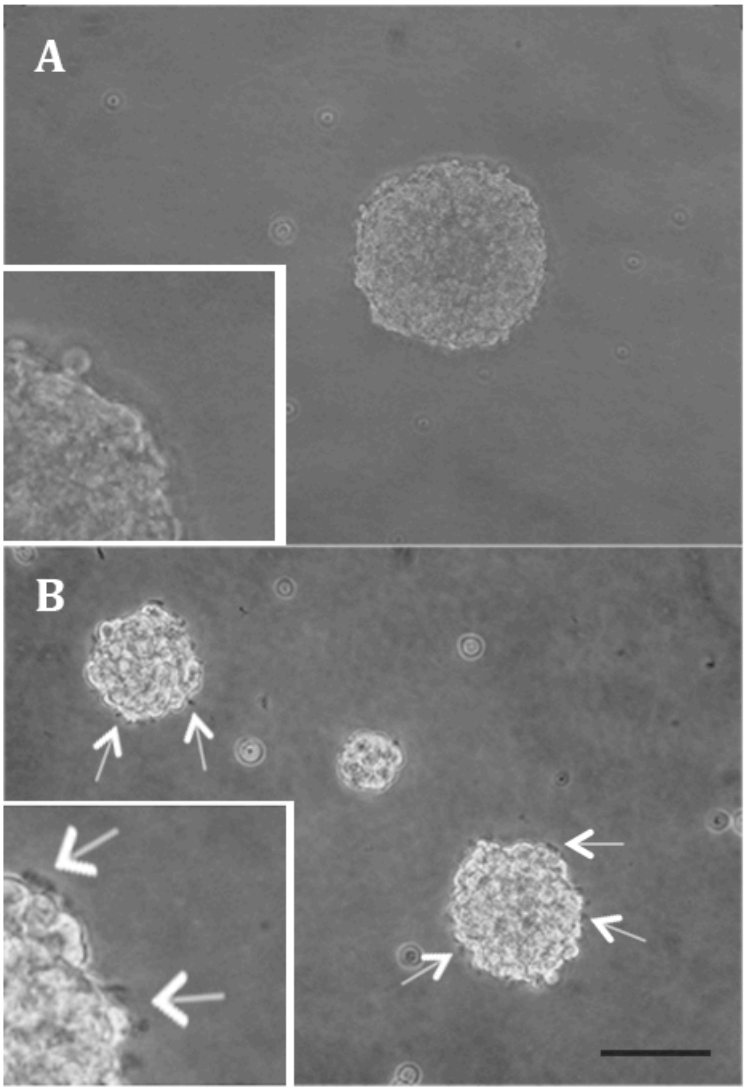

Figure 2-1: **Sphere morphology of control and mutant *Pik3ca*^{H1047R}*/PTEN*$^{del/del}$ neurospheres.** (A) Control and (B) *Pik3ca*^{H1047R}*/PTEN*$^{del/del}$ neurospheres are cultured in 3D culture system with defined culture media. The scale bar is 100µm.

2.3.2 Mutant neurospheres exhibit enhanced proliferation compared to wild-type neurospheres

As shown in Figure 2-2, Mutant *Pik3ca*^{H1047R}/*PTEN*$^{del/del}$ neurospheres treated with tamoxifen to initiate the Cre-mediated excision, showed a higher proliferation rate than control cells over a period of 24h. This may have been due to the Cre-mediated excision of *PTEN* gene coupled with the Cre-mediated mutation of the *Pik3ca* gene, both of which result in over-activation of the PI3K pathway, resulting in higher cell proliferation than the control cells. However, as the passage number increased, mutant *Pik3ca*^{H1047R}/*PTEN*$^{del/del}$ neurospheres appeared to exhibit an increasing proliferation rate in late passages as compared to early passages, whereas the proliferation rate of control cells remained stable. This observation was not validated quantitatively for this study, but would be worthy of further investigation. This observation may suggest that more progressive and malignant properties develop in mutant *Pik3ca*^{H1047R}/*PTEN*$^{del/del}$ cells; they appear to adapt to the culture conditions and adapt themselves towards aberrant and aggressive proliferation. This phenomenon was also observed in a study of human glioblastoma multiforme-derived cell lines conducted by Vescovi's group (Rossella et al., 2004).

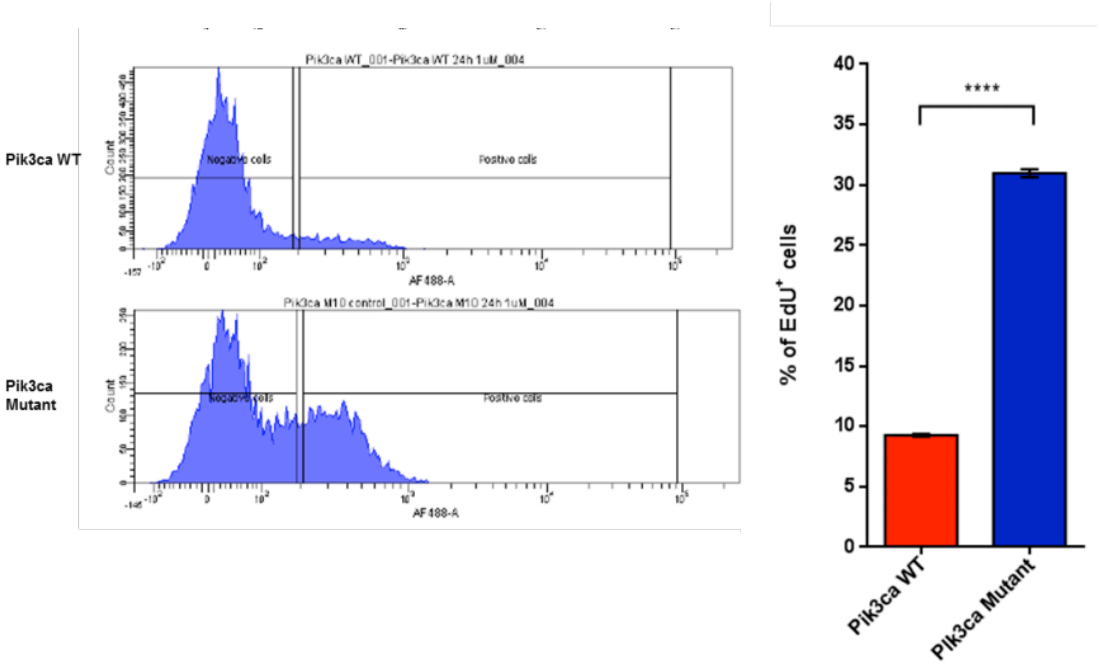

Figure 2-2: Flow cytometry based proliferation assay using mouse control and mutant *Pik3ca*^{H1047R}/*PTEN*$^{del/del}$ cells at early passages. The cell proliferation rate was determined based on 1µM EdU added 24h earlier. The results show a significant difference in cell proliferation between control and mutant *Pik3ca*^{H1047R}/*PTEN*$^{del/del}$ cells, with a three fold higher incidence of EdU positive cells in mutant cells than in control cells. Results are expressed as mean ± S.E.M. with n=3 per group. Data were analysed by t test ($p<0.0001$, n=3).

2.3.3 Mutant NSPCs exhibit enhanced sphere-forming potential compared to wild-type NSPCs

The sphere-forming efficiency is a valuable tool to characterize neural stem cells, as it shows the percentages of cells that are capable of re-forming spheres from just a single stem-like cell in a 3D culture system. Only the cells with stem-like properties would grow and proliferate. Thus, we next examined the stem cell capacity of these cells lines using limiting dilution assays and the results are analyzed by extreme-limiting dilution analysis (ELDA) (Hu and Smyth, 2009).

As neurospheres can be generated by spontaneous cell aggregation, we determined to seed the cells at extremely low concentrations, ranging from 1 to 30 cells per well into a 96-well ultra-low attachment plate. Both control and mutant *Pik3ca*^{H1047R}*/PTEN*$^{del/del}$ cells were able to form neurospheres from only a small number of cells in the clonal formation assay. It was observed that even one cell was able to re-form a neurosphere efficiently, which suggested that the neurospheres of both control and transgenic NSPCs contained a high proportion of neural stem cells or neural progenitor cells. Seeding with 7 cells or more from the neurospheres resulted in complete re-forming of neurospheres in all assayed wells. However mutant NSPCs, with 1 NSFU (neurospheres forming unit) /1.27 cells seeded, exhibit higher sphere-forming efficiency than wild-type NSPCs (1 NSFU/ 2.01 cells seeded) in early passage (Figure 2-3).

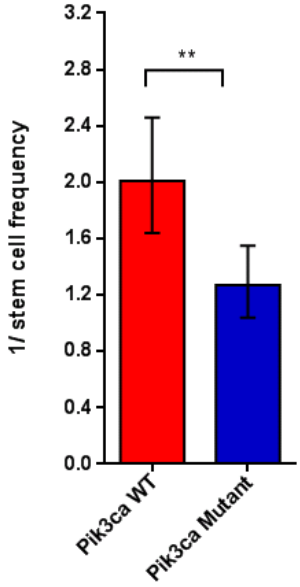

Confidence intervals for 1/(stem cell frequency)

Group	Lower	Estimate	Upper
Pik3ca WT	2.46	2.01	1.64
Pik3ca Mutant	1.55	1.27	1.04

Overall test for differences in stem cell frequencies between any of the groups

Chisq	DF	P.value
9.73	1	0.00181

Figure 2-3: Characterization of the ability of WT and mutant *Pik3ca^{H1047R}/PTEN$^{del/del}$* cells to form neurospheres using the limiting dilution assay. The results show a significant difference (p=0.00181, p<0.05) of 1/stem cell frequency between control and mutant *Pik3ca^{H1047R}/PTEN$^{del/del}$* neurospheres. 1/stem cell frequency indicates the number of stem cells to give a neurosphere. The estimates of 1/stem cell frequency were 2.01 and 1.27 for WT and mutant *Pik3ca^{H1047R}/PTEN$^{del/del}$* neurospheres respectively. The value of 1/stem cell frequency for WT *Pik3ca^{H1047R}/PTEN$^{del/del}$* neurospheres was significantly larger than that for mutant *Pik3ca^{H1047R}/PTEN$^{del/del}$* neurospheres. Data were analysed by ELDA online software (Hu and Smyth, 2009).

2.3.4 Effect of reduced concentration of growth factor on cell clonal forming ability of WT and mutant cells

One of the main objectives of this project was to compare cell signalling in control and mutant neural stem cells. It was originally assumed, based on literature observations, that cells extracted from brain and grown as neurospheres would contain a mixture of neural stem cells and transit amplifying cells. Thus not all cells would be expected to possess clone forming ability. To avoid this problem, the intention had been to reprogram cells to form induced pluripotent stem cells (iPSC), from which neural stem cells can be obtained (this concept is discussed in more detail in Chapter 3). However, due to the high proportion of neural stem cells or neural progenitor cells inside the primary neurosphere populations, the *Pik3ca*^{H1047R}/*PTEN*$^{del/del}$ cells were considered to be suitable models for direct investigation of the phosphorylated proteins of PI3K pathway in neural stem (i.e control) and glioblastoma (i.e mutant) stem cells. To prepare for signalling studies, the growth of cells was investigated under conditions of reduced EGF and FGF2 concentration. These two growth factors are typically used to maintain neural stem cells and avoid differentiation but they are likely to activate the PI3K pathway. Thus it seemed sensible to investigate the properties of the two cell types under conditions of reduced growth factor stimulation. We hypothesised that in order to compare proteomics of the WT and mutant cells, which will be discussed in detail in Chapter 4, the growth factor concentration should be optimized to reduce or minimize direct activation of the PI3K pathway. Thus, a clonal formation assay was conducted using different concentrations of EGF and FGF2, or either EGF or FGF2 alone. From previous limiting dilution assays, it was known that a seeding density of one cell per well in 96 well plates could form a neurosphere in a majority of wells. Therefore, one cell per well was used as the seeding density in this clonal formation assay to investigate the effect of different concentrations of EGF and FGF2 on the cell lines.

As shown in Table 2-1, a mimimum of 1ng/mL growth factors could maintain the clonal abiliity for both the control and mutant cells. Even at 500pg/mL of both growth factors the cells were able to form clones, but the size of spheres was significantly reduced compared with the normal size of neurospheres formed at 1ng/mL or higher

concentrations. This implied that 500pg/mL was a limiting concentration for both growth factors to maintain the clonal ability of the *Pik3ca*^{H1047R}*/PTEN*$^{del/del}$ cell line. Thus, 1ng/mL was considered to be the minimum concentration of EGF and FGF2 required when used together to maintain the normal growth and clonal ability of both control and mutant *Pik3ca*^{H1047R}*/PTEN*$^{del/del}$ cell lines.

Table 2-1: Effect of different concentrations of EGF and FGF2 growth factors on clonal fomation ability of *Pik3ca*^{H1047R}/*PTEN*$^{del/del}$ cell line using limiting dilution assay. Confidence intervals for 1/(stem cell frequency) of (A) Control and (B) Mutant *Pik3ca*^{H1047R}/*PTEN*$^{del/del}$ cells are analyzed by ELDA software (Hu and Smyth, 2009). In this experiment both growth factors were present at the same concentration as defined for each group.

(A) Confidence intervals for 1/(stem cell frequency) of control cells

Group	Estimate	Lower	Upper
0 (none)	Inf	Inf	10.014
10fg/mL	Inf	Inf	10.014
100fg/mL	Inf	Inf	10.014
1pg/mL	Inf	Inf	10.014
10pg/mL	Inf	Inf	10.014
100pg/mL	Inf	Inf	10.014
500pg/mL	1.19	0.757	0.483
1ng/mL	1.19	0.757	0.483
5ng/mL	0.831	1.308	0.527
10ng/mL	0.434	0.692	0.272
20ng/mL	0.558	0.872	0.357

(B) Confidence intervals for 1/(stem cell frequency) of mutant *Pik3ca*^{H1047R}/*PTEN*$^{del/del}$ cells

Group	Estimate	Lower	Upper
0 (none)	Inf	Inf	10.014
10fg/mL	Inf	Inf	10.014
100fg/mL	Inf	Inf	10.014
1pg/mL	Inf	Inf	10.014
10pg/mL	Inf	Inf	10.014
100pg/mL	Inf	Inf	10.014
500pg/mL	2.17	1.310	0.794
1ng/mL	2.17	1.310	0.794
5ng/mL	0.687	1.070	0.440
10ng/mL	0.496	0.780	0.361
20ng/mL	1.091	1.720	0.676

Note: Inf: Infinity

No clonal spheres were formed in the complete absence of EGF and FGF2 (Table 2-1), which is consistent with the work of Conti et al. (2009) who suggested that EGF and FGF2 were essential for maintenance of the growth of neural stem cells. Interestingly, growth media supplemented with either 20ng/mL EGF alone or 20ng/mL FGF2 alone were each capable of maintaining the clonal ability of both cell types (Table 2-2 B to E). There were no significant differences amongst each of the groups studied, though it was noted that in the absence of either growth factor the sizes of the spheres generated were significantly reduced.

Interestingly, the only condition that produced a significant difference in clonal ability between control and mutant *Pik3ca*^{H1047R}*/PTEN*$^{del/del}$ cells was under the original conditions using 20ng/mL of both EGF and FGF2. Futher data on phosphorylation of proteins in the PI3K pathway were obtained via western blot in Dr Mantamadiotis' laboratory. These studies indicated that there was no PI3K pathway phosphorylation observed in control cells at the normal concentration of 20ng/mL EGF and 20ng/mL FGF2, whereas the tamoxifen-treated mutant cells did have higher levels of phosphorylation of AKT, presumablely resulting from activiation of the PI3K pathway. Given the data presented above, it was decided that the concentration of both growth factors, EGF and FGF2, would remain at 20ng/mL for all future studies carried out in Chapter 3 and Chapter 4. This would at least ensure that differentiation did not occur during the investigation of cell signalling.

Table 2-2: Effect of concentration of one growth factor on clonal formation ability of *Pik3ca^{H1047R}/PTEN$^{del/del}$* cells using limiting dilution assay. (A) confidence intervals for 1/(stem cell frequency) of control and mutant *Pik3ca^{H1047R}/PTEN$^{del/del}$* cells. (B to E) Overall test for differences in stem cell frequencies between any of the groups. The results show no significant difference ($p>0.05$) of 1/stem cell frequency between the groups compared. Data are analyzed by ELDA software (Hu and Smyth, 2009).

(A) Confidence intervals for 1/(stem cell frequency) of control and mutant *Pik3ca^{H1047R}/PTEN$^{del/del}$* cells

Group	Estimate	Lower	Upper
Control 20ng/mL FGF2 only	0.97	0.621	0.398
Control 20ng/mL EGF only	1.19	0.757	0.483
Mutant 20ng/mL FGF2 only	1.31	0.831	0.527
Mutant 20ng/mL EGF only	1.59	0.997	0.624

(B) Overall test for differences in stem cell frequencies between control cell groups with only FGF2 or EGF only

Chisq	DF	P.value
0.374	1	0.541

(C) Overall test for differences in stem cell frequencies between Mutant cell groups with only FGF2 or EGF only

Chisq	DF	P.value
0.300	1	0.584

(D) Overall test for differences in stem cell frequencies between control and mutant cell groups with EGF only

Chisq	DF	P.value
0.804	1	0.370

(E) Overall test for differences in stem cell frequencies between control and mutant cell groups with FGF2 only

Chisq	DF	P.value
0.695	1	0.404

2.3.5 Multi-potency of control and mutant NSPCs under defined differentiation media

To investigate the multi-potency of the two *Pik3ca*^{H1047R}/*PTEN*$^{del/del}$ cell lines, the control and mutant *Pik3ca*^{H1047R}/*PTEN*$^{del/del}$ neurospheres were plated as monolayers to access their differentiation properties in defined differentiation conditions (modified N2B27 medium as described in session 2.2.4), which were frequently used for neural differentiation in our Lab (Zeng et al., 2011), for 5 and 10 days. The expression of multiple lineage-specific markers, including nestin, glial fibrillary acidic protein (GFAP) and neuron-specific class III beta-tubulin (Tuj-1), were analyzed by immunocytochemistry and the corresponding numbers of cells positive for each marker were counted by flow cytometry.

As shown in Figure 2-4, both control and mutant cell lines showed reduced numbers of nestin-positive cells and GFAP-positive cells, as well as a dramatic increase in the number of Tuj-1-positive cells during differentiation for the first 5 days of differentiation. This indicated differentiation of neural stem cells and neural progenitor cells into neurons in this defined neural differentiation media. Interesting, it was observed that the cell lines were all prone to form aggregated areas in adhesion culture at the beginning of differentiation period. The mutant cells were observed to form larger aggregated areas than control cells during the first 5 days. Immunocytochemistry analysis indicated that there were more nestin-positive cells expressed within these aggregated areas, but more Tuj-1-positive cells expressed around the edges of the clusters as monolayers. The observed existence of these cell clumps or aggregations during the early stages of differentiation may reflect the retention of NSPCs in the culture, which may “provide the structural conditions for contact communication required for neuronal differentiation” (Schlett et al., 2000). Osafune’s group (Toyoda et al., 2015) also observed similar cell aggregation in adhesion culture during differentiation of human ESCs and IPSCs towards pancreatic bud-like progenitor cells, and demonstrated that these cell aggregations in the early differentiation culture media were critical for the efficiency of cell lineage commitment

and cell aggregation.

Figure 2-4: Immunochemistry analysis of control and mutant *Pik3ca*^{H1047R}*/PTEN*$^{del/del}$ cells under defined differentiation conditions for up to 10 days. (a) Differentiation of adhesive control cell culture. The percentage of nestin+ cells were observed to be 61.0%, 37.7% and 72.1% at day 1, day 5 and day 10 under defined differentiation media respectively. The percentages of Tuj-1+ cells were 25.9%, 73.4% and 82.2% on day 1, day 5 and day 10. The percentage of GFAP+ cells were 10.9%, 1.8% and 2.5% respectively at day 1, day 5 and day 10 under defined differentiation media. (b) Differentiation of adhesive mutant *Pik3ca*^{H1047R}*/PTEN*$^{del/del}$ cell culture. The percentage of each cell type during cell differentiation was measured using the BD FACSCanto™ II flow cytometry. The percentage of nestin+ cells were 77.7%, 63.7% and 56.9% on day 1, day 5 and day 10 cultures respectively. The percentages of Tuj-1+ cells were 20.6%, 75.5% and 82.5% on day 1, day 5 and day 10. The percentage of GFAP+ cells were 17.5%, 1.3% and 0.7% respectively in day 1, day 5 and day 10 cultures. The scale bar is 100μm.

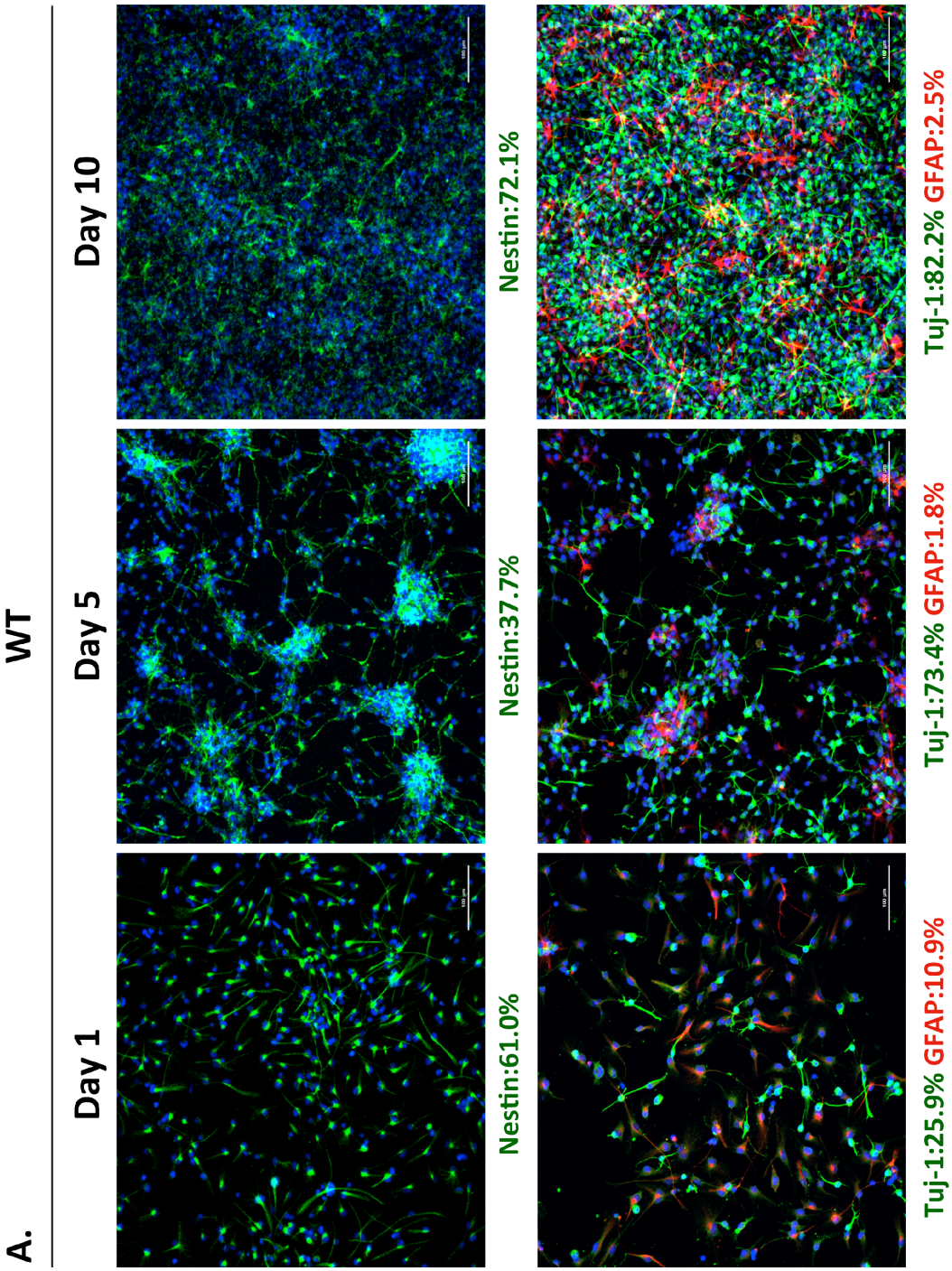
A.
WT
Day 1
Day 5
Day 10
Nestin:61.0%
Nestin:37.7%
Nestin:72.1%
Tuj-1:25.9% GFAP:10.9%
Tuj-1:73.4% GFAP:1.8%
Tuj-1:82.2% GFAP:2.5%

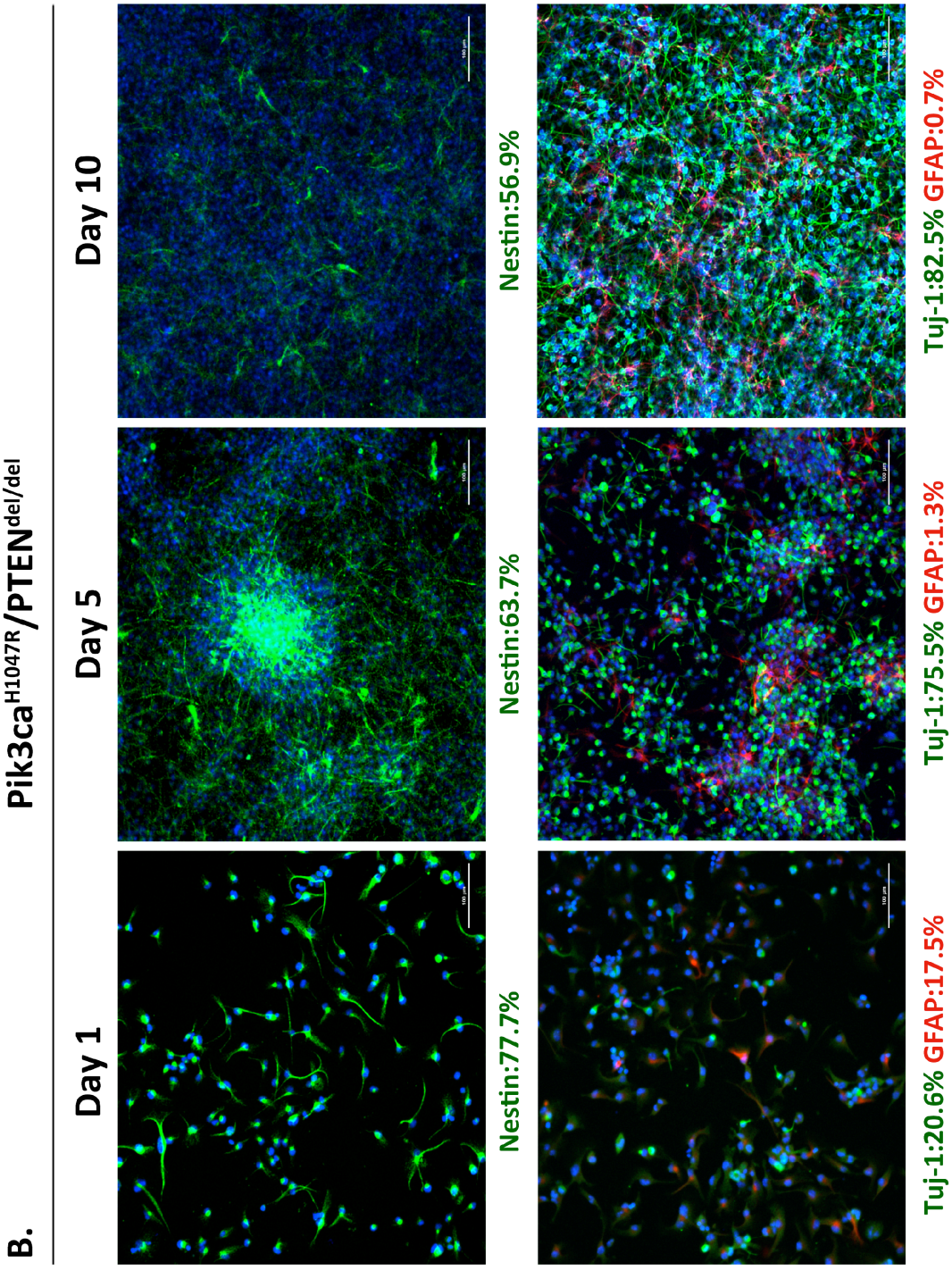
B.
Pik3ca^{H1047R}/PTEN$^{del/del}$
Day 1
Day 5
Day 10
Nestin:77.7%
Nestin:63.7%
Nestin:56.9%
Tuj-1:20.6% GFAP:17.5%
Tuj-1:75.5% GFAP:1.3%
Tuj-1:82.5% GFAP:0.7%

To summarize, this chapter provided some basic information about the growth and differentiation of the control cells and mutant *Pik3ca*^{H1047R}*/PTEN*$^{del/del}$ cell lines. Mutant *Pik3ca*^{H1047R}*/PTEN*$^{del/del}$ neurospheres exhibit more tightly packed spheres with more microvilli at sphere surface than the control cell line. Flow cytometry based proliferation assay and limiting dilution assays showed the enhanced proliferation rate and enhanced sphere-forming potential of mutant *Pik3ca*^{H1047R}*/PTEN*$^{del/del}$ cells when compared to control cells. In addition, both control cells and mutant cells could survive and grow in the defined media supplemented with a minimum of 1ng/mL of EGF and FGF2, but show significant differences when the concentration of growth factors were maintained at 20ng/mL. Both control and mutant NSPCs demonstrated multi-potency and were able to differentiate towards neurons in defined media.

Thus, this Cre-mediated mouse *Pik3ca*^{H1047R}*/PTEN*$^{del/del}$ cell line could be used as a source to provide continuous undifferentiated NPSCs for our modeling of glioblastoma initiating cells as well as for the study of key pathways involved in the development of glioblastoma.

Chapter 3

Modelling Glioblastoma initiating cells using induced pluripotent stem cells generated from conditional Cre-induced mouse transgenic *Pik3ca^{H1047R}/PTEN$^{del/del}$* tissues

3.1 Background

A recent paper published in Nature pointed out that a restricted cell population, glioblastoma stem cells, propagates the growth of glioblastoma and went some way to establishing that glioblastoma is a cancer stem cell disease (Chen et al., 2012). Jacques et al. (2009) also found that stem cells, but not astrocytes could give rise to glioblastoma through a cell autonomous mechanism. Thus, the building of a glioblastoma initiating cell model seems to be a tool for exploring the therapeutic targets that may specifically target these recurrent cells. An initial objective of this project was to use induced pluripotent stem cell (iPSC) technology to achieve this objective, as described below. The reasoning behind this objective was that whilst growth of primary neural stem cells from mice as neurospheres is an established technique, it has been assumed that such neurospheres are heterogeneous cultures, containing some neural stem cells and other downstream progenitors and transit amplifying cells. Under such circumstances it was considered that probing signalling mechanisms within the whole neurosphere population could be a poor reflection of the specialized population of neural stem cells. Methods have been established for differentiation and propagation of neural stem cells from mouse embryonic stem cells (ESCs) and these cells can be maintained as a pure population of neural stem cells for

over 100 passages (Conti et al, 2005). Thus it was considered that ESCs or iPSCs might be an excellent source of neural stem cells for comparative studies. An additional advantage of obtaining iPSCs is that in principle they could be a source of other cell types, allowing comparisons to be made between signalling defects in control and mutant cells from other tissues.

The opportunity to make use of iPSCs was made possible by a breakthrough discovery from a Japanese research group in 2006. This work first identified that pluripotent stem cells with remarkable similarities to ESCs could be reprogrammed from mouse fibroblasts by simultaneously inducing expression of four proteins, Oct4, Sox2, Klf4 and c-Myc (Takahashi and Yamanaka, 2006). These induced pluripotent stem cells (iPSCs) were remarkably similar to ESCs not only in gene expression and DNA methylation (Guenther et al., 2010; Newman and Cooper, 2010; Bock et al., 2011), but also in ability to differentiate into multiple lineages (Boulting et al., 2011). Thus, in principle this technique provided a tool to reprogram tissue isolated from transgenic mice.

Current gene expression systems used for iPSC generation include integrating vectors such as retroviral vectors (Takahashi and Yamanaka, 2006; Takahashi et al., 2007; Silva et al., 2008) or lentiviral vectors (Montini et al., 2006), non-integrating vectors including plasmid vectors (Okita et al., 2008), episomal plasmids (Yu et al., 2009) and adenovirus vectors (Stadtfeld et al., 2008). In addition, excisable integrating vectors have been developed by engineering constructs in viral vectors with floxed transgenes (Soldner et al., 2009) or piggyback transposon systems (Woltjen et al., 2009; Tsukyama et al., 2011). The field of reprogramming has developed rapidly with alternative vector systems coming in and out of favor rapidly. In this study, a reprogramming system that used a commercial lentiviral vector with the four Yamanaka transgenes flanked by loxP sequences was proposed for iPSC generation. This approach was chosen because generally speaking, integrating vectors give rise to higher iPSC reprogramming efficiency than non-integrating vectors. It was hypothesized that lentiviral vectors would be the best option for this study since they are efficiently integrated into both dividing and non-dividing cells. It was thought that this would be suitable for reprogramming neural samples that contains a mixture of neural stem and neural

progenitor cells. The concept was that the Cre-LoxP excisable system would allow us to excise the reprogramming construct from the reprogrammed iPSCs so that studies would not be compromised by ongoing expression of pluripotency transgenes that may compromise the subsequent studies. It was hypothesized, based on general observations in the iPSC field that reprogramming primary cultures of neurospheres would be easier than reprogramming fully differentiated cells, such as the skin fibroblasts that are routinely used for generating iPSCs.

Data collected by The Cancer Genome Atlas (TCGA), together with published molecular studies, have identified genetic abnormalities in glioblastomas that cover four core signalling pathways, including EGFR pathway, p53 pathway, Pi3k pathway and retinoblastoma (RB) tumor suppressor pathway (Rao, S.K., 2010). In the RB pathway, CDKN2A/CDKN2B locus was deleted in 46% of the combined cases. In the EGFR pathway, *EGFR* gene amplification accounted for 45%. In the p53 pathway and PI3K pathway, *p53* and *PTEN* gene mutation correspondingly accounted for around 30%. (Rao, S.K., 2010) Usually, *EGFR* amplifications and *PTEN* mutations happened more frequently in primary GBM and p53 mutations occurred more frequently in secondary GBM (Ohgaki H. et al., 2004).

Researchers from Peter MacCallum Cancer Centre (Kinross et al., 2012) demonstrated using a mouse model that $Pik3ca^{H1047R}$ mutations, coexistent with loss of *PTEN*, when activated in adult mice using a Cre-LoxP strategy are sufficient to promote cell transformation, thus promoting tumorigenesis. This study demonstrated that abnormal Pik3ca kinase activity and loss of PTEN's phosphatase activity cooperated to not only cause an increased PIP3 level that would finally lead to cell transformation, but also overcome negative feedback loops as a result of promoting tumorigenesis (Kinross, et al., 2012).

Together with the genetic analysis of glioblastoma, it was hypothesized that *Pik3ca* mutation with loss of *PTEN* could also be sufficient to generate glioblastoma from neural stem cells. Hence, tissues prepared from this engineered $Pik3ca^{H1047R}/PTEN^{del/del}$ mouse should be useful as a source of induced pluripotent stem cells (iPSCs) in this

study.

3.1.2 Outline of modeling design

The following strategy was proposed to produce the glioblastoma model. Primary cells, neurospheres and fibroblasts in this case, would be obtained from Cre-mediated conditional transgenic *Pik3ca*^{H1047R}*/PTEN*$^{del/del}$ mice and subsequently transformed to produce iPSCs by use of the four Yamanaka factors. Then, these derived iPSCs would be differentiated into neural stem cells and neural progenitor cells (NPSCS) using the well-established differentiation method in our laboratory. With the expression of Cre-recombinase, the *Pik3ca*^{H1047R} mutations and the loss of PTEN would later be activated in order to give glioblastoma-like cells (Figure 3-1). As explained above it was hypothesized that the use of iPSCs to obtain neural stem cells would generate a more uniform and homogenous cell population than propagation of primary neurospheres. Then, the iPSCs-derived NSCs could be investigated using proteomics techniques such as SILAC to determine expression of potential target proteins and phosphorylated proteins indicating new targets downstream of the mutations in PI3K signalling. The use of SILAC to study our glioblastoma model is described in Chapter 4 of this thesis.

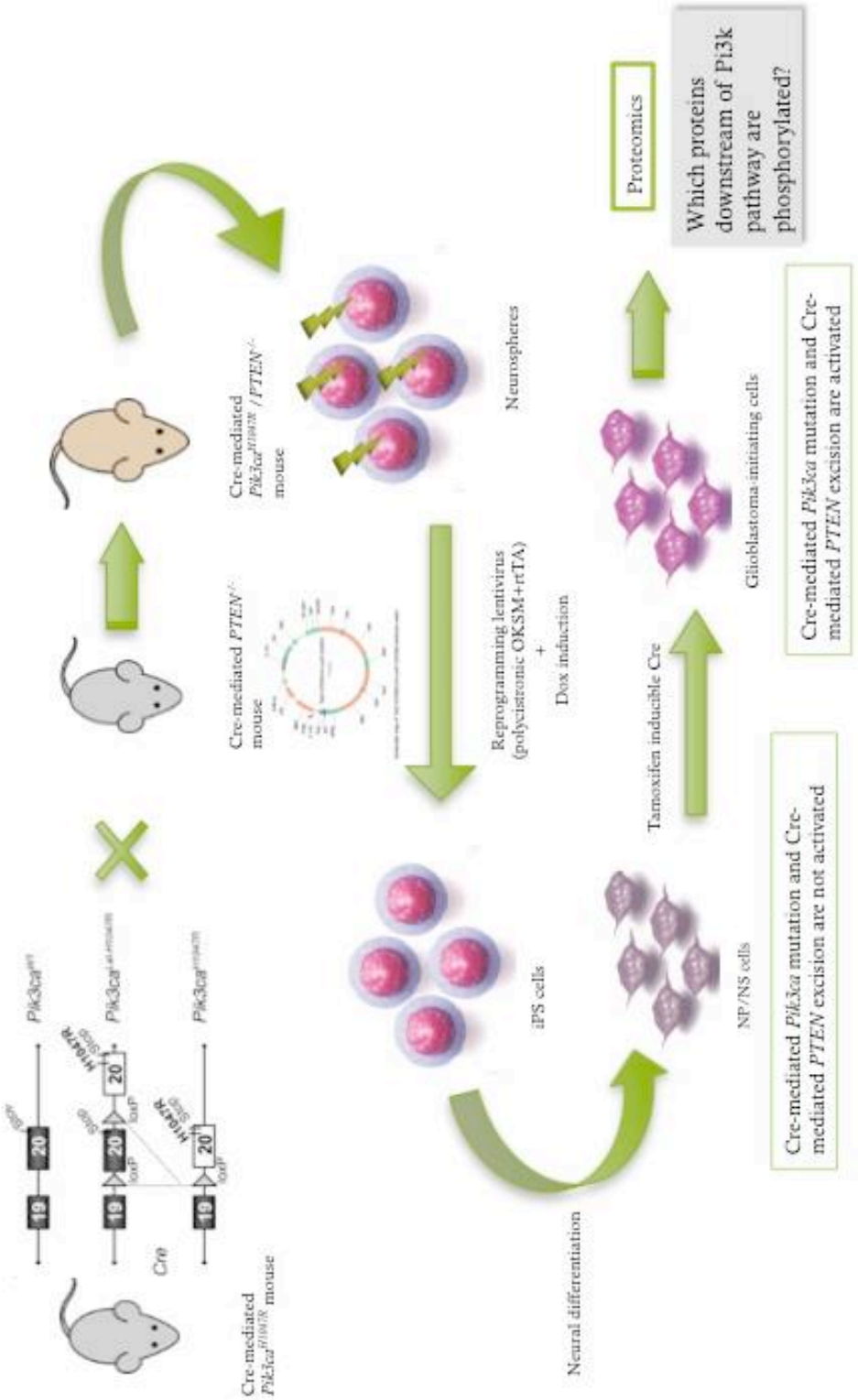

Figure 3-1: Outline of the design of glioblastoma initiating cells model

In this chapter, a step by step process of building from tissue cells towards glioblastoma initiating cell model was validated initially using a mouse embryonic fibroblast (MEF) cell line transformed with a pluripotency reporter, in the form of OCT-4 promoter-controlled expression of green fluorescent protein (GFP). OCT-4 is a key pluripotency gene that should be expressed in ESCs and iPSCs but is not expressed in MEFs. Later, iPS reprogramming from Cre-mediated transgenic mouse *Pik3ca*^{H1047R}*/PTEN*$^{del/del}$ cell lines were attempted and a comparison of various reprogramming conditions are discussed. The aim of this study was to generate a stable transgenic mouse *Pik3ca*^{H1047R}*/PTEN*$^{del/del}$ cell-derived iPSC line for subsequent modeling of glioblastoma initiating cells.

3.2 Materials and Methods

3.2.1 Cell Culture

The Cre-mediated mouse transgenic *Pik3ca*^{H1047R}*/PTEN*$^{del/del}$ neurospheres were cultured as described in Chapter 2 (2.2.1.1 and 2.2.1.2).

Transgenic *Pik3ca*^{H1047R}*/PTEN*$^{del/del}$ mouse embryonic fibroblasts (MEF) were also obtained from Dr. Theo Mantamadiotis' Lab at the University of Melbourne. The mouse OCT-4-GFP embryonic fibroblast (OCT-4-GFP MEF) cell line was obtained from colleagues in Monash University. Both populations of MEFs were cultured in mouse MEF growth medium, which contains Dulbecco's Modified Essential Medium (DMEM; Invitrogen, Australia), 10% fetal bovine serum (FBS; Invitrogen, Australia) and 1000U/mL penicillin G and streptomycin sulfate (Life Technologies, Australia). Cultures were maintained at 37 ^{o}C in a 5% CO_2 incubator and passaged when cells were 70% to 80% confluent.

A mouse Sox-1-eGFP embryonic stem (ES) cell line was available from the stem cell research group at Monash Institute of Pharmaceutical Science. This cell line was cultured in GMEM-based mouse embryonic stem cell (mESC) growth medium, which contains Glasgow's Modified Essential Medium (GMEM; Invitrogen, Australia), 10% ES

qualified FBS (Invitrogen, Australia), 100mM Sodium Pyruvate (Invitrogen, Australia), 10mM MEM non Non-Essential Amino Acids (Invitrogen, Australia), 55mM β–mercaptoethanol (Invitrogen, Australia), 1000U/mL penicillin G and streptomycin sulfate (Life Technologies, Australia). Cultures were maintained at 37 ^{o}C in a 5% CO_2 incubator and passaged when cells were 70% to 80% confluence.

3.2.2 Verification of the iPSC reprogramming process

3.2.2.1 IPSC generation from the mouse Oct4-GFP MEF cell line

IPSCs were generated using the Mouse STEMCCA Cre-Excisable Dox-Inducible Polycistronic (OKSM) Lentivirus Reprogramming Kit (Millipore, US), according to the manufacture's protocol. In brief, Oct4-GFP MEF cells were seeded at 1.4 x 10^4cells/cm^2 on 0.1% gelatin coated plates in MEF growth media for 24 hours at 37 ^{0}C in a 5% CO_2 incubator. After one day, the medium was exchanged with low serum complete medium, which consists of all the components in MEF growth medium, except that the FBS was replaced with 2% v/v FBS. TetO-STEMCCA-LoxP (OKSM) and rtTA lentiviruses were added at MOI=10, followed by the addition of 5µg/mL Polybrene transfection reagent, for 24 hours at 37 ^{0}C in a 5% CO_2 incubator. The medium was exchanged with DMEM based mouse complete ES cell medium (with 15% FBS) containing 2µM doxycycline (Dox), to induce OKSM expression, and 10ng/mL of recombinant mouse leukemia inhibitory factor (LIF; Life technologies, Australia) every other day, until the appearance of mouse iPSC-like cell colonies was observed. The iPSC-like colonies were picked based on the morphology of the colonies. The colonies should be tight colonies of small cells that have clear boundaries and the size of the colonies should approximately fit into the frame of view under a microscope using a 10X objective. Doxycycline induction was expected to produce colonies of iPSCs after 4-6 weeks, when the iPS-like colonies reach a sufficient size for replating. After this period, iPS-like colonies were picked off, trypsinized and reseeded onto mitotically irradiated inactivated MEFs in the serum free iPS culturing medium with 2i inhibitors (GSK3β inhibitor and Mek1/2 inhibitor) (without doxycycline) at 37 ^{0}C in a 5% CO_2 incubator. Mouse iPS colonies were further passaged until they reached 70% to 80% confluence.

3.2.2.2 Differentiation of mouse ES cells into NPSCs

The protocol used was adapted from Conti's (Conti et al., 2005) and Zeng's (Zeng et al., 2011) protocol, which was well established in our lab. For neural induction, the mouse ES cell line and Sox1-GFP ESC cell line were seeded at 1.5 x 10^4cells/cm^2 on 0.1% gelatin coated plates in ESC growth media overnight at 37 ^{0}C in a 5% CO_2 incubator. Then, the medium was replaced with modified N2B27 media, a 1:1 mixture of DMEM/F-12 supplemented with N2 additives, 50ug/mL bovine albumin fraction V, 25ng/mL insulin and neurobasal media supplemented with B27 serum free additive for 10 days, with media exchanged every day. On day 10, the cells were reseeded at 4x10^4cells/cm^2 on ultra-low attachment plates in NS culture medium to allow neurosphere formation. For around 4-6 days, neurospheres were collected and filtered through a 40mm filter onto 0.1% gelatin coated plates to allow NPSC cell expansion. Expansion took about 4 days, with media changes every second day, and then the cells were routinely passaged every 48h in NS culture media containing 20ng/mL EGF and 20ng/mL FGF2.

3.2.3 Building iPS cell lines from Cre-mediated *Pik3ca^{H1047R}/PTEN$^{del/del}$* mouse transgenic tissue

The Cre-mediated *Pik3ca^{H1047R}/PTEN$^{del/del}$* tissue cells were transformed using Mouse STEMCCA Cre-Excisable Dox-Inducible Polycistronic (OKSM) Lentivirus Reprogramming Kit (Millipore, US) or the Mouse STEMCCA Cre-Excisable Constitutive Polycistronic (OKSM) Lentivirus Reprogramming Kit (Millipore, US), according to the manufacture's protocol. Mouse STEMCCA Cre-Excisable Constitutive Polycistronic (OKSM) Lentivirus Reprogramming Kit was used in the same way as that described above in Chapter 3.2.2.1, except that doxycycline was not used in combination with the iPS induction medium. The latter system was used in some of the studies because the doxycycline-inducible kit was discontinued by the manufacturer during the study. This was frustrating but reflected the rapidly changing nature of the materials available for reprogramming.

3.2.4 Immunocytochemistry

Unless specified, the cells were stained as the same way as that described in Chapter 2 (2.2.4.2).

3.3 Results and discussion

3.3.1 Validation of the techniques toward building the glioblastoma initiating cell model

3.3.1.1 Successful validation of iPSCs reprogramming techniques using the Cre-excisable, Dox-inducible, polycistronic lentivirus reprogramming system in OCT-4-GFP MEF cells

In these studies, the Mouse STEMCCA Cre-Excisable Dox-Inducible Polycistronic (OKSM) Lentivirus Reprogramming Kit from Millipore was used. The Cre-LoxP system combined with Dox-inducible system was chosen because the Dox-induction could efficiently be turned on and off, allowing iPSCs to be generated but then propagated and differentiated in the absence of Yamanaka OKSM genes induced by doxycycline. Later expression of Cre-recombinase would allow excision of the floxed cassette of Yamanaka OKSM genes, ensuring that there was absolutely no expression of pluripotency genes in later experiments. The mouse OCT-4-GFP embryonic fibroblast (OCT-4-GFP MEF) cell line was used here to test the validity of the proposed iPSCs derivation technique. This cell line contained a green fluorescent reporter gene under the control of an Oct4 promoter, such that GFP was only expressed in the presence of Oct4. Therefore, only successfully reprogrammed iPSC colonies, with the expression of Oct-4 gene, expressed green fluorescent protein.

As shown in Figure 3-2 below, OCT-4-GFP MEF cells began to form iPSC-like colonies from day 10 and finally formed an identified colony at around day 22 during doxycycline (Dox) induction.

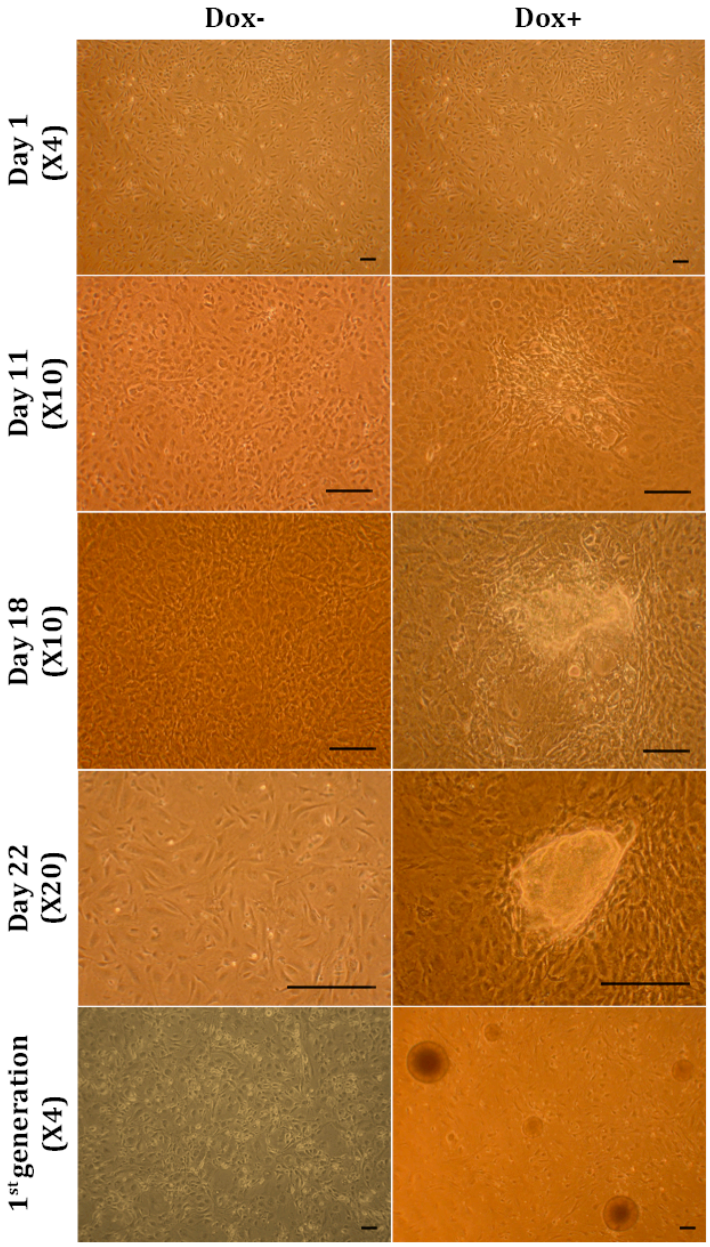

Figure 3-2: Representative photomicrographs of the progress of iPSC reprogramming of the OCT-4-GFP MEF cell line. Cell clusters were observed to start to merge together from day 11 in the presence of doxycycline (Dox). Colonies that morphologically resembled mouse ES cells were generated by day 22 in the presence of Dox. OCT-4-GFP MEF cell-derived iPS colonies were successfully passaged and maintained on mitotically inactivated MEF cells. Scale bar is 100µm.

To examine whether these iPSC-like colonies were fully reprogrammed, the iPSC-like colonies were characterized under the Nikon confocal microscope to determine whether they were expressing green fluorescent protein. Figure 3-3A and 3-3B showed an identified colony formed in the presence of Dox which showed green fluorescence, suggesting expression of the *Oct4* gene. In addition, the first passage of this newly established iPSC line (Figure 3-3C and 3-3D) maintained very good round-shaped stem cell morphology on inactivated MEF feeder layers. It also maintained the green fluorescent signal, indicating successful generation of iPSC colonies.

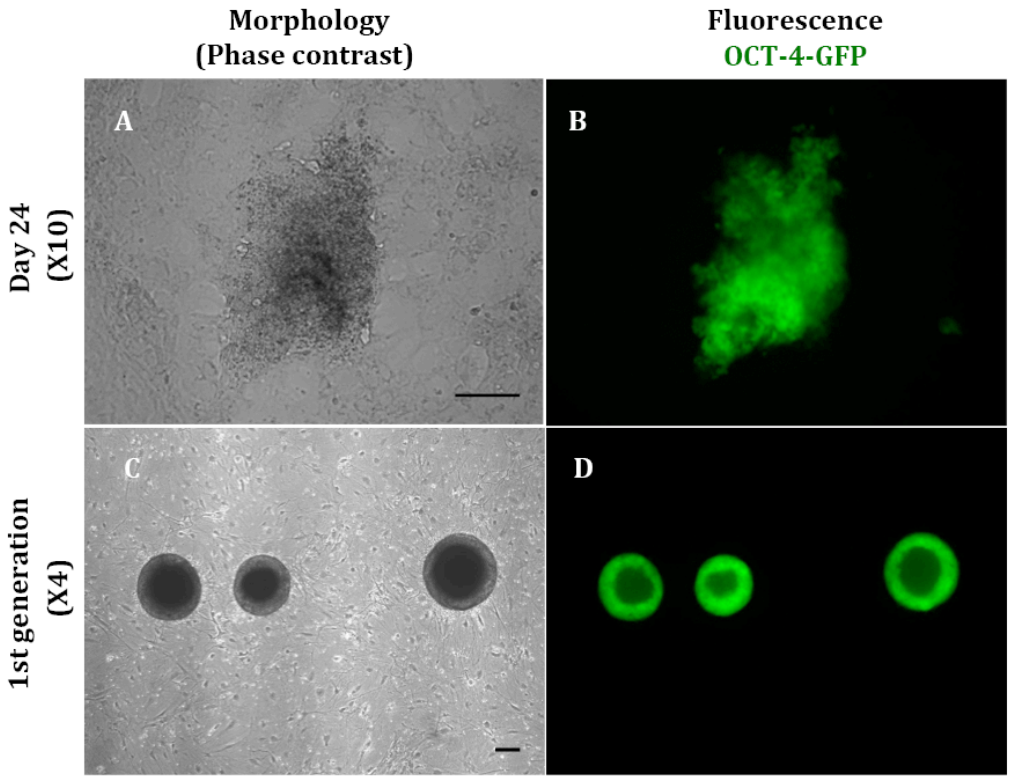

Figure 3-3: Characterization of iPSC-like colonies derived from the mouse embryonic fibroblast OCT-4-GFP cell line. (A) Phase contrast photo (10X) of reprogrammed iPSC colony as cells merged together. (B) Fluorescent photo (10X) of reprogrammed iPSC colony that activates the endogenous expression of OCT-4-GFP. In (A) and (B), images were taken at day 22 of Dox-induction. Green fluorescence was the result of GFP expression. (C) Phase contrast photo (4X) of first passaged iPSC colonies maintained on irradiated MEF feeder cells. (D) Fluorescent photo (4X) of first passaged iPSC colonies maintained on irradiated MEF feeder cells. Scale bar is 100µm.

3.3.1.2 Differentiation of mouse embryonic stem cells into neural progenitor and neural stem cells using Sox-1-egfp ES cells

The most widely used method to differentiate mESCs into NPSCs involves neural induction in serum-free adherent N2B27 medium followed by cell aggregation in suspension culture. The protocol used in this study was adapted from Conti's (Conti et al., 2005) and Wendy Zeng's protocols (Zeng et al., 2011). As shown in Figure 3-4A, the mouse Sox-1-egfp ES cell line (46C), was exposed to serum-free adherent N2B27 medium for 10 days. This period was selected for neural induction because prolonged neural induction over 10 days has been reported to give rise to a significant proportion of NPSCs with a more bipolar morphology and enhanced potential to generate multiple neuronal lineages, when compared to cells derived after 4 days or 7 days neural induction (Zeng et al., 2011). After 10 days neural induction, the culture medium was replaced with NS culture media to form cell aggregates termed neurospheres in ultra-low attachment plates as shown in Figure 3-4B. This generated neurospheres that were assumed to be a heterogeneous mixture of various cell types (Conti et al., 2005). NPSCs were then propagated from these neurospheres in NS culture media supplemented with FGF2 and EGF as shown in Figure 3-4C. Figure 3-4D is representative of the first passaged NPSCs derived from Sox-1-egfp ES cells. The bipolar morphology and lattice growth of these derived NPSCS was consistent with the morphology shown in the Conti paper (Conti et al., 2005).

To determine if these Sox-1-egfp ESC derived cells were NPSCs, the cells were stained with antibodies to the neural stem cell protein, nestin. As shown in Figure 3-5a, 3-5c and 3-5e, nestin-positive cells were evident in the culture, indicating that the majority of cells in this culture were NPSCs. The cultures were also stained with the neuron marker Tuj-1 to show the proportion of early neurons in the culture. As shown in Figure 3-5b, 3-5d and 3-5f, there were some Tuj-1 positive cells in the culture, which was consistent with the published proportions of cells in 10-day neural induction neurospheres. The expectation was that there would be approximately 20% ±5% βIII-tubulin positive neurons and 65%±3% nestin positive NPSCs (Zeng et al., 2011).

Taken together these features of nestin-positive, proliferative cells, bipolar morphology and lattice growth, the results were consistent with the expectation that the Sox-1-egfp cells had been differentiated to produce NPSCs, which indicated that the published protocol for derivation of NPSCs was reliable.

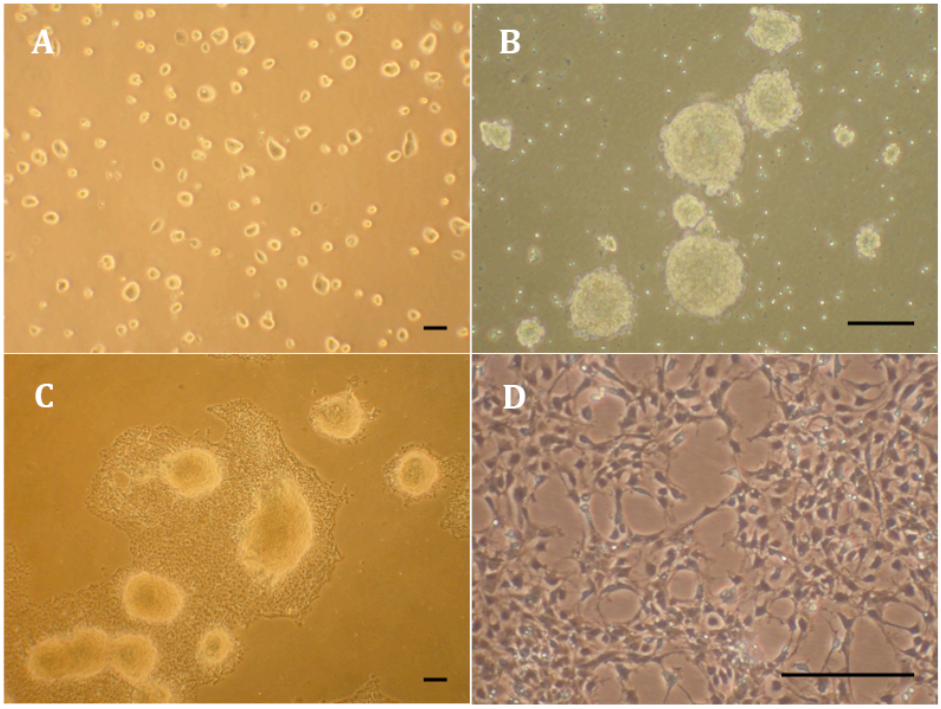

Figure 3-4: Representative micrographs of differentiation of mouse Sox-1-egfp embryonic stem (mES) cells into NPSCs. (A) Representative micrograph (X4) of mES cells maintained in ES growth media on 0.1% gelatin coated plate. (B) Representative micrograph (X10) of formation of neurospheres maintained in NS culture media on Ultra low attachment plate. (C) Representative micrograph (X4) of expansion of NPSCs from neurospheres. (D) Representative micrograph (X20) of NPSCs. Scale bar is 100µm.

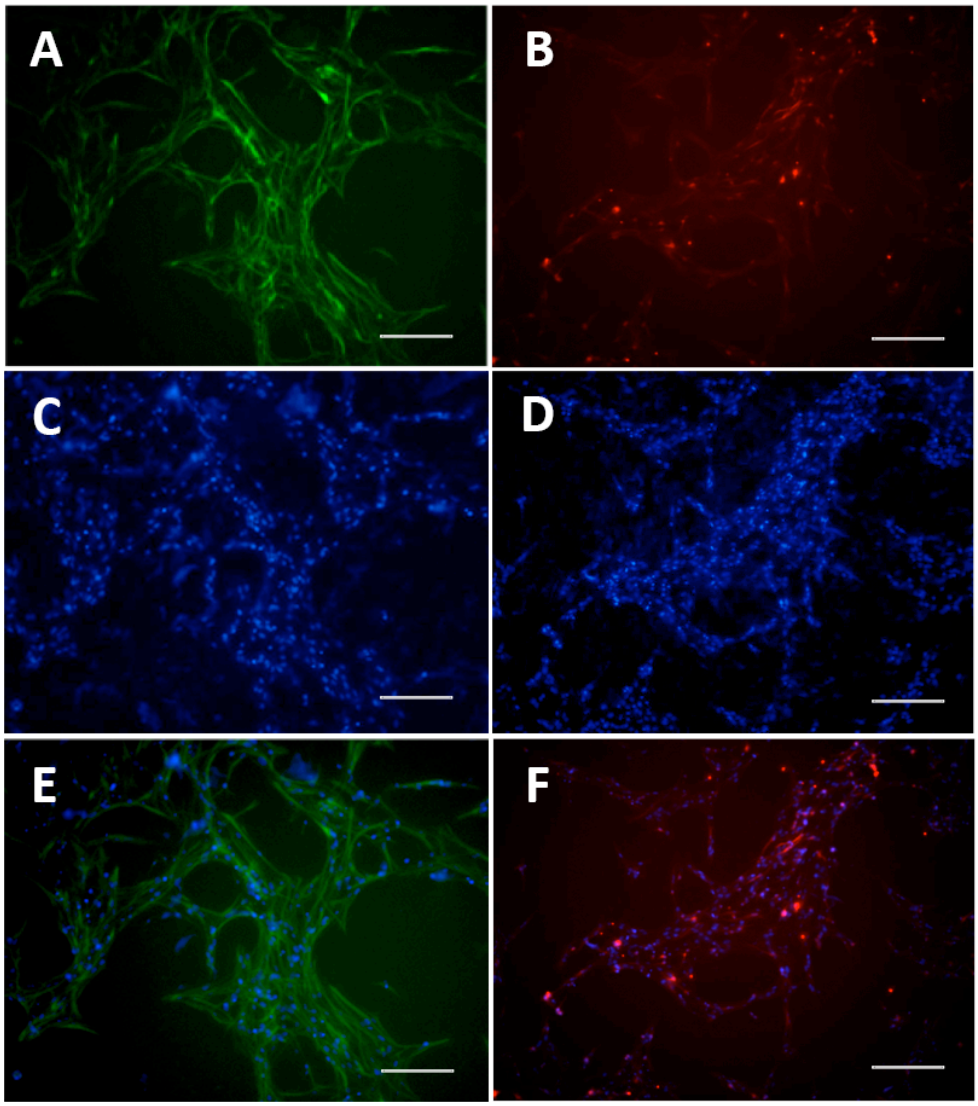

Figure 3-5: Representative micrographs (10X) of immunocytochemistry of NPSCs derived from Sox1-egfp mES cell line. (A) and (B) Immunostaining of Nestin and Tuj-1 respectively. (C) and (D) Immunostaining of DAPI. (E) Combined image of (A) and (C). (F) Combined image of (B) and (D). Scale bar is 100µm.

3.3.2 Establishment of iPSC-derived glioblastoma initiating cells

3.3.2.1 Derivation of iPSC-derived glioblastoma initiating cells from Cre-mediatd mouse transgenic *Pik3ca^{H1047R}/PTEN$^{del/del}$* neurospheres

Having validated the reprogramming system using MEFs, the same lentiviral particles were applied to the Cre-induced conditional mouse transgenic *Pik3ca^{H1047R}/PTEN$^{del/del}$* neurospheres for iPSC derivation. The reason neurospheres were used initially rather than fibroblasts here is that reprogramming is allegedly easier from stem or progenitor cells than from fully differentiated cells. Once genuine ground state iPSCs have been produced the epigenetic memory of the neural cells should be eradicated, thus the source of cells used to generate iPSCs should not affect their final properties.

As shown in Figure 3-6, Cre-mediated *Pik3ca^{H1047R}/PTEN$^{del/del}$* neurospheres were collected from Dr. Mantamadiotis' laboratory. These neurospheres were previously cultured in Knockout DMEM/F12 medium supplemented with knockout serum replacement, 20ng/mL EGF and 20ng/mL FGF2. These cells were cultured as a monolayer on 0.1% gelatin coated plate for three passages in order to enrich a uniform of NPSCs before reprogramming. After adding reprogramming lentivirus (Mouse STEMCCA Cre-Excisable Dox-Inducible Polycistronic (OKSM) Reprogramming Kit (Millipore, US)) using the validated reprogramming protocol, doxycyline (Dox) was added one day after treating with lentivirus to induce the process of reprogramming. The virus was used at a multiplicity of infection (MOI) of 5 or 10. MOI <5 were not tried based on the assumption that low MOI would yield very few or no colonies. Cell death was observed one day after lentivirus addition at MOI=10, suggesting that the lentivirus at this concentration may have been toxic to the transgenic neural cells. At MOI=5, ESC-like colonies began to form after a prolonged period of 88 days of docycyline induction. This was an unusual length of time for iPSC colony formation (Figure 3-6).

A heterogenous mixture with few bona fide colonies was observed and the majority of

the culture comprised incompletely or partially reprogrammed “by-products” at different stages (Figure 3-7). The appearance of this heterogenous reprogramming experiment may have been due to the triggering of non-specific innate immunity that triggered a protein degradation program to prevent the host cells from infection by foreign cells (Buckley et al., 2012; Polo et al., 2012). Such responses can limit transition from the initiation phase to the maturation phase of reprogramming, or even prevent cells from passing through the barriers during initiation phase or maturation phases of reprogramming. What appeared to be bona fide colonies were detected sporadically on different days, indicating a gradual transcriptional activation of pluripotency-associated genes (Meissner et al., 2007). There are still many unknowns in the process of iPS reprogramming. Despite the irregular are rare incidence of iPSC colony formation, with a defined boundary that resembles the undifferntiated ES cell colonies were picked off, and passaged onto inactivated MEF cells (Figure 3-7). These cells were incubated in a knockout serum replacement (KSR)-based knockout medium supplemented with LIF and 2i inhibitors to promote the maturation phase, as well as to enhance the buidling toward stabilization phase during reprogramming. It has been suggested (Liu et al., 2014) that KSR-based medium could facilitate the efficiency and also improve the number of bona fide iPSC colonies. 2i and LIF supplemented medium was formulated to promote passage of the pre-pluripotent-iPS cell colonies (pre-iPSC) to pass the initiation phase towards ground state pluripotency by inhibition of Erk and GSK signalling pathways (Silva et al., 2008). Other colonies, which showed a merged cell area without forming a tight colony, or with the differentiated boundary, were left on the same plates for further continous induction with Dox. However, the second subset of cells did not survive long-term culture, which suggested that these cells could be partially reprogrammed cells that were not capable of self-renewal using the conditions adopted in this study.

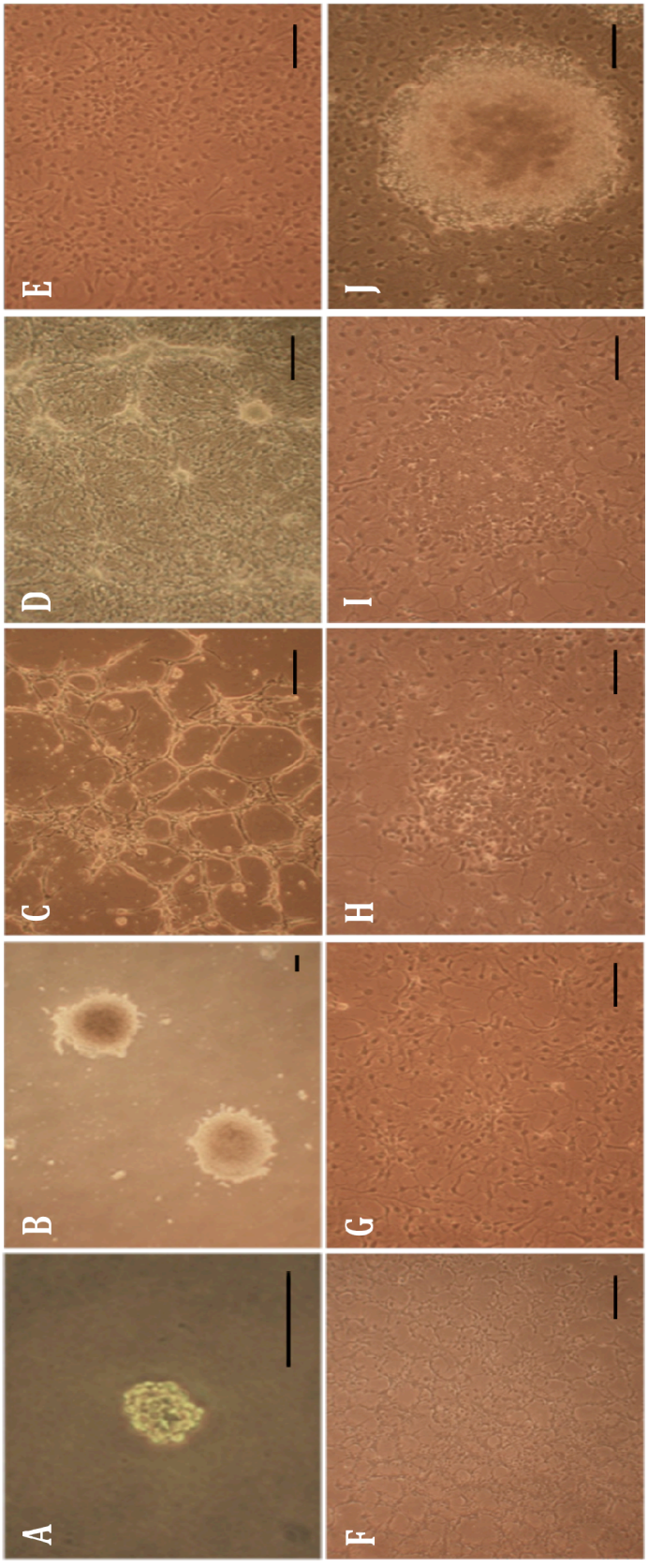

Figure 3-6: Representative micrographs of attempts to generate iPSCs from mouse neurospheres (1st reprogramming campaign) (A) Mouse neurospheres on ultra-low attachment plate. (B) NPSCs expansion on 0.1% gelatin coated plate. (C) First passage of *Pik3ca*^{H1047R}/*PTEN*$^{del/del}$ cells on 0.1% gelatin coated plate. (D) Third passage of *Pik3ca*^{H1047R}/*PTEN*$^{del/del}$ NPSCs on 0.1% gelatin coated plate. (E-J) The process of iPSC-like colony formation at day 0, day 7, day 88, day 92, day 95 and day 98 during induction with doxycycline. Scale bar is 100µm.

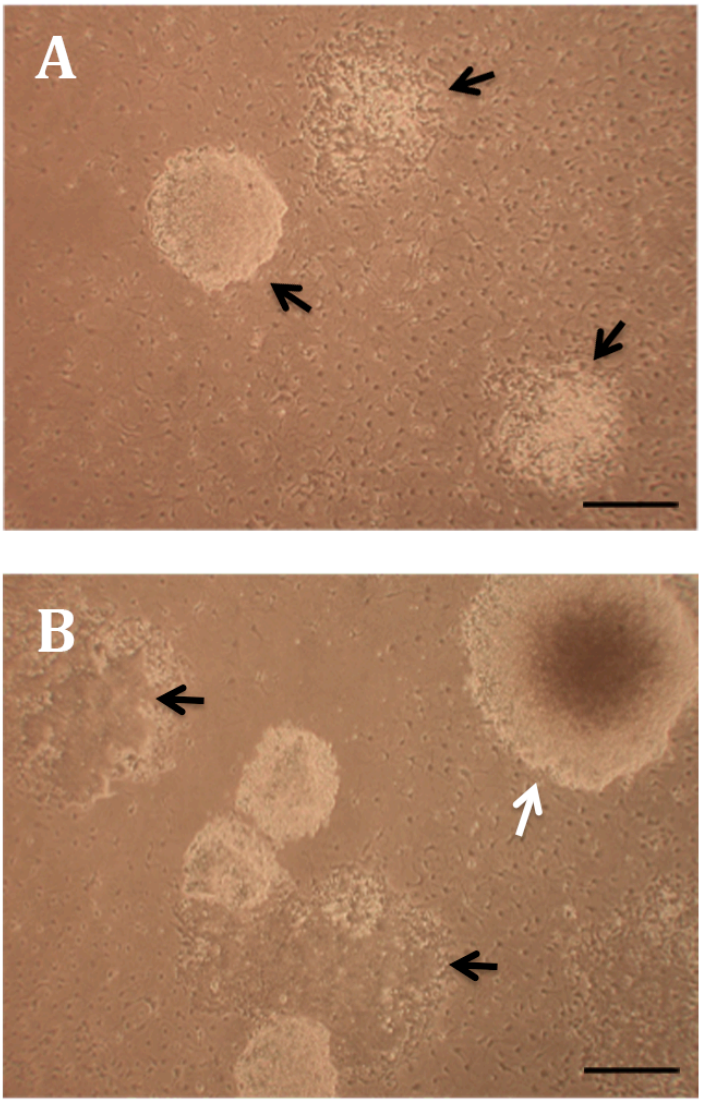

Figure 3-7: Representative micrographs of different stages of iPSC-like colony formation under heterogeneous expression of 4 reprogramming factors. (A) iPSC-like colonies derived from mouse *Pik3ca*^{H1047R}*/PTEN*$^{del/del}$ neurosphere at day 94. (B) iPSC-like colonies derived from mouse *Pik3ca*^{H1047R}*/PTEN*$^{del/del}$ neurosphere at day 97. These figures show mixed population of iPSC-like colonies at different reprogramming stages, with majority of partially reprogrammed iPSC-like colonies in the culture (see black arrow). White arrow indicates bona fide iPSC-like colonies. Scale bar is 100µm.

3.3.2.2 Further refinement of culture medium and passaging strategies for derivation of iPSCs from mouse transgenic *Pik3ca^{H1047R}/PTEN$^{del/del}$* neurospheres

In order to explore methods to produce more stable mature iPSC lines, the Dox induction conditions were manipulated and alternative media and passaging strategies were investigated. Firstly, the medium used during doxycycline induction was optimized by comparing the previously used complete ES medium (containing 15% FBS; ES medium) with serum-free medium (KO medium) during the first 7 days of docycycline induction. This method was tried because the starting neurospheres were originally cultured in serum free medium. In contrast, the cultures for reprogramming of embryonic fibroblasts or adults fibroblasts had been cultured in serum containing medium. It was postulated that the sudden change of neurospheres into serum containing medium one day after lentivirus additon may have stressed the cells, resulting in an increased period of time required to adapt to the new medium enviroment, ultimately preventing reprogramming. Indeed, the transgenic neurospheres had been found to be very sensitive to the growth medium in previous experiments (Appendix A).

Using the modified protocol, again a mixture of cells and colonies at different regrogramming stages formed at around day 22 in Dox induction medium. As shown in Figure 3-8, the colonies generated by the ES medium were much larger in size and had a relatively flat morphology with differentiation around the colony boundary. After incubation in the KO medium for the first 7 days of doxycycline induction period which was gradually switched into ES medium, cell colonies were observed to adopt a more ESC-like appearance. This supports previous evidence that the mouse transgenic neurospheres were sensitive to the medium and may need a period of time to adapt to the serum containing medium conditions prior to the preparation of reprogramming.

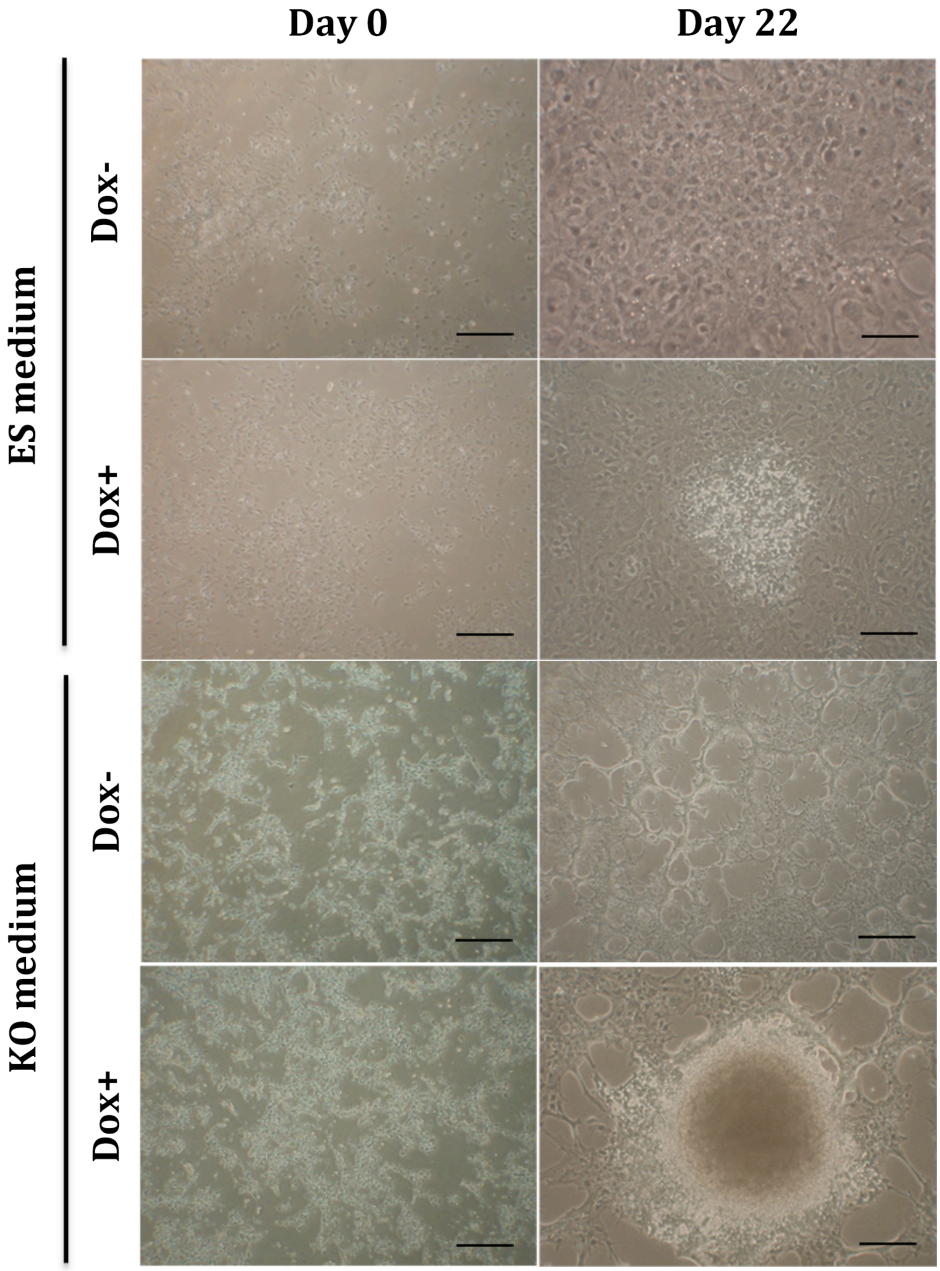

Figure 3-8: Representative micrographs of iPSCs generation from *Pik3ca*^{H1047R}/*PTEN*$^{del/del}$ neurospheres in ES and KO media during doxycycline induction at day 0 and day 22. The result show partially reprogrammed iPSCs formed at day 22 when induced with doxycycline. Scale bar is 100µm.

Colonies that had a defined boundary and morphologically resembled embryonic stem cells, were picked and passaged either as single cell suspensions or small clumps. At this stage two types of iPSC culturing media were tested for propagation of replated iPSC-like cells or colony cuts. This work aimed to test if the iPSC-like colonies were capable of self-renewal as single cell suspension. Self-renewal, independent of the four Yamanaka factors is one of the most definitive characteristics for the stabilization phase during iPS reprogramming (Wernig et al., 2007). By withdrawing the doxycycline (Dox) in the iPS culturing media, the Dox-inducible tetO operator no longer induces the expression of four Yamanaka factors, leaving the "transgene-free" iPS cells. Once Dox has been removed, only fully reprogrammed iPSCs that gained full pluripotent state would survive and expand further. The stabilization phase of reprogramming could theoretically be characterized by expression of the pluripotency-aasociated genes such as Nanog and Oct-4 (Brambrink et al., 2008). Due to the poor yields of iPSC-like colonies, the statistical characterization of pluripotency of the iPSC-like cells could not be carried out.

As shown in Figrue 3-9, only the iPSC-like colony passaged as a single cell suspension in the Knockout medium with LIF and 2i inhibitors survived and these colonies could be further passaged. In contrast, there was no formation of iPSC-like colonies when cells were passaged as single cell suspensions in the complete ES media (containing 20%FBS) with LIF and 2i inhibitors. Although iPSC-like cells passaged as clumps survived in both media conditions, these clumps remained the same size and did not grow any further. This may indicate that the process of iPSC reprogramming was suspended such that cell clumps could only be maintained in the culture media but were not supported to renew or expand. Again these cells appeared to be partially reprogrammed cells, perhaps unable to progress through the maturation phase, and unable to adapt to maturation medium.

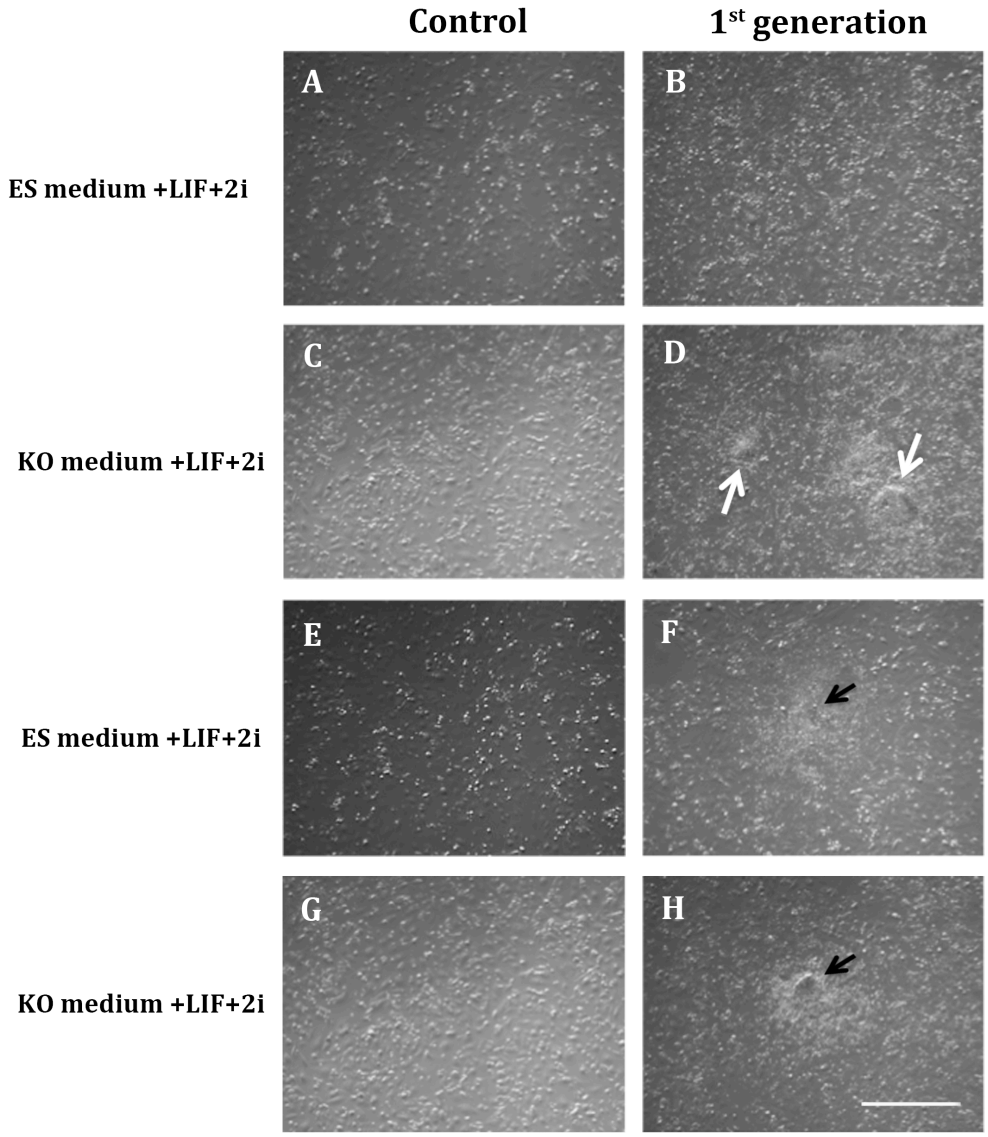

Figure 3-9: Representative photomicrographs (X10) of early passage iPSC-like cell generation from *Pik3ca*^{H1047R}/*PTEN*$^{del/del}$ neurospheres (3rd campaign using different colony pick-up strategies and medium conditions). (A to D) iPSC-like cells passaged after dissociation as single cells. (E to H) iPSC-like cells passaged as clumps. The result indicated that iPSC-like colonies survived and grew when cells were passaged as single cells in Knockout medium condition (D) (see white arrow). Passaged iPSC-like colonies survive but do not continue growing when cells were passaged as clumps (F and H) (see black arrow). Scale bar is 100µm.

According to these comparisons, it seemed to be better to use single cell suspensions as the passage strategy and to culture iPSC-like cells reprogrammed from *Pik3ca*^{H1047R}/*PTEN*$^{del/del}$ neural cells in Knockout media with LIF and 2i inhibitors.

When the surviving iPSC-like cells were passaged further as a single cell suspension in Knockout medium, with LIF and 2i inhibitors, differentiation was observed to occur at the boundary of each colony. In addition, the size of the remaining surviving colony was observed to become smaller and smaller at each passage, and eventully die after the third passage. This may be an indication that the passaged iPSC-like cells were either partially reprogrammed cells, in transition from maturation phase to stabilization phase of reprogramming, and that pluripotency medium was unable to sustain their growth. Thus, the cells were not stable, and lost their self-renewal abilities. Perhaps this may have been due to insufficient exposure to the four Yamanaka transgenes. Indeed, these cells were picked after two and half weeks under the expression of Yamanaka factors, which may not have allowed enough time for the gradual or sequential activation of pluripotency-associated genes in order to be fully reprogrammed. Research from Rudy Jaenisch's group (Brambrink et al., 2008) suggested a minimum of 12 to 16 days for the expression of transgene during reprogramming, and that prolonged expression with Yamanaka transgene would give rise to a higher yield of iPSC cells. However these authors also raised the concern that the differentiation capacity of iPSCs may be affected by long reprogramming times. Another possibility is that the cells just returned to their original cell type, neural stem cells in this case, due to the epigenetic memory that was not eradicated during the attempts to reprogram the cells. It seemed that correlations between the length of transgene expression and the efficiency of iPS reprogramming need to be studied in more detail for reprogramming of primary neural cells. To investigate whether prolonged exposure to the Yamanaka factors helped, the time of expression of four Yamanaka transgenes was extended to at least 3 weeks.

In addition, ROCK inhibitors were used to help with plating during passaging. ROCK inhibitors have been shown to prevent cell death due to anoikis when ESCs are re-plated. The extended process (reprogramming campaign 4) resulted in a few

iPSC-like colonies as before, but regrettably they were still not capable of self-renewal, in subsequent generations (Table 3-1). Even when some picked iPSC-like cells were exposed to continuous provision of doxycycline, they were unable to survive.

Table 3-1: The outline of the comparison of iPSC culture conditions for reprogramming mouse transgenic neurospheres

Culture media of first generation of iPS-like cells	Survival status	Further expand
ES+LIF+ 2i	_	_
KO+LIF+ 2i	+	_
ES +LIF+ 2i +ROCK	_	_
KO + LIF+2i+ROCK	_	_
ES+Dox+LIF	_	_

Note: "-" indicates a negative result and "+" indicates a positive result

In summary, insufficient stable iPSC colonies were generated from primary neurospheres, and this prevented a full analysis of the partially programmed cells.

3.3.2.3 Derivation of iPSC-derived glioblastoma initiating cells from mouse transgenic *Pik3ca^{H1047R}/PTEN$^{del/del}$* MEF cells

As reprogramming *Pik3ca^{H1047R}/PTEN$^{del/del}$* neurospheres was unsuccessful, it seemed sensible to attempt to reprogram another tissue type with the same genetic background. Indeed, Schnabel et al. (2012) suggested that there may be a positive correlation of the proliferation rate with reprogramming efficiency. Thus, Cre-mediated transgenic *Pik3ca^{H1047R}/PTEN$^{del/del}$* mouse embryonic fibroblasts (MEF), were used instead for the later studies.

With this system, iPSC-like colonies with a clear boundary were generated and the number of these iPSC-like colonies was twice as high as achieved from mouse transgenic neurospheres. This may suggest that higher reprogramming efficiency was

correlated to the higher proliferation rate of MEF cells compared to neurospheres. As shown in Figure 3-10, some areas of cells began to merge together as early as day 8 with the expression of Dox-induced Yamanaka factors. However, the cell areas that merged at early time points, prior to day 15, all eventually formed unidentified flat cell clusters. Cell clusters that appeared later (usually after day 15) aggregated quickly into cell colonies and finally formed colonies with a much clearer boundary, that were morphologically similar to mouse ESCs after 20 days. When these iPSC-like colonies were passaged by either single cell suspension or cell clumps in either the Knockout medium with 2i inhibitors or ES (with 15%FBS) media with 2i inhibitors, only one colony passaged as single cell suspension in Knockout media was observed to survive for the 1st generation. Due to the limitation in number of surviving cells, the culture failed to be passaged and expanded further. At this stage of the project, the doxycycline inducible lentiviral kit was discontinued and the decision was made to abandon the campaign.

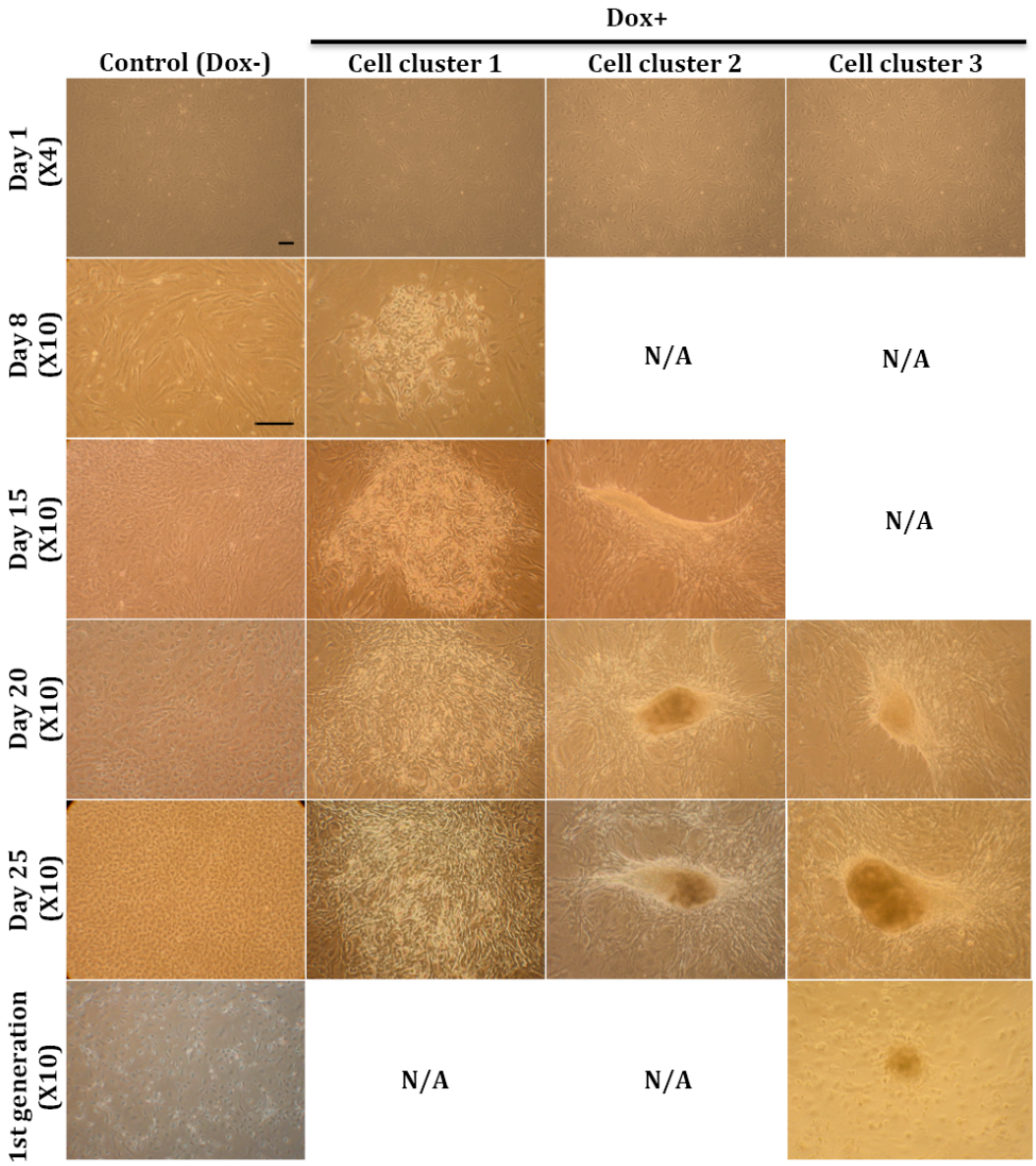

Figure 3-10: Representative photomicrographs of progress of iPS reprogramming from mouse transgenic *Pik3ca*^{H1047R}/*PTEN*$^{del/del}$ MEF cell line. Cell clusters such as cluster 1 were observed to start to merge together from day 8 in the presence of doxycycline (Dox). Cell clusters like cluster 2 and 3 were started to merge from day 15 and generated cell colony that are morphologically resembles mouse ESCs at around day 20 in the presence of Dox. Only one colony, from cell cluster 3, survived for the 1st passage, but was refractory to further expansion. Scale bar is 100µm.

Due to the unexpected discontinued production of Mouse STEMCCA Cre-Excisable Dox-Inducible Polycistronic (OKSM) Lentivirus Reprogramming Kit, it became necessary to consider alternative systems. Currently, the most commonly used and commercially available reprogramming systems are Sendai reprogramming systems and lentivirus system. However, since Sendai reprogramming systems at this stage had only been applied to reprogramming human cells, and not been tested on mouse cells before, an alternative lentivirus system, mouse STEMCCA Cre-Excisable constitutive Polycistronic (OKSM) Lentivirus Reprogramming Kit was used instead. This is the corresponding constitutive expression system to the system we tried, so we investigated this system. One limitation of this reprogramming system is that since it is not an inducible reprogramming system, the polycistronic (OKSM) genes could not be turned off until the four Yamanaka factors are excised, i.e. by expressing Cre recombinase in the iPSCs. Prolonged expression under the Yamanaka factors during reprogramming may affect the differentiation ability of iPS cells (Brambrink et al., 2009), which may affect our subsequent differentiation assay from the tissue-derived iPSCs to the desired NPSCs.

The OCT-4-GFP MEF cell line was to test the reprogramming efficiency of this new kit. In addition, the Cre-mediated mouse transgenic *Pik3ca*^{H1047R}*/PTEN*$^{del/del}$ MEF cells were treated alongside the OCT-4-GFP MEF cells for comparison. As shown in Figure 3-11, one of the OCT-4-GFP MEF cell-derived iPSC-like colonies was positive for GFP, indicating the success in using kit for reprogramming. Interestingly, one colony, as shown in Figure 3-11, appeared to differentiate into cardiac muscle, since it was spontaneously contracting. Some authors have reported that mouse embryonic fibroblasts have the potential to be directly reprogrammed into cardiac-like cells while bypassing the pluripotent intermediate state (Efe et al., 2011; Ieda et al., 2010; Lalit et al., 2016). Another possible explanation of this phenomenon could have been that the highly heterogenous mouse embryonic fibroblasts contained a distinct subpopulation with cardiac attributes (Singhal et al., 2016; Lalit et al., 2016). It has been suggested that MEFs, within a subpopulation, could be reprogrammed into induced cardiac progenitor cells but then differentiated into contracting cardiomyocyte-like cells in a very short time. However, the detailed mechanisms of reprogramming in this respect have not been established.

When the constitutive lentiviral OKSM vector was applied to the Cre-mediate *Pik3ca*^{H1047R}*/PTEN*$^{del/del}$ MEF cells, there appeared only one colony that morphylogically like an embryoid body (Figure 3-12).

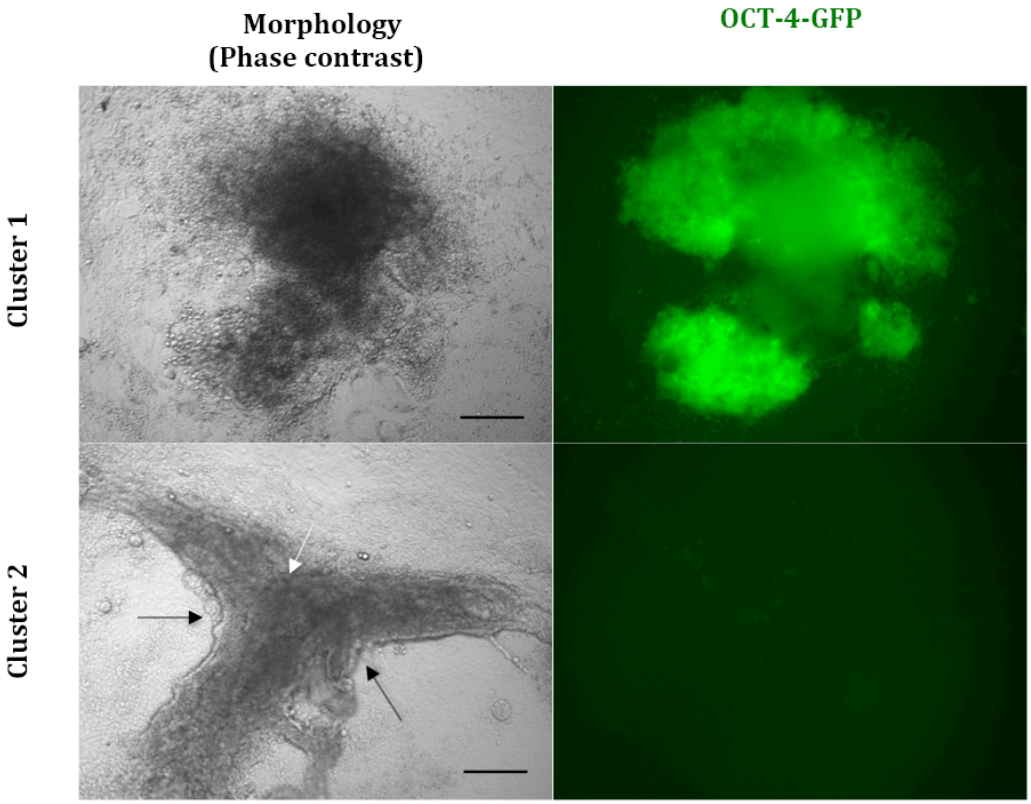

Figure 3-11: The expression of OCT-4 promoter controlled GFP signals in two cell clusters at day 35 during Dox-induced lentiviral expression of the four reprogramming factors. Only colony 1 exhibited mouse ESC-like morphology and showed GFP positive signal. Colony 2 showed spontaneous contractions starting from the original spot (white arrow) to the "wing-like" side (black arrow) and colony 2 was GFP negative. Scale bar is 100µm.

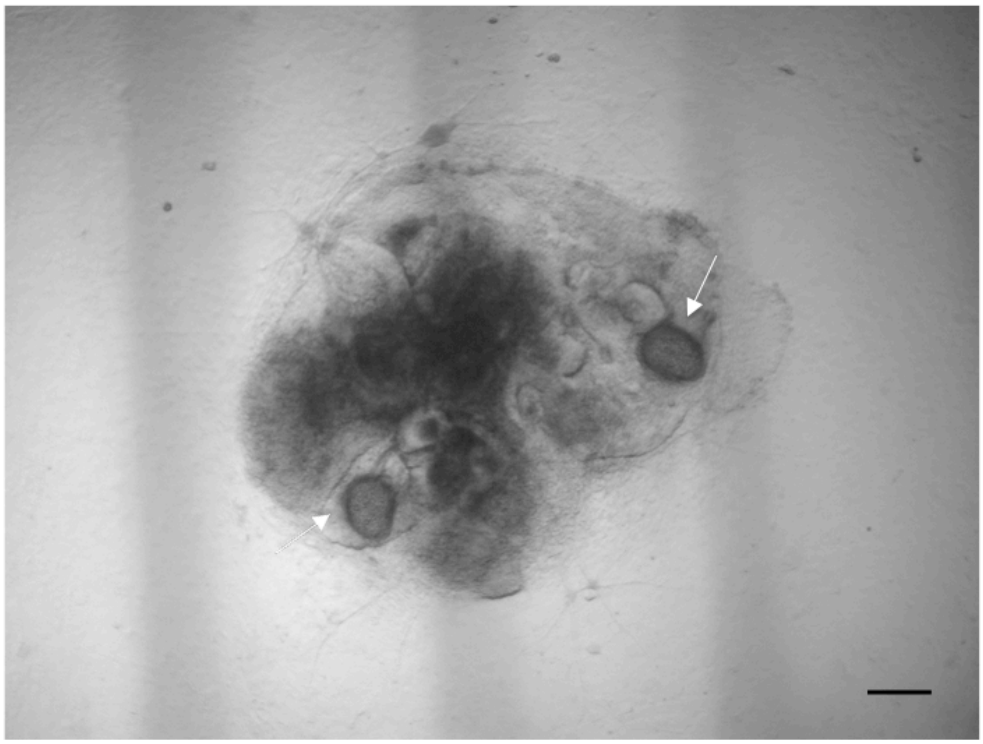

Figure 3-12: Live phase contract imaging (X4) of an unidentified cell cluster generated from Cre-mediated *Pik3ca*^{H1047R}/*PTEN*$^{del/del}$ MEF cells at day 34 during Dox-induced lentiviral expression of the four reprogramming factors. The cell cluster was shown to be like an embryoid body. Cells within two small areas (white arrow) appeared morphologically like mouse ESCs. Scale bar is 100µm.

After 5 different campaigns to reprogram either neural cells or MEFs from the transgenic mice the decision was made to abandon this objective. The reprogramming process was time consuming and there were no signs that iPSCs could be stabilized using either lentiviral system. Each campaign had taken approximately 3 months from the beginning of the culture to evaluation and as there is a practical limit to the time available for PhD study with regret it was necessary to move on with other aspects of the PhD program.

In conclusion, whilst the lentiviral system worked well for reprogramming Oct4-GFP MEFs, a stable iPSC line derived from Cre-mediated transgenic mouse *Pik3ca*^{H1047R}*/PTEN*$^{del/del}$ tissue cells was not established. The reasons for failure of the iPSC reprogramming for this transgenic mouse tissue cells are not fully understood, since iPSC reprogramming is currently a series of undefined stochastic events. However, these results suggested the following: (1) The reprogramming efficiency may be related to the exposure period to OKSM reprogramming factors and the proliferation rate of original cells, but cannot be predicted simply by these two factors, due to the stochastic nature of the process. (2) There appeared to be greater chance of obtaining mature iPSCs from colonies that formed quickly at later stages of reprogramming, but culture conditions for maintenance of these colonies were not established. It would make sense to investigate the culture conditions in more detail. (3) The genetic background of the source cells that are used for iPSC reprogramming may affect the likelihood of success. It is possible that the engineered mouse lines were refractory to reprogramming for as yet unknown reasons.

Chapter 4

Investigation of protein expression and phosphorylation downstream of PI3K activation in neural stem/progenitor cells

4.1 Background

Comprehensive large-scale studies of proteins help to identify disease-associated proteins and to reveal differences in comparative protein expression between samples of interest. In relation to glioblastoma，this approach can reveal expression differences between wild type and mutant cells of interest and has the potential to identify new candidate targets related to the regulation of glioblastoma initiating cells.

Current available proteomics techniques include traditional two-dimensional polyacrylamide gel electrophoresis (2D-electrophoresis) and mass spectrometry (MS) based approaches like isotope-coded affinity tag (ICAT), isobaric tagging for relative and absolute quantitation (iTRAQ) and stable isotope labeling with amino acids in cell culture (SILAC). In this project, we used the SILAC technique to study our cells of interest. SILAC offers several advantages, including a simple and straightforward labeling system which is carried out directly in cell culture, requiring no further chemical or peptide labeling, unlike ICAT (Ong et al., 2002). The label incorporation efficiency of SILAC is theoretically close to 100%, and proteins are generally labeled uniformly which avoids differences in labeling efficiency amongst samples of interest. In addition, the use of SILAC offers the opportunity to quantitate change in non-cysteine containing proteins, which can not be quantitated by the use of ICAT

(Ong et al., 2002). SILAC has been recently applied to studies of protein phosphorylation and protein–protein interaction, which is appropriate in relation to the objective of this thesis, to reveal any specific therapeutic targets in models of glioblastoma initiating cells.

Since mammalian cells are not capable of synthesizing all amino acids, specific amino acids, including leucine, lysine, threonine, methionine etc., that are essential, are usually supplied in the culture medium. The SILAC technique relies on the *in vivo* incorporation of one or more of these essential amino acids, which are isotopically labeled with non-radioactive isotopes, directly on the cell population of interest in the culture system, allowing the differences in protein abundance between samples to be quantified using mass spectrometry (MS).

Figure 4-1 shows the typical flowchart of the SILAC technique. Basically, two cell populations of interest are cultured in two different culture media, one containing the amino acids labeled with non-radioactive isotopes (heavy medium), another containing normal amino acids for cell growth (light medium). The cells grown in the presence of heavy medium incorporate labeled amino acids into their newly synthesized proteins, allowing the proteins containing these labeled isotopes to be identified and quantified by MS.

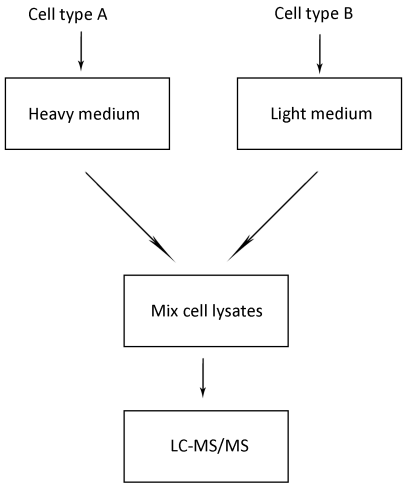

Figure 4-1: Overview of the SILAC flowchart (redrawn with reference to http://www.thermofisher.com)

The aim of the study described in this chapter was to investigate the difference in protein expression levels and possibly phosphorylation levels of proteins between wildtype neural stem cells and mutant *Pik3ca*^{H1047R}/*PTEN*$^{del/del}$ neural stem/progenitor cells. This study focused on analysis of gene expression levels of kinases, also known as kinome profiling, which aimed to reveal differences caused by activation of PI3K/AKT signalling networks in mutant *Pik3ca*^{H1047R}/*PTEN*$^{del/del}$ neural stem/progenitor cells. It is hypothesized that these cells resemble glioblastoma initiating cells and therefore were compared directly with wild type stem/progenitor cells with the same genetic background.

4.2 Materials and Methods

4.2.1 Cell culture

Both control and mutant *Pik3ca*^{H1047R}/*PTEN*$^{del/del}$ neurospheres were cultured using the same conditions as those described in Chapter 2.

4.2.2 Detection of PI3K/AKT pathway-associated phosphoproteins

The PI3K/AKT pathway-associated phosphoproteins of both control and mutant mouse *Pik3ca*^{H1047R}/*PTEN*$^{del/del}$ cell lines were detected using the PathScan® AKT Signalling Antibody Array Kit (Fluorescent Readout) (Cell Signalling Technology, US) according to manufacturer's instruction. Briefly, control and mutant mouse *Pik3ca*^{H1047R}/*PTEN*$^{del/del}$ cells were cultured in *Pik3ca*^{H1047R}/*PTEN*$^{del/del}$ cell culturing medium as described in Chapter 2.2.1.1, but for this experiment supplemented with different concentrations of growth factors (EGF and FGF2), ranging from 0ng/mL to 50ng/mL, for at least three passages at 37 ^{o}C in a 5% CO_2 incubator, in order to allow the cells to adapt to the effects caused by exchanging the concentrations of growth factors from the original 20ng/mL. Then, cells were washed with ice-cold 1X PBS and lysed with ice-cold 1X Cell Lysis Buffer (Cell Signalling Technology, US) which consisted of 20mM Tris-HCl (pH7.5), 150mM NaCl, 1mM disodium EDTA, 1mM EGTA, 1% Triton, 20mM sodium pyrophosphate, 25mM sodium fluoride, 1mM β-glycerophosphate, 1mM Na_3VO_4 and

1µg/mL leupeptin. Cells were micro-centrifuged at maximum speed for 10 minutes at 4 ^{o}C and then each lysate was diluted into Array Dilution Buffer (Cell Signalling Technology, US), which is a proprietary buffer provided by the manufacturer as part of the kit, on ice to make the final protein concentration of 0.5mg/mL. For the assay, 100µL Array blocking buffer (Cell Signalling Technology, US), which is also a proprietary buffer provided by the manufacturer as part of the kit, was added to each well of prepared multi-well slides for 15 minutes at room temperature on an orbital shaker. Then, the buffer in each well was replaced by 75µL of prepared diluted lysate at each condition and incubated overnight at 4 ^{o}C on an orbital shaker. The medium was then exchanged with 100µL 1X Array wash buffer (Cell Signalling Technology, US), which consisted with 2% Tween-20 and 98% 20X PBS, and incubated for 5 minutes at room temperature on an orbital shaker three times to ensure adequate washing. Subsequently the wash buffer was replaced with 75µL 1X Detection antibody cocktail (Cell Signalling Technology, US), to each well and incubated for 1 hour at room temperature on an orbital shaker. The Detection antibody cocktail is a proprietary antibody cocktail provided by the manufacturer as part of the kit, but it contained antibody to work on the phosphorylation site as listed in Table 4-1. Following four washes with 100µL 1X Array wash buffer, each well was incubated with 75µL 1X DyLight 680®-linked Streptavidin (Cell Signalling Technology, US) for 30 minutes at room temperature on an orbital shaker to allow for fluorescence visualization. After another repeat wash with 100µL 1X Array wash buffer and a wash for 10 seconds with 10mL de-ionized water, slides were dried completely. An infrared image of the slide was captured using a LI-COR® Biosciences Odyssey® imaging system and the pixel intensity was quantified by use of the LI-COR® ImageStudio™ Lite analysis software.

4.2.3 Stable isotope labeling by amino acids in cell culture (SILAC)

4.2.3.1 Preliminary assay to determine minimal concentration of amino acids that do not affect cell viability

Due to the high cost of heavy amino acids, the first assay carried out was designed to identify the minimum concentration of amino acids in the medium that would support

cell growth. Both control and mutant mouse *Pik3ca*^{H1047R}*/PTEN*$^{del/del}$ neurospheres were trypsinized and seeded at 2 x 10^4 cells/ml, 100µL/well in light SILAC^{-Arg} (light SILAC media without light Arginine) media, supplemented with different fractions of the total L-Arginine (Light arginine; Sigma-Aldrich, Australia) concentration in normal media, in 96-well ultra-low attachment plates (Sigma-Aldrich, Australia) for 4 days at 37 ^{o}C in a 5% CO_2 incubator. The light SILAC^{-Arg} media consisted of Dulbecco's Modified Eagle Medium/Nutrient Mixture F-12 for SILAC (DMEM/F12 for SILAC; Thermo Scientific, Australia), B-27® supplement minus vitamin A (Thermo Fisher Scientific, Australia), 1000U/mL penicillin G and streptomycin sulfate (Life Technologies, Australia), L-lysine (Sigma-Aldrich, Australia), supplemented with 20ng/mL EGF (Invitrogen, Australia) and 20ng/ml FGF2 (Invitrogen, Australia). Regular serum was not used in SILAC medium as it contained free amino acids that would reduce the labeling efficiency. After 4 days incubation, 20µL CellTiter-Blue® Reagent (Promega, US) was added into each well and incubated for 1 hour at 37 ^{o}C in a 5% CO_2 incubator. The fluorescence was measured using an EnVision® Series Multilabel Plate Reader with excitation filter 530-570nm and emission filter 580-620nm.

4.2.3.2 Preliminary assay to determine arginine to proline conversion

Due to the issue that the labeled arginine will convert metabolically into proline for some cell lines, which would result in the multiple signals in the following MS analysis, another preliminary assay was carried out to reduce the conversion of proline from arginine, thus reducing the unnecessary signals generated from conversion. Both control and mutant mouse *Pik3ca*^{H1047R}*/PTEN*$^{del/del}$ neurospheres were cultured in heavy SILAC^{-Arg} (heavy SILAC media without heavy arginine) media, supplemented with the nominated minimal concentration of $^{13}C^{15}N$ labeled Arginine-HCl (Heavy arginine; Silantes, Germany) in ultra-low attachment plates (Sigma-Aldrich, Australia) for at least 6 doublings at 37 ^{o}C in a 5% CO_2 incubator to ensure the full complete incorporation of labeled amino acids. The heavy SILAC^{-Arg} medium consisted of Dulbecco's Modified Eagle Medium/Nutrient Mixture F-12 for SILAC (DMEM/F12 for SILAC; Thermo Scientific, Australia), B-27® supplement minus vitamin A (Thermo Fisher Scientific,

Australia), 1000U/mL penicillin G and streptomycin sulfate (Life Technologies, Australia), $^{13}C^{15}N$ labeled Lysine-HCl (Heavy Lysine; Silantes, Germany), 20ng/mL EGF (Invitrogen, Australia) and 20 ng/mL FGF2 (Invitrogen, Australia). Once cells were ready, the cells were lysed with urea lysis buffer (pH 8), which consisted of 8M urea (Sigma-Aldrich, Australia), 20mM HEPES (Sigma-Aldrich, Australia), 2.5mM sodium-pyrophosphate (Sigma-Aldrich, Australia), 2.5mM β-glycerol phosphate (Sigma-Aldrich, Australia), 1mM sodium orthovanadate (Sigma-Aldrich, Australia), 1mM EDTA (Sigma-Aldrich, Australia), 1mM TCEP (Sigma-Aldrich, Australia). The cell suspension was micro-centrifuged at maximum speed for 10 minutes at 4 ^{o}C. The cell lysate was collected and transferred to the laboratory of Roger Daly's group at Monash Clayton Campus for analysis by mass spectrometry to determine the incorporation of labeled isotopes as well as to determine the minimum arginine to proline conversion for subsequent SILAC labeling.

4.2.3.3 Protein harvest for SILAC labeling

After determination of the optimum composition of growth medium for cell labeling, control cells and mutant mouse *Pik3ca^{H1047R}/PTEN$^{del/del}$* neurospheres were cultured respectively in light SILAC media and heavy SILAC media with a pre-determined concentration of light arginine and heavy arginine (see below) in ultra-low attachment plates for 4 days at 37 ^{o}C in a 5% CO_2 incubator. The culture program was maintained for approximately 2 months for the culture to expand to a large enough mass to ensure extraction of the target of 20mg total protein for each sample. Once the culture has reached the required volume, the cells were lysed with kinome profiling buffer (pH 7.4), which consisted of 50mM HEPES-NaOH (Sigma-Aldrich, Australia), 150mM NaCl (Sigma-Aldrich, Australia), 0.5% Triton™ X-100 (Sigma-Aldrich, Australia), 1mM Ethylenediaminetetraacetic acid (EDTA; Sigma-Aldrich, Australia), 1mM Ethylene Glycol Tetraacetic acid (EGTA; Santa Cruz Biotechnology, US) and 10µL/mL Halt™ Protease and Phosphatase inhibitor cocktail (ThermoFisher Scientific, Australia) to prevent protein degradation. The cell suspension was micro-centrifuged at maximum speed for 10 minutes at 4 ^{o}C. The cell lysate was then collected and transferred to the laboratory of Roger Daly at the Monash University Clayton Campus for further analysis by mass

spectrometry.

4.2.3.4 Kinome profiling

The kinome profiling analysis was carried out by the laboratory of Roger Daly at the Monash University (Clayton campus). Briefly, equal masses of lysates prepared from light and heavy isotope-labeled samples were mixed and transferred through prepared Econo-Pac columns which were pre-coupled with 200µL of each CTx-0294885, purvalanol B, SU6668 and VI16832 inhibitors to inhibit a broad range of kinases. CTx-0294885 is a novel bisanilino pyrimidine, which was shown to give the largest kinome-enrichment coverage, including all AKT family members when combined with another three kinase inhibitors (Zhang et al., 2013). To wash off any non-binding or non-specific binding proteins, each Econo-Pac column was washed with 7 mL washing buffer A which was constituted of 50mN HEPES-NaOH (pH 7.5), 1M NaCl, 0.5% Triton X-100, 1mM EDTA, 1mM EGTA, 10mM NaF and 0.1mM Na_3VO_4, then washing buffer B which constituted of the same ingredients as washing buffer A, except that 150mM NaCl was used instead of 1M NaCl, then washing buffer C which was constituted of 50mM HEPES, 10mM NaF and 0.1 mM Na_3VO_4. Each wash was applied three times at 4°C before progressing to the next. Kinases were then eluted five times with 1mL of pre-equilibrated buffer C, which constituted of 5mM dithiothreitol (DTT) and 0.5% sodium dodecyl sulfate (SDS). Eluted kinases were centrifuged and stored at -80°C for future use.

4.2.3.5 Sample preparation for mass spectrometry

Sample preparation for mass spectrometry was carried out by Roger Daly's laboratory at the Monash University (Clayton campus). Briefly, samples were twice centrifuged and re-suspended with 100µL of milliQ water. 5 volumes of cold 100% acetone was then added to the sample and incubated overnight at -20°C. Samples were centrifuged at 16000xg for 15 minutes at 4°C and the pellets were rinsed twice with 100% acetone. Samples were then re-suspended with buffer that constituted of 6M guanidine, 50mM

tris HCl (pH 8), 2.5mM β–glycerophosphate, 5mM sodium orthovanadate, 5mM K_2HPO_4 and 5mM sodium fluoride (NaF) at room temperature for 10 minutes. Samples were reduced with 5µL of 100mM tris(2-carboxyethyl)phosphine (TCEP) at 37°C for one hour, followed by alkylation with 2.1µL of 500mM iodoacetamine and chloroacetamide at room temperature for one hour in the dark. Samples were adjusted with 50mM ammonium bicarbonate solution to dilute quinidine concentration below 0.6M. Trypsin was added according to the mass of protein available in a 1:50 ratio by weight and the samples were incubated overnight at 37°C. Samples were finally adjusted with 80% trifluoroacetic acid (TFA) to give pH value of 2-3, prior to be processed by mass spectrometry.

4.2.3.6 Mass spectrometry analysis

Samples were analyzed using an UltiMate™ 3000 RSLCnano LC system (ThermoFisher Scientific) coupled to an LTQ Orbitrap XL™ mass spectrometer (ThermoFisher Scientific). 1µg of sample peptides was trapped on a 2cm long pre-column and separated on a 50cm analytical column (Dionex, Sunnyvale, CA). Peptides were eluted using a two-hour linear gradient of 80% acetonitrile/0.1% formic acid (FA) gradient flowing at 250nL per minute using a mobile phase gradient of 2.5-42.5% acetonitrile. The eluting peptides were interrogated with an Orbitrap mass spectrometer in data dependent acquisition for the top 20 ions. Mass spectra were processed with MaxQuant software (version 1.5.8.3) against the UniPort with a setting of mouse database, common contaminants and reverse sequences. A ratio of heavy to light required a fold change of 1.5 for differential expression. Functional annotation was conducted using Database for Annotation, Visualization and Integrated Discovery (DAVID) software and STRING software.

4.2.3.7 Gene ontology analysis and protein interaction network analysis

Gene ontology analysis and protein interaction network analysis was conducted using DAVID software and STRING software. Briefly, a total of 1447 protein were identified and calculated for the ratio in the heavy medium and light medium respectively. 127 proteins with the ratio of concentration in heavy medium over light medium more

than 1 were identified as over-expressed in mutant cells, whereas 158 proteins with ratio of concentration in light medium over heavy medium more than 1 were identified as over-expressed in control cells. These over expressed proteins were analysed by software for mapping the gene ontology term and protein interaction network.

4.2.4 Statistical analysis

All data were expressed as mean ±S.E.M and the data were analyzed with ANOVA to determine statistical significance. Results were considered significant when $p<0.05$. All analysis was performed by use of GraphPad Prism, version 5 for Mac.

4.3 Results and Discussion

4.3.1 Mutant *Pik3ca*^{H1047R}/*PTEN*$^{del/del}$ cells exhibit enhanced PI3K downstream activity

In order to study the differences in phosphorylation of proteins related to PI3K signalling, between control and mutant *Pik3ca*^{H1047R}/*PTEN*$^{del/del}$ cells, a fluorescent-based AKT signalling antibody array was acquired. This array was designed for the simultaneous detection and quantitation of 16 phosphorylated proteins associated with AKT signalling network (Table 4-1).

Figure 4-2 indicates that mutant *Pik3ca*^{H1047R}/*PTEN*$^{del/del}$ cells had higher phosphorylation levels of several proteins associated with AKT, the largest differences being in AKT itself and GSK-3β when compared with levels present in the wild-type NPSCs. The expression of phosphorylated PTEN in control cells was significantly higher, approximately 13 fold higher, which was expected as a result of the deletion of PTEN in the mutant cells. Overall, the array results were consistent with the expectation that mutant cells had higher activation of proteins downstream of PI3K. Ideally, it will be useful to validate these results by western blotting.

Of the 16 phosphorylated proteins, it is interesting to observe that phosphorylated GSK-3β is significantly higher in the mutant cells. GSK-3β was found to be consistently over-expressed and over-phosphorylated in GBM in comparison with normal brain tissues (Miyashita et al., 2009; Li et al., 2010). Its high expression is likely to be related to the self-renewal capability of mutant *Pik3ca*^{H1047R}/*PTEN*$^{del/del}$ cells. GSK-3β is a component of the Wnt pathway that is critical in maintenance of self-renewal ability of normal NPSCs (Shakoori et al., 2005). Serine 9 of GSK-3β is a target of AKT and this phosphorylation inhibits the activity of GSK-3β which is then no longer able to phosphorylate β-catenin (Shakoori et al., 2005). This allows β-catenin to enter the nucleus and activate Wnt target genes (Shakoori et al., 2005).

Table 4-1: Target map of the PathScan AKT signalling antibody array kit

	Target	Phosphorylation Sites
1	Positive Control	N/A
2	Negative Control	N/A
3	AKT	Thr308
4	AKT	Ser473
5	S6 Ribosomal Protein	Ser235/236
6	AMPKα	Thr172
7	PRAS40	Thr246
8	mTOR	Ser2481
9	GSK-3α	Ser21
10	GSK-3β	Ser9
11	p70 S6 Kinase	Thr389
12	p70 S6 Kinase	Thr421/Ser424
13	Bad	Ser112
14	RSK1	Ser380
15	PTEN	Ser380
16	PDK1	Ser241
17	Erk1/2	Thr202/Tyr204
18	4E-BP1	Thr37/46

A.

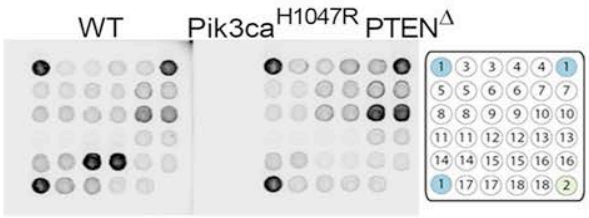

B.

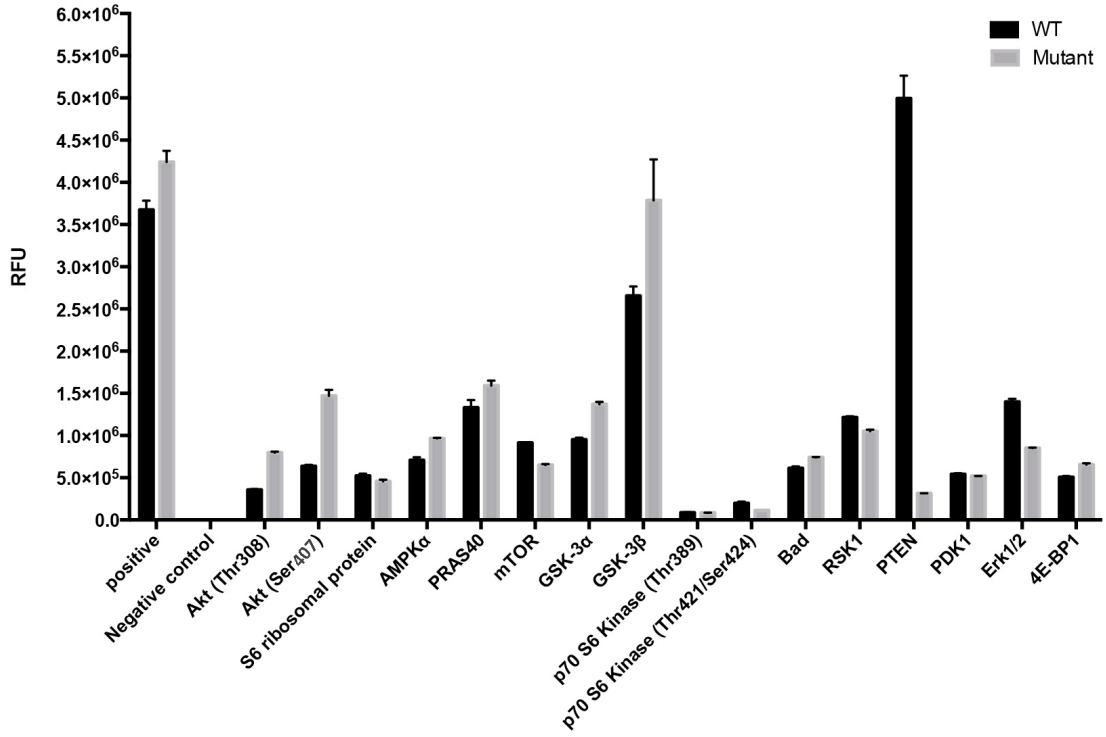

Figure 4-2: Different phosphorylation activities between control and mutant *Pik3ca^{H1047R}/PTEN$^{del/del}$* cells using PathScan® AKT Signalling Antibody Array. The cells were cultured in medium containing 20ng/mL of EGF and 20ng/mL of FGF2. (A) Image of chemiluminescent probing acquired using LI-COR® Biosciences Odyssy® imaging system. (B) Quantitative analysis of spots in (A) (Error bars are plotted and calculated based on mean±standard deviation, n=2).

4.3.2 Effect of different concentrations of growth factors on phosphorylation of proteins associated with PI3K/AKT signalling

As PI3K/AKT signalling is usually activated by upstream growth factors, such as EGF and FGF2, and these growth factors were used in the culture medium, it was important to consider how the growth medium influenced signalling experiments. To investigate this, a series of different concentrations of growth factors on the PI3K/AKT signalling network were investigated using the antibody array (0, 1, 20 and 50ng/ml of each growth factor). It was important to ensure that the PI3K signalling in the cultured cells was not over-stimulated. Ideally, activation by growth factors would be kept to a minimum to ensure that the fundamental differences between control and mutant *Pik3ca*^{H1047R}/*PTEN*$^{del/del}$ cells could be compared.

As previously discussed in Chapter 2 and Chapter 3, the minimum concentration of EGF and FGF2 required in the culture medium to maintain the cells was determined to be 1ng/mL. For general maintenance, the concentration of both growth factors was usually 20ng/mL as suggested by the literature. In fact, higher concentrations of 50ng/mL have been preferred by the Mantamadiotis lab at The University of Melbourne to ensure robust cell culture of *Pik3ca*^{H1047R}/*PTEN*$^{del/del}$ cells, hence we tested 1, 20 and 50 ng/mL using the antibody array. In summary, the results (Figure 4-3) suggested that it would be acceptable to use 20ng/mL of both EGF and FGF2 for preparation of cells for SILAC experiments. The data for the mutant cells indicated that there was little or no difference in levels of phosphoproteins in the presence or absence of EGF and FGF2. For the control cells there were some differences in phosphoprotein levels as the growth factor concentration was raised from 1ng/mL to 20ng/mL. AKT, mTOR, PTEN, RSK1 and Erk1/2 phosphorylation levels increased. Several other proteins were not differentially phosphorylated, including the GSK3 proteins (Figure 4-3 panel A). The observation that the control cells were activated to some extent by EGF and FGF2, but that the mutant cells were not activated, correlated with the expectation that the mutant cells had constitutively activated PI3K signalling. This contributed to their increased clonal capacity. It was concluded that preparing the

control cells in 20ng/mL growth factors was not ideal. It would lead to a level of activation over and above their basal levels. However a compromise had to be made to allow the growth of a large population of control cells. It was felt that to attempt to expand the control cells culture at 1ng/ml would be risky, could be a slow process, and may lead to some cell death. Colonies of control cells did form at 1ng/ml but large-scale expansion may have been unsuccessful.

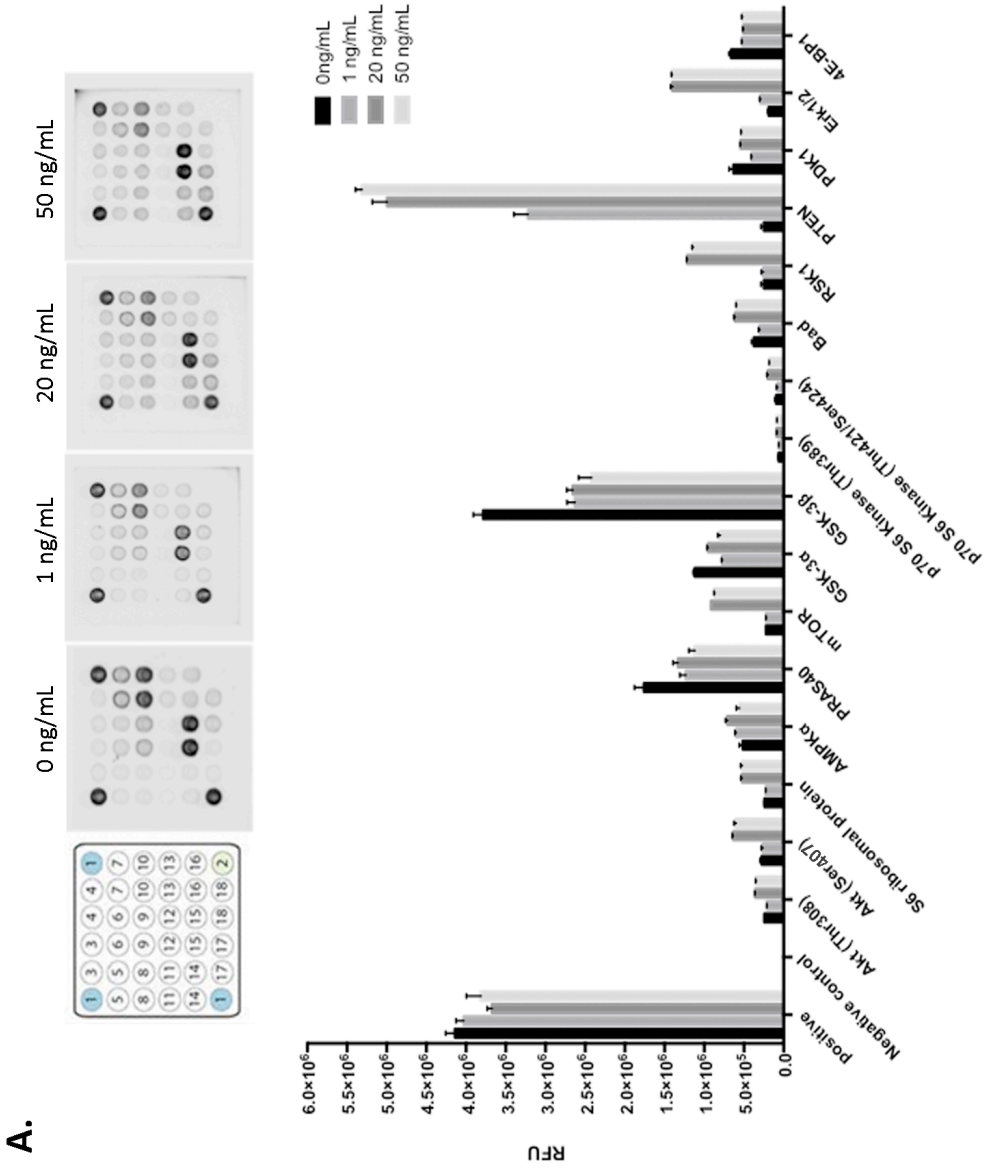
A.
0 ng/mL
1 ng/mL
20 ng/mL
50 ng/mL
0ng/mL
1 ng/mL
20 ng/mL
50 ng/mL
RFU
6.0×10^6
5.5×10^6
5.0×10^6
4.5×10^6
4.0×10^6
3.5×10^6
3.0×10^6
2.5×10^6
2.0×10^6
1.5×10^6
1.0×10^6
5.0×10^5
0.0
positive
Negative control
Akt (Thr308)
Akt (Ser473)
S6 ribosomal protein
AMPKα
PRAS40
mTOR
GSK-3α
GSK-3β
p70 S6 Kinase (Thr389)
p70 S6 Kinase (Thr421/Ser424)
Bad
RSK1
PTEN
PDK1
Erk1/2
4E-BP1

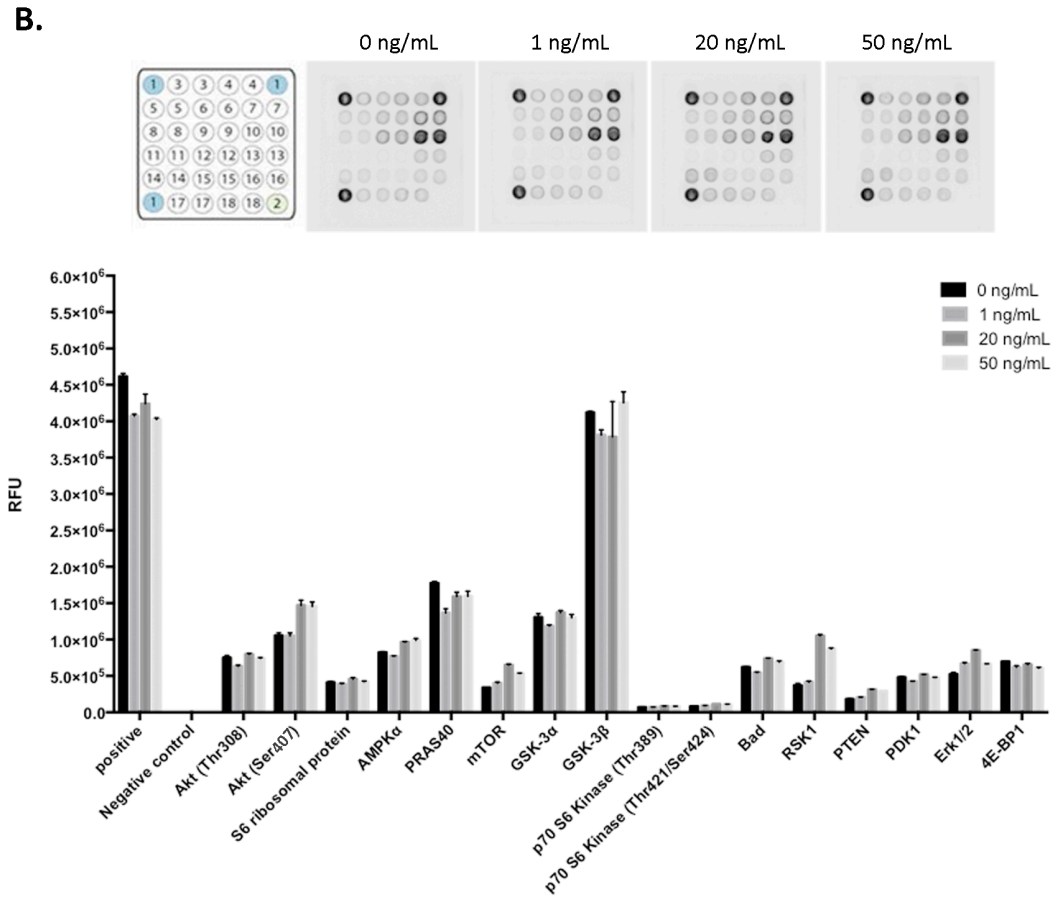

Figure 4-3: Phosphorylation activities affected by the supplied growth factors concentration between control and mutant *Pik3ca*^{H1047R}*/PTEN*$^{del/del}$ cells using PathScan® AKT Signalling Antibody Array. The cells were cultured in medium containing both EGF and FGF2 at the same concentrations in each case, 0ng/mL, 1ng/mL, 20ng/mL and 50ng/mL respectively. (A) Image of chemiluminescent probing and quantitative analysis of spots for control cells (n=2). (B) Image of chemiluminescent probing and quantitative analysis of spots for mutant cells (Error bars are plotted and calculated based on mean±standard deviation, n=2).

4.3.3 Efficient incorporation of SILAC isotopes into control and mutant Pik3caH1047R/PTENdel/del neural stem/progenitor cells

The lowest arginine (Arg) concentration needed for the cells to grow healthily and the minimal Arg to proline (Pro) conversion levels were determined prior to the preparation of cell lysate for subsequent SILAC labeling. This was carried out to minimize the cost of incubating cells in media containing the expensive heavy arginine and lysine reagents.

As shown in Figure 4-4, the growth rate of mutant *Pik3ca*^{H1047R}/*PTEN*$^{del/del}$ cells decreased considerably when cells were grown in concentrations of arginine less than 1/16 of the normal concentration in culture medium. Subsequently cells were cultured using 1/4 and 1/8 of the usual concentration of arginine, as heavy arginine, and samples were analyzed by Roger Daly's lab (Monash University, Clayton campus) to determine Arg to Pro conversion. All labeling samples tested were efficiently incorporated and the labeling efficiency was determined to be greater than 95%. Control cells were observed to exhibit delayed proliferation after prolonged incubation in the heavy arginine and lysine SILAC medium, which was a further indication that the control cells were more sensitive and less likely to be expanded under stressful conditions. It was possible to label control cells with heavy amino acids but it made more sense to label the mutant cells, given their more robust growth (Figure 4-4).

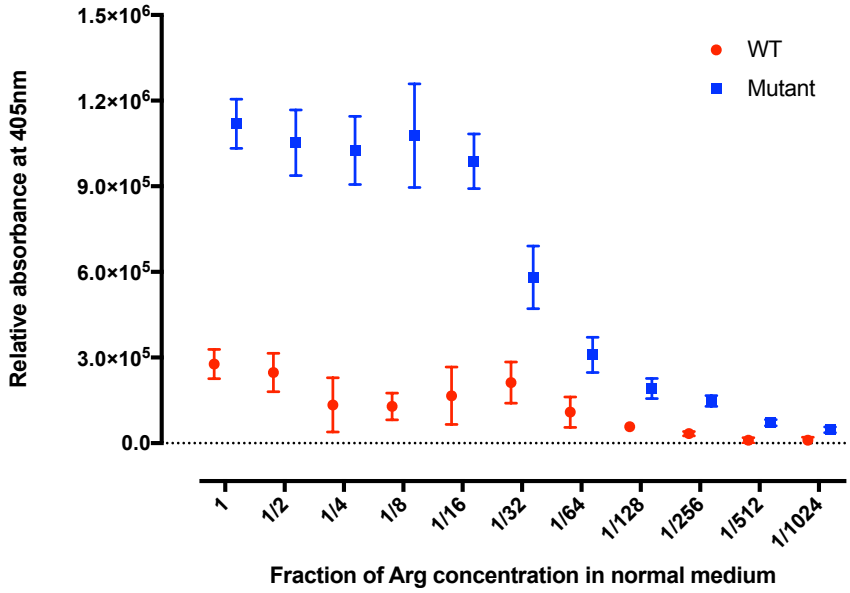

Figure 4-4: Optimization of arginine at different concentration in control and mutant *Pik3ca*^{H1047R}/*PTEN*$^{del/del}$ cells. Both cell lines were cultured in SILAC specific culture medium supplemented with different fractions of arginine concentration in the normal culture medium. After 4 days the cell growth was compared using Cell Titer Blue. The results show a dramatic decrease of cell viability when cells received a fraction of arginine concentration below 1/16 for mutant and 1/32 for control cells respectively. Results are expressed as mean ± S.E.M. with n=6 per group.

4.3.4 Over-expression of ten kinases in mutant *Pik3ca^{H1047R}/PTEN$^{del/del}$* cells

Kinome profiling using mass spectrometry conducted by Roger Daly's proteomics lab (Monash University, Clayton campus) identified ten kinases that were significantly over-expressed in the mutant *Pik3ca^{H1047R}/PTEN$^{del/del}$* cells (Figure 4-5), including Focal adhesion kinase 1(FAK1), Never-in Mitosis A related kinase 1 (NEK1), Rho associated coiled-coil containing protein kinase 1 (ROCK1), Insulin receptor (INSR), cyclin dependent kinase 2 and 9 (CDK2, CDK9), dual specificity mitogen-activated protein kinase kinase 5 and 6 (MP2K5, MP2K6), calcium/calmodulin-dependent protein kinase kinase 1 (KKCC1) and calcium/calmodulin-dependent protein kinase type 1-like (KCC1A). Of particular interest are FAK1, NEK1 and ROCK1 in relation to published glioblastoma research, as discussed below. The other upregulated kinases have not been associated with glioblastoma in the literature and thus may represent interesting targets for further investigation.

The overexpression of FAK1 may indicate a negative feedback loop that effectively reduces the impact caused by the loss of PTEN on PI3 kinase activity, as PTEN can directly dephosphorylate tyrosine-phosphorylated FAK (You et al., 2015). FAK has previously been reported to be elevated in glioblastoma cells and anaplastic astrocytoma cells rather than other brain cells (Natarajan et al., 2003).

NEK1, a serine/threonine kinase, is involved in DNA damage response and proper checkpoint activation of the cell cycle (Chen Y et al., 2011). Overexpression of NEK1 in our mutant glioblastoma initiating-like cells might implicate a possible underlying mechanism of chemo-resistance of mutant NPSCs. Chen et al. (2014) suggested a possible relationship between raised NEK1 levels and cellular tolerance to DNA-damaging agents. Although NEK1 was found to be frequently over-expressed in human Glioma cells (Zhu et al., 2016), there does not seem to be any published studies on glioblastoma initiating cells. Thus, future studies could be initiated to evaluate potential NEK1 inhibitors and the effect of siRNA knockdown of NEK1 expression. An

NEK1 inhibitor could be an adjuvant therapy to support the use of currently available cytotoxic agents to improve their effects on glioblastoma initiating cells.

Apart from FAK 1 and NEK1, the high expression of ROCK1 in the mutant glioblastoma initiating-like cells was worthy of attention. Accumulating evidence in recent years has revealed a potential key role of ROCK1 in cancer progression including breast cancer, lung cancer, ovarian cancer and gliomas (Wei L et al., 2016). High expression levels of ROCK1 have been found in glioblastoma cells in comparison to normal tissue cells, and the expression level of ROCK1 was an indicator of malignancy of glioma (Zhou et al., 2016). Moreover, one interesting study (Inaba et al., 2010) suggested a role of ROCK1 in relation to the cellular sensitivity to cytotoxic drugs. Inhibition by ROCK1 inhibitor alone had no effect on cell proliferation, but ROCK1 inhibition combined with other cell cycle agents was effective (Inaba et al., 2010). Although ROCK1 has been well characterized and well studied in the past few years, the role of ROCK1 in glioblastoma initiating cells, and the potential therapeutic value in treating glioblastoma with ROCK1 inhibitors is worthy of further discovery and development.

(A)

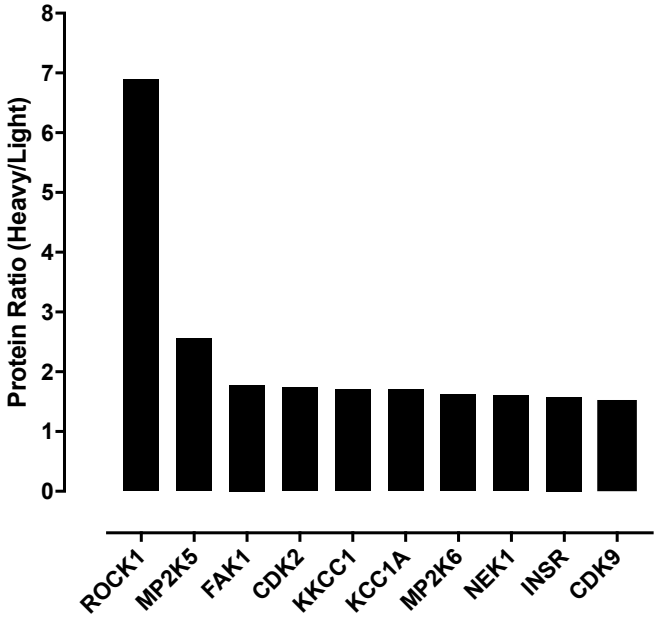

(B)

Accession	Protein	Protein Ratio (H/L) [a]
P70335	ROCK1	6.89
Q9WVS7	MP2K5	2.56
P34152	FAK1	1.78
P97377	CDK2	1.74
Q8VBY2	KKCC1	1.71
Q91YS8	KCC1A	1.71
P70236	MP2K6	1.62
P51954	NEK1	1.60
P15208	INSR	1.58
Q99J95	CDK9	1.53

a: indicate relative protein abundances from heavy and light medium

Figure 4-5: Kinome profiling of over-expressed kinases in heavy-labeled mutant *Pik3ca*^{H1047R}*/PTEN*$^{del/del}$ cells. (A) Column bar indicating relative SILAC ratio of ten identified kinases. (B) Table list of information of ten identified kinases. Protein ratio (H/L) was calculated using MaxQuant software.

4.3.5 Glioblastoma initiating-like cells exhibit over-expressed proteins of the proteasome system

Gene ontology analysis (Figure 4-6) and protein interaction network analysis (Figure 4-7 and Figure 4-8) were conducted to characterize the molecular functions of enriched proteins. Most proteins were identified to be associated with the proteasome complex and tRNA synthesis in mutant cells. This may provide justification to target the proteasome system of glioblastoma initiating-like cells as a possible strategy for therapeutic intervention.

A recent publication from Lee et al. (2016) explored a targetable class of proteins, the ubiquitin-specific proteases (USPs), which are associated with stem cell maintenance in GBM. USP1 was specifically identified to be over-expressed in GBM and even in glioblastoma initiating cells relative to the normal brain tissues (Lee et al., 2016). Inhibition of USP1 was reported to attenuate the proliferation of GICs, as well as promote radiosensitivity of GBM cells to therapeutic treatments (Lee et al., 2016). Proteasome inhibitor, bortezomib (BTZ) also showed some effects on inducing cell apoptosis of GBM cells (Styczynski et al., 2006). However, bortezomib failed in a phase II study to treat relapsed GBM patients (Friday et al., 2012). However, the role of the proteasome system in GBM, especially in glioblastoma initiating cells is worthy of further research, and the combination of a proteasome inhibitor with other agents in GBM treatment would be a particularly worthy of investigation.

In summary, mutant *Pik3ca*^{H1047R}/*PTEN*$^{del/del}$ cells, which resemble GICs in this case, exhibited more PI3K/AKT signalling activities than the wild-type NPSCs. Kinome profiling identified at least ten over-expressed kinases that may have potential therapeutic value as targets for GBM drug development. FAK1, NEK1 and ROCK1 are particularly interesting as there are reports of their association with GBM. In addition, gene ontology analysis, together with protein interaction network analysis revealed that the proteasome system might be an important target to disrupt the functions of glioblastoma initiating cells.

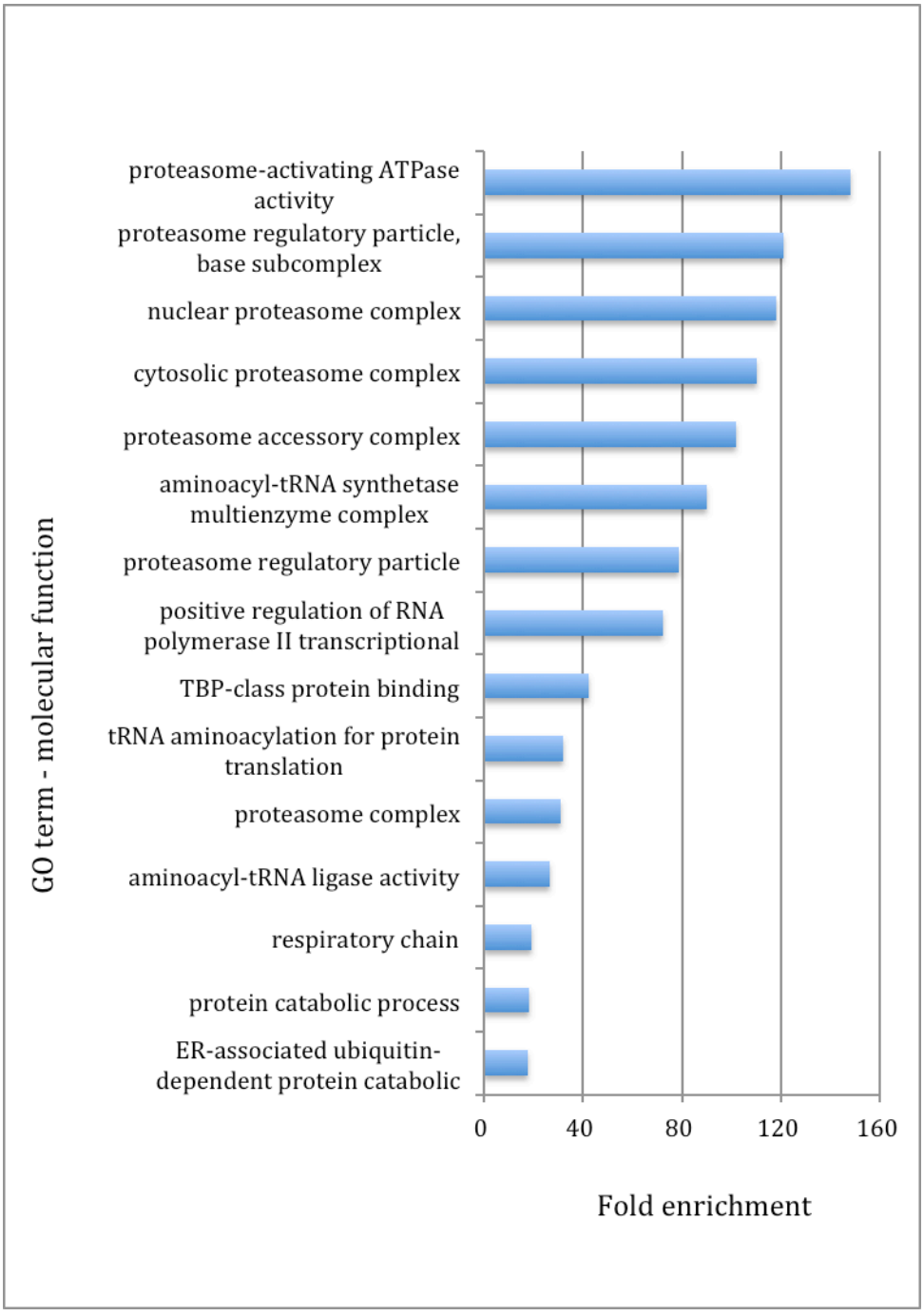

Figure 4-6: Gene ontology (GO) classification of the top 15 molecular functions of overexpressed kinases identified in mutant *Pik3ca*^{H1047R}/*PTEN*$^{del/del}$ cells.

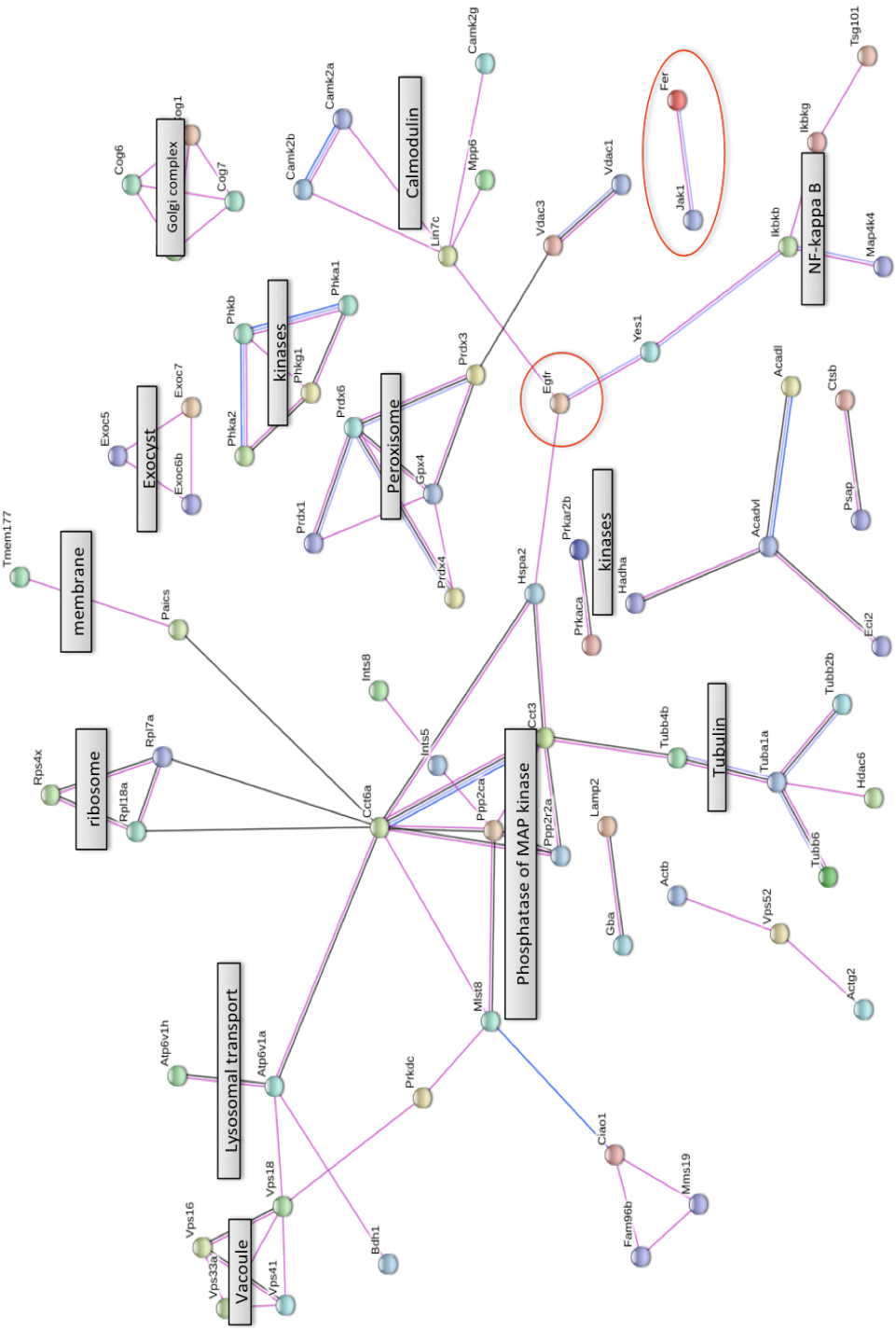

Figure 4-7: Protein interaction network analysis of over-expressed proteins in control NPSCs

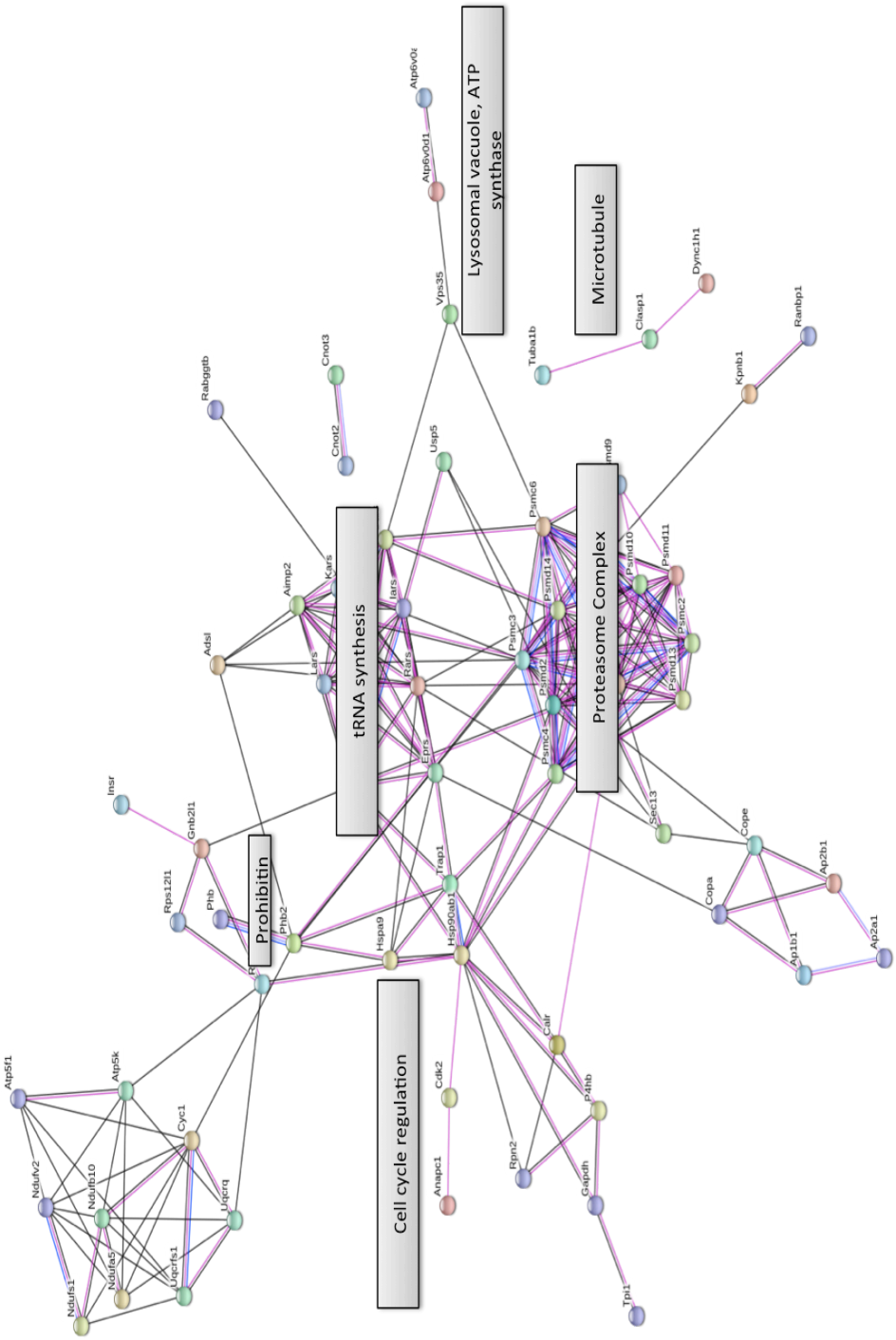

Figure 4-8: Protein interaction network analysis of over-expressed proteins in mutant *Pik3ca*^{H1047R}*/PTEN*$^{del/del}$ cells

Chapter 5

Biological activity of novel SANT-1 analogues as inhibitors of Hedgehog signalling

5.1 Background

Hedgehog (Hh) signalling plays very important roles in cell proliferation, cell differentiation, regulation of organ patterning during embryonic development, and regulation of stem cell self-renewal in adult tissues. Hedgehog signalling has been implicated as a major factor in specific forms of cancer that are known to be hedgehog dependent, including basal cell carcinoma (Epstein et al., 2008) and some medulloblastomas (Berman et al., 2002). There is also increasing interest in the influence of hedgehog signalling on the progression of a variety of other solid cancers, including pancreatic cancer (Thayer et al., 2003), small-cell lung cancer (Watkins et al., 2003), prostate cancer (Berman et al., 2004), breast cancer (Cui et al., 2010) and glioma (Bar et al., 2007). These tumors frequently show abnormal activation or mutation of components of the Hh pathway. Thus, antagonists targeting components of the Hh pathway, especially smoothened (SMO), have considerable potential in cancer therapy.

In relation to brain tumors, some researchers (Dahmane et al., 2001) have reported consistent expression of Hh signalling activities in primary brain tumors and some GBM derived cell lines. Recent research (Bar et al., 2007) found that blockade of the Hedgehog pathway following standard radiation treatment on glioblastoma multiforme (GBM) neurospheres, could inhibit the growth and formation of radio-resistant glioma neuropheres. In addition, research from Cooper's group

(Ehtesham et al., 2007) revealed a ligand-dependent regulatory role of Hh pathway on glioma progenitor cells, within grade II and grade III gliomas, but not within GBM. The development of drug candidates that inhibit Hh signalling has generated considerable commercial interest and there are several clinical trials in progress. Inhibition of SMO activity may be a potential approach for the treatment of GBM, given that glioblastoma initiating cells resemble neural stem cells, because in some tumours Hedgehog signalling appears to be necessary for survival and proliferation of repopulating cancer stem cells after a course of chemotherapy.

The Hh signalling pathway was first reported in Drosophila by Nusslein-Volhard and Wieschaus' group (Nusslein-Volhard C and Wieschaus E, 1980) in 1980 and it is now known that the functional mechanisms of its signalling cascade are evolutionarily conserved from Drosophila to mammals (Krauss et al., 1993). Molecular studies have identified the main protein components of Hh signalling pathway in mammalian cells as Hedgehog interacting protein (HHIP), Patched (PTCH), Smoothened (SMO), Suppressor of Fused (SUFU) and Glioma-associated oncogene homologs (GLI).

In mammalian cells, the initial activation of Hh signalling pathway occurs specifically in the primary cilia (Figure 1-6). The primary cilia are non-motile, microtubule-rich surface projections that have been identified as essential structural features in activation of Hh signalling pathway (Wilson et al., 2009). PTCH is a twelve-transmembrane protein receptor integral within the plasma membrane that has been observed to localize and enrich in and around the primary cilia (Rohatgi et al., 2007). PTCH acts as a receptor for Hh ligand binding and regulates the translocation and activation of Smoothened (SMO) (Rohatgi et al., 2007). SMO is a seven-pass transmembrane protein (Wang et al., 2013) which is structurally similar to members of the G protein coupled receptor (GPCR) superfamily, and has recently been classified as a member of the Frizzled family (class F) of GPCR-like receptors (Ayers et al., 2010). Glioma-associated oncogene homologs (GLI) consist of three proteins, Gli1, Gli2 and Gli3. Gli1 acts as a transcriptional activator due to its C-terminal activation domain, whereas Gli2 and Gli3 act as repressors in regulation of Hh signalling.

The detailed mechanisms of Hh signalling are still somewhat unclear. Briefly speaking, in the absence of Hh ligands, PTCH inhibits the activation of SMO by a poorly understood mechanism. This enables the Gli protein complex, Gli2/3, to undergo proteolytic cleavage into its repressor forms, resulting in failure in transcription of Hh target genes. In the presence of Hh ligands, the Hh ligands induce a conformational change in PTCH that relieves the repression of SMO, allowing SMO to transport from cytoplasm to primary cilia for its activation. The activation of SMO requires a conformational switch from an inactive closed conformation to active open conformation, which requires Hh-activation-induced neutralization to break the electrostatic interactions in the C-terminal domain within SMO dimers (Zhao et al., 2007). The activated open conformation of SMO allows increased levels of SUFU-Gli2/Gli3 transport within the primary cilia, where the dissociated Gli2/Gli3 complex can bypass proteolytic cleavage, entering into the nucleus and binding to the targeting gene promoter, thus initiating the expression of target genes (Kim et al., 2009; Wen et al., 2010).

Due to the central role of SMO in Hh signalling and its tractability as a target for small molecule ligands, many Hh pathway inhibitors targeted to SMO have been investigated and developed. Cyclopamine, identified from the plant *Veratrum californicum*, was the first reported natural ligand, which inhibits SMO by direct binding to the heptahelical transmembrane domain of SMO receptor (Chen et al., 2002). However, cyclopamine was determined to be unsuitable for clinical use due to non-specific toxicity, short elimination half-life and poor bioavailability (Lipinski et al., 2008).

Several synthetic SMO inhibitors have entered clinical development for the treatment of Hh-mediated cancers and products have been approved for human use over the past five years. The oral SMO inhibitor LDE-225 was in Phase I in clinical trial (Rodon et al., 2014). GDC-0449 was approved by the US Food and Drug Administration (FDA) in 2012 for the treatment of metastatic or locally advanced basal cell carcinoma (BCC) (Fellner C, 2012). An orally available Hedgehog inhibitor IPI-926, derived from cyclopamine, was in Phase II clinical trial for treatment of Myelofibrosis (Sasaki et al.,

2016) and Phase I trial for treatment of BCC (Jimeno A et al., 2013). The potent and orally bioavailable inhibitor PF-04449913 was developed to treat acute myeloid leukemia and is in clinical development (Munchhof et al., 2012).

Although the current inhibitors appear to be effective in treating some solid tumors, there is still much to be learned about SMO inhibitors and there is room for new compounds to be evaluated against different forms of malignant disease. In this study, an assay for SMO inhibition was developed to allow evaluation of some novel structural analogues of SANT-1. SANT-1, is a potent inhibitor of SMO, prevents the accumulation of cytoplasmic SMO to the primary cilia (Rohatgi et al., 2008), and drew our attention as a potential lead compound. With this in mind, a collaboration was initiated with medicinal chemists at Monash Institute of Pharmaceutical Science (MIPS), led by Professor Peter Scammells, which aimed to synthesize analogues of SANT-1 and evaluate them using cell culture assays. A number of these compounds are described in this chapter.

SMO activation and inhibition can be evaluated using cell culture models. The most commonly used assays are induction of alkaline phosphatase (AP) expression and a Gli-luciferase reporter gene assay. Both of these assays in principle are suitable for compound screening of small molecules that could potentially target the Hh pathway. The AP assay measures expression of AP produced during Hh-induced differentiation of the mouse mesoderm fibroblast C3H10T1/2 cell line. During differentiation, the fibroblast-like cells differentiate into osteoblast-like cells that are regulated by the activation of the Hh pathway. This results in elevation of AP levels that can be assayed using the well-known ρ-nitrophenyl phosphate (PNPP) substrate, to yield a water-soluble yellow product that absorbs light at 405nm (Tremblay et al., 2009). The Gli-luciferase reporter gene assay is based on the measurement of luciferase activity, the expression of which is under the control of a Gli-responsive element. Once Hh signalling is activated, PTCH releases its inhibition on SMO, allowing SMO to activate the Gli transcription factors, thus resulting in Gli-responsive expression of luciferase. The level of the luciferase expression usually corresponds to the level of Hh signalling activation. The Gli-luciferase gene reporter assay, according to the literature, is more

sentitive than using the AP assay. (Mahindroo et al., 2009)

In this study, efficacy testing systems for studying newly synthesized SANT-1 derived small molecules were compared and optimized. A total of 26 newly synthesized SANT-1 analogues were screened for their potential anticancer efficacy. Later, the IC_{50} of pre-selected small molecules were determined as appropriate.

5.2 materials and methods

5.2.1 Cell culture

The mouse NIH/3T3 (ATCC® CRL-1658™) embryonic fibroblast cell line was purchased from the American Type Culture Collection (ATCC). Mouse C3H10T1/2 embryonic fibroblast cell line and 293-ShhN-pIND cell lines were obtained from Prof. Neil Watkins' Lab in Monash Institute of Medical Research (MIMR) respectively. These cells were cultured in mouse MEF growth medium, which contains Dulbecco's Modified Essential Medium (DMEM; Invitrogen, Australia), 10% fetal bovine serum (FBS; Invitrogen, Australia) and 1000U/mL penicillin G and streptomycin sulfate (Life Technologies, Australia). Cultures were maintained at 37 ^{o}C in a 5% CO_2 incubator and passaged when cells were at 80% to 90% confluency.

5.2.2 Preparation of compounds

Novel synthesized SANT-1 analogues were obtained from Professor Peter Scammells' Laboratory in the Department of Medical Chemistry in MIPS. SANT-1 was purchased from TOCRIS. Smoothened agonist, SAG, was purchased from Merck Millipore. The recombinant mouse sonic Hedgehog/Shh-C25II N-Terminus, or so-called super Shh, was purchased from R&D Systems and was prepared by dissolving the protein in sterile PBS containing 0.1% bovine serum albumin. All other compounds were prepared by dissolving the weighed compounds into dimethyl sulfoxide (DMSO; Sigma, Australia) to make 25mM solutions as stock and stored at -20°C freezer until use.

5.2.3 Preparation of conditioned medium containing active Shh

The conditioned medium containing active Shh (Shh conditioned medium), used as positive control, was prepared by growing 293-ShhN-pIND cells in mouse MEF growth medium with 400µg/mL Geneticin® Selective Antibiotic (G418 sulfate) (G418; Thermo Fisher Scientific, Australia) for one week at 37 ^{o}C in a 5% CO_2 incubator. After one week, the growth medium was removed and exchanged with low serum DMEM growth medium, in which Dulbecco's Modified Essential Medium (DMEM; Invitrogen, Australia) was supplemented with 2% fetal bovine serum (FBS; Invitrogen, Australia) and 1000U/mL penicillin G and streptomycin sulfate (Life Technologies, Australia). After three days incubation, the conditioned medium containing active Shh was collected and filtered through a 0.22µM filter and stored at 4°C for future use.

5.2.4 Gli-luciferase reporter gene assay

5.2.4.1 Establishing stable cell lines containing Gli reporter gene

The stable cell lines containing Gli reporter gene were established by using Cignal Lenti Gli Reporter assay kit (QIAGEN, Australia) according to manufacturer's instruction. Briefly, mouse NIH/3T3 or mouse C3H10T1/2 embryonic fibroblast cells were seeded into 24-well plate at 1x10^{4}cells/cm^2 in MEF growth media and the seeded cells were incubated overnight at 37°C in a 5% CO_2 incubator. The media was replaced on the following day with MEF complete growth media, which contains Dulbecco's Modified Essential Medium (DMEM; Invitrogen, Australia), 10% fetal bovine serum (FBS; Invitrogen, Australia), 0.1mM Gibco® MEM non-essential amino acids (NEAA; Invitrogen, Australia) and 1mM sodium pyruvate (Invitrogen, Australia) without any antibiotics. Then, 50µl of Cignal™ lentiviral particles and 8µg/ml SureENTRY™ Transduction Reagent was added into the media and the cell incubated overnight at 37°C in a 5% CO_2 incubator. The medium containing Cignal™ lentiviral particles was removed the next day and the cells were incubated in fresh MEF complete growth media with 1000U/mL penicillin G and streptomycin sulfate (Life Technologies, Australia) overnight. Stable antibiotic-resistant cell lines were

identified following incubation with 3µg/mL puromycin (InvivoGen, USA) for several days. Puromycin titration was performed on targeted cell line before selection.

5.2.4.2 Puromycin titration

Mouse C3H10T1/2 cells were seeded into 24-well plates at $1.6x10^4$cells/cm^2 in MEF growth media and the cells were incubated overnight at 37°C in a 5% CO_2 incubator. The media was replaced with MEF growth media containing one of a series of concentrations of puromycin ranging from 1ng/mL to 10µg/mL to the corresponding wells. The cells were cultured for 14 days, and the growth media containing puromycin replaced every three days. Cell deaths were recorded every day. The minimum concentration of puromycin that caused complete cell death after 3-4 days would be used for this cell type.

5.2.4.3 Establishing Gli-luciferase gene reporter assay

The Gli-luciferase gene reporter assay was performed by using Steady-Glo® Luciferase Assay System (Promega, USA). Transfected cells were seeded at 5000 cell/well in 96-well plate overnight at 37°C in a 5% CO_2 incubator. The Glo Lysis Buffer (GLB) and cells were equilibrated to room temperature before use. Cells were washed with PBS and 50µL GLB was added to each well to rapidly lyse cultured mammalian cells within 5 min at room temperature. The cell lysate was centrifuged and the supernatant were transferred into luminometer 96-well plate (Promega, USA). The lysate was then diluted with 50µL GLB and then 100µL Steady-Glo® Luciferase Assay Reagent was added into each well. Following 5 minutes incubation at room temperature, the luminescence was measured using a LUMIstar® Omega luminometer according to the manufacturer's instruction.

5.2.5 IC_{50} determination

5.2.5.1 Assay preparation

Mouse C3H10T1/2 cells were seeded into normal 96-well plate at 5000 cells per well in 100µL MEF growth medium and incubated overnight at 37°C in a 5% CO_2 incubator. The medium was then replaced with the ultra-low serum MEF growth medium, which contains Dulbecco's Modified Essential Medium (DMEM; Invitrogen, Australia), 0.5 % fetal bovine serum (FBS; Invitrogen, Australia) and 1000U/mL penicillin G and streptomycin sulfate (Life Technologies, Australia), the following day. After 24 hours incubator at 37°C in a 5% CO_2 incubator, the medium was replaced with fresh ultra-low serum MEF growth medium one-hour prior to performing the assay. Then, mouse C3H10T1/2 cells were incubated with inhibitors at a series of concentrations ranging from 1nM to 10µM for 1 hour at 37°C in a 5% CO_2 incubator. After that, 600nM Smoothened agonist, SAG, or a 1:4 split of Shh conditioned media was added as an agonist for 5 days at 37°C in a 5% CO_2 incubator.

5.2.5.2 Alkaline phosphatase assay

The IC_{50} of SANT-1 analogues was determined by their inhibition of the expression of alkaline phosphatase in mouse C3H10T1/2 cell, having stimulated the cells with agonists of the sonic Hedgehog (Shh) signalling pathway. The alkaline phosphatase (AP) assay was performed using Pierce™ PNPP Substrate Kit (Thermo Fisher Scientific, USA). The protocol for AP assay was adapted from Williams *et al.* (Williams et al., 1999). Briefly, treated C3H10T1/2 cells were washed with cold PBS and lysed with AP lysis buffer containing 150mM Sodium chloride, 1 % Triton™ X-100, 0.5% Tween® 20 (Sigma-Aldrich, Australia), 0.1% SDS and Calbiochem® Protease inhibitor cocktail set III (1:200; Merck Millipore, Germany) for 30 minutes on ice. Cell lysates were then centrifuged at 200x g at 4°C for 20 minutes and ρ-Nitrophenylphosphate (PNPP) substrate was added to supernatant for 1 hour at room temperature. Development of yellow colour was an indicator of AP activity. Absorbance of alkaline phosphatase bounded with PNPP substrate was measured using an EnVision® Series Multilabel

Plate Reader at a wavelength of 405nm.

5.2.6 Immunochemistry of primary cilia

Mouse C3H10T1/2 cells were seeded under different seeding density into Ibidi® 8-well μ-Slides in MEF growth medium and incubated overnight at 37°C in a 5% CO_2 incubator. The cells were then prepared in the same way as that described in section 5.2.4.1 (Assay Preparation), where the antagonist of Shh signalling was not added in this case. After 5 days incubation at 37°C in a 5% CO_2 incubator, the treated cells were washed with phosphate-buffered saline (PBS) and then fixed with 4% paraformaldehyde at room temperature (RT) for 30 minutes. The fixation, blocking and permeabilization procedures were as the same as those described in section 2.2.4.2 (Immunocytochemistry). Then, treated cells were stained with mouse monoclonal anti-γ-tubulin antibody conjugated with Dyomics® 647 (1:100; Abcam, UK) at 4°C overnight. After three washes with PBS, cells were blocked with 20μg/mL AffiniPure Fab fragment goat anti-rabbit IgG(H+L) (Jackson ImmunoResearch, USA) for 30 minutes at RT. Then, cells were stained with a second primary antibody, acetylated mouse monoclonal anti-α-tubulin (1:2000; Sigma-Aldrich, USA), at 4°C overnight, followed by two washes with PBS. The next day, after three more washes with PBS, the cells were stained with a corresponding secondary antibody, donkey anti-mouse Alexa Fluor® 594 (1:1000). With three more washes with PBS, cells were stained with 50ng/mL DAPI at RT for 5 minutes. Then, cells were washed twice again with PBS immediately prior to visualization under the Nikon A1-R confocal microscope.

5.2.7 Data analysis

All assays were carried out at least three times in triplicate. All data were analysed using GraphPad Prism, version 5 for Mac and expressed as mean ± SEM. The grouped data were analysed by one-way ANOVA post-doc Dunnett's test. Results were considered significant when $p<0.05$.

5.3 Results and discussion

5.3.1 A stable cell line with luciferase gene under the control of Gli responsive element was generated

In order to construct a stable cell line (Gli-Luc-NIH3T3) used for Gli-luciferase gene reporter assay, a luciferase gene under the control of Gli responsive elements was incorporated into mouse NIH3T3 embryonic fibroblast cell line using Cignal Lenti reporter assay kit. Before starting this transformation, the cell seeding density and toxicity of puromycin were optimized. For optimization of cell seeding density, NIH3T3 cells were seeded at $5x10^3$cells/cm^2, $10x10^3$cells/cm^2 and $20x10^3$cells/cm^2 and incubated overnight. Cells reached around 70%-90% confluence the next day only when cells were initially seeded at $10x10^3$cells/cm^2. Therefore, a seeding density of $10x10^3$cells/cm^2 was used as initial point prior to treatment with lentivirus. In addition, a puromycin titration was carried out to optimize the amount of puromycin for selection of successfully transduced Gli-Luc-NIH3T3 cells. As shown in Table 5-3-1A, the minimum concentration of puromycin that was required to completely kill NIH3T3 cells was 3µg/mL. As shown in Figure 5-1, concentrations below 300ng/mL did not affect this cell line significantly. 300ng/mL of puromycin caused very little cell death. 1µg/mL of puromycin completely killed NIH3T3 cells after a 9-day exposure. Therefore, it was decided that 3µg/mL puromycin would be used as the minimum concentration for selection of transfected Gli-Luc-NIH3T3 cells. An MOI of 50 was selected as a starting point for transduction.

A.

Days	Control	Concentrations of puromycin (µg/mL)								
		0.001	0.003	0.01	0.03	0.1	0.3	1	3	10
1	-	-	-	-	-	-	-	*	***	x
2	-	-	-	-	-	-	*	**	*****	x
3	-	-	-	-	-	-	*	**	x	x
4	-	-	-	-	-	-	*	**	x	x
5	-	-	-	-	-	-	*	**	x	x
6	-	-	-	-	-	-	*	***	x	x
7	-	-	-	-	-	-	*	*****	x	x
8	-	-	-	-	-	-	*	*****	x	x
9	-	-	-	-	-	-	*	x	x	x
10	-	-	-	-	-	-	*	x	x	x
11	-	-	-	-	-	-	*	x	x	x
12	-	-	-	-	-	-	*	x	x	x
13	-	-	-	-	-	-	*	x	x	x
14	-	-	-	-	-	-	*	x	x	x

Note: -: no cell death; *: cell death increased with the number of stars; x: complete cell death

B.

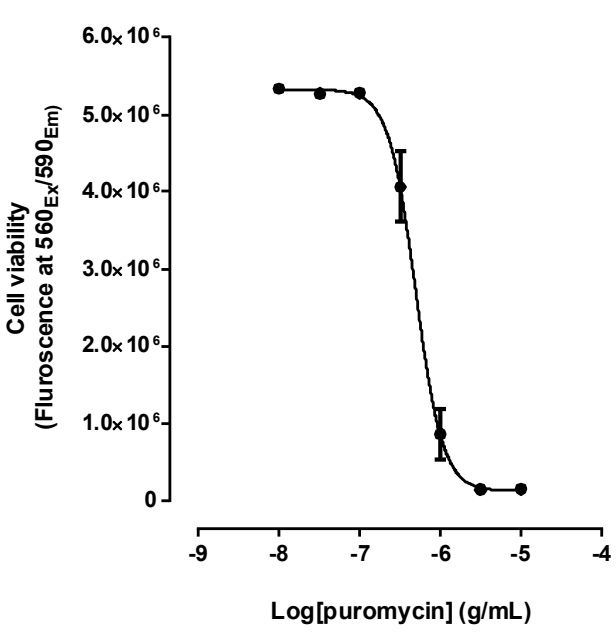

Figure 5-1: Puromycin titration for selection of transfected NIH3T3 cells. (A) Observations of cell death after treatment with different concentrations of puromycin for 14 days. (B) Puromycin titration kill curve using the transformed NIH3T3 cell line. The minimum concentration of puromycin that can affect complete cell death was 3µg/mL. Results are expressed as mean ± S.E.M. with n=4 per group.

The selected transfected Gli-Luc-NIH3T3 MEF cells were then used to evaluate whether Hh signalling by this transfected cell line could be activated by SAG or Shh-conditioned media. As shown in Figure 5-2, the luciferase activity was not detectable for WT NIH3T3 cells but was evident in Gli-Luc-NIH3T3 cells, which indicated the successful incorporation of the luciferase expression construct under the control of Gli responsive element. However, when the Gli luciferase gene reporter assay was further evaluated to see if the activated Hh pathway could be inhibited by Hh pathway antagonist, there was no significant inhibitory activity after treating cells with SANT-1 or other Hh pathway antagonists. In addition, a high background level of luciferase activity was detected in Gli-Luc-NIH3T3 cell line compared with non-transfected NIH3T3. Due to this inconsistency, the AP assay was developed in parallel.

5.3.2 Optimization of compound screening and efficacy testing systems for SANT-1 analogues targeted to Smoothened in the Hh pathway

5.3.2.1 Cell confluence affects primary cilia formation

As cell cyle and starvation are two critical steps for the primary cilium formation which is then an essential step for the Hh signalling activation, the first optimization of cell density just before starvation was done to ensure majority of cells were at resting state, G0 phase of cell cycle, which allow for the followed Hh signalling activation. Cell density was optimized by seeding WT NIH3T3 and Gli-Luc-NIH3T3 mouse embryonic fibroblast cells both at 5000 cells/well and incubating for different times, at 24h, 48h and 72h. When cells were cultured for 24h, the cell confluence at the time of starvation was observed to be around 40% to 50% (sub-confluent). Cells were observed to reach confluence when they were incubated for 48h and were observed to become over-confluent once the incubation period was 72h. The cells were stimulation by a 1:4 split of Shh-conditioned media respectively and the performance of the luciferase assay was compared after incubation periods of 24h, 48h and 72h respectively. As shown in Figure 5-2, only the Gli-Luc-NIH3T3 cells, which was successfully incorported with luciferase gene, showed a significant increase in

relative luciferase activity under the conditions when Gli-Luc-NIH3T3 cells reach confluency or over-confluency. This result may imply that the activation of Hh signaling requires cells at resting state to allow the primary cilium formation prepared as a site for signaling activation. Further evident of relationship between cell cycle and primary cilium foramtion will be shown later in this section.

In addition, cell seeding density was also optimized for the AP assay, a similar increase of AP activity that was proportional to cell confluence was observed. Thus, it was related to the percentage of cells in G0 phase (Figure 5-3). Hh pathway activity was significantly increased as the cells reached confluence before starvation. This was consistent with the previous conclusion that cell confluence before starvation is the critical step for the primary cillia formation. However, it was observed that there was a slight decrease of Hh pathway activity when cells were seeded at $40x10^3$ cells/mL. This slight decrease may be due to the death of cells as they became too confluent. Thus, the optimized seeding density was $20x10^3$ cells/mL for the AP assay.

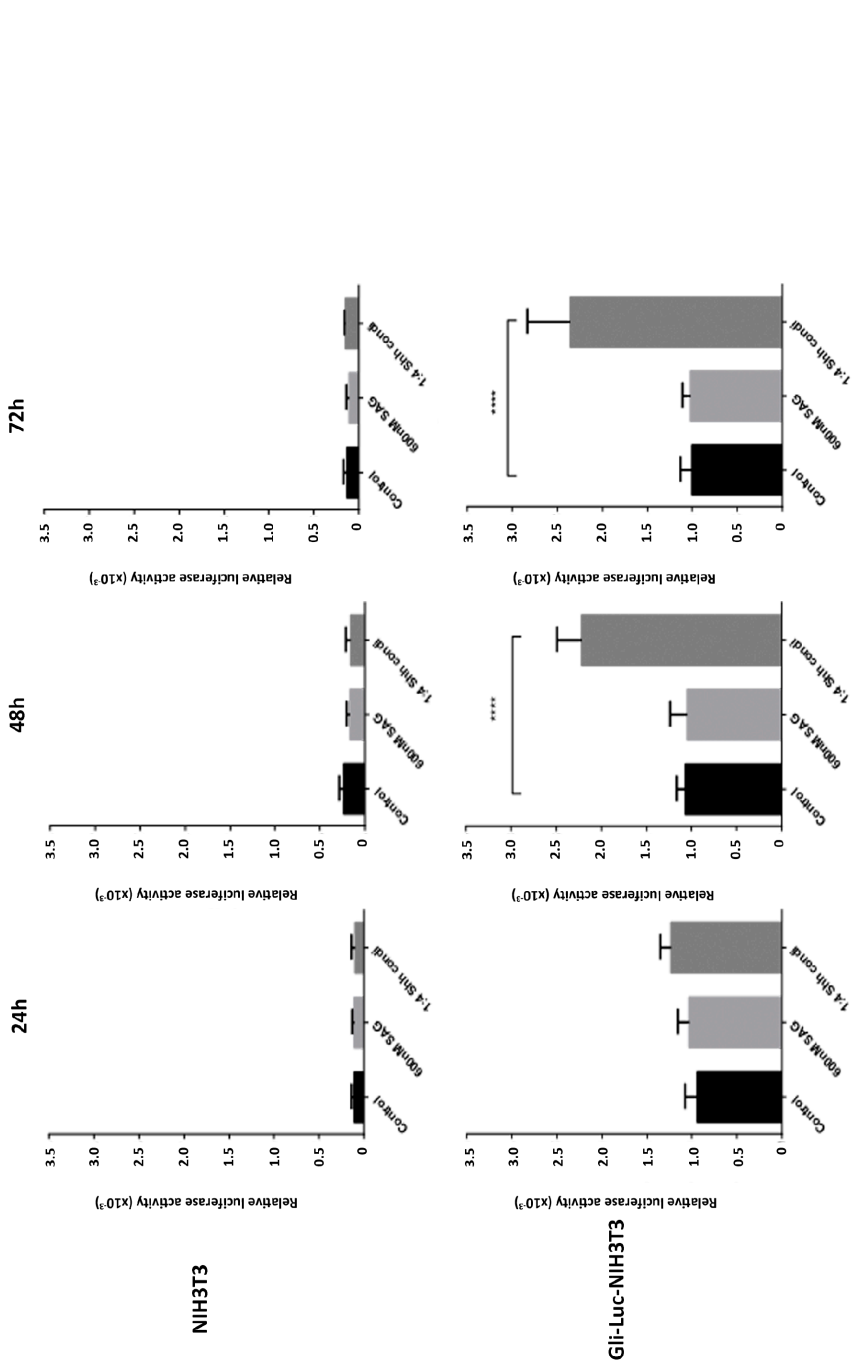

Figure 5-2: Optimization of cell confluence on Hh signalling activation of mouse NIH3T3 embryonic fibroblasts using Gli-luciferase gene reporter assay. NIH3T3 and Gli-luc-NIH3T3 cells were cultured for different periods followed by 24h starvation. Both cell lines were treated with SAG and Shh-conditioned media for Hh pathway activation. The results show that significant luciferase activity was detected only when Gli-Luc-NIH3T3 MEFs were stimulated with 1:4 split Shh-conditioned media after seeding for 48 h and 72h. Results are expressed as mean ± S.E.M. with n=6 per group. Data were analysed by one-way ANOVA post-hoc Dunnett's test.

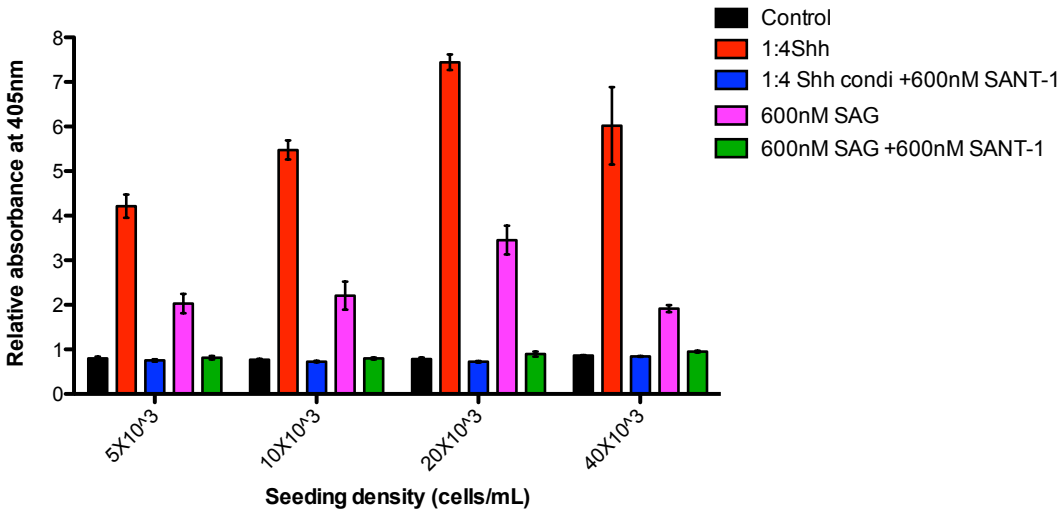

Figure 5-3: Optimization of seeding density for Hh signalling activation of mouse C3H10T1/2 embryonic fibroblasts using the AP assay. C3H10T1/2 MEFs were seeded at different density, followed by serum starvation for 24h. The Hh pathway was activated by either 600nM SAG or a 1:4 split of Shh conditioned media, and some wells were inhibited by co-administration of 600nM SANT-1. The results show a significant increase of AP activity when cells were treated with either SAG or Shh-conditioned media, and this increase was inhibited by Hh pathway antagonist SANT-1. Also, there was an increase in AP activity measured with the increase in seeding density when cells are treated with either SAG or Shh-conditioned media. However, there was a slightly decrease of AP activity measured when cells were seeding at $40x10^3$ cells/mL. Results are expressed as mean ± S.E.M. with n=9 per group. Data is analysed by one-way ANOVA post-hoc Dunnett's test.

To further test these observations, primary cilia and basal body of the primary cilia were immunolabelled with anti-acetylated α-tubulin and γ-tubulin respectively. As the primary cilia are microtubule-based and their formation involves polymerized microtubules that are acetylated, the primary cilia can be stained with anti-acetylated α-tubulin. The primary cilium originates from the mother centriole, which differentiates into the basal body containing a centriole which can be stained with the centrosome marker γ-tubulin (Dawe et al., 2007). Thus, anti-acetylated α-tubulin and γ-tubulin were used together to stain primary cilia and basal body respectively. It was speculated that the cell confluence that induces arrest in G0/G1 phase of cell cycle would affect the primary cilia formation. As cell confluency can efficiently induce quiescence of cells, it was assumed that a prolonged culture of cells to reach higher cell density, would lead to a higher percentage of cells in the G0/G1 phase or G0 phase of the cell cycle (Hayes et al., 2005). As shown in Figure 5-4, more basal bodies were observed at the base of primary cilia and more primary cilia were evident when cells were fully confluent at the time of serum starvation rather than at a sub-confluent stage. This was consistent with the observation that cell confluency affected the sensitivity of cells to Hh signal activation, and confirmed the literature reports that primary cilia formation is one of the essential steps in Hh signal activation. It has been reported (Barzi et al., 2010) that Shh-induced activation of Hh signalling pathway allowed the previously dispersed Protein kinase A (PKA) to accumulate at the base of the primary cilia. The primary cilia are prolonged, allowing activated SMO to migrate from the cytoplasm to the primary cilia via an intraflagellar transport pathway (Wang et al., 2009).

Further investigation of the mechanism of Hedgehog signalling was beyond the scope of this study, but it was useful to observe formation of cilia using immunocytochemistry and this clearly explained the need for diligent preparation of cells prior to running the SMO inhibition assays. The optimized AP assay was used in subsequent studies to test the activity of newly synthesized small molecules derived from SANT-1, as AP assay was more sensitive for detection Hh signalling than the Gli-luciferase gene reporter assay in our case. The parent compound is a potent SMO inhibitor but has not been developed as a clinical agent, in all likelihood it lacks

appropriate pharmacokinetic properties. In addition, SANT-1 was disclosed as a probe compound, originally identified by a screening exercise. Hence SANT-1 would not be a realistic commercial prospect for clinical development. Whether SANT-1 has been used as a lead for further development is not clear from the literature, so it was interesting to begin to study the structure-activity relationships of some analogues.

Figure 5-4: Immunofluorescence detection of primary cilium anchoring and basal body localization at the base of primary cilium and its dependence on the cell proliferation cycle. Culture of C3H10T1/2 cells with different seeding densities were grow in the presence of SAG molecule followed by 24h serum starvation. The nuclei are stained with DAPI (blue). Primary cilia are stained with anti-acetylated α-tubulin (red). Basal bodies are stained with γ-tubulin (yellow). (A) More primary cilia were observed when cells were fully confluent at the time of serum starvation. (B) Localization of basal body shift out of nuclear membrane. (C) Cells, which are over confluent at the time of serum starvation, have more basal body and primary cilia projection out of nucleus membrane. Scale bars = 10µm.

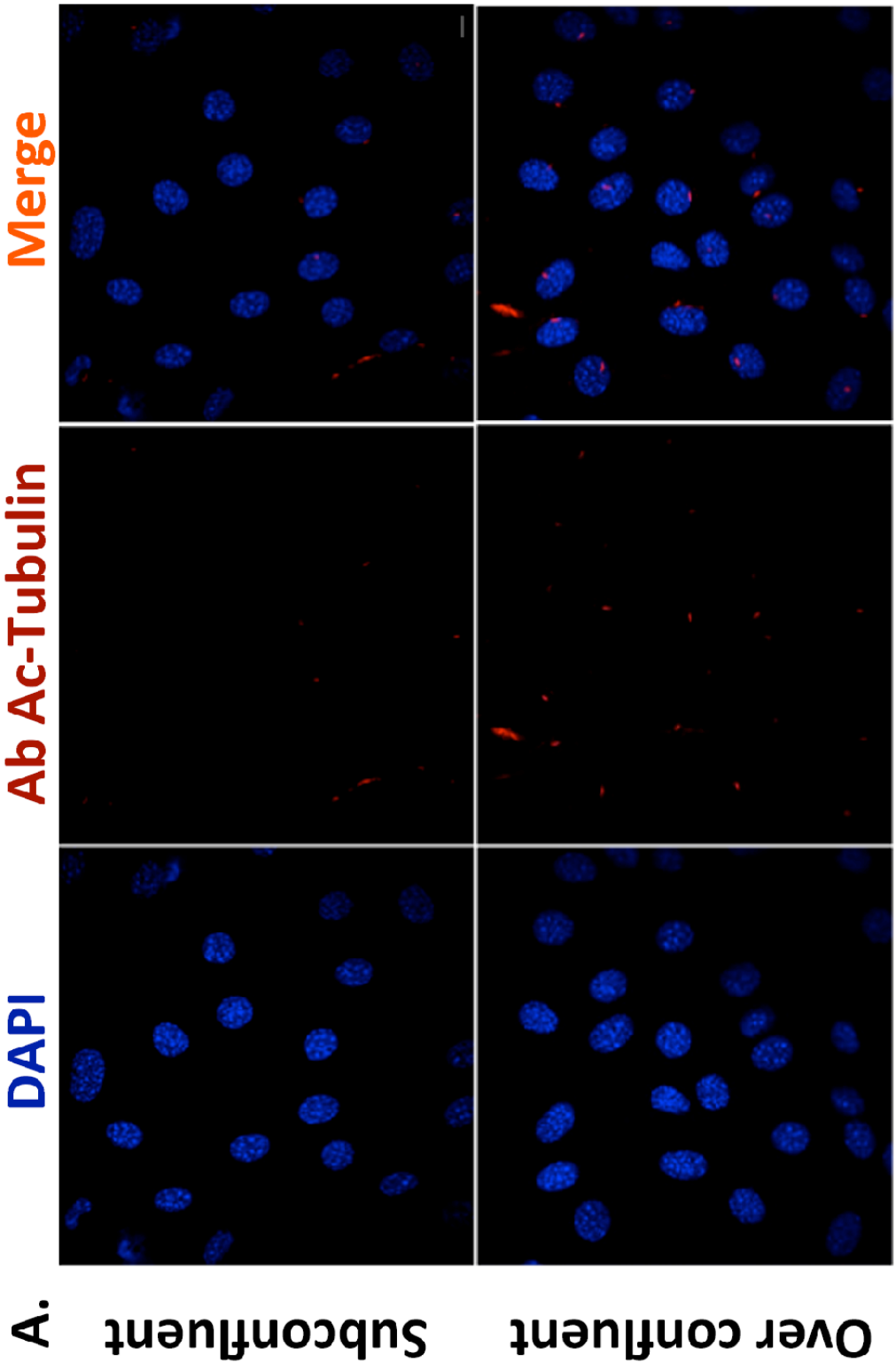
A.
Subconfluent
Over confluent
DAPI
Ab Ac-Tubulin
Merge

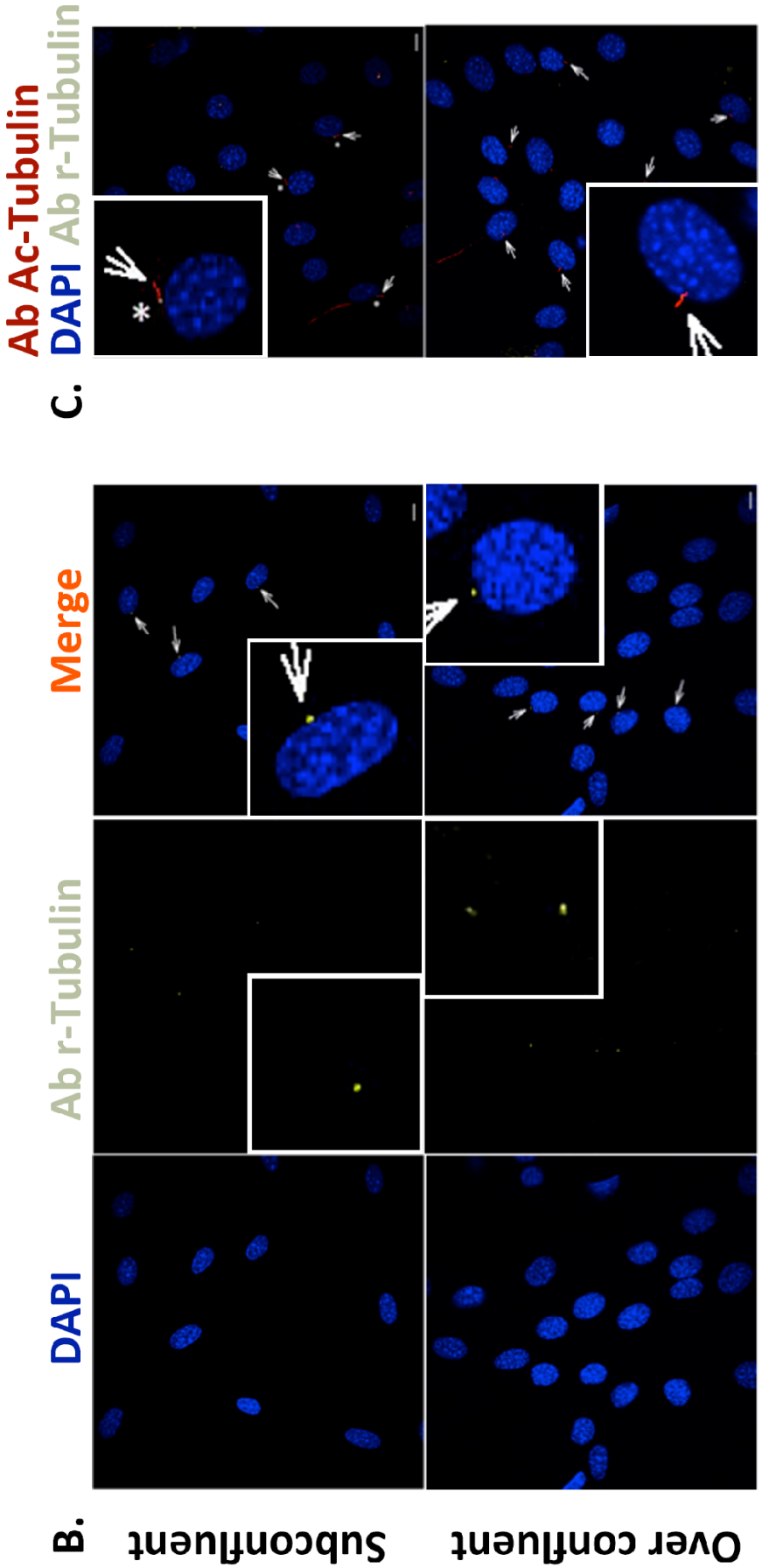
C.
DAPI Ab r-Tubulin
Ab Ac-Tubulin
B.
Over confluent
Subconfluent
DAPI
Ab r-Tubulin
Merge

5.3.3 Identification of Hedgehog pathway inhibitors

5.3.3.1 Testing of currently available agonists

As shown in the Figure 5-5, SAG and super Shh were tested using the optimized AP assay in order to vadidate the performance and the consistency of the assay. SAG was observed to have EC_{50} of 2.2±1.2nM, which was consistent with the literature. This compound was discovered during a high-throughput screen in Shh-LIGHT2 cells and reported to have an EC_{50} of 3nM (Chen et al., 2002). "Super Shh" is a recombinant mouse sonic hedgehog with a modification of non-glycosylated N-terminal fragment and cholesterol addition at C-terminal, in order to enhance the membrane tethering and receptor binding affinity (Feng et al., 2004). The EC_{50} of ''Super Shh", a recombinant form of Shh with reported high activity, was found to be 154.0±1.1ng/mL. Due to its cheaper cost, SAG molecule was used to stimulate the Hh pathway and a 1:4 split of Shh-conditioned medium was used as qualitative positive control.

5.3.3.2 Evaluation of current available antagonists

Two well-known SMO inhibitors, SANT-1 and GDC-0449 were used to evaluate whether the activated Hh pathway could be inhibited as measured by the AP assay. Under these conditions SANT-1 and GDC-0449 were effective inhibitors of the Hh pathway with IC_{50} of 40.3±1.1nM and 37.7±1.2nM respectively (Figure 5-6). The tested IC_{50} of SANT-1 was slightly higher than the literature value (20nM), but this value will depend on the conditions used for the competition assay (Chen et al., 2002). GDC-0449 was slightly more potent than SANT-1 in this case. All novel small Hh pathway molecules were synthesized based on the structure of SANT-1.

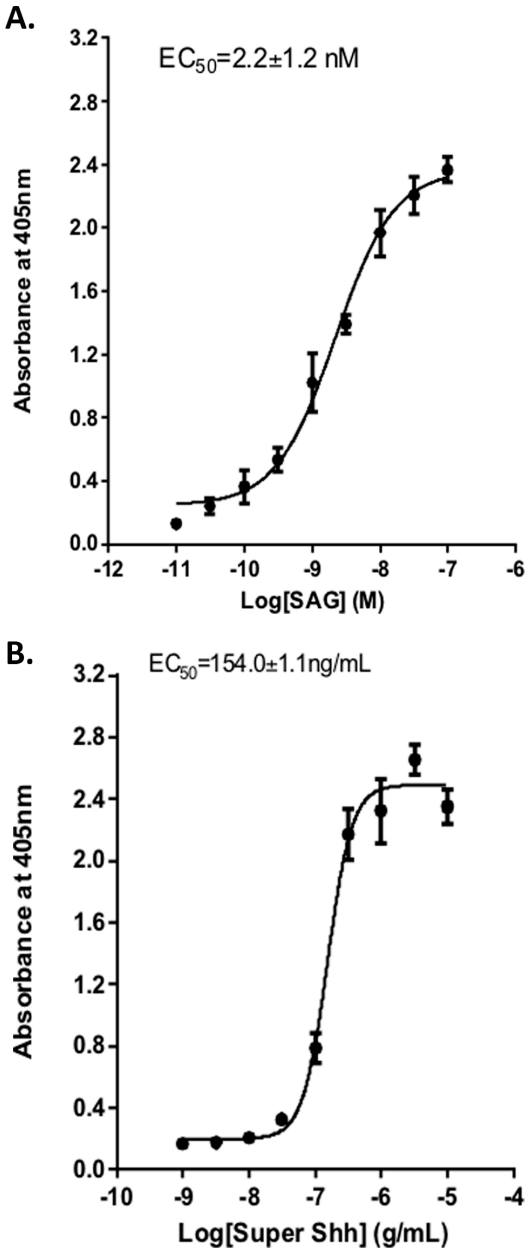

Figure 5-5: Dose response curves for activation of Hh signalling by SAG and super Shh, as determined by AP activity in C3H10T1/2 cells. (A) EC_{50}(SAG)=2.2±1.2nM. (B) EC_{50}(super Shh)=154.0±11.1ng/mL. Results are expressed as mean ± S.E.M. with n=9 per group. Data were analysed by either nonlinear regression log (agonist) vs. response (three parameters) or log (agonist) vs. response-variable slope (four parameters).

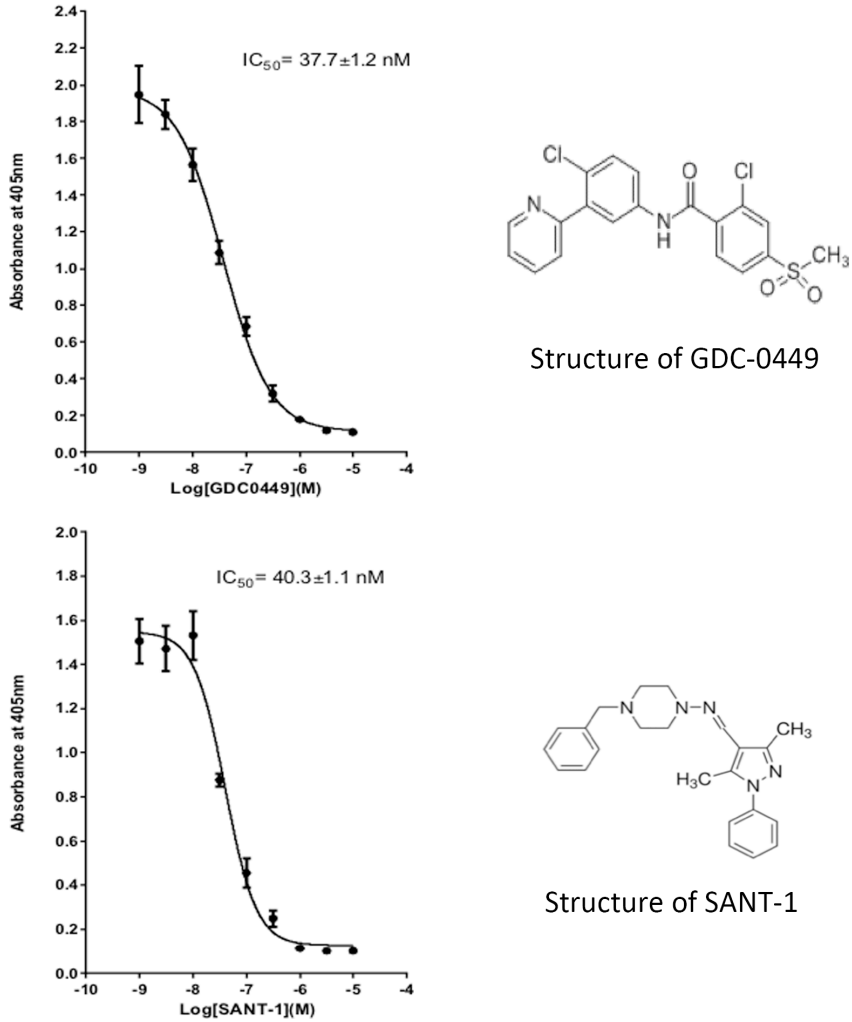

Figure 5-6: Competition dose-response assay for SMO inhibition by GDC-0449 and SANT-1 using the AP activity in C3H10T1/2 cells. (A) IC_{50} (GDC-0449)=37.7±1.2nM. (B) IC_{50} (SANT-1)=40.3±1.1nM. Results are expressed as mean ± S.E.M. with n=9 per group. Data were analysed by either nonlinear regression log (inhibitor) vs. response (three parameters) or log (inhibitor) vs. response-variable slope (four parameters).

5.3.3.3 SMO inhibitory activity of novel SANT-1 analogues

A total of 31 novel SANT-1 analogues were evaluated firstly by screening for inhibition at 300nM (against 30nM SAG). Three compounds (**5a**, **7** and **10**) were shown to have significant activity though they were less potent than SANT-1. The compounds are presented as six groups based on the structural differences between analogues.

5.3.3.3.1 The secondary aldimine (-N–N=CH-) functional group in SANT-1 cannot be replaced by a carbonyl (-N-CO-CH_2-) functional group

A group of 13 compounds (compound **1** to **4c**), as shown in Table 5-1, were synthesized to investigate whether the secondary aldimine functional group (-N –N=CH-) could be replaced by an alternative carbonyl functional group (-N-CO-CH_2-). Compounds **1** to **4c** (Table 5-1) all included the alternative linker and had various substitutions to one of the benzyl rings. The compounds were all analogues of 1-(4-benzylpiperazin-1-yl)-2-(3,5-dimethyl-1-phenyl-1H-pyrazol-4-yl)ethan-1-one. This series of analogues had no inhibitory activity on Hh signalling pathway in C3H10T1/2 MEF line (Figure 5-7). When the -N–N=CH- linker was retained, the ethylbenzene tolerated methyl substitution in one positions but with loss of activity (Table 5-2). One compound (Compound **5a**) with methyl substitution in the meta position of the benzene ring structure had some SMO inhibitory ability. The data confirmed that the –N-CO-CH_2- linker could not be tolerated and this strategy was not pursued further. Replacement of the -N–N=CH- linker with -C=O-NH- linker also resulted in complete loss of SMO inhibitory activity (compound **6**) (Figure 5-8 and Table 5-2).

Interestingly, compound **5b** had a similar structure with **5a**, the only difference being in the position of methyl group substitution to the benzene ring. However, compound **5b** was clearly less potent than **5a**, which suggests that the position of functional group on benzene ring of ethylbenzene terminal had a significant effect on antagonist activity, though both compounds were less potent than SANT-1.

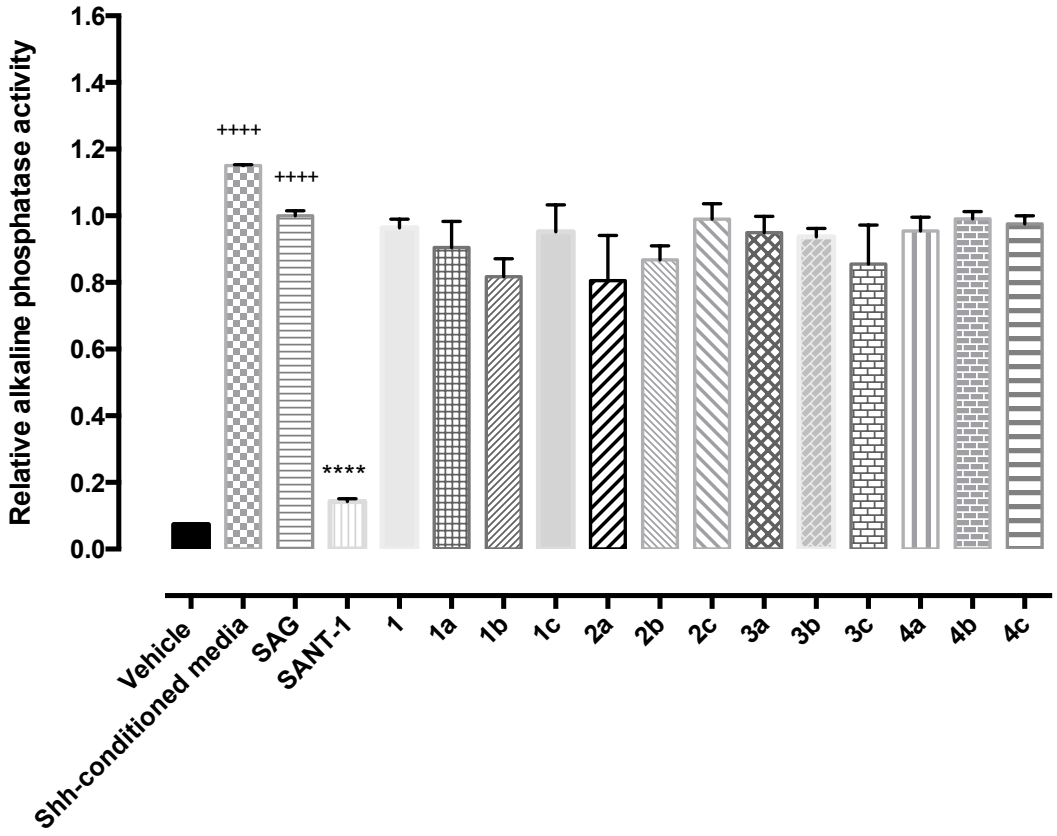

Figure 5-7: Screen of 13 SANT-1 derived small molecules as potential SMO inhibitors by assaying AP activity in C3H10T1/2 cells. The graph shows relative AP activity of cells with the treatment of 13 novel SANT-1 derivatives at 600nM following stimulation treatment with 600nM SAG. All synthesized compounds were unable to inhibit the action of SAG. Results are expressed as mean ± S.E.M. with n=9 per group. ++++: Significant different from vehicle group (P<00001). ****: Significant different from SAG treatment group (P<0.0001). Data were analysed by one-way ANOVA post-hoc Dunnett's multiple comparisons test.

Table 5-1: 13 SANT-1 derived analogues with the common feature that the -N-N=CH- linker was replaced by –N-CO-CH2-. The table lists structural changes in the structure of SANT-1 derived analogues, and IC_{50} values when possible assayed using the AP assay on C3H10T1/2 cell line.

1-(4-benzylpiperazin-1-yl)-2-(3,5-dimethyl-1-phenyl-1H-pyrazol-4-yl)ethan-1-one derivatives

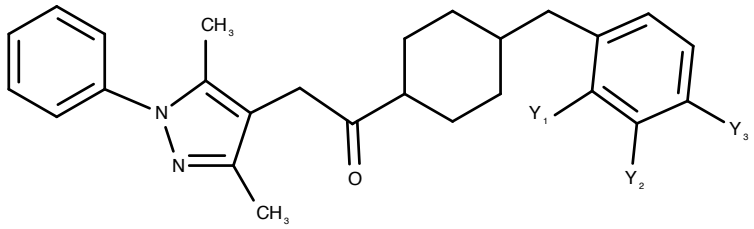

No.	Y_1	Y_2	Y_3	IC_{50} (μM)
1				NA
1a	Br			NA
1b		Br		NA
1c			Br	NA
2a	NO_2			NA
2b		NO_2		NA
2c			NO_2	NA
3a	OMe			NA
3b		OMe		NA
3c			Ome	NA
4a	Me			NA
4b		Me		NA
4c			Me	NA

Note: NA: not active.

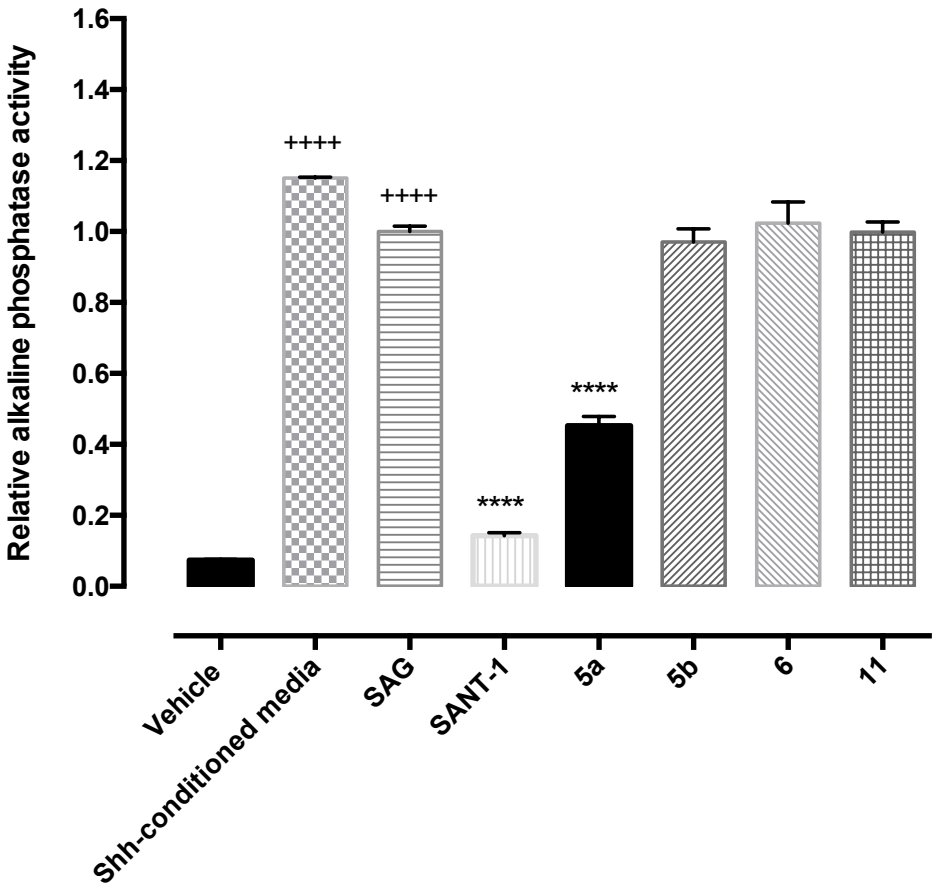

Figure 5-8: Compound screening of 4 novel SANT-1 analogues using the AP assay on C3H10T1/2 MEF cells. The graph shows relative AP activity of cells with the treatment of 4 novel synthesized SANT-1 derivatives at 600nM following stimulation treatment with 600nM SAG molecule. Only compound **5a** shows significant difference from SAG treatment group. Results are expressed as mean ± S.E.M. with n=9 per group. ++++: Significant different from vehicle group (P<00001). ****: Significant different from SAG treatment group (P<0.0001). Data were analysed by one-way ANOVA post-hoc Dunnett's multiple comparisons test.

Table 5-2: 4 alternative SANT-1 derived analogues as potential SMO inhibitors. The table lists structural changes in the structure of SANT-1 derived analogues, and IC_{50} values when possible assayed using the AP assay on C3H10T1/2 cell line.

SANT-1 derivatives

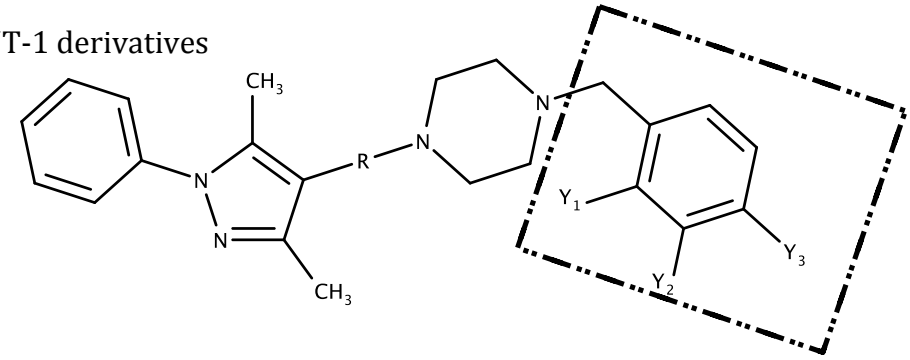

No.	R	Y_1	Y_2	Y_3	IC_{50} (μM)
5a	-N=CH-		Me		0.2
5b	-N=CH-			Me	NA
6	-C=O-NH-				NA
11	-N=CH-	Dot-square selected part: $-CH_3$			NA

Note: NA: not active.

5.3.3.3.2 Piperazine ring may contribute to SMO inhibitory properties of SANT-1

The 6 compounds (**12a** to **16**) retained the -N–N=CH- linker but deleted the piperazine ring structure (Table 5-3). These compounds lacked SMO inhibitory properties as shown in Figure 5-9. All three active agents tested in this study (compounds, **5a**, **7** and **10)** retained the piperazine structure, suggesting that it may be an essential feature. The active compound **5a**, with the highest inhibitory potency (0.2µM), retained the piperazine structure in conjugation with the -N–N=CH- linker. Compounds **7** and **10**, with IC_{50} of 0.8 and 4.1µM correspondingly (Table 5-4), showed less potency than compound **5a,** were active in the absence of the -N–N=CH- linker, but retained the piperazine moiety of SANT-1. This further indicates an essential role of piperazine structure but suggests that there are alternatives to the -N–N=CH- linker. Substitution of either piperazine structure or -N–N=CH- linker decreased the potency of compounds, but the -N–N=CH- linker is perceived to be the part of the molecule that might be unsuitable for clinical use. Hence, the activity of compounds **7** and **10**, particularly compound **7**, offers hope. Compounds **17** and **18** were modified with regard to both piperazine structure and -N–N=CH- linker, and duly had no activity at the concentration tested (Table 5-5 and Figure 5-11). This provided further evidence to support our conclusion of an essential functional role of piperazine structure in SMO inhibition.

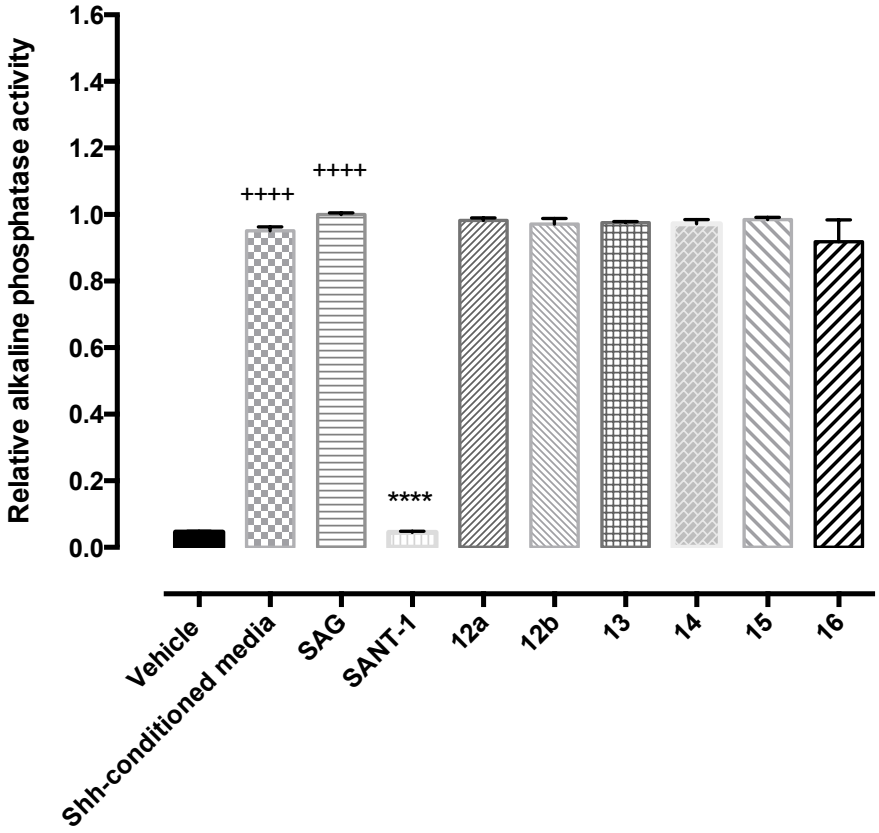

Figure 5-9: Compound screening of 6 novel SANT-1 derivatives as potential SMO inhibitors tested using the AP assay on C3H10T1/2 MEF cells. The graph shows relative AP activity of cells with the treatment of 6 novel synthesized SANT-1 derivatives at 600nM following stimulation treatment with 600nM SAG molecule. All synthesized compounds were unable to inhibit the action of SAG. Results are expressed as mean ± S.E.M. with n=9 per group. ++++: Significant different from vehicle group (P<00001). ****: Significant different from SAG treatment group (P<0.0001). Data were analysed by one-way ANOVA post-hoc Dunnett's multiple comparisons test.

Table 5-3: Structures of 6 SANT-1 derived analogues. The table lists changes in the structure of SANT-1 derived analogues, and IC_{50} values where possible assayed using the AP assay on C3H10T1/2 cell line.

3,5-dimethyl-1-phenyl-4-[(1E)-(2-phenylhydrazin-1-ylidene)methyl]-1H-pyrazole derivatives

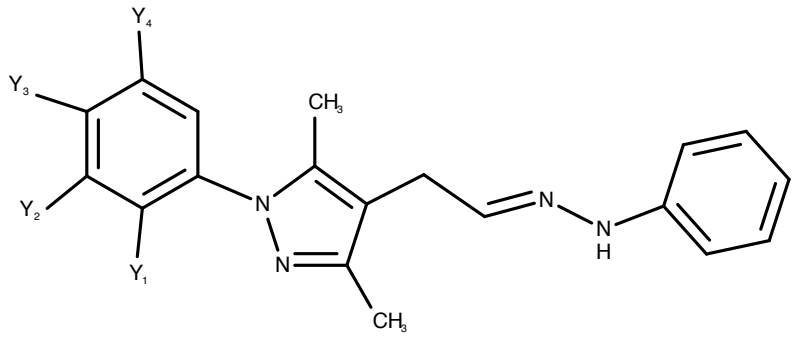

No.	Y_1	Y_2	Y_3	Y_4	IC_{50} (µM)
12a	F				NA
12b			F		NA
13		Cl			NA
14		Br			NA
15				$-NO_2$	NA
16			$-NO_2$ (no HCl)		NA

Note: NA: not active.

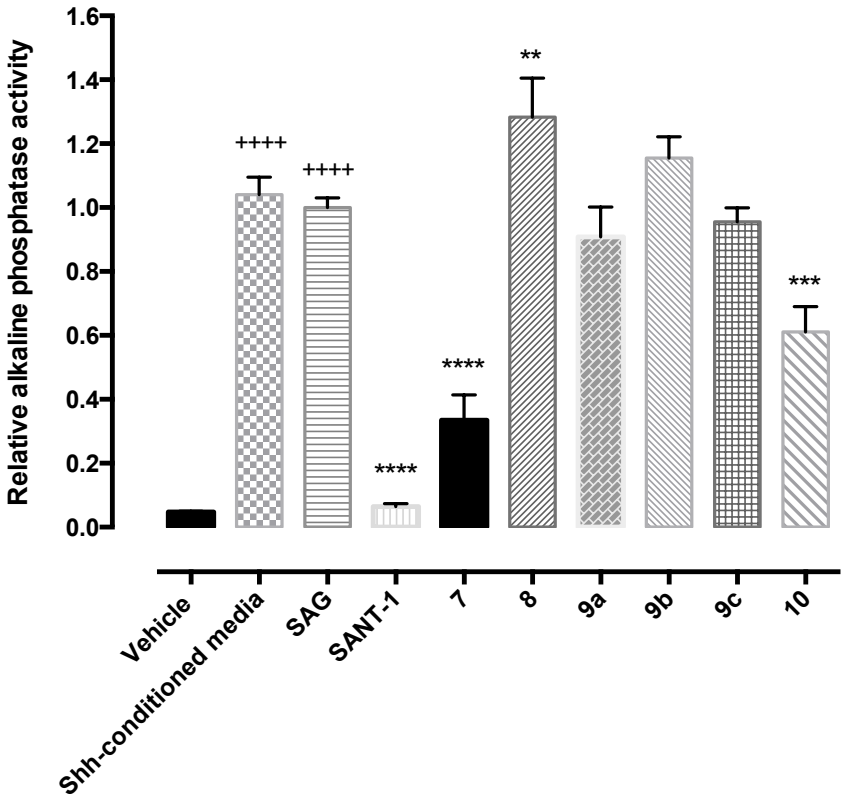

Figure 5-10: Compound screening of 6 novel synthesized SANT-1 derived small molecules with -CH2-CH2- linker as SMO inhibitors using the AP assay using C3H10T1/2 MEF cells. The graph shows relative AP activity of cells with the treatment of 6 novel synthesized SANT-1 derivatives at 600nM following stimulation treatment with 600nM SAG molecule. Compounds **7**, **8** and **10** show significant difference from SAG treatment group. Results are expressed as mean ± S.E.M. with n=3 per group. ++++: Significant different from vehicle group (P<0.0001). ****: Significant different from SAG treatment group (P<0.0001). **: Significant different from SAG treatment group (P<0.01). Data were analysed by one-way ANOVA post-hoc Dunnett's multiple comparisons test.

Table 5-4: Structure of SANT-1 derivatives with -CH2-CH2- linker. The table lists changes in the structure of SANT-1 derived analogues, and IC_{50} values where possible assayed using the AP assay on C3H10T1/2 cell line.

1-benzyl-4-[2-(3,5-dimethyl-1-phenyl-1H-pyrazol-4-yl)ethyl]piperazine derivatives

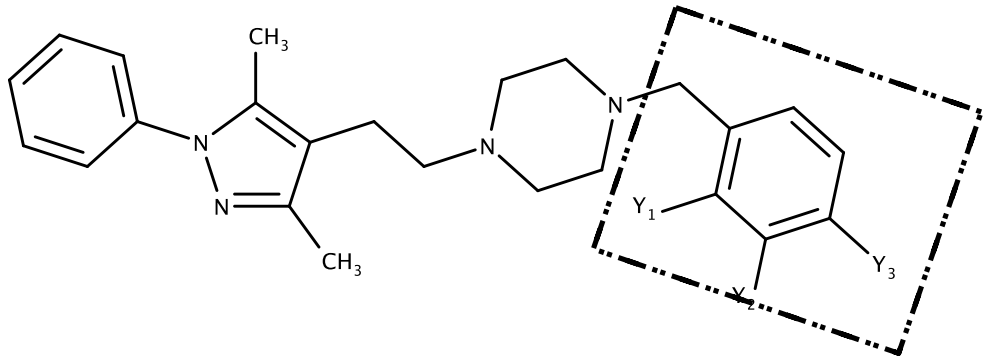

No.	Y_1	Y_2	Y_3	IC_{50} (μM)
7				0.8
8		-O-CH_3-		NA
9a	F			NA
9b		F		NA
9c			F	NA
10	Dot-square selected part: 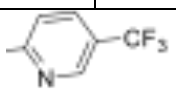			4.1

Note: NA: not active.

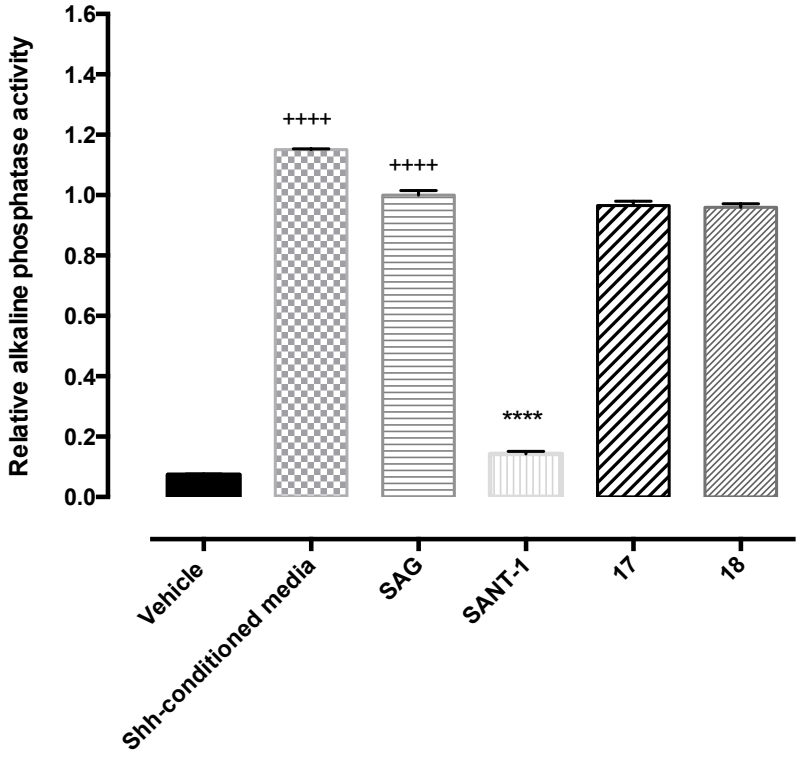

Figure 5-11: Compound screening of 2 novel synthesized SANT-1 analogues as SMO inhibitors using the AP assay on C3H10T1/2 MEF cells. The graph shows relative AP activity of cells with the treatment of 2 novel SANT-1 derivatives at 600nM following stimulation treatment with 600nM SAG molecule. These two compounds were unable to inhibit the action of SAG. Results are expressed as mean ± S.E.M. with n=9 per group. ++++: Significant different from vehicle group (P<0.0001). ****: Significant different from SAG treatment group (P<0.0001). Data were analysed by one-way ANOVA post-hoc Dunnett's multiple comparisons test.

Table 5-5: Structure of 2 SANT-1 derivatives. The table lists changes in the structure of SANT-1 derived analogues, and IC_{50} when possible using the AP assay on C3H10T1/2 cell line.
Note: NA: not active.

SANT-1 derivatives

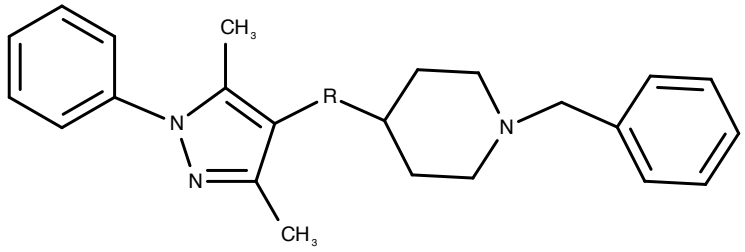

No.	R	IC_{50} (μM)
17	- CH_2- NH_2^+ - with Cl^-	NA
18	-C=O-NH-	NA

5.3.3.3.3 Functional groups coupled to the benzene ring were not well tolerated

The coupling of functional groups to the benzene ring of ethylbenzene terminal generally reduced the activity of SANT-1 analogues. As shown in Table 5-4, the structure of compounds **8**, **9a**, **9b** and **9c** were based on the structure of active compound **7** (IC_{50}=0.8µM), with only the coupling of different functional group or coupling to different positions on the benzene ring of the ethylbenzene terminal. These compounds lost all SMO inhibition activity at the concentration tested when compared to active compound **7** (Figure 5-10). By withdrawing the whole ethylbenzene terminal (compound **10**), the compound seemed to regain some inhibitory activity, with the IC_{50}=4.1µM, but this compound was not as potent as compound **7**. This may suggest that coupling of functional groups to the benzene ring of ethylbenzene terminal are poorly tolerated and should be avoided while work continues on the replacement of the -N–N=CH- linker. The only substitution that was tolerated to some extent was the meta-methyl substitution to the benzene ring of ethylbenzene terminal.

In conclusion, the AP assay proved to be reliable to investigate the effect of small molecule SMO inhibitors. The assay was optimized and validated to allow robust routine screening and potency determination. The newly synthesized SANT-1-derived small molecules **5a**, **7** and **10** were shown to have some inhibitory activity on Hh pathway, with IC_{50} of 0.2, 0.8 and 4.1µM respectively. These were at least five-fold less potent than SANT-1 (IC_{50} =40nM). The structure activity studies emphasised the importance of the -N–N=CH- linker and the piperazine moiety present in SANT-1. However, the activity retained by compounds **7** and **10** indicated that the -N–N=CH- linker can be replaced, which was considered to be encouraging. The piperazine group is present in many drugs and is unlikely to be a liability in relation to human use of a drug candidate. Substitution of the benzene ring of ethylbenzene did not offer any improvement to potency and should be avoided in the next stages of lead development.

Chapter 6

Biological investigation of the anticancer effect of novel noscapine analogues on cancer cell lines

6.1 Background

Noscapine was firstly isolated from a plant source, *Papaver Somniferum,* and been used as a cough suppressant since 1950s (Winter et al., 1961). Noscapine is an orally available phthalideiso-quinoline alkaloid that has been reported to act as microtubule-depolymerizing agent to induce cell mitotic arrest and cell apoptosis, but with no obvious side effects (Winter et al., 1961). As the second-most abundant alkaloid from the opium poppy, noscapine has biological properties similar to colchicine and podophyllotoxin. It has been reported to bind to tubulin in a stoichiometric manner, altering microtubule assembly and resulting in cells being trapped in G_2/M phase of cell cycle (Ye et al., 1998).

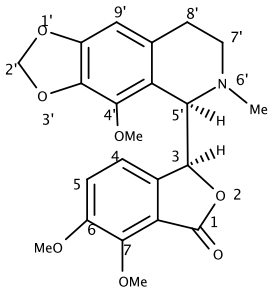

Figure 6-1: Chemical structure of noscapine

The cell cycle (Figure 6-2) is a series of continuous events during which cells prepare for division and eventually divide into two daughter cells. In its simplest form the eukaryotic cell cycle consists of interphase, the mitotic phase and cytokinesis. The

interphase consists of three continuous phases, described as the Gap 1 (G_1), Synthesis (S) and Gap 2 (G_2) phases, during which cells are preparing for DNA synthesis (G_1 phase), replicating DNA (S phase) and preparing for mitosis (G_2 phase). Following the G_2 phase, cells undergo nuclear division (Mitotic phase, or M phase) and then immediately separate all prepared cell components into two daughter cells (cytokinesis). Antimitotic reagents, like noscapine, that affect microtubule dynamics during cell cycle, result in the cessation of cell cycle progression at the metaphase/anaphase transition, and eventually induce apoptosis. (Yvon et al., 1999)

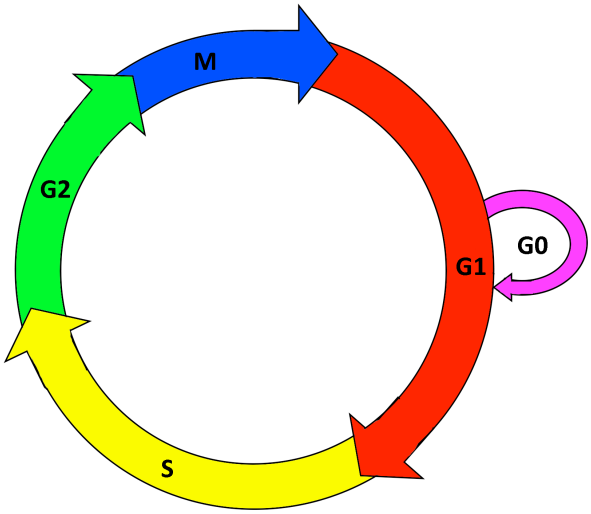

Figure 6-2: Scheme of cell cycle (redrawn with reference to http://www.jargonwall.com)

Noscapine has been reported to have weak antimitotic activity, and has at least 10 to 20 times lower cytotoxicity than other microtubule-binding alkaloids, such as vinblastine, homoharringtonine and some benzophenanthridine alkaloids (Wang et al., 2016). Potent microtubule-depolymerizing agents produce a wide variety of side effects and also have the disadvantage of having poor water solubility, and low oral bioavailability. Thus, there has been interest in the potential of noscapine as a candidate lead compound for development of an oral therapeutic treatment that requires chemical modification to improve its potency.

Previous studies by Scammells' group (DeBono et al., 2012) generated a series of cyclic ether analogues of *N*-nornoscapine, including *N*-acyl, *N*-carbamate, *N*-urea and

N-thiourea classes, and demonstrated that *N*-urea compounds possessed the most promising anticancer activity. The *N*-carbamate class also generated promising compounds but these were less potent than *N*-urea class of noscapine analogues. In addition, the phenyl group promoted cell arrest in G_2/M phase of the cell cycle for both *N*-acyl and *N*-carbamate classes (DeBono et al., 2012). The most promising compound identified in this study was *N*-ethyl-aminocarbonyl Noscapine (analogue **1**), which had an EC_{50} value of 6.7µM and 3.6µM on prostate (PC3) and breast (MCF-7) cancer cell lines, respectively (Table 6-1) (DeBono et al., 2012).

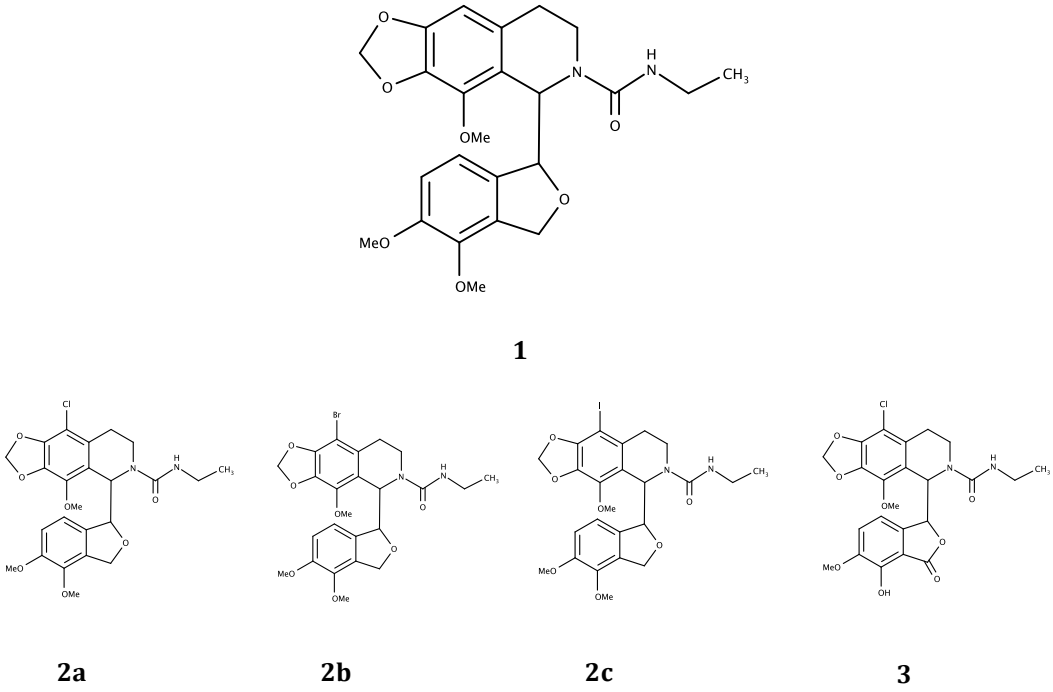

Figure 6-3: Chemical structure of leading noscapine analogues from first generation (1) and second generation (2a to 3)

Later, a series of second derivatives was generated based on the modification of 7- and 9'- positions of the previously identified active lead scaffold, *N*-ethyl-aminocarbonyl noscapine analogue **1**. The results (DeBono et al., 2014) showed some improved anticancer activity amongst these secondary-derivatives, with their potency at least fourfold greater than the previous active lead scaffold **1**. Four compounds **2a**, **2b**, **2c** and **3** were selected as the lead compounds for the next generation investigated in this

study, as they showed an better EC_{50} of less than 2µM across three different cancer cell lines (Table 6-1) (DeBono et al., 2014).

Table 6-1: Cell cytotoxicity of noscapine derivatives in MCF-7, PC3 and PANC-1 cells.[a]

Compd	EC_{50}[µM]		
	MCF-7	PC3	PANC-1[b]
1	3.58	6.7±1.2	nd
2a	1.7±0.1	1.5±0.4	0.9±0.08
2b	1.8±0.2	1.6±0.1	1.0±0.01
2c	2.9±0.2	1.4±0.1	0.9±0.2
3	1.2±0.1	1.5±0.1	1.3±0.1

[a] DeBono et al., 2012; DeBono et al., 2014
[b] EC_{50} was not determined (nd) in MCF-7 and PANC-1 cells if the mean EC_{50} value of the test compound in PC3 cells was >3µM.

Following this path, the Scammells group synthesized a third generation of noscapine analogues, whose structures were based on the previously identified lead compounds. These series of newly synthesized compounds included *N*-sulfonyl cyclic ether noscapine analogues, 9'-chloronoscapine analogues with modification in 1, 6', 7-substitions, 2-pyrrolidone moiety or ρ–dioxane moiety containing noscapine-like analogues, as well as some related Tetrahydroisoquinolines (THIQ) derivatives. The activities of 63 new compounds were evaluated in this study. For consistency and comparison with published work, the same three cells lines were used as before. However these compounds may have useful activity against glioblastoma if the compounds are able to enter the brain.

Temozolomide (TMZ) is currently the only chemotherapeutic treatment available to treat glioblastoma multiform (GBM) and it only kills the proliferating glioma cells. There is an urgent need to develop or improve therapeutic treatments, and in particular it would be desirable to target the recurrent TMZ-resistant glioblastoma initiating cells.

Interestingly, in 2011, Chen's group (Jhaveri et al., 2011) showed that noscapine could

effectively target recurrent human temozolomide (TMZ)-resistant glioma cells and prevent growth and invasion *in vitro*. The *in vivo* treatment with noscapine of a xenograft TMZ-resistant tumor model also produced promising survival data (Jhaveri et al., 2011). The IC_{50} values for noscapine against across three tested human glioblastoma cell lines, including LN229, A172 and U251 cell lines, were 70μM, 20μM and 40μM correspondingly (Jhaveri et al., 2011). In addition, a limitation for the development of therapeutical drugs targeted on brain tumor is the ability to cross the blood brain barrier (BBB). However, noscapine was found to be able to cross the experimental BBB efficiently *in vitro* (Landen et al., 2004). Thus, the development of noscapine analogues may provide an alternative opportunity in treatment of GBM, especially those TMZ-resistant glioblastoma initiating cells which caused the recurrence of glioblastoma.

6.2 Materials and Methods

6.2.1 Cell culture

Human prostate cancer cell line (PC3), human breast cancer cell line (MCF-7) and human pancreatic cancer cell line (PANC-1) were all obtained from colleagues at Monash University. These cells were cultured in PC3 cell culture medium, MCF-7 cell culture medium and PANC-1 cell culture medium respectively at 37 ^{o}C in a 5% CO_2 incubator. PC3 cell culture medium contained Ham's F-12K Kaighn's) Medium (F-12K; Invitrogen, Australia), 10% FBS, 1000U/mL penicillin G and 1000U/mL streptomycin sulfate. MCF-7 cell culture medium contained Minimum Essential Medium α (MEM α; Invitrogen, Australia), 10% FBS, 1000U/mL penicillin G and 1000U/mL streptomycin sulfate. PANC-1 cell culture medium contained DMEM, 10% FBS, 1000U/mL penicillin G and 1000U/mL streptomycin sulfate. The cultures were passaged when cells were at 80% to 90% confluence.

6.2.2 Preparation of compounds

Noscapine, vincristine and all noscapine analogues were obtained from Professor Peter Scammell's lab at Monash University. All compounds were prepared for biological evaluation by dissolving a known mass of each compound into DMSO to prepare 0.1M stock solutions, which were stored at -20°C until use.

6.2.3 Evaluation of cell cycle arrest by noscapine analogues

Cells were seeded at $4x10^4$ cells per well in regular 24 well plates and incubated for 48 hours at 37 ^oC in a 5% CO_2 incubator. After this two-day incubation, cells were treated with one of the noscapine analogues at 10μM and returned to an incubator for 18 hours at 37 ^oC in 5% CO_2. The treated cells were then detached, washed with PBS and re-suspended in the appropriate culture medium containing the nucleic acid stain, Hoechst 33342 (Thermo Fisher Scientific, Australia), at a final concentration of 10μg/mL. Cell suspensions were incubated in a 37^oC incubator and protected from light. Cell samples were analyzed by flow cytometry with a BD FACSCanto™ II flow cytometer (BD Biosciences, US) using a DAPI filter set, in order to access the degree of cell cycle arrest. 100nM vincristine was used as a positive control.

6.2.4 Determination of growth inhibition by noscapine analogues

Noscapine analogues that clearly arrested the cell cycle were further analyzed to determine their ability to prevent cell growth. Cells were exposed to a series of concentrations of each noscapine analogue to determine theIC_{50} via a cell viability assay. 2000 cells per well were seeded into regular 96 well plates in the appropriate cell culture medium and incubated for 48 hours at 37 ^oC in a 5% CO_2 incubator. After this two-day period cells were treated with a noscapine analogue and incubated for a further 5 days at 37 ^oC in a 5% CO_2 incubator. Cell viability was evaluated after this 5-day period using the CellTiter-Blue® Cell Viability Assay Kit (Promega, USA) according to the manufacturer's instructions. Briefly, CellTiter-Blue® Reagent, a highly purified

resazurin buffer solution, was added directly to each well and the cells were incubated for 2 hours at 37 ^{o}C in a 5% CO_2 incubator. The fluorescence was detected using an EnVision® Series Multilabel Plate Reader (PerkinElmer, USA) with excitation filter at 560nm and emission filter at 590nm.

6.2.5 Statistical analysis

All assays were carried out at least three times in triplicate. All data were analyzed using GraphPad Prism, version 5 for Mac and expressed as mean ± SEM. The percentage of cells arrested at G2/M phase ($Cells_{G2/M}$) was determined from the flow cytometry data by estimating the number of cells in G2/M phase and normalizing for untreated cells using the following formula:

$$\text{Arrest index} = \frac{\left(\%\ \text{of}\frac{\text{CellsG2}}{\text{M}}\text{after treatment} - \%\ \text{of}\frac{\text{CellsG2}}{\text{M}}\text{in vehicle control}\right)x\ 100}{\%\ \text{of CellsG2/M in vehicle control}}$$

A noscapine analogue with an arrest index over 100 was regarded as a highly active compound, and was selected for determination of its half maximal inhibitor concentration (IC_{50}). An arrest index lower than 30 was regarded as non-active. The IC_{50} of active noscapine analogues was analyzed based on nonlinear dose responsive curve using GraphPad Prism.

6.3 Results and Discussion

A total of 63 Noscapine analogues were first screened at 10µM to evaluate their effects on the cell cycle arrest of MCF-7, PC3 and PANC-1 cancer cell lines by way of flow cytometry. Cells treated with various noscapine analogues, or so called noscapinoids, were stained with nucleic acid dye, Hoechst 33342, to investigate the cell cycle distribution. The cell cycle distribution is determined based on the difference in DNA content in various phase of cell cycle. Hoechst 33342 can preferentially bind to the adenine-thymine (A-T) regions of DNA and emits blue fluorescence that can be

detected at wavelength ranging from 460nm to 490nm (Filby et al., 2016). Thus, only cells with disrupted microtubules caused by the treatment with active noscapinoids would halt cycling in G_2/M phase. This was evident when cells contain double the normal DNA content, detected by a larger proportion of cells with higher blue fluorescence intensity (Figure 6-4). The arrest index was used to identify active compounds. An arrest index of less than 10 was considered to represent an inactive compound. An arrest index between 10 and 50 was considered to represent an active compound. Highly active noscapinoids were those with arrest indices greater than 50.

Although noscapine has been reported to inhibit cell growth with IC_{50} of 16.81±9.79μM, 35.20±8.18μM, 60.85±12.17μM in HeLa, MCF-7 and U2OS cancer cell lines respectively (Wang et al., 2016), in this study noscapine was evaluated to be inactive at trapping cells in G_2/M phase of cell cycle at 10μM on MCF-7, PANC-1 and PC3 cancer cell lines (Figure 6-4). Noscapine solubility was found to be lower than 100μM, which realistically prevents the acquisition of enough data to confidently estimate IC_{50} values above 10μM. In this study, the focus was on estimating parameters of more active compounds and a precise estimate of noscapine activity was not of great importance. It is possible that the antimitotic activity of noscapine is cell line dependent, given the value of IC_{50} for HeLa cells quoted above. The cell lines we examined were certainly less sensitive than HeLa cells. Unlike noscapine, vincristine, as a positive control, exhibited similar IC_{50} across all three cancer cell lines in this study. As shown in Figure 6-5, the IC_{50} was determined to be 4.6nM, 4.3nM and 6.9nM on PC3, MCF-7 and PANC-1 cancer cell lines respectively, suggesting that vincristine is at least 1000 fold more active in the assay than noscapine.

A.

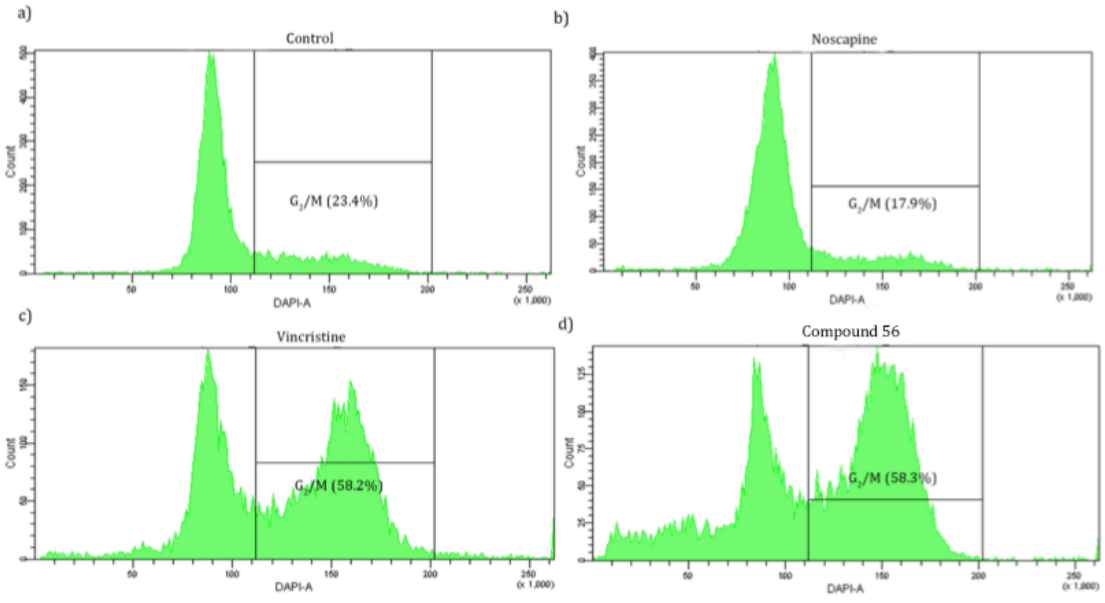
a)
Control
G2/M (23.4%)
b)
Noscapine
G2/M (17.9%)
c)
Vincristine
G2/M (58.2%)
d)
Compound 56
G2/M (58.3%)
Count
DAPI-A
(x 1,000)

B.

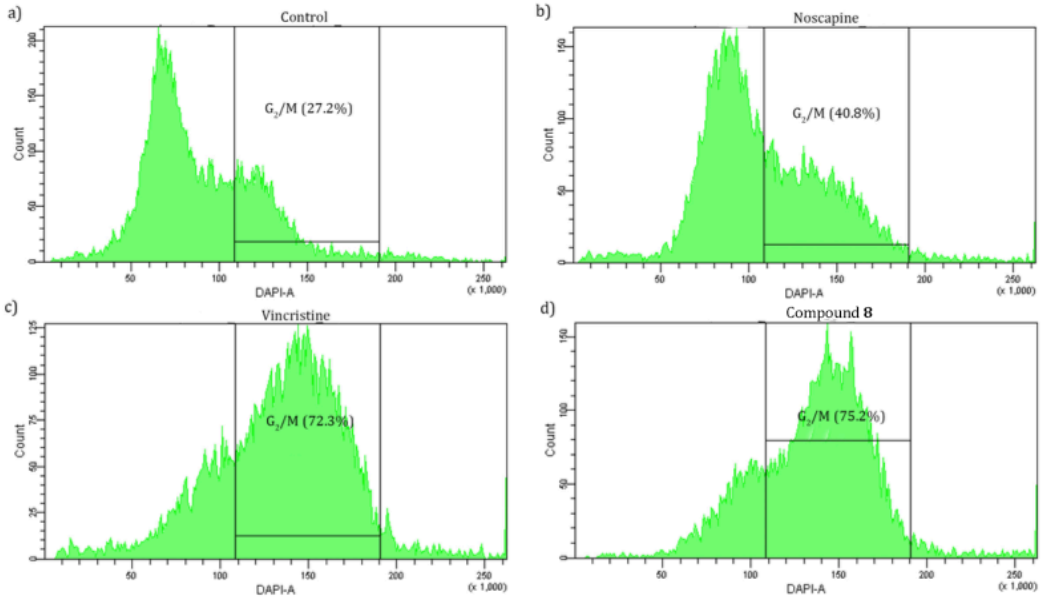
a)
Control
G2/M (27.2%)
b)
Noscapine
G2/M (40.8%)
c)
Vincristine
G2/M (72.3%)
d)
Compound 8
G2/M (75.2%)
Count
DAPI-A
(x 1,000)

C.

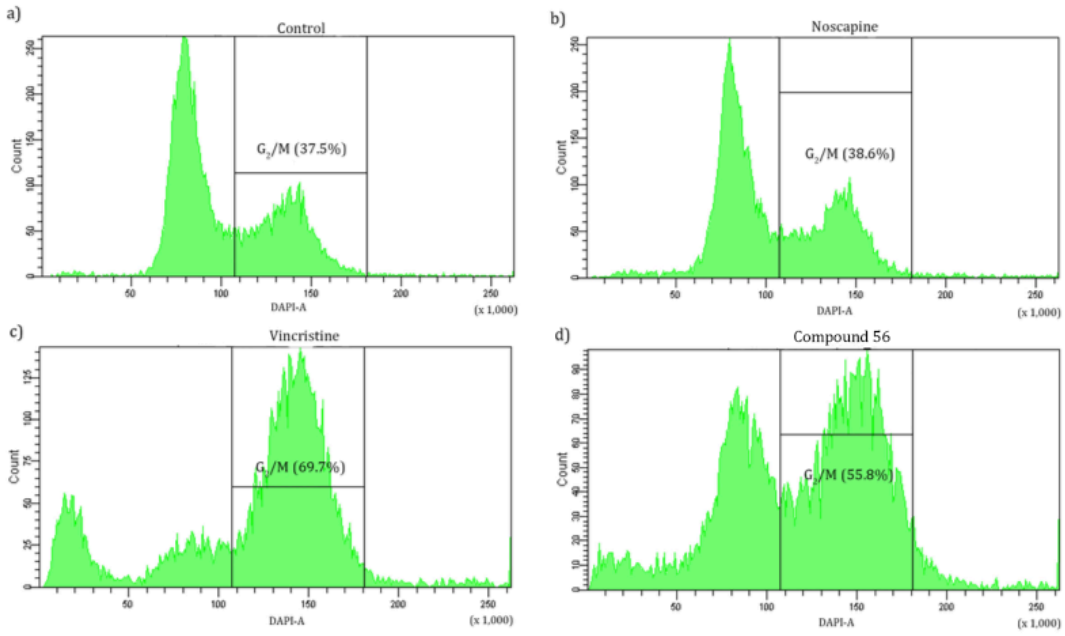

Figure 6-4: Representative FACS analysis of cell populations in various stages of the cell cycle when treated with noscapine analogues or vincristine. MCF-7 cell line (A), PANC-1 cell line (B) and PC3 cell line (C) were all treated with vehicle control (a), 10µM Noscapine (b), 5.36nM (IC80) vincristine (c) and 10µM noscapine analogues respectively for 21 hours. Examples involving active compound **56** and **8** are shown as representative here and they are discussed later in Table 6-9 and Table 6-3 respectively. The cell-cycle distribution of G_2/M phase was calculated.

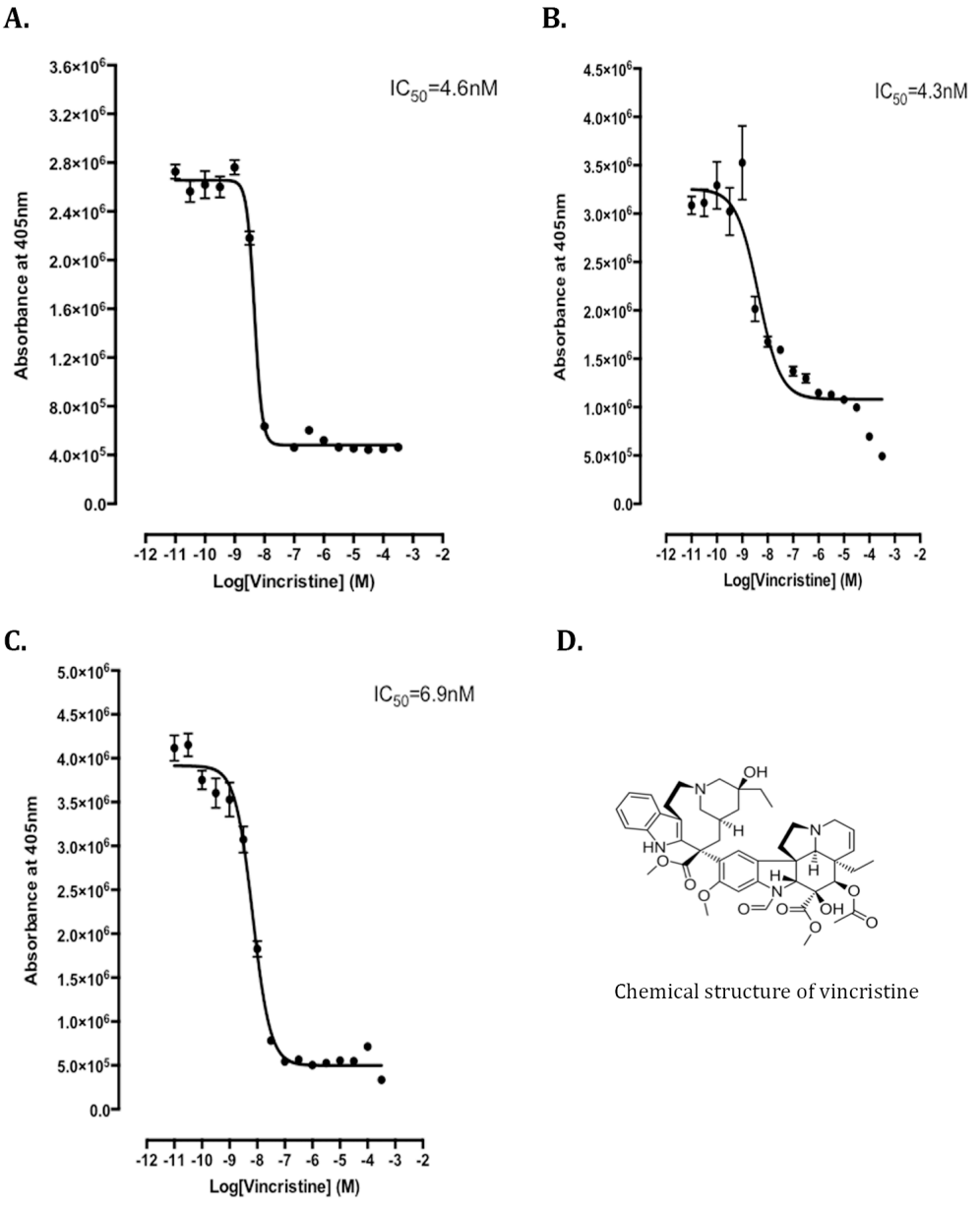

Figure 6-5: Determination of cytostatic activity of vincristine on PC3, MCF-7 and PANC-1 cancer cell lines. (A) IC_{50}(vincristine)=4.6nM on PC3 cell line. (B) IC_{50}(vincristine)=4.3nM on MCF-7 cell line. (C) IC_{50}(vincristine)=6.9nM on PANC-1 cell line. (D) Chemical structure of vincristine. Results are expressed as mean ± S.E.M. with n=9 per group. Data were analyzed by either nonlinear regression log (inhibitor) versus response (three parameters), or log (inhibitor) versus response-variable slope (four parameters).

6.3.1 *N*-sulfonyl cyclic ether noscapine analogues

As previous studies by Scammells' group (2012) demonstrated that the 6'-*N*-demethylation of noscapine across various series, including *N*-alkyl, *N*-amide, *N*-carbmate, *N*-thiourea and *N*-urea series, could give rise to very different activities, a small series of *N*-sulfonyl compounds were generated to see if they possess any higher efficiency. Results showed that *N*-sulfonyl cyclic ethers of noscapine (compounds **5** and **6**) exhibited some activity (arrest index ≤50%) as shown in Table 6-2. Further modification with by changing the 7-methoxy into 7-hydroxy produced a more active compound in MCF-7 cells. This suggested that modification by 7-substitution was a promising strategy as discussed later.

Table 6-2: Changes in the arrest index following treatment with four N-sulfonyl cyclic ether noscapine analogues at 10μM, and IC_{50} values for active compounds.

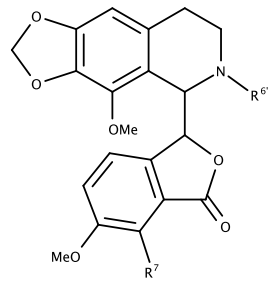

No.			Arrest index		IC_{50} (μM)	
	$R^{6'}$	R^7	MCF-7	PANC-1	MCF-7	PANC-1
4	CONHEt	OMe	INA	INA	NA	NA
5	SO_2OH	OMe	47	27	NA	NA
6	$SO_2NH(CO)OC(CH3)_3$	OMe	33	25	NA	NA
7	SO_2NH_2	OH	195	33	Na	NA

Inactive (INA): arrest index ≤ 10
NA: IC_{50} was not assayed if the arrest index ≤ 100
Na: IC_{50} was not assayed

6.3.2 9’-chloronoscapine analogues

6.3.2.1 Tetrahydrofuran moiety combined with 7-methoxy structure retained potent cytotoxic activity

As shown in Table 6-3, a series of 1,6’-substituted 9’-chloronoscapine analogues were generated based on the structure of one of the existing lead compounds (**2a**). 1,6’-substituted 9’-chloronoscapine analogues contained a 6’-sulfonyl-group-containing group along with the 9’chloro, 7-methoxy. In addition, the tetrahydrofuran (THF) moiety was retained as in compound **2a**. Most of these analogues had similar activity to compound **2a** (Table 6-3). However, when the modification was made to change the THF moiety in 1,6’-substituted 9’-chloronoscapine analogues into the γ-butyrolactone (GBL) moiety (Table 6-4), compounds had significantly lower activity. This suggested an important role of THF moiety combined with 7-methoxy. In addition, these active 1,6’-substituted 9’-chloronoscapine analogues were less active when the compounds were substituted with a longer sulfonyl groups.

Table 6-3: Changes in the arrest index of 1,6-substituted 9'-chloronoscapine analogues all at 10μM, and IC_{50} values for active compounds.

1,6'-substituted 9'-chloronoscapine analogues

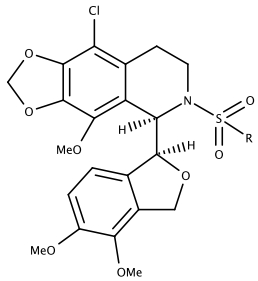

No.	R	Arrest index		IC_{50} (μM)	
		MCF-7	PANC-1	MCF-7	PANC-1
8	NH_2	290	158	1.3	2.1
9	NHPr	282	140	≥10	2.9
10	$NH(CH_2)_2N(CH_3)_2$	123	39	Na	NA
11	$NHCH_3CF_3$	307	116	≥10	1.6
12	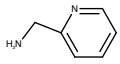	260	122	≥10	4.8
13	$NH(CH_2)_2COOH$	75	29	NA	NA
14	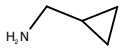	260	130	≥10	5.2
15	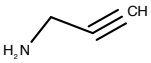	265	154	9.4	6.4
16	NHEt	191	151	2.5	5.5
17	NHBn	60	29	NA	NA
18	2-thiophene	260	134	Na	2.7
19	3-NO_2Ph	27	47	NA	NA
20	4-ClPh	96	74	NA	NA
21	4-CH_3Ph	219	83	Na	Na
22	2-FPh	228	141	Na	Na
23	2-NO_2Ph	229	138	Na	Na
24	OH	197	153	Na	Na
25	ethylurea	22	50	NA	NA

NA: IC_{50} was not assayed if the arrest index ≤ 100

Na: IC_{50} was not assayed

Table 6-4: Changes in the arrest index for three noscapine analogues all at 10μM, and IC_{50} for active compounds.

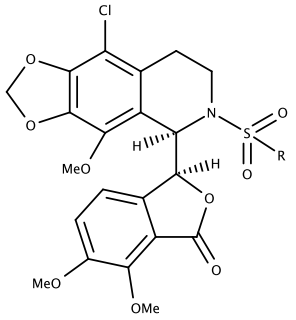

No.	R	Arrest index			IC_{50} (μM)		
		MCF-7	PANC-1	PC3	MCF-7	PANC-1	PC3
26	NH_2	46	24	NA	NA	NA	NA
27	NHEt	52	37	NA	NA	NA	NA
28	$NH(CH_2)_2NH(CH_3)_2$	18	24	NA	NA	NA	NA
NA: IC_{50} was not assayed if arrest index ≤ 100							

6.3.2.2 γ-butyrolactone moiety combined with 7-hydroxy structure retained potent cytotoxic activity

A previous lead compound **3** provided a promising structure containing a THF moiety and the 7-hydroxy group, which gave rise to an improved cytotoxic activity compared with compound **1**. Thus, a series of six, 7-substitute-9'-chloronoscapine analogues were synthesized (Table 6-5). Most compounds exhibited similar activity to the 1,6'-substituted 9'-chloronoscapine analogues, which provided further another evidence of the value of GBL coupled with 7-hydroxy. The combination of GBL moiety with 7-methoxy or the combination of THF moiety with 7-hydroxy resulted in loss of functional activity.

Table 6-5: Changes in arrest index for four noscapine analogues all at 10μM, and IC_{50} for active compounds.

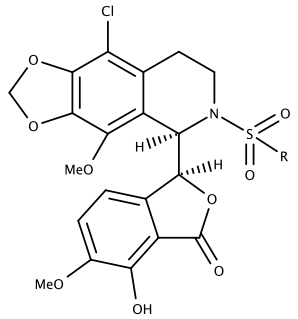

No.	R	Arrest index		IC_{50} (μM)	
		MCF-7	PANC-1	MCF-7	PANC-1
29	NH_2	242	143	Na	Na
30	NHEt	220	128	Na	Na
31	NHPr	277	145	Na	Na
32	$NH(CH_2)_2NH(CH_3)_2$	33	25	NA	NA

Inactive (INA): arrest index ≤ 10
NA: IC_{50} was not assayed if the arrest index ≤ 100
Na: IC_{50} was not assayed

6.3.3 2 Value of the pyrrolidone moiety in noscapine-like analogues

Compounds **33a** to **34** are the series that contained a 2-pyrrolidone moiety. As shown in Table 6-6, compounds within this series are active, but less active than the best compounds on MCF-7 and PC3 cancer cell lines, and inactive on PANC-1 cells. One possibility for this may be due to the combination of GBL moiety coupled with 7-methoxy that generally resulted in the loss of functional activity.

Table 6-6: Changes in arrest index for 4 noscapine analogues all at 10µM, and IC_{50} for active compounds.

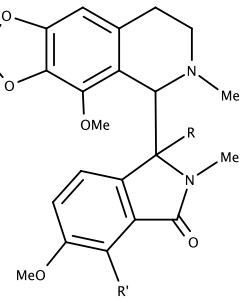

33a to **34**

No.			Arrest index			IC_{50} (µM)		
	R	R'	MCF-7	PC3	PANC-1	MCF-7	PC3	PANC-1
33a	H	OMe	44	25	INA	NA	NA	NA
33b	H	OMe	35	22	INA	NA	NA	NA
33	Me	OMe	39	29	INA	NA	NA	NA
34	H	H	30	33	INA	NA	NA	NA

Inactive (INA): arrest index ≤ 10
NA: IC_{50} was not assayed if the arrest index ≤ 100
Note: **33a** and **33b** are one compound with different diastereomer structure

6.3.4 Value of ρ-dioxane moiety in noscapine-like analogues

Another series of compounds were made with modification with dioxolane moiety into ρ–dioxane moiety (Table 6-7). Apart from compound **38**, most ρ-dioxane moiety containing compounds show no activity in PANC-1 cell line, and modest activity in MCF-7 and PC3 cell lines. Compound **38** was the only highly active compound (≥50% of the changes in mitotic arrest) in this series, which may be due to the inclusion of the tetrhydrofuran (THF) moiety in compound **38**. As discussed before, this combination was determined to give an improved anticancer activity compared to noscapine. To date, compound **38** is the most promising compound in this study, with IC_{50} value of 3.6, 1.1 and 2.5µM on MCF-7, PANC-1 and PC3 cell line respectively. However, compound **38** is still not as potent as the 2nd generation noscapine compounds (**2a** to **3**).

Table 6-7: Changes in arrest index for 7 noscapine analogues all at 10µM, and IC_{50} for active compounds.

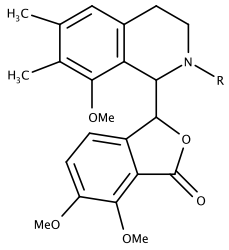

35a to **36c**

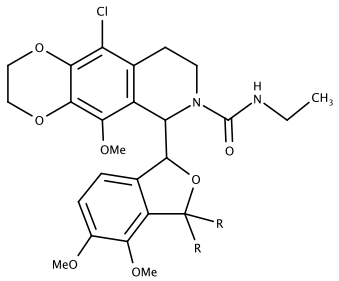

37 to **38**

No.	R	R'	Arrest index			IC_{50} (µM)		
			MCF-7	PANC-1	PC3	MCF-7	PANC-1	PC3
35a	Me		20	INA	16	NA	NA	NA
35b	Me		17	INA	23	NA	NA	NA
36a	EA		28	INA	29	NA	NA	NA
36b	EA		50	INA	42	NA	NA	NA
36c	EA		INA	INA	INA	NA	NA	NA
37	=O		26	INA	32	NA	NA	NA
38	H		374	89	120	3.6	1.1	2.5

Inactive (INA): arrest index ≤ 10
NA: IC_{50} was not assayed if arrest index ≤ 100
EA: ethylacetamide

6.3.5 Related Tetrahydroisoquinolines derivatives

Research conducted by Zimmerman et al. (2013) demonstrated a noscapine-inspired collection of tetrahydroisoquinolines (THIQs) that possess more potent activity in disrupting microtubule dynamics compared with noscapine. In addition, the group of THIQs was reported to have the ability to overcome drug resistance in the multidrug-resistant HeLa cell line due to their limited interaction with P-glycoprotein

or other efflux pumps (Zimmerman et al., 2013). Therefore, the MIPS group elected to synthesize some related THIQ derivatives as shown in Table 6-8 and Table 6-9.

6.3.5.1 Dioxolane moiety retained some activity in mitotic arrest

The structure of compounds **39** to **52** are based on the structure of THIQ core combined with benzofuran, as shown in Table 6-8. This series of compounds were modified to examine compounds lacking the dioxolane moiety. Most of compounds within this series lost the ability to arrest cells in G_2/M phase, with marginal activity on PC3 and MEF-7 cell lines. However, the compounds in Table 6-2 and Table 6-4 retained the dioxolane moiety and these had some activity across all three cell lines. This suggests that the dioxolane moiety within the structure of noscapine is not essential for activity but promotes mitotic arrest. Interesting, one exception was compound **51**, which had high activity. This was thought to be due to the presence of the THF moiety as well as the 7-methoxy group, which consistently shows higher activity than compounds with GBL substitution. In addition, compound **51** is a 9'-chloro substituted analogue with *N*-ethylacetamide, and therefore retained several of the features that promote arrest at G2/M. This feature was also absent in compounds **50** and **52.**

6.3.5.2 9-bromo THIQ derivatives

Another series of THIQ derivatives retained the THIQ core, 9-bromo and 4-methoxy substitutions as well as the dioxolane moiety, but differed in the substitutions at *N*-position and 5-position (Table 6-9). Compounds **53** to **56** are *N*-ethylacetamide based analogues and compounds **57** to **58** are *N*-methyl based analogues. These compounds were inactive with exception of compound **56** that was active in mitotic arrest and showed a moderate cytotoxic activity (≥5μM) across the three cell lines.

Table 6-8: Changes in arrest index for 17 noscapine analogues all at 10µM, and IC_{50} for active compounds.

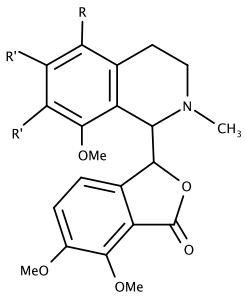

39 to **42**

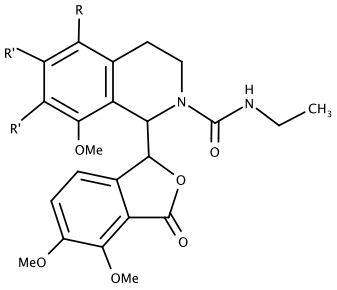

43 to **49b**

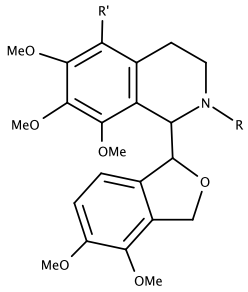

50 to **52**

No.				Arrest index			IC_{50} (µM)		
	R	R’	R’’	MCF-7	PANC-1	PC3	MCF-7	PANC-1	PC3
39	Cl	OMe	OMe	INA	INA	INA	NA	NA	NA
40	H	$OCH(CH_3)_2$	$OCH(CH_3)_2$	INA	INA	INA	NA	NA	NA
41	H	OMe	OMe	INA	INA	INA	NA	NA	NA
42	H	1:1 mixture of OH and OCH_2Ph		INA	INA	INA	NA	NA	NA
43	H	OMe	OMe	INA	INA	INA	NA	NA	NA
44	H	OH	OH	INA	INA	INA	NA	NA	NA
45	Cl	OMe	OMe	INA	INA	INA	NA	NA	NA
46	H	$OCH(CH_3)_2$	$OCH(CH_3)_2$	17	INA	21	NA	NA	NA
47	H	Ph	OH	51	INA	28	NA	NA	NA
48a	H	2-FPh	OH	50	INA	27	NA	NA	NA
48b	H	3-FPh	OH	61	INA	21	NA	NA	NA
48c	H	4-FPh	OH	14	INA	23	NA	NA	NA
49a	H	2-OMePh	OH	33	INA	25	NA	NA	NA
49b	H	3-OMePh	OH	18	INA	26	NA	NA	NA
50	EA	H		INA	INA	INA	NA	NA	NA
51	EA	Cl		208	112	48	28.0	6.0	7.4
52	Me	Cl		INA	INA	INA	NA	NA	NA

Inactive (INA): arrest index ≤ 10
NA: IC_{50} was not assayed if arrest index ≤ 100
EA: ethylacetamide

Table 6-9: Changes in arrest index for 6 noscapine analogues all at 10µM, and IC_{50} for active compounds.

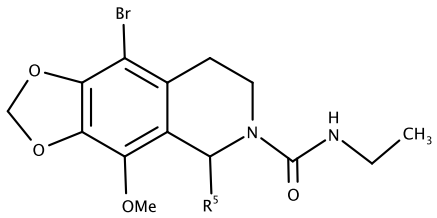

53 to **56**

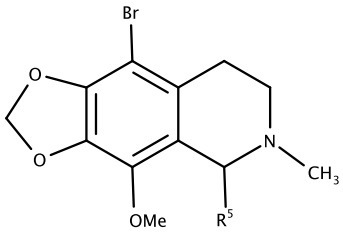

57 to **58**

No.	R^5	Arrest index			IC_{50} (µM)		
		MCF-7	PC3	PANC-1	MCF-7	PC3	PANC-1
53	Ph	INA	INA	INA	NA	NA	NA
54	2,3,4-OMePh	INA	INA	INA	NA	NA	NA
55	CH_2(Ph)	INA	INA	INA	NA	NA	NA
56	CH_2(3-OMePh)	294	117	101	54.3	9.5	8.9
57	Ph	INA	INA	INA	NA	NA	NA
58	CH_2(Ph)	INA	INA	INA	NA	NA	NA

Inactive (INA): arrest index ≤ 10
NA: IC_{50} was not assayed if arrest index ≤ 100

In summary, the biological evaluation of novel noscapine analogues and noscapine-like analogues further developed our understanding of the structure-activity relationships and revealed some promising cues for the next steps in designing more potent microtubule-depolymerizing agents. *N*-sulfonyl cyclic ether noscapine analogues had some activity in trapping cells in G_2/M phase compared with *N*-alkyl classes, but were not as potent as *N*-urea and *N*-thiourea classes. The studies indicated the importance of the THF moiety combined with 7-methoxy, or GBL coupled with 7-hydroxy, in developing more potent compounds compared with other combinations. The dioxolane moiety did not appear to offer any advantages. The most promising compound in this study was compound **38**, with IC_{50} values of 3.1, 1.1 and 2.5µM on MCF-7, PANC-1 and PC3 cell line respectively. However, although it is potent, this compound still not as potent as our second generation of Noscapine analogue (compound **2a** to **3**).

Chapter 7

Discussion and future implications

Glioblastoma multiform (GBM) is a lethal heterogeneous tumor population that appears to have its origin in neural stem cells within the subventricular zone of central nervous system (CNS). Recent studies show that the relapse and recurrence of GBM is a function of a small subpopulation of GBM cells, referred to as glioblastoma initiating cells (GICs), which are capable of self-renewal, proliferation and differentiation into the various cell types observed in GBM (Chen et al., 2012). GICs are typically resistant to chemotherapy and radiotherapy, and new approaches will be needed to modulate their activity (Bao et al., 2006; Chen et al., 2012). The malignancy and complication of this tumor bring difficulties and challenges in identification, isolation and characterization of the GICs targeted for specific therapeutics.

Currently there are no clinically approved biomarkers for GICs. A combination of embryonic stem cell (ESC) markers and neural stem cell (NSCs) markers are the most common approaches to identification and isolation (Galli et al., 2004; Singh et al., 2004). However, these markers still lack specificity for GICs. Recent proteomics and genomics analysis has identified consistently higher expression of a cell surface marker, CD9, in GICs, compared with normal neural stem cells (NSCs), which may provide a promising marker in the identification and isolation of GICs (Okawa et al., 2017).

Given the lack of detailed knowledge of GICs, the development of new identification markers for GICs, and a model of GICs, are expected to be helpful for basic research using GICs and for the development of drug therapies for GBM. One of the aims of this study was to establish a model of GICs and to use this model to identify potential therapeutic targets in GICs. The original idea to produce iPSCs from Cre-mediated

transgenic mouse *Pik3ca*^{H1047R}/*PTEN*$^{del/del}$ cell lines was discontinued due to the unexpected lack of success using our reprogramming strategy. This was disappointing, particularly because the lentiviral reprogramming system worked well with mouse embryonic fibroblasts, but became too time-consuming. Some suggestions were provided to promote reprogramming efficiency for future studies. The original reason for attempting to make iPSCs was that they should provide a good source of neural stem cells, whereas primary neurospheres from mouse brain have generally been described to be heterogeneous (Llieva and Dufva, 2013). In our study most of the cells in primary neurospheres were capable of clonal expansion of new spheres from single cells, suggesting that the neurospheres were a rich source of neural stem cells. This allowed the kinome profiling study (in Chapter 4) to make direct use of primary cells. The study identified some kinases that are over-expressed in mutant NPSCs. Notably FAK1, NEK1 and ROCK1 that are associated with GBM were upregulated, which gives some confidence in the method and suggests that other kinases identified may provide targets for future discovery for drug therapeutics. Moreover, the gene ontology analysis and protein interaction network analysis revealed that the proteasome system might be an important target to disrupt the functions of GICs. However, due to the time limitation of the PhD period, the investigation of phosphorylation of PI3K pathways on our *Pik3ca*^{H1047R}/*PTEN*$^{del/del}$ cells was limited to experiments conducted using the AKT signalling antibody array, which limited the identification of the range of the potential phosphorylation sites. Thus, future work should be more focused on identification of a broader range of phosphorylation sites, and the differences in phosphorylation between our control NPSCs and mutant *Pik3ca*^{H1047R}/*PTEN*$^{del/del}$ cells. Phosphorylation sites are related to PI3K signalling pathways could also be identified using the SILAC technique, which may provide an opportunity to identify the potential targets for discovery of kinase inhibitors for GICs treatment. In addition, as FAK1, NEK1 and ROCK1 were over-expressed in our mutant cells, future work towards investigation of the effects of any FAK1, NEK1 or ROCK1 inhibitors on our cells would be a valuable focus for investigation in the future.

The current standard treatments for GBM consist of maximal resection by surgery or radiation therapy, followed by adjuvant chemotherapies targeting either fast

proliferating non-GICs or recurrent-associated GICs (Ohba and Hirose, 2016; Szopa et al., 2017).

Recent genomic and molecular analysis from The Cancer Genome Atlas (TCGA) suggested the potential pathways and genetic aberrations involved in the regulation of proliferation, self-renewal and differentiation of GICs. As multiple concurrent mutations are common in GBM, and there are currently no individual therapeutics that can efficiently target GICs, the development of new therapeutic drugs for GBM treatment, or the use of new therapeutic modalities combining conventional treatments would be valuable. Therapeutic inhibitors targeted to the pathways specifically involved in regulation of self-renewal, proliferation and differentiation of GICs may shed on light on new treatment options for treating GBM. Although most cases of GBM are associated with the amplification of *EGFR* or the presence of EGFR protein variants, like EGFRvIII, there are limitations and difficulties in the development of therapeutics targeted to EGFR due to specific nature (Schulte et al., 2013). In addition, as the amplification of *EGFR* or the presence of EGFR variants are not used as prognostic markers for the median survival, this may also limit the therapeutic value of developing EGFR-associated targets. Current chemotherapies targeting IDH or RTK signaling pathways, so far, have shown limited efficacy in clinical trials (Huse and Holland, 2010). Thus, our studies addressed the discovery of potential targets involved in the PI3K signaling pathways specifically in GICs. The parallel studies on development of novel SANT-1 analogues and novel noscapine analogues are relevant in that they may provide agents for adjuvant or combinatorial approaches to therapeutics for GBM.

The existing inhibitors of Wnt, Shh, PI3K and Notch signaling pathways are good candidates for treating GICs. Combined therapeutic treatments with STAT3 inhibitor, STX-0119, and mTOR inhibitor, rapamycin, were recently reported to effectively suppress the TMZ-resistant glioma cells in vitro (Miyata et al., 2017). PF403 was recently reported to have promising effect on tumor growth inhibition for GBM, as PF403 can direct bind to Smoothened (SMO) receptor to inhibit the interaction of SMO with Patched 1 (Ptch1), thus disrupting the Hedgehog signaling pathway (Chen et al.,

2016). Current clinical Phase II and Phase III studies targeting GICs for recurrent GBM included using Erlotinib (van den Bent et al., 2009), Galunisertib (Brandes et al., 2016a), ezataurin (Wick et al., 2010), cediranib (Batchelor et al., 2013), bevacizumab (Taal et al., 2014; Wick et al., 2015), fotemustine (Brandes et al., 2016b) or their combinations. These approaches all showed effects on prolonged median survival, however, in the best case, the median survival was increased by five months, with most only for one or two months.

The investigations in this thesis on evaluation of novel SANT-1-derived small molecules identified some hints for future studies. The secondary aldimine (-N-N=CH-) functional group and piperazine structures presented in SANT-1 structure may be the key and essential structural composition in retaining the high potency as an antagonist. We identified three novel active SANT-1-derived small molecules, with the most effective IC_{50} at 0.2μM, which is around five fold less potent than SANT-1 (IC_{50}=40nM). Recent structural studies conducted by de Sauvage's group (Sharpe et al., 2015) investigated the cocrystal structures of SMO and revealed two key binding sites within SMO that in particular interacted with small molecule regulators, one is in the transmembrane (TM) helical domain which forms a deep hydrophobic pocket, and the other binding site is in an extracellular domain (ECD) of SMO. The same study (Sharpe et al., 2015) identified a common feature of three residues, including Asp384, Tyr394 and Glu518, in SMO that are capable of interacting with small molecules. Thus, this part of study, together with the information revealed by de Sauvage's group, provided a clue to synthesize our next generation of SANT-1 derivatives that may offer additional insights for potential GBM therapeutics or chemotherapy for other Hh-signalling associated tumors.

Apart from direct targeting GICs, the development for radiation and chemotherapy for proliferative non-GICs are also within the regime of discovery. To date, Temozolomide (TMZ) is still the main standard chemotherapy for GBM (Wilson et al., 2014). However, due to the high administrative dose and a series of side effects, there is a need to find a way to improve the efficacy and to reduce the side effects of TMZ, or to develop alternative drugs for TMZ. Previous studies by European Organization for Research and Treatment of Cancer Brain Tumour and Radiation Oncology Group, together with the

National Cancer Institute for Canada demonstrated that, with the combination of radiation therapy followed by TMZ, the time of median survival was significantly increased for patients with GBM compared with treatment with radiation therapy or TMZ alone, in a Phase III study (Stupp et al., 2009). The combination therapy of TMZ with GDC-0941 (Shi et al., 2017), nimotuzumab (Nitta et al., 2016), Shikonin (Matias et al. 2017), Tubastatin A (Li et al., 2017), or lithium (Han et al., 2017) all showed promising results in relation to decreased cell proliferation, cell migration, drug resistance and tumor recurrence compared with using TMZ alone in newly diagnosed GBM patients. These reports all suggest a future modality for GBM, using TMZ concomitant with other adjuvant drugs. In addition, TMZ delivery using biodegradable nanocarriers, such as polysorbate-80 coated polybutylcyanoacrylate nanoparticles (Tian et al., 2011) and PLGA nanoparticles (Ling et al., 2012; Jain et al., 2014), is now being widely studied to reduce side effects and alleviate the problems caused by poor drug delivery across the BBB into brain.

The most promising alternatives to TMZ are cucurmin, nimotuzumab, bevacizumab and ZOL-loaded transferrin-PEGylated nanoparticles. Cucurmin shows ability to cross the BBB to inhibit brain tumor growth (Purkayastha et al., 2009) and promotes differentiation of GICs (Zhuang et al., 2012). Nimotuzumab, a humanized anti-EGFR antibody, demonstrated a significant effect on inhibition of the cell proliferation and angiogenesis, and promoted the sensitivity of glioma cells to radiation therapy (Solomon et al., 2013) and TMZ therapy (Nitta et al., 2016). Particularly when the glioma cells had amplification of EGFR or mutant EGFRvIII. This antibody may provide future strategies for newly diagnosed GBM patients with aberrant EGFR status. However, recurrent GICs were still resistant either in the combination therapy with TMZ (Nitta et al., 2016) or when administed its antibody alone. Bevacizumab, a monoclonal antibody targeting vascular endothelial growth factor (VEGF), which is capable of blocking the VEGF pathway, thus inhibiting the cell proliferation and angiogenesis, was initially approved for GBM treatment in 2009 due to a high response rate (Cohen et al., 2009). However, based on some Phase III studies (Chinot et al., 2014; Gilbert et al., 2014), this drug has failed to show any beneficial effects on overall median survival, for newly diagnosed GBM patients or patients with recurrent GBM,

and has been associated with some adverse effects (Narita Y, 2015; Field et al., 2015). The use of bevacizumab still remains controversial, as the heterogeneity of GBM really influences the activity of the cell response. Thus, future trials are needed to obtain more relevant data.

One obstacle for GBM treatment is the presence of the blood-brain barrier (BBB) that prevents most drugs getting access to the brain. One promising strategy in the future for targeted brain delivery would be use of direct injection of nano-carriers, like PLGA nanoparticles or silver nanoparticles (Liang et al., 2017), to overcome the inability of drugs to cross the BBB, as well as to minimize the serious cytotoxicity side effects which result from chemotherapeutics. Another strategy is to continue developing and modifying the current potential compounds that are capable of crossing the BBB. Researchers (Landen et al., 2004) found that the opium alkaloid noscapine may have potential for the treatment of GBM, as noscapine shows the ability to cross the blood-brain barrier. Noscapine can also inhibit the growth of glioblastoma cells, and shows synergistic anti-tumor activities on glioblastoma cells *in vivo* when combined with FDA-approved traditional drugs including temozolomide (TMZ), bis-chloroethylnitrosourea (BCNU) or cisplatin (CIS) (Qi et al., 2013).

In this study, as discussed in Chapter 6, novel noscapine analogues synthesized from our department (Monash Institute of Pharmaceutical Science) were also evaluated. These noscapine analogues are third generation agents with new modifications to the structure of noscapine. One (compound **38**) with promising efficacy on all tested cell lines MCF-7, PANC-1 and PC3 has EC_{50} values of 3.1, 1.1 and 2.5µM respectively. However, it will be necessary to develop compounds with even a better efficacy, and these novel analogues need to undergo pharmacokinetics study for further investigation *in vivo.* The development of noscapine analogues may provide opportunity to improve therapeutic outcomes for treating GBM as well as other solid tumors.

There is scope for future work towards development of clinical candidates based on SANT-1 derivatives or more potent selective noscapine-like analogues. The studies

reported here as well as previous studies conducted at MIPS on noscapine analogues have identified lead compounds and a basis for collaborative studies that could be conducted together with our department of medicinal chemistry. In addition, those SANT-1 derivatives or noscapine-like analogues that are shown to be promising anti-cancer agents would be valuable agents to test on our *Pik3ca*^{H1047R}*/PTEN*$^{del/del}$ cell lines to investigate the effects of both lasses of drugs on the glioblastoma stem cell model. This would also require establishing a new test system to evaluate the effects of using SANT-1 derivatives and noscapine-like analogues on our neural cell lines.

An alternative approach to prolong the median survival of GBM patients, is the development of immunotherapies, such as the development of DCVav-L, based on the cancer vaccine hypothesis. This is a dendritic cell vaccine, which has shown improvement in median survival of GBM patients and this vaccine is currently undergoing phase III studies (Chang et al., 2011; Ardon et al., 2012). This may bring more opportunities for the fight against the GBM cells.

In summary, future work towards developing therapies for GBM will likely combine the development or modification of traditional therapies with new innovative immunotherapies. Current standard care of TMZ or radiotherapy to kill or arrest fast proliferating tumor cells could be more beneficial if incorporated into glioma cell-targeted nanocarriers. Adjuvant therapies targeting kinases overexpressed in GBM may become valuable components of drug therapy. This study provided some hints on potential therapeutic targets identified by proteomics studies, provided more information about improvements for new generations of SANT-1 derivatives and noscapine analogues, both of which may be useful for the generation of therapeutic drugs for GBM treatment in the future.

References

Abdouh M, Facchino S, Chatoo W, Balasingam V, Ferreira J, Bernier G (2009). BMI1 sustains human glioblastoma multiforme stem cell renewal. *Neurobiology of Desease* **29**:8884-8896.

Adams JM and Strasser A (2008). Is tumor growth sustained by rare cancer stem cells or dominant clones. *Cancer Res* **68**:4018-4021

Anido A, Saez-Borderias A, Gonzalez-Junca A, Rodon L, Folch G, Carmona MA, Prieto-Sanchez RM, Barba I, Martinez-Saez E, Prudkin L, Cuartas I, Raventos C, Martinez-Ricarte F, Poca MA, Garcia-Dorado D, Lahn MM, Yingling JM, ROdon J, Sahuquillo J, Baselga J, Seoane J (2010). TGF-β receptor inhibitors target the CD44 (high)/Id1 (hight) glioma-initiating cell population in human glioblastoma. *Cancer Cell* **18**:655-668.

Ardon, H, van Gool SW, Verschuere T, Maes W, Fieuws S, Sciot R, Wilms, G, Demaerel P, Goffin J, van Calenbergh F, Menten J, Clement P, Debiec-Rychter M, De Vleeschouwer S (2012). *Cancer Immuno Immunother* **61**:2033-2044.

Arias-Carrion O (2008). Basic mechanisms of rTMS: Implications in Parkinson's disease. *Int Arch Med* **1**:2.

Ayers KL, Therond PP (2010). Evaluating Smoothened as a G-protein-coupled receptor for Hedgehog signaling. *Trends Cell Biol* **20**:287-298.

Ballabh P, Braun A, Nedergaard M (2004). The blood-brain barrier: an overview: structure, regulation and clinical implication. *Neurobiol Dis* **16**:1-13.

Bao S, Wu Q, Li Z, Sathornsumetee S, Wang H, McLendon RE, Hjelmeland AB, Rich JN (2008). Targeting cancer stem cells through L1CAM suppresses glioma growth. *Cancer Res* **68**:6043-6048.

Bao S, Wu Q, McLendon RE, Hao Y, Shi Q, Hjelmeland AB, Dewhirst MW, Bigner DD, Rich JN (2006). Glioma stem cells promote radioresistance by preferential activation of the DNA damage response. *Nature* **444**:756-760.

Bar EE, Chaudhry A, Lin A, Fan X, Schreck K, Matsui W, Piccirillo S, Wescovi AL, Dimeco F, Olivi A, Eberhart CG (2007). Cyclopamine-mediated hedgehog pathway inhibition depletes stem-like cancer cells in glioblastoma. *Stem Cells* **25**:2524-2533.

Barzi M, Berenguer J, Menendez A, Alvarez-Roderiguez R Pons S (2010). Sonic-hedgehog-mediated proliferation requires the localization of PKA to the cilium base. *Journal of Cell Science* **123**:62-69.

Batchelor TT, Mulholland P, Neyns B, Nabors LB, Campones M, Wick A, Mason W, Mikkelsen T, Phuphanich S, Ashby LS, Degroot J, Gattamaneni R, Cher L, Rosenthal M, Payer F, Jurgensmeier JM, Jain RK, Sorensen AG, Xu J, Liu Q, van den Bent M (2013). Phase III randomized trial comparing the efficacy of cediranib as monotherapy, and in combination with lomustine, versus lomustine alone in patients with recurrent globlastoma. *J Clin Oncol* **31**:3212-3218.

Berman DM, Desai N, Wang X, Karhadkar SS, Reyon M, Abate-Shen C, Beachy PA, Shen MM (2004). Roles for Hedgehog signaling in androgen production and prostate ductal morphogenesis. *Dev Biol* **267**:387-398.

Berman DM, Karhadkar SS, Hallahan AR, Pritchard JI, Eberhart CG, Watkins DN, Chen JK, Cooper MK, Taipale J, Olson JM, Beachy PA (2002). Medulloblastoma growth inhibition by hedgehog pathway blockade. *Science* **297**:1559-1561.

Bock C, Kiskinis E, Verstappen G, Gu H Boulting G, Smith ZD, Ziller M, Croft GF, Amoroso MW, Oakley DH (2011). Reference maps of human ES and iPS cell variation enable high-throughput characterization of pluripotent cell lines. *Cell* **144**:439-452.

Boulting GL, Kiskinis E, Croft GF, Amoroso MW, Oakley DH, Wainger BJ, Williams DJ, Kahler DJ, Yamaki M, Davidow L (2011). A functionally characterized test set of human induced pluripotent stem cells. *Nature Biotechnology* **29**: 279-286.

Brambrink T, Foreman R, Welstead GG, Lengner C, Wernig M, Suh H, Jaenisch R (2008). Sequential expression of pluripotency markers during direct reprogramming of mouse somatic cells. *Cell Stem Cell* **2**:151-159.

Brandes AA, Carpentier AF, Kesari S, Sepulveda-Sanchez JM, Wheeler HR, Chinot O, Cher L, Steinbach JP, Capper D, Specenier P, Rodeon J, Cleverly A, Smith C, Gueorguieva I, Miles C, Guba SC, Desaiah D, Lahn MM, Wick W (2016a). A phase II randomized study of galunisertib monotherapy or galunisertib pluas lomustine compared with lomusting monotherapy in patiernts with recurrent Glioblastoma. *Neuro Oncology* **18**:1146-1156.

Brandes AA, Finocchiaro G, Zagonel V, Reni M, Caserta C, Fabi A, Clavarezza M, Maiello E, Eoli M, Lombardi G, Monteforte M, Proietti E, Agati R, Eusebi V, Franceschi E (2016b). AVAEGE: a phase II, randomized, noncomparative study of fotemustine or bevacizumab for patients with recurrent Glioblastoma. *Neuro Oncology* **18**:1304-1312.

Briscoe J, Therond PP (2013). The mechanisms of hedgehog signaling and its roles in development and disease. *Nature Reviews Molecular Cell Biology* **14**:416-429.

Buckley SM, Aranda-Origilles B, Strikoudis A, Apostolou E, Loizou E, Moran-Crusio K, Farnsworth CL, Koller AA, Dasgupta R, Silva JC et al (2012). Regulation of pluripotency and cellular reprogramming by the ubiquitin-proteasome system. *Cell Stem Cell* **11**:783-798.

Cancer Genome Atlas Research Network (2008). Comprehensive genomic characterization defines human glioblastoma genes and core pathways. *Nature* **455**:1061-1068.

Cantley LC (2002). The phosphoinositide 3-kinase pathway. *Science* **296**:1655-1657.

Cao XX, Xu JD, Xu JW, Liu XL, Cheng YY, Li QQ, Xu ZD, Liu XP (2011). ROCK1 promotes breast carcinoma migration/metastasis via activation of the RhoA/Rho kinase pathway. *Breast Cancer Res Treat* **126**:555-563.

Capdevila C, Rodriguez-Vazquez L, Marti J (2017). Glioblastoma Multiforme and Adult Neurogenesis in the Ventricular-Subventricular Zone: A Review. *J Cell Physio* **232**:1596-1601.

Chalhoub N, Baker SJ (2009). PTEN and the PI3-kinase pathway in cancer. *Annu Rev Pathol* **4**:127-150.

Chang CN, Huang YC, Yang DM, Kikuta K, Wei KJ, Kubota T, Yang WK (2011). A phase I/II clinical trial investigating the adverse and therapeutic effects of a postoperative autologous dendritic cell tumor vaccine in patients with malignant glioma. *J Clin Neurosci* **18**:1048-1054.

Chen J, Lv H, Hu J, Ji M, Xue N, Li C, Ma S, Zhou Q, Lin B, Li Y, Yu S, Chen X (2016). CAT3, a novel agent for medulloblastoma and Glioblastoma treatment, inhibits tumor growth by disrupting the hedgehog signaling pathway. *Cancer Lett* **381**:391-403.

Chen JK, Taipale J, Cooper MK, Peachy PA (2002). Inhibition of Hedgehog signaling by direct binding of cyclopamine to Smootherned. *Genes Dev* **16**:2743-2748.

Chen JK, Taipale J, Young KE, Maiti T, Beachy PA (2002). Small molecule modulation of Smoothened activity. *PNAS* **99**: 14071-14076.

Chen Y, Chen CF, Polci R, Wei R, Riley DJ, Chen PL (2014). Increased Nek1 expression in renal cell carcinoma cells is associated with decreased sensitivity to DNA-damaging treatment. *Oncotarget* **5**:4283-4294.

Chen Y, Chen CF, Riley DJ, Chen PL (2011). Nek1 kinase functions in DNA damage response and checkpoint control through a pathway independent of ATM and ATR. *Cell cycle* **10**:655-663.

Chinot OL, Wick W, Mason W, Henriksson R, Saran F, Nishikawa R, Carpentier AF, Hoan-Xuan K, Kavan P, Cernea D, Brandes AA, Hilton M, Abrey L, Cloughesy T (2014). Bevacizumab plus radiotherapy-temozolomide for newly diagnosed gliobalstoma. *N Engl J Med* **370**:709-722.

Chu Q, Orr BA, Semenkow S, Bar EE, Eberhart CG (2013). Prolonged inhibition of Glioblastoma xenograft initiation and clonogenic growth flowing *in vivo* Notch blockade. *Clin Cancer Res* **19**:3224-3233.

Clevers H (2006). Wnt/β-Catenin signaling in development and disease. *Cell* **127**:469-480.

Cohen MH, Shen YL, Keegan P, Pazdur R. FDA drug approval summary: bevacizumab (Avastin) as treatment of recurrent glioblastoma multiforme. *Oncologist* **14**:1131-1138.

Conti L, Pollard SM, Gorba T, Reitano E, Toselli M, Biella G, Sun Y, Sanzone S, Ying QL, Cattaneo E, Smith A (2005). Niche-independent symmetrical self-renewal of a mammalian tissue stem cell. *PLoS Biology* **3**:1594-1606.

Cui W, Wang LH, Wen YY, Song M, Li BL, Chen XL, Xu M, An SX, Zhao J, Lu YY, Mi XY, Wang EH (2010). Expression and regulation mechanisms of Sonic Hedgehog in breast cancer. *Cancer Sci* **101**:927-933.

Dahmane N, Sanchez P, Gitton Y, Palma V, Sun T, Beyna M, Weiner H, Altaba AR (2001). The Sonic Hedgehog-Gli pathway regulates dorsal brain growth and tumorigenesis. *Development* **128**:5201-5212.

Daneman R (2012). The blood-brain barrier in health and disease. *Ann Neurol* **72**:648-672.

Dawe HR, Farr H, Gull K (2007). Centriole/basal body morphogenesis and migration during cliogenesis in animal cells. *J Cell Sci* **120**:7-15

DeBono AJ, Mistry SJ, Xie JH, Muthiah D, Phillips J, Ventura S, Callaghan R, Pouton CW, Capuano B, Scammells PJ (2014). Sythesis and biological evaluation of a functionalized derivatives of Noscapine as cytotoxic agents. *ChemMedChem* **9**:399-410.

DeBono AJ, Xie JH, Ventura S, Pouton CW, Capuano B, Scammells PJ (2012). Synthesis and biological evaluation of *N*-substituted Noscapine analogues. *ChemMedChem* **7**:2122-2133.

Doetch F, Petreanu L, Caille I, Garcia-Verdugo JM, Alvarez-Buylla A (2002). EGF converts transit-amplifying neurogenic precursors in the adult brain into multipotent stem cells. *Neuron* **36**:1021-1034.

Doetsch F, Caille I, Lim DA, Garcia-Verdugo JM, Alvarez-Buylla A (1999). Subventricular zone astrocytes are neural stem cells in the adult mammalian brain. Cell **97**:703-716.

Efe JA, Hilcove S, Kim J, Zhou H, Ouyang K, Wang G, Chen J, Ding S (2011). Conversion of mouse fibroblasts into cardiomyocytes using direct reprogramming strategy. *Nature Cell Biology* **13**:215-222.

Ehtesham M, Sarangi A, Valadez JG, Chanthaphaychith S, Becher MW, Abel TW, Thompson RC, Cooper MK (2007). Ligand-dependent activation of the hedgehog pathway in glioma progenitor cells. *Oncogene* **26**:5752-5761.

Eng LF, Ghirnikar RS, Lee YL (2000). Glial fibrillary acidic protein: GFAP-thirty-one years (1969-2000). *Neurochemical Research* **25**:1439-1451.

Epstein EH (2008). Basal cell carcinomas: attack of the hedgehog. *Nat. Rev. Cancer* **8**:743-754.

Eyler CE, Foo WC, LaFiura KM, McLendon RE, Hjelmeland AB, Rich JN (2008). Brain cancer stem cells display preferential sensitivity to Akt inhibition. *Stem Cells* **26**:3027-3036.

Fan X, Khaki L, Zhu TS, Soules ME, Talsma CE, Gul N, Koh C, Zhang J, Li YM, Maciaczyk J, Nikkhah G, Dimeco F, Piccirillo S (2010). NOTCH pathway blockade depletes CD133-positive Glioblastoma cells and inhibits growth of tumor neurospheres and xenografts. *Stem Cells* **28**:5-16.

Fellner C (2012) Vismodegib (Erivedge) for advanced basal cell carcinoma. *P T* **37**:673-677.

Feng J, White B, Tyurina OV, Guner B, Larson T, Lee HY, Karlstrom RO, Kohtz JD (2004). Synergistic and antagonistic roles of the Sonic hedgehog N- and C-terminal lipids. *Development* **131**:4357-4370.

Ferlay J, Soerjomataram I, Ervik M, Dikshit R, Eser S, Mathers C, Rebelo M, Parkin DM, Forman D, Bray F (2015). Cancer incidence and mortality worldwide: sources, methods and major patterns in 2012. *Int J Cancer* **136**:E359-86.

Field KM, Jordan JT, Wen PY, Rosenthal MA, Reardon DA (2015). Bevacizumab and Glioblastoma: scientific review, newly reported updates, and ongoing controversies. *Cancer* **121**:997-1007.

Filby A, Day W, Purewal S, Martinez-Martin N (2016). The analysis of cell cycle, proliferation, and asymmetric cell division by imaging flow cytometry. *Methods Mol Biol* **1389**:71-95.

Flahaut M, Meier R, Coulon A, Nardou KA, Niggli FK, Martinet D, Beckmann JS, Joseph JM, Muhlethaler-Mottet A, Gross N (2009). The Wnt receptor FZD1 mediates chemoresistance in neuroblastoma through activation of the WNT/β-caternin pathway. *Oncogene* **28**:2245-2256.

Friday BB, Anderson SK, Buckner J, Yu C, Giannini C, Geoffroy F, Schwerkoske J, Mazurczak M, Gross H, Pajon E, et al., (2012). Phase II trial of vorinostat in combination with bortezomib in recurrent glioblastoma: a north central cancer treatment group study. *Neuro Oncol* **14**:215-221.

Furnari FB, Fenton T, Bachoo RM, Mukasa A, Stommel JM, Stegh A, Hahn WC, Ligon KL, Louis DN, Brennan C, Chin L, DePinho RA, Cavenee WK (2007). Malignant astrocytic glioma: genetics, biology, and paths to treatment. *Genes Dev* **21**:2683-2710.

Gage FH (2000). Mammalian neural stem cells. *Science* **287**:1433-1438.

Galli R, Binda E, Orfanelli U, Cipelletti B, Gritti A, De Vitis S, Fiocco R, Foroni C, Dimeco F, Vescovi A (2004). Isolation and characterization of tumorigenic, stem-like neural precursors from human glioblastoma. *Cancer Res* **64**:7011-7021.

Gallia GL, Tyler BM, Hann CL, Siu IM, Giranda VL, Vescovi AL, Brem H, Riggins GJ (2009). Inhibition of Akt inhibits growth of glioblastoma and glioblastoma stem-like cells. *Mol Cancer Ther* **8**:386-393.

GBD 2015 Disease and Injury Incidence and Prevalence Collaborators (2016). Global, regional, and national incidence, prevalence, and years lived with disability for 310 diseases and injuries, 1990-2015: a systematic analysis for the Global Burden of Disease Study 2015. *Lancet* **388**:1545-1602.

Gilbert CA, Daou MC, Moser RP, Ross AH (2010). Gamma-secretase inhibitors enhance temozolomide treatment of human gliomas by inhibiting neurospheres repopulation and xenograft recurrence. *Cancer Res* **70**:6870-6879.

Gilbert MR, Dignam JJ, Armstrong TS, Wefel JS, Blumenthal DT, Vogelbaum MA, Colman H, Chakravarti A, Pugh S, Won M, Jeraj R, Brown PD, Jaeckle KA, Schiff D, Stieber VW, Brachman DG, Werner-Wasik M, Tremont-Lukats IW, Sulman EP, Aldape KD, Curran WJ Jr, Mehta MP (2014). A randomized trial of bevacizumab for newly diagnosed Glioblastoma. *N Engl J Med* **370**:699-708.

Gilbertson RJ, Rich JN (2007). Making a tumor's bed: glioblastoma stem cells and the vascular niche. *Nature reviews* **7**:733-736.

Gong A, Huang S (2012). FoxM1 and Wnt/β-catenin signaling in glioma stem cells. *Cancer Res* **72**:5658-5662.

Gu C, Banasavadi-Siddegowda YK, Joshi K, Nakamura Y, Kurt H, Gupta S, Nakano I (2013). Tumor-specific activation of the c-JUN/MELK pathway regulates glioma stem cell growth in a p53-dependent manner. *Stem Cells* **31**:870-881.

Guenther MG, Frampton GM, Soldner F, Hockemeyer D, Mitalipova M, Jaenisch R, Young RA (2010). Chromatin structure and gene expression programs of human embryonic and induced pluripotent stem cells. *Cell Stem Cell* **7**:249-257.

Hamaya K, Doi K, Tanaka T, Nishimoto A (1985). The determination of glial fibrillary acidic protein for the diagnosis and histogenetic study of central nervous system tumors: a study of 152 cases. *Acta Med Okayama* **39**:453-462.

Han S, Meng L, Jiang Y, Cheng W, Tie X, Xia J, Wu A (2017). Lithium enhances the antitumour effect of temozolomide against TP53 wild-type Glioblastoma cells via NFAT1/FasL signaling. *Br J Cancer* doi:1038/bjc.2017.89.

Hayes O, Ramos B, Rodriguez LL, Aguilar A, Badia T, Castro FO (2005). Cell confluency is as efficient as serum starvation for inducing arrest in the G0/G1 phase of the cell cycle in granulosa and fibroblast cells of cattle. *Anim Reprod Sci* **87**:181-192.

Hebard LW, Maurer J, Miller A, Lesperance J, Hassell J, Oshima RG, Terskikh AV (2010). Maternal embryonic leucine zipper kinase is upregulated and required in mammary tumor-initiating cells in vivo. *Cancer Res* **70**:8863-8873.

Hoa N, Ge L, Kuznetsov Y, McPherson A, Cornforth AN, Pham JT, Myers MP, Ahmed N, Salsman VS, Lamb LS Jr, Bowersock JE, Hu Y, Zhou YH, Jadus MR (2010). Glioma cells display complex cell surface topogrphies that resist the actions of cytolytic effector lymphocytes. *J Immunol* **185**:4793-4803.

Hu Y, Smyth GK (2009). ELDA: extreme limiting dilution analysis for comparing depleted and enriched populations in stem cell and other assays. *J Immunol Methods* **347**:70-78.

Huse JT, Holland EC (2010). Targeting brain cancer:advances in the molecular pathology of malignant glioma and medulloblastoma. *Nature Reviews Cancer* **10**:319-331.

Ieda M, Fu JD, Delgado-Olguin P, Vedantham V, Hayashi Y, Bruneau BG, Srivastava D (2010). Direct reprogramming of fibroblasts into functional cardiomyocytes by defined factors. *Cell* **143**:375-386.

Imura T, Kornblum HI, Sofroniew MV (2003). The predominant neural stem cell isolated fro postnatal and adult forebrain but not early embryonic forebrain expresses GFAP. *J Neurosci* **23**:2824-2832.

Izumoto S, Ohnishi T, Arita N, Hiraga S, Taki T, Hayakawa T (1996). Gene expression of neural cell adhesion molecule L1 in malignant gliomas and biological significance of L1 in glioma invasion. *Cancer Research* **56**:1440-1444.

Jackson EL, Garcia-Verdugo JM, Gil-Perotin S, Roy M, Quinones-Hinojosa A, VandenBerg S, Alvarez-Buylla A (2002). PDGFRα-positive B cells are neural stem cells in the adult SVZ that form glioma-like growths in response to increased PDGF signaling. *Neuron* **51**:187-199.

Jacque CM, Vinner C, Kujas M, Raoul M, Racadot J, Baumann NA (1978). Determination of glial fibrillary acidic protein (GFAP) in human brain tumors. *Journal of the Neurological Sciences* **35**:147-155.

Jacques TS, Swales A, Brzozowshi MJ, Henriquez NV, Linehan JM, Mirzadeh Z, Malley CO, Naumann H, Alvarez-Buylla A, Brandner S (2010). Combinations of genetic mutations in the adult neural stem cell compartment determine brain tumour phenotypes. *The EMBO Journal* **29**: 222-235.

Jain DS, Athawale RB, Bajaj AN, Shrikhande SS, Goel PN, Nikam Y, Gude RP (2014). Unraveling the cytotoxic potential of temozolomide loaded into PLGA nanoparticles. *Daru* **22**:18-26.

Jhaveri N, Cho H, Torres S, Wang WJ, Schonthal AH, Petasis NA, Louie SG, Hofman FM, Chen TC (2011). Noscapine inhibits tumor growth in TMZ-resistant gliomas. *Cancer Letters* **312**:245-252.

Jimeno A, Weiss GJ, Jr WHM, Gettinger S, Eigl BJC, Chang ALS, Dunbar J, Devens S, Faia K, Skliris G, Kutok J, Lewis KD, Tibes R, Sharfman WH, Ross RW, Rudin CM (2013). Phase I study of the hedgehog pathway inhibitor IPI-926 in adult patients with solid tumors. *Clin Cancer Res* **19**:2766-2774.

Johansson CB, Momma S, Clarke DL, Risling M, Lendahl U, Frisen J (1999). Identification of a neural stem cell in the adult mammalian central nervous system. *Cell* **96**:25-34.

Johnson DR, Fogh SE, Giannini C, Kaufmann TJ, Raghunathan A, Theodosopoulos PV, Clarke JL (2015). Case-based review: newly diagnosed glioblastoma. *Neuro Oncology Practice* **2**:106-121.

Jung CS, Foerch C, Schanzer A, Heck A, Plate KH, Seifert V, Steinmetz H, Raabe A, Sitzer M (2007). Serum GFAP is a diagnostic marker for glioblastoma multiforme. *Brain* **130**:3336-3341.

Kaur N, Chettiar S, Rathod S, Rath P, Muzumdar D, Shaikh ML, Shiras A (2013). Wnt3a mediated activation of Wnt/β-catenin signaling promotes tumor progression in glioblastoma. *Mol Cell Neurosci* **54**:44-57.

Kempermann G, Gage FH (1999). New nerve cells for the adult brain. *Sci Am* **280**:48-53.

Kenney-Herbert E, Al-Mayhani T, Piccirillo SGM, Fowler J, Spiteri I, Jones P, Watts C (2015). CD15 expression does not identify a phenotypically or genetically distinct glioblastoma population. *Stem Cells Transl Med* **4**:822-831.

Kim J, Kato M, Beachy PA (2009). Gli2 trafficking links Hedgehog-dependent activation of Smoothened in the primary cilium to transcriptional activation in the nucleus. *Proc Natl Acad Sci USA* **106**:21666-21671.

Kim K, Zhao R, Doi A, Ng K, Unternaehrer J, Cahan P, Huo H, Loh YH, Aryee MJ, Lensch MW, Li H, Collins JJ, Feinberg AP, Daley GQ (2011). Donor cell type can influence the epigenome and differentiation potential of human induced pluripotent stem cells. *Nat Biotechnol* **29**:1117-1119.

Kinross KM, Montgomery KG, Kleinschmidt M, Waring P, Ivetac I, Tikoo A, Saad M, Hare L, Roh V, Mantamadiotis T, Sheppard KE, Ryland GL, Campbell IG, Gorringe KL, Christensen JG, Cullinane C, Hicks RJ, Pearson RB, Johnstone RW, McArthur GA, Phillips WA (2012). An activating *Pik3ca* mutation coupled with *Pten* loss is sufficient to initiate ovarian tumorigenesis in mice. *The Journal of Clinical Investigation* **122**:553-557.

Kita D, Yonekawa Y, Weller M, Ohgaki H (2007). *PIK3CA* alterations in primary (de novo) and secondary glioblastomas. *Acta Neuropathol* **113**:295-302.

Knobbe CB, Reifenberger G (2003). Genetic alterations and aberrant expression of genes related to the phosphatidyl-inositol-3'-kinase/protein kinase B (Akt) signal transduction pathway in glioblastomas. *Brain Pathol* **13**:507-518.

Koten JW, Neijt JP, Zonnenberg BA, Den-Otter W (1993). The difference between benign and malignant tumours explained with the 4-mutatin paradigm for carcinogenesis. *Anticancer Res* **13**:1179-1182.

Krauss S, Concordet JP, Ingham PW (1993). A functionally conserved homolog of the *Drosophila* segment polarity gene hh is expressed in tissues with polarizing activity in zebrafish embryos. *Cell* **75**:1431-1444.

Kreso A, Dick JE (2014). Evolution of the cancer stem cell model. *Cell Stem Cell* **14**:275-291.

Lalit PA, Salick MR, Nelson DO, Squirrell JM, Shafer CM, Patel NG, Saeed I, Schmuck EG, Markandeya YS, Wong R, Lea MR, Eliceiri KW, Hacker TA, Crone WC, Kyba M, Garry DJ, Stewart R, Thomson JA, Downs KM, Lyons GE, Kamp TJ (2016). Lineage Reprogramming of fibroblasts into proliferative induced cardiac progenitor cells by defined factors. *Cell Stem Cell* **18**:354-367.

Lan F, Pan Q, Yu H, Yue X (2015). Sulforaphane enhances temozolomide-induced apoptosis because of down-regulation of miR-21 via WNT/β-caternin signaling in glioblastoma. *J Neurochem* **134**:811-818.

Landen JW, Hau V, Wang M, Davis T, Ciliax B, Wainer BH, Van Meir EG, Glass JD, Joshi HC, David RA (2004). Noscapine crosses the blood-brain barrier and inhibits Glioblastoma growth. *Clinical Cancer Research* **10**:5187-5201.

Lee JK, Chang N, Yoon Y, Yang H, Cho H, Kim E, Shin Y, Kang W, Oh YT, Mun GI, Joo KM, Nam DH, Lee J (2016). USP1 targeting impedes GBM growth by inhibiting stem cell maintenance and radioresistance. *Neuro Oncol* **18**:37-47.

Li Y, Lu H, Huang Y, Xiao R, Cai X, He S, Yan G (2010). Glycogen synthase kinases-3beta controls differentiation of malignant Glioma cells. *Int J Cancer* **127**:1271-1282.

Li ZY, Zhang C, Zhang Y, Chen L, Chen BD, Li QZ, Zhang XJ, Li WP (2017). A novel HDAC6 inhibitor Tubastatin A: controls HDAC6-p97/CVP-mediated ubiuitination-autophagy turnover and reverses temozolomide-induced ER stress-tolerance in GBM cells. *Cancer Lett* **391**:89-99.

Liang P, Shi HM, Zhu WG, Gui QF, Xu Y, Meng JF, Guo XY, Gong Z, Cheng HQ (2017). Silver nanoparticles enhance the sensitivity of temozolomide on human glioma cells. *Oncotarget* **8**:7533-7539.

Ling Y, Wei K, Zou F, Zhong S (2012). Temozolomide loadedPLGA-based superparamagnetic naoparticales for magnetic resonance imaging and treatment of malignant glioma. *Int J Pharm* **430**:266-275.

Lipinski RJ, Hutson PR, Hannam PW, Nydza RJ, Washington IM, Moore RW, Girdaukas GG, Peterson RE, Bushman W (2008). Dose- and route- dependent teratogenicity, toxicity, and pharmacokinetic profiles of the hedgehog signaling antagonist cyclopamine in the mouse. *Toxicol Sci* **104**:189-197.

Liu K, Wang F, Ye XY, Wang LL, Yang J, Zhang JZ, Liu L (2014). KSR-based medium improves the generation of high-quality mouse iPS cells. *PLOS ONE* **9**(8): e105309.

Liu L, Luo GZ, Yang W, Zhao X, Zheng Q, Lv Z, Li W, Wu HJ, Wang L, Wang XJ (2010). Activation of the imprinted Dlk1-Dio3 region correlates with pluripotency levels of mouse stem cells. *The Journal of Biological Chemistry* **285**:19483-19490.

Llieva M, Dufva M (2013). SOX2 and OCT4 mRNA-expressing cells, detected by molecular beacons, localize to the center of neurospheres during differentiation. *PLoS One* **8**:e73669.

Louis DN, Perry A, Reifenberger G, von Deimling A, Figarella-Branger D, Cavenee WK, Ohgaki H, Wiestler OD, Kleihues P, Ellison DW (2016). The 2016 World Health Organization classification of tumors of the central nervous system: asummary. *Acta Neuropathol* **131**:803-820.

MacDonald BT, Tamai K, He X (2009). Wnt/beta-catenin signaling: components, mechanisms and diseases. *Dev Cell* **17**:9-26.

Mahindroo N, Punchihewa C, Fujii N (2009). Hedgehog-Gli signaling pathway inhibitors as anticancer agents. *J Med Chem* **52**:3829-3845.

Manoranjan B, Wang X, Hallett RM, Venugopal C, Mack SC, McFarlane N, Nolte SM, Scheinemann K, Gunnarsson T, Hassell JA, Taylor MD, Lee C, Triscott J, Foster CM, Dunham C, Hawkins C, Dunn SE, Singh SK (2013). FoxG1 interacts with Bmi1 to regulate self-renewal and tumorigenicity of medulloblastoma stem cells. *Stem Cells* **31**:1266-1277.

Martini FH, Timmons MJ, Tallitsch RB (2012). *Human anatomy* (7th ed.). Boston: Benjamin Cummings.

Matias D, Balca-Silva J, Dubois LG, Pontes B, Ferrer VP, Rosario L, do Carmo A, Echevarria-Lima J, Sarmento-Ribeiro AB, Lopes MC, Moura-Neto V (2017). Dual treatment with shikonin and temozolomide reduces Glioblastoma tumor growth, migration and glial-to-mesenchymal transition. *Cell Oncol* doi:10.1007/s13402-017-0320-1.

Meissner A, Wernig M, Jaenisch R (2007). Direct reprogramming of genetically unmodified fibroblasts into pluripotent stem cells. *Nat Biotechnol* **25**:1177-1181.

Memmel S, Sukhorukov VL, Horing M, Westerling K, Fiedler V, Katzer A, Krohne G, Flentje M, Djuzenova CS (2014). Cell surface area and membrane folding in glioblastoma cell lines differing in PTEN and p53 status. *PLoS One* **9**: e87052.

Ming GL, Song H (2005). Adult neurogenesis in the mammalian central nervous system. *Annu Rev Neurosci* **28**:223-250.

Mirzadeh Z, Merkle FT, Soriano-Navarro M, Garcia-Verdugo JM, Alvarez-Buylla A (2008). Neural stem cells confer unique pinwheel architecture to the ventricular surface in neurogenic regions of the adult brain. Cell Stem Cell **3**:265-278.

Miyashita K, Kawakami K, Nakada M, Mai W, Shakoori A, Fujisawa H, Hayashi Y, Hamada J, Minamoto T (2009). Potential therapeutic effect of glycogen synthase kinase 3beta inhibition against human glioblastoma. *Clin Cancer Res* **15**:887-897.

Miyata H, Ashizawa T, Iizuka A, Kondou R, Nonomura C, Sugino T, Urakami K, Asai A, Hayashi N, Mitsuya K, Nakasu Y, Yamaguchi K, Akiyama Y (2017). Combination of a STAT3 inhibitor and an mTOR inhibitor against a temozolomide resistant Glioblastoma cell line. *Cancer Genomics Proteomics* **14**:83-91.

Montini E, Ceasana D, Schmidt M, Sanvito F, Ponzoni M, Bartholomae C, Sergi-Sergi L, Benedicenti F, Ambrosi A, Di-Serio C, Doglioni C, von-Kalle C, Naldini L (2006). Hematopoietic stem cell gene transfer in a tumor-prone mouse model uncovers low genotoxicity of lentiviral vector integration. Nat Biotechnol **24**:687-696.

Munchhof MJ, Li QF, Shavnya A, Borzillo GV, Boyden TL, Jones CS, LaGreca SD, Martinez-Alsina L, Patel N, Pelletier K, Reiter LA, Robbins MD, Tkalcevic GT (2012). Discovery of PF-04449913, a potent and orally bioavailable inhibitor of Smoothened. *ACS Med Chem Lett* **3**:106-111.

Nakabayashi H, Shimizu K (2011). HA1077, a Rho kinase nhibitor, suppresses Glioma-induced angiogenesis by targeting the Rho-ROCK and the mitogen-activated protein kinase kinase/extracellular signal-regulated kinase (MEK/ERK) signal pathways. *Cancer Sci* **102**:393-399.

Nakano I, Masterman-Smith M, Saigusa K, Paucar AA, Horvath S, Shoemaker L, Watanabe M, Negro A, Bajpai R, Howes A, Lelievre V, Waschek JA, Lazareff JA, Freije WA, Liau LM, Gibertson RJ, Cloughesy TF, Geschwind DH, Nelson SF, Mischel PS, Terskikh AV, Kornblum HI (2008). Maternal embryonic leucine zipper kinase is a key

regulator of the proliferation of malignant brain tumors, including brain tumor stem cells. *J Neurosci Res* **86**:48-60.

Narita Y (2015). Bevacizumab for Glioblastoma. *Therapeutics and Clinical Risk Management* **11**:1759-1765.

Natarajan M, Hecker TP, Gladson CL (2003). FAK signaling in anaplastic astrocytoma and glioblastoma tumors. *Cancer J* **9**:126-133.

Newman AM, Cooper JB (2010). Lab-specific gene expression signatures in pluripotent stem cells. *Cell Stem Cell* **7**:258-262.

Nitta Y, Shimizu S, Shishido-Hara Y, Suzuki K, Shiokawa Y, Nagane M (2016). Nimotuzumab enhances temozolommide-induced growth suppression of glioma cells expressing mutant EGFR in vivo. *Cancer Medicine* **5**:486-499.

Nusslein-Volhard C, Wieschaus E (1980). Mutations affecting segment number and polarity in Drosophila. *Nature* **287**:795-801.

Ohba S, Hirose Y (2016). Current and future drug treatments for glioblastomas. *Current Medicinal Chemistry* **23**:4309-4316.

Ohgaki H, Dessen P, Jourde B, Horstmann S, Nishikawa T, Patre PLD, Burkhard C, Schuler D, Probst-Hensch NM, Maiorka PC, Baeza N, Pisani P, Yonekawa Y, Yasargil MG, Lutolf UM, Kleihues P (2004). Genetic pathways to glioblastoma: a population-based study. *Cancer Res* **64**: 6892-6899.

Okawa S, Gagrica S, Blin C, Ender C, Pollard SM, Krijgsveld J (2017). Proteome and secretome characterization of Glioblastoma-derived neural stem cells. *Stem Cell* **35**:967-980.

Okita K, Nakagawa M, Hyenjong H, Ichisaka T, Yamanaka S (2008). Generation of mouse induced pluripotent stem cells without viral vectors. *Science* **322**:949-953.

Ong SE, Blagoev B, Kratchmarova I, Kristensen DB, Steen H, Pandey A, Mann M (2002). Stable isotope labeling by amino acids in cuture, SILAC, as a simple and accurate approach to expression proteomics. *Mol Cell Proteomics* **1**:376-386.

Ostrom QT, Gittleman H, Fulop J, Liu M,Blanda R, Kromer C, Wolinsky Y, Kruchko C, Barnholtz-Sloan J (2015). CBTRUS statistical report: primary brain and central nervous system tumors diagnosed in the United States in 2008-2012. *Neuro Oncology* **17**:iv1-62.

Ostrom QT, Gittleman H, Liao P, Rouse C, Chen Y, Dowling J, Barnholtz-Sloan J (2014). CBTRUS statistical report: primary brain and central nervous system tumors diagnosed in the United States in 2007-2011. *Neuro-Oncology* **16**:iv1-63.

Park IK, Morrison S, Clarke MF (2004). Bmi1, stem cells, and senescence regulation. *J Clin Invest* **113**:175-179.

Pecina-Slaus N, Kafka A, Varosanec AM, Markovic L, Krsnik Z, Njiric N, Mrak G (2016). Expression patterns of Wnt signaling component secreted freizzled-related protein 3 in astrocytoma and glioblastoma. *Molecular Medicine Reports* **13**:4245-4251.

Peukert S, Miller-Moslin K (2010). Small-molecule inhibitors of the Hedgehog signaling pathway as cancer therapeutics. *ChemMedChem* **5**: 500-512.

Pietras A, Katz A, Wee B, Halliday JJ, Pitter KL, Werbeck JL, Amankulor NM, Huse JT, Holland EC (2014). Osteopontin-CD44 signaling in the glioma perivascular niche enhances cancer stem cell phenotypes and promotes aggressive tumor growth. *Cell Stem Cell* **14**:357-369.

Polo JM, Anderssen E, Walsh RM, Schwarz BA, Nefzger CM, Lim SM, Borkent M, Apostolou E, Alaei S, Cloutier J et al (2012). A molecular roadmap of reprogramming somatic cells into iPS cells. *Cell* **151**:1617-1632.

Ponti G, Obernier K, Guinto C, Jose L, Bonfanti L, Alvarez-Buylla A (2013). Cell cycle and lineage progression of neural progenitors in the ventricular-subventricular zones of adult mice. *Proc Natl Acad Sci USA* **110**:E1045-1054.

Prestegarden L, Svendsen A, Wang J, Sleire L, Skaftnesmo KO, Bjerkvig R, Yan T, Askland L, Persson A, Sakariassen PQ, Enger PQ (2010). Glioma cell populations grouped by different cell type markers drive brain tumor growth. *Cancer Res* **70**:4274-4279.

Purkayasha S, Berliner A, Fernando SS, Ranasinghe B, Ray I, Tariq H, Banerjee P (2009). Curcumin blocks brain tumor formation. *Brain Res* **1266**:130-138.

Purow BW, Haque RM, Noel MW, Su Q, Burdick MJ, Lee J, Sundaresan T, Pastorino S, Park JK, Mikolaenko I, Maric D, Eberhart CG, Fine HA (2005). Expression of Notch-1 and its ligands, Delta-like-1 and Jagged-1, is critical for glioma cell survival and proliferation. *Cancer Res* **65**:2353-2363.

Qi Q, Liu X, Li SY, Joshi HC, Ye KQ (2013). Synergistic suppression of noscapine and conventional chemotherapeutics on human Glioblastoma cell growth. *Acta Pharmacologia Sinica* **34**:930-938.

Rao SK, Edwards J, Joshi AD, Siu IM, Riggins GJ (2010). A survey of glioblastoma genomic amplications and deletions. *Journal of Neuro-Oncology* **96**:169-179.

Ren F, Sheng WQ, Du X (2013). CD133: a cancer stem cells marker, is used in colorectal cancers. *World J Gastroenterol* **19**:2603-2611.

Reya T, Morrison SJ, Clarke MF, Weissman IL (2001). Stem cells, cancer, and cancer stem cells. *Nature* **414**:105-111.

Rodon J, Tawbi HA, Thomas AL, Stoller RG, Turtschi CP, Baselga J, Sarantopoulos J, Mahalingam D, Shou Y, Moles MA, Yang L, Granvil C, Hurh E, Rose KL, Amakye DD, Dummer R, Mita AC (2014). A Phase I, multicenter, open-label, first-in-human,

dose-escalation study of the oral smoothened inhibitor Sonidegib (LDE225) in patients with advanced soled tumors. *Clinical Cancer Research* **20**:1900-1909.

Rohatgi R, Milenkovic L, Corcoran RB, Scott MP (2008). Hedgehog signal transduction by Smoothened: Pharmacologic evidence fro a 2-step activation process. *PNAS* **106**:3196-3201.

Rohatgi R, Milenkovic L, Scott MP (2007). Patched 1 regulates Hedgehog signaling at the primay cilium. *Science* **317**:372-376.

Rossella G, Binda E, Orfanelli U, Cipelletti B, Gritti A, De Vitis S, Foroni C, Dimeco F, Vescovi A (2004). Isolation and characterization of tumorigenic, stem-like neural precursors from human glioblastoma. *Cancer Research* **64**:7011-7201.

Samuels Y, Wang Z, Bardelli A, Silliman N, Ptak J, Szabo S, Yan H, Gazdar A, Powell SM, Riggins GJ, Willson JK, Markowitz S, Kinzler KW, Vogelstein B, Velculescu VE (2004). *Science* **304**:554.

Sarkar S, Mirzaei R, Zemp FJ, Wu W, Senger DL, Robbins SM, Yong VW (2017). Activation of Notch signaling by tenascin-c promotes growth of human brain tumor-initiating cells. *Cancer Res* doi:10.1158/0008-5472.

Scales SJ, de Sauvage FJ (2009). Mechanisms of hedgehog pathway activation in cancer and implications for therapy. *Trends Pharmacol Sci* **30**:303-312.

Schlett K, Czirok A, Tarnok K, Vicsek T, Madarasz E (2000). Dynamics of cell aggregation during in vitro neurogenesis by immortalized neuroectodermal progenitors. *Journal of Neuroscience Research* **60**:184-194.

Schmid AC, Byrne RD, Vilar R, Woscholski R (2004). Bisperoxovanadium compounds are potent PTEN inhibitors. *FEBS letters* **566**: 35-38.

Schnabel LV, Abratte CM, Schimenti JC, Southard TL, Fortier LA (2012). Genetic background affects induced pluripotent stem cell generation. *Stem Cell Research & Therapy* **3**:30.

Schneider M, Huber J, Hadaschik B, Siegers GM, Fiebig HH, Schuler J (2012). Characterization of colon cancer cells: a functional approach characterizing CD133 as a potential stem cell marker. *BMC Cancer* **12**:96.

Schulte A, Liffers K, Kathagen A, Riethdrorf S, Zapf S, Merlo A, Kolbe K, Westphal M, Lamszus K (2013). Erlothinib resistance in EGFR-amplified Glioblastoma cells is associated with the upregulation of EGFRvII and PI3Kp100odelta. *Neuro-oncology* **15**:1289-1301.

Shahi MH, Lorente A, Castresana JS (2008). Hedgehog signaling in medulloblastoma, glioblastoma and neuroblastoma. *Oncol Rep* **19**:681-688.

Shakoori A, Ougolkov A, Yu ZW, Zhang B, Modarressi MH, Billadeau DD, Mai M, Takahashi Y, Minamoto T (2005). Deregulated GSK3beta activity in colorectal cancer: its association with tuor cell survival and proliferation. *Biochem Biophys Res Commun* **334**:1365-1373.

Sharpe HJ, Wang W, Hannoush RN, de Sauvage FJ (2015). Regulation of the oncoprotein Smoothened by small molecules. *Nature Chemical Biology* **11**:246-255.

Shi F, Guo H, Zhang R, Liu H, Wu L, Wu Q, Liu J, Liu T, Zhang Q (2017). The PI3K inhibitor GDC-0941 enhances radiosensitization and reduces chemoresistance to temozolomide in GBM cell lines. *Neuroscience* **346**:298-308.

Shi L, Fei X, Wang Z, You Y (2015). PI3K inhibitor combined with miR-125b inhibitor sensitize TMZ-induced anti-glioma stem cancer effects through inactivation of WNT/β-caternin signaling pathway. *In vitro Cell Dev Biol Anim* **51**:1047-1055.

Shmelkov SV, St Clair R, Lyden D, Rafii S (2005). AC133/CD133/Prominin-1. *Int J Biochem Cell Biol* **37**:715-719.

Silva J, Barrandon O, Nichols J, Kawaguchi J, Theunissen TW, Smith A (2008). Promotion of reprogramming to ground state pluripotency by signal inhibition. *PLoS Biology* **6**:e253.

Singh M, Manoranjan B, Mahendram S, McFarlane N, Venugopal C, Singh SK (2014). Brain metastasis-initiating cells: survival of the fittest. *Int J Mol Sci* **15**:9117-9133.

Singh SK, Clarke ID, Terasaki M, Bonn VE, Hawkins C, Squire J, Dirks PB (2003). Identification of a cancer stem cell in human brain tumors. *Cancer Research* **63**:5821-5828.

Singh SK, Hawkins C, Clarke ID, Squire JA, Bayani J, Hide T, Henkelman RM, Cusimano MD, Dirks PB (2004). Identification of human brain tumour initiating cells. *Nature* **432**:396-401.

Singhal PK, Sassi S, Lan L, Au P, Halvorsen SC, Fukumura D, Jain RK, Seed B (2016). Mouse embryonic fibroblasts exhibit extensive developmental and phenotypic diversity. *Proc Natl Acad Sci USA* **113**:122-127.

Soeda A, Inagaki A, Oka N, Ikegame Y, Aoki H, Yoshimura SI, Nakashima S, Kunisada T, Iwama T (2008). Epidermal growth factor plays a crucial role in mitogenic regulation of human brain tumor stem cells. *J Biol Chem* **283**:10958-10966.

Soldner E, Hockemeyer D Breard C, Gao Q, Bell GW, Cook EG, Hargus G, Blak A, Cooper Q, Mitalipova M, Isacson O, Jaenisch R (2009). Parkinson's disease patient-derived induced pluripotent stem cells free of viral reprogramming factors. *Cell* **136**:964-977.

Solomon MT, Selva JC, Figueredo J, Vaquer J, Toledo C, Quintanal N, Salva S, Domingez R, Alert J, Marinello JJ, Catala M, Griego MG, Martell JA, Luaces PL, Ballesterols J, de-Castro N Bach F, Crombet T (2013). *BMC Cancer* **13**:299-306.

Son MJ, Woolard K, Nam DH, Lee J, Fine HA (2009). SSEA-1 is an enrichment marker for tumor-initiating cells in human Glioblastoma. *Cell Stem Cell* **4**:440-452.

Stadtfeld M, Nagaya M, Utikal J, Weir G, Hochedlinger K (2008). Induced pluripotent stem cells generated without viral integration. *Science* **322**:945-949.

Standring S (2008). *Gray's Anatomy* (40th Edition). Churchill Livingstone.

Stupp R, Hegi ME, Mason WP, van den Bent MJ, Taphoorn MJ, Janzer RC, Ludwin SK, Allgeier A, Fisher B, Belanger K, Hau P, Brandess AA, Gijtenbeek J, Marosi C, Vecht CJ, Mokhtari K, Wesseling P, Villa S, Eisenhauer E, Gorlia T, Weller M, Lacombe D, Cairncross JG, Mirimanoff RO (2009) Effects of radiotherapy with concomitant and adjuvant temozolomide versus radiotherapy alone on survival I glioblastoma in a randomized phase III study: 5-year analysis of the EORTC-NCIC trial. *Lancet Oncol* **10**:459-466.

Styczynski J, Olszewska-Slonina D, Kolodziej B, Napieraj M, Wysocki M (2006). Activity of bortezomib in glioblastoma. *Anticancer Res* **26**:4499-4503.

Suwala AK, Hanaford A, Kahlert UD, Maciaczyk J (2016). Clipping the wings of clioblastoma: modulation of WNT as a novel therapeutic strategy. *J Neuropathol Exp Neurol* **75**:388-396.

Suzuki T, Izumoto S, Fujimoto Y, Maruno M, Ito Y, Yoshimine T (2005). Clinicopathological study of cellular proliferation and invasion in gliomatosis cerebri: important role of neural cell adhesion molecule L1 in tumour invasion. *Journal of Clinical Pathology* **58**:166-171.

Suzuki Y, Shirai K, Oka K, Mobaraki A, Yoshida Y, Noda SE, Okamoto M, Suzuki Y, Itoh J, Itoh H, Ishiuchi S, Nakano T (2010). Higher pAkt expression predicts a significant worse prognosis in glioblastomas. *J Radiat Res* **251**:343-348.

Szerlip NJ, Pedraza A, Chakravarty D, Azim M, McGuire J, Fang Y, Ozawa T, Holland EC, Huse JT, Jhanwar S, Leversha MA, Mikkelsen T, Brennan CW (2012). Intratumoral heterogeneity of receptor tyrosine kinases EGFR and PDGFRA amplification in glioblastoma defines subpopulations with distinct growth factor response. *Proc Natl Acad Sci USA* **109**:3041-3046.

Szopa W, Burley TA, Kramer-Marek G, Kaspera W (2017). Glioblastoma: current status and future perspectives. *BioMed Research International* doi:10.1155/2017/8013575.

Taal W, Oosterkamp HM, Walenkamp AM, Dubbink HJ, Beerepoot LV, Hanse MC (2014). Single-agnet bevacizumab or lomustine versus a combination of bevacizumab plus lomustine versus a combination of bevacizumab plus lomustine in patients with recurrent Glioblastoma (BELOB trail): a randomized controlled phase 2 trial. *Lancet Oncol* **15**:943-953.

Takahashi K, Tanabe K, Ohnuki M, Narita M, Ichisaka T, Tomada T, Yamanaka S (2007). Induction of pluripotent stem cells from adult human fibroblasts by defined factors. *Cell* **131**:861-872.

Takahashi K, Yamanaka S (2006). Induction of pluripotent stem cells from mouse embryonic and adult fibroblast cultures by defined factors. *Cell* **126**: 663-676.

Teodorczyk M, Schmidt MHH (2014). Notching on Cancer's door: Notch signaling in brain tumors. *Front Oncol* **4**:341.

Thakkar JP, Dolecek TA, Horbinski C, Ostrom QT, Lightner DD, Barnholtz-Sloan JS, Villano JL (2014). Epidemiologic and molecular prognostic review of glioblastoma. *Cancer Epidemiology, Biomarkers and Prevention* **23**:1985-1996.

Thayer SP, di Magliano MP, Heiser PW, Nielsen CM, Roberts DJ, Lauwers GY, Qi YP, Gysin S, Fernandez-del Castillo C, Yajnik V, Antonium B, McMahon M, Warshaw AL, Hebrok M (2003). Hedgehog is an early and late mediator of pancreatic cancer tumorigenesis. *Nature* **425**:851-856.

Tian XH, Lin XN, Wei F, Feng W, Huang ZC, Wang P, Ren L, Diao Y (2011). Enhanced brain targeting of temozolomide in polysorbate-80 coated polybutylcyanoacrylate nanoparticles. *Int J Nanomedicine* **6**:445-452.

Tichy J, Spechtmeyer S, Mittelbronn M, Hattingen E, Rieger J, Senft C, Foerch C (2016). Prospective evaluation of serum glial fibrillary acidic protein (GFAP) as a diagnostic marker for glioblastoma. *J Neurooncol* **126**:361-369.

Tirino V, Desiderio V, d'Aquino R, De Francesco F, Pirozzi G, Graziano A, Galderisi U, Cavaliere C, De Rosa A, Papaccio G, Giordano A (2008). Detection and characterization of CD133+ cancer stem cells in human solid tumours. *PLoS One* **3**:e3469.

Toyoda T, Mae SI, Tanaka H, Kondo Y, Funato M, Hosokawa Y, Sudo T, Kawaguchi Y, Osafune K (2015). Cell aggregation optimizes the differentiation of human ESCs and iPSCs into pancreatic bud-like progenitor cells. *Stem cell Research* **14**:185-197.

Tremblay MR, Lescarbeau A, Grogan MJ, Tan E, Lin G, Austad BC, Yu LC, Behnke ML, Nair SJ, Hagel M, White K, Conley J, Manna JD, Alvarez-Diez TM, Hoyt J, Woodward CN, Sydor JR, Pink M, MacDougall J, Campbell MJ, Cushing J, Ferguson J, Curtis MS, McGovern K, Read MA, Palombella VJ, Adams J, Castro AC (2009). Discovery of a potent and orally active hedgehog pathway antagonist (IPI-926). *J. Med. Chem* **52**:4400-4418.

Tsukiyama T, Asano R, Kawaguchi T, Kim N, Yamada M, Minami N, Ohinata Y, Imai H (2011). Simple and efficient method for generation of induced pluripotent stem cells using piggyback transposition of docycycline-inducible factors and an EOS reporter system. *Genes Cells* **16**:815-825.

Urban N, Guillemot F (2014). Neurogenesis in the embryonic and adult brain: Same regulators, different roles. *Front Cell Neurosci* **8**:396.

Van den Bent MJ, Brandes AA, Rampling R, Kouwenhoven MC, Kros JM, Carpentier AF, Clement PM, Frenay M, Campone M, Baurain JF, Armand JP, Taphoorn MJ, Tosoni A,

Kletzl H, Klughammer B, Lacombe D, Gorlia T (2009). Randomized phase II trial of erlotinib versus temozolomide or carmustine in recurrent Glioblastoma: EORTC brain tumor group study 26034. *J Clin Oncol* **27**:1268-1274.

Verhaak RG, Hoadley KA, Purdom E, Wang V, Qi Y, Wilkerson MD, Miller CR, Ding L, Golub T, Mesirov JP, Alexe G, Lawrence M, O'Kelly M, Tamayo P, Weir BA, Gabrie S, Winckler W, Gupta S, Jakkula L, Feiler HS, Hodgson JG, James CD, Sarkaria JN, Brennan C, Kahn A, Spellman PT, Wilson RK, Speed TP, Gray JW, Meyerson M, Getz G, Perou CM, Hayes DN (2010). An integrated genomic analysis identifies clinically relevant subtypes of Glioblastoma characterized by abnormlities in PDGFRA, IDH1, EGFR and NF1. *Cancer Cell* **17**:98-110.

Visvader JE (2011). Cells of origin in cancer. *Nature* **469**:314-322.

Wang J, Sakariassen PO, Tsinkalovasky O, Immervoll H, Boe SO, Svendsen A, Prestegarden L, Rosland G, Thorsen F, Stuhr L, Molven A, Bjerkvig R, Enger PO (2008). CD133 negative glioma cells form tumors in nude rats and give rise to CD13 positive cells. *Int J Cancer* **122**:761-768.

Wang XJ, Tanaka Mine, Krstin S, Peixoto HS, Wink M (2016). The interference of selected cytotoxic alkaloids with the cytoskeleton: an insight into their modes of action. *Molecules* **21**:E906.

Wang Y, Zhou Z, Walsh CT, McMahon AP (2009). Selective translocation of intracellular Smoothened to the primary cilium in response to Hedgehog pathway modulation. *PNAS* **106**:2623-2628.

Watkins DN, Berman DM, Burkholder SG, Wang B, Beachy PA, Baylin SB (2003). Hedgehog signaling within airway epithelial progenitors and in small-cell lung cancer. *Nature* **422**:313-317.

Wei L, Suram M, Stephanie S, Lambert-Cheatham N (2016). Novel insights into the roles of Rho kinase in cancer. *Arch Immuno Ther Exp* **64**:259-278.

Wen X, Lai CK, Evangelista M, Hongo JA, de Sauvage FJ, Scales SJ (2010). Kinetics of hedgehog-dependent full-length Gli3 accumulation in primary cilia and subsequent degradation. *Mol Cell Biol* **30**:1910-1922.

Wernig M, Meissner A, Foreman R, Brambrink T, Ku M, Hochedlinger K, Bernstein BE, Jaenisch R (2007). In vitro reprogramming of fibroblasts into a pluripotent ES-cell-like state. *Nature* **448**:318-324.

Wick W, Brandes A, Gorlia T, Bendszus M, Sahm F, Taal W, Taphoorn MJB, Domont J, Idbaih A, Campone M, Clement PM, Stupp R, Fabbro M, Le Rhun E, Dubois F, Klein M, Platten M, Weller M, Golfinopoulos V, van den Bent MJ (2015). Phase III trial exploring the combination of bevacizumab and lomustine in patients with first recurrence of Glioblastoma: the EORTC 26101 trial. *Neuro Oncol* **17**:v1.

Wick W, Puduvalli VK, Chamberlain MC, van den Bent MJ, Carpentier AF, Cher LM, Mason W, Weller M, Hong S, Musib L, Liepa AM, Thornton DE, Fine HA (2010). Phase III study of enzastaurin compared with lomustine in the treatment of recurrent intracranial Glioblastoma. *J Clin Oncol* **28**:1168-1174.

Wilson CW, Chen MH, Chuang PT (2009). Smoothened adopts multiple active and inactive conformations capable of trafficking to the primary cilium. *PLoS ONE* **4**:e5182.

Wilson TA, Karajannis MA, Harter DH (2014). Glioblastoma multiforme: State of the art and future therapeutics. *Surgical neurology international* **5**:64-62.

Winter CA, Flataker L (1961). Toxicity studies on noscapine. *Toxicol. Appl. Pharmacol* **3**:96-106.

Woltjen K, Michael IP, Mohseni P, Desai R, Mileikovsky M, Hamalainen R, Cowling R, Wang W, Liu P, Gertsenstein M, Kaji K, Sung HK, Nagy A (2009). piggyback transposition reprograms fibroblasts to induced pluripotent stem cells. *Nature* **458**:766-770.

Xiao A, Wu H, Pandolfi PP, Louis DN, Van Dyke T (2002). Astrocyte inactivation of the pRb pathway predisposes mice to malignant astrocytoma development that is accelerated by PTEN mutation. *Cancer Cell* **1**:157-168.

Yahyanejad S, Henry K, Iglesias VS, Granton PV, Barbeau LMO, van Hoof SJ, Groot AJ, Habets R, Prickaerts J, Chalmers AJ, Eekers DBP, Theys J, Short SC, Verhaegen F, Vooijs M (2016). NOTCH blockade combined with radiation and therapy and temozolomide prolongs survival of orthotopic Glioblastoma. *Oncotarget* **7**:41251-41264.

Ye K, Ke Y, Keshava N, Shanks J, Kapp JA, Tekmal RR, Petros J, Josh HC (1998). Opium alkaloid noscapine is an antitumor agent that arrests metaphase and induces apptosis in dividing cells. *Pro. Natl. Acad. Sci. U.S.A.* **95**:1601-1606.

You DW, Xin JP, Wolk A, Wei W, Schmidt R, Scurti G, Nand S, Breuer EK, Kuo PC, Breslin P, Kini AR, Nishimura MI, Zeleznik-Le NJ, Zhang JW (2015). FAK mediates a compensatory survival signal parallel to PI3K-AKT in PTEN-null T-all cells. *Cell Reports* **10**:2055-2068.

Yu J, Hu K, Smuga-Otto K, Tian S, Stewart R, Slukvin LL, Thomson JA (2009). Human induced pluripotent stem cells free of vector and transgene sequences. *Science* **324**:797-801.

Yvon AMC, Wadsworth P, Jordan MA (1999). Taxol suppresses dynamics of individual microtubules in living human tumor cells. *Mol Biol Cell* **10**:947-959.

Zaguia F, Schneider R (2011). Microvilli expressed on glioma cells keep cytotoxic cells at a distance. *Cancer Biol Ther* **11**:1-3.

Zeng W, Fabb S, Haynes J, Pouton C (2011). Extended periods of neural induction and propagation of embryonic stem cell-derived nerural progenitors with EGF and FGF2 enhances Lmx1a expression and neurogenic potential. *Neurochemistry International* **59**:394-403.

Zhang S, Yu D (2010). PI(3)King Apart PTEN's role in cancer. *Clinical Cancer Research* **16**:4325-4330.

Zhao Y, Tong C, Jiang J (2007). Hedgehog regulates smoothened activity by inducing a conformational switch. *Nature* **450**:252-258.

Zheng H, Ying H, Yan H, Kimmelman AC, Hiller DJ, Chen AJ, Perry SR, Tonon G, Chu GC, Ding Z, Stommel JM, Dunn KL, Wiedemeyer R, You MJ, Brennan C, Wang YA, Ligon KL, Wong WH, Chin L, DePinho RA (2008). P53 and Pten control neural and glioma stem/pprogenitor cell renewal and differentiation. *Nature* **455**:1129-1133.

Zhu J, Cai Y, Liu P, Zhao WG (2016). Frequent Nek1 overexpression in human gliomas. *Biochemical and biophysical research communication* **476**:522-527.

Zhuang WZ, Long LM, Zheng BX, Ji WJ, Yang N, Zhang QQ, Liang ZQ (2012). Curcumin promotes differentiation of glioma-initiating cells by inducing autophagy. *Cancer Science* **103**:684-690.

Zimmermann TJ, Roy S, Martinez NE, Ziegler S, Hedberg C, Waldmann H (2013). Biology-oriented synthesis of a tetrahydroisoquinoline-based compound collection targeting microtubule polymerization. *Chembiochem* **14**:295-300.

Zlokovic BV (2008). The blood-brain barrier in health and chronic neurodegenerative disorders. *Neuron* **57**:178-201.

Appendix A

As shown in Appendix Figure 1, we noticed that the normal B2 supplement contains retinoic acid which will stimulate neuronal differentiation. Indeed, there was a significant morphology change when these cells were cultured in DMEM/F12+B27 (containing Vitamin A) medium compared to that cultured in DMEM/F12+B27 (no Vitamin A) medium. The one cultured in the medium containing no vitamin A is healthier and the spheres are more spherical, and the cells were more compact. These neurospheres could be further passaged without any noticeable change of the morphology. However, the cells cultured in medium supplemented with B27 (containing Vitamin A) have a loose packed morphology. These cells died after 2 to 3 passages, which may be due to neuronal differentation. The previous medium, which supported the growth of neurospheres for other cell lines, could not support the growth of *Pik3ca*^{H1047R}/*PTEN*$^{del/del}$ cell line. This might be due to the neural suplement containing a small amount of retinoic acid. Thus, we noticed that the growth of this *Pik3ca*^{H1047R}/*PTEN*$^{del/del}$ cell line is very sensitive to a small amount of retinoic acid.

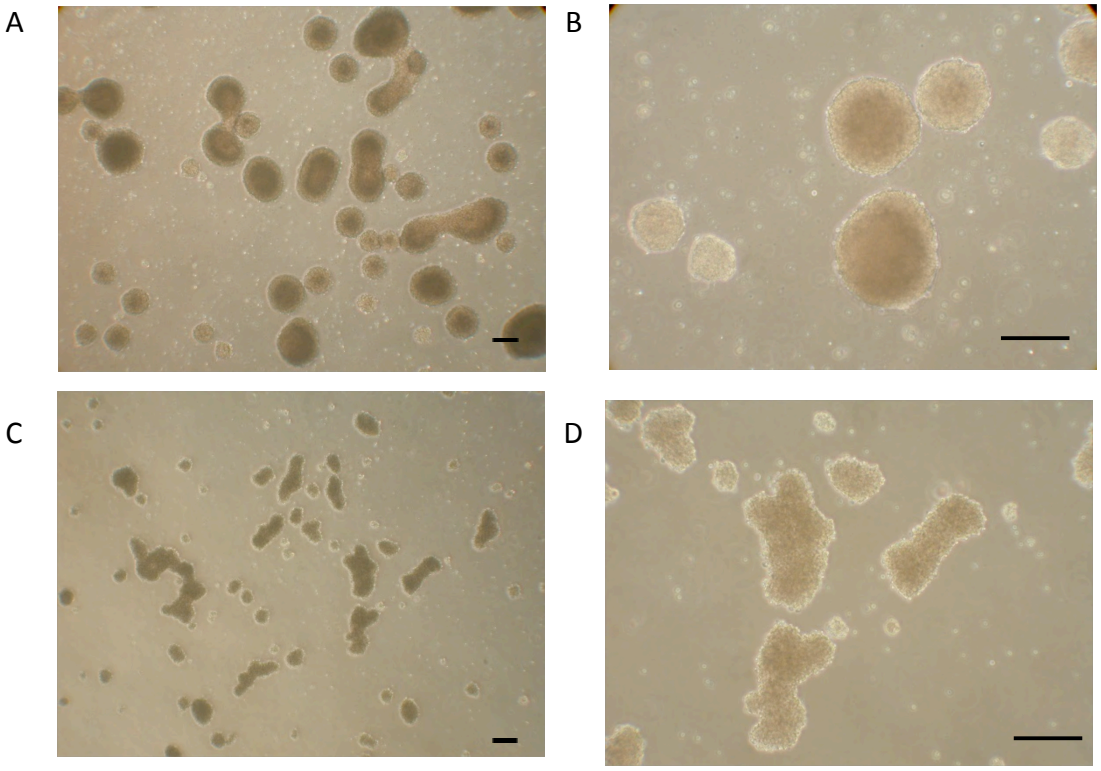

Appendix figure 1: Culture media for growing mouse *Pik3ca*^{H1047R}/*PTEN*$^{del/del}$ neurospheres. The growth media were compared to optimize the growth conditions for mouse *Pik3ca*^{H1047R}/*PTEN*$^{del/del}$ neurospheres. (A and B): DMEM/F12 supplemented with B27 serum free supplement (without Vitamin A), and 20ng/mL EGF and FGF2. (C and D): DMEM/F12 supplemented with B27 serum free supplement (contain Vitamin A), and 20ng/mL EGF and FGF2. Scale bar is 100µm.

Appendix B

PI3K activation in neural stem cells drives tumorigenesis which can be suppressed by targeting CREB

Paul M. Daniel[1], Gulay Filiz[1], Daniel V. Brown[1], Michael Christie[1], Paul M. Waring[1], Yi Zhang[2], John M. Haynes[2], Colin Pouton[2], Dustin Flanagan[3], Elizabeth Vincan[3,4,5], Terrance G. Johns[6], Karen Montgomery[7], Wayne A. Phillips[7,8], Theo Mantamadiotis[1]*

[1]Department of Pathology, School of Biomedical Sciences, University of Melbourne, Parkville, Australia

[2]Stem Cell Biology Group, Drug Discovery Biology, Monash Institute of Pharmaceutical Sciences, Monash University, Parkville, VIC, Australia

[3]Molecular Oncology Laboratory, University of Melbourne

[4]Victorian Infectious Diseases Reference Laboratory, Doherty Institute

[5]School of Biomedical Sciences, Curtin University, WA, Australia

[6] Centre for Cancer Research, Hudson Institute of Medical Research, Clayton, Australia

[7]Cancer Biology and Surgical Oncology Research Laboratory, Peter MacCallum Cancer Centre, Melbourne, Australia

[8]Sir Peter MacCallum Department of Oncology, University of Melbourne, Parkville, 3010, Australia

*E-mail: Correspondence to: Theo Mantamadiotis, theom@unimelb.edu.au

Running Title: PI3K mutations drive mouse neural stem cell tumors

Keywords: PI3K; PIK3CA; PTEN; CREB; WNT; neural stem cells; brain cancer; glioma; GBM; mouse model

Hyperactivation of the PI3K signaling is common in human cancers, including gliomas, but the precise role of the pathway in glioma biology remains to be determined. Some limited understanding of PI3K signaling in brain cancer come from studies on neural stem/progenitor cells (NSPCs) where signals transmitted via the PI3K pathway cooperate with other intracellular pathways and downstream transcription factors to regulate NSPC proliferation. To investigate the role for the PI3K pathway in glioma initiation and development, we generated a mouse model targeting the inducible expression of a Pik3ca^{H1047A} oncogenic mutation and simultaneous deletion of the PI3K negative regulator, Pten, in NSPCs. We show that the expression of a Pik3ca^{H1047A} was sufficient to initiate tumorigenesis but that simultaneous loss of Pten, was required for the development of invasive, high-grade glioma. Mutant NSPCs exhibited enhanced neurosphere forming capacity which correlated with increased Wnt signaling. We also show that loss of CREB in *Pik3ca-PTEN* tumors led to a longer symptom-free survival in mice. Taken together, our findings present a novel mouse model for high-grade glioma with which we demonstrate that the PI3K pathway is important for initiation of tumorigenesis and that disruption of downstream CREB signaling attenuates tumor expansion.

INTRODUCTION

Although our understanding of the cellular and molecular mechanisms controlling brain cancer pathogenesis has progressed over the last decades, the therapies available have not translated to improved patient outcome. This is exemplified in the most common and deadly high-grade glioma (HGG) in adults, glioblastoma (GBM), where post-therapy survival for most patients ranges between 8-14 months. Since the pioneering work by Holland and colleagues [22], genetically engineered mouse models have demonstrated that various gene combinations, overexpressing and/or targeting growth factors, growth factor receptors, oncogenic pathways and tumor suppressors in both brain progenitor or differentiated cells can initiate glioma development. These models, particularly those mimicking genetic alterations seen in patient tumors have proven to be invaluable in understanding the molecular events underlying the development of brain tumors, with the first models expressing constitutively activated mutant growth factor receptors (EGFR) or mutated key downstream signaling molecule (Ras, Akt) [21, 22]. Numerous mouse models have since been generated using transgenic or gene modifying technologies targeting many genes [1, 58]. Genes enabling the initiation of high-grade gliomas include combinations of *NF1, TP53, PTEN, AKT, Ras, INK4a/ARF* [1, 2, 10, 43]. Many models have targeted glial cells, which are the cells enriched in human glioma [10, 13, 21]. Other mouse models show that gene mutations in oligodendrocyte precursor cells or fully differentiated astrocytes or neurons can initiate glioma development[16, 35]. The role of brain tumor stem cells (BTSCs) in fueling tumor growth has been demonstrated in a number of mouse models targeting genetic mutations/deletions in NSPCs[1, 2, 22, 26, 35, 43, 49] and highlighted by a study demonstrating that ablation of BTSCs inhibited tumor growth [59]. With the better understanding of single gene or gene combinations driving HGG development, recent translational research has turned to

modelling HGG by manipulating specific factors of cell signaling networks which can been targeted by pathway-specific drugs.

The signaling pathways driving HGG pathobiology overlap with those activated in many cancers and involve complex interactions between oncogenes and tumor suppressors. Most oncogenes and tumor suppressors are regulatory factors of the phosphoinositide 3-kinase (PI3K) and mitogen-activated protein kinase (MAPK) pathways. Both pathways activate a cascade of downstream kinases which lead to the activation of specific transcription factors, including the cAMP response element binding protein (CREB), which is upregulated in GBM and has a role in NSPC and GBM cell proliferation [12, 45]. Emerging evidence suggest that oncogenic PI3K and MAPK signals converge with Wnt signaling to regulate cancer cell growth and proliferation[44] and that in GBM, Wnt signaling has a role in cancer stem cell maintenance[48].

When one considers the upstream components of the PI3K pathway including the epidermal growth factor receptor (EGFR) and the PI3K catalytic and regulatory subunits, PIK3CA and PIK3R1 as well as the pathway's main negative regulator, phosphatase and tensin homolog (PTEN), up to 63% of HGGs, including GBM, exhibit an alteration in at least one of these genes [31]. A recent study of cancer driver mutations shows that the catalytic subunit of PI3K, encoded by the *PIK3CA* gene, is amongst the three major oncogenic drivers in GBM; the other drivers are the *EGFR* and *TP53* [52]. Indeed, *PIK3CA* mutations are reported to be present in up to 17% of all pediatric and adult brain cancer types with primary higher grade and treatment resistant brain tumors exhibiting the highest mutation rates [31]. The full activation of the PI3K pathway not only requires enhanced catalytic activity to drive key downstream kinases such as Akt but also requires the inactivation of the lipid phosphatase activity of PTEN, which dephosphorylates phosphatidylinositol (3,4,5)-trisphosphate (PIP3) to the inactive PIP2 form[8, 14]. The precise role

of PTEN in PI3K-driven HGG/GBM remains unclear, since recent discoveries demonstrate multiple PI3K-independent biochemical and cellular PTEN functions[6, 51]. Deletion of PTEN in neural stem and progenitor cells leads to enhanced proliferative activity in the stem cell niche but no tumor development [19, 20]. However, *Pten* deletion in combination with *p53* and/or *Rb1* loss results in the development of astrocyte-derived high-grade tumors [10]. An inducible viral expression system targeting NSPCs or glial cells, established the importance of platelet-derived growth factor-A (PGFA) in high-grade glioma initiation and the role of additional mutations of other genes, including *Pten* and *NF1*, in accelerating tumor development and determining the proneural GBM subtype[43]. The effects of pro-oncogenic mutations involving the PI3K catalytic (p110α) and regulatory (p85) subunits have not been investigated in mouse brain but combined activation of Ras and Akt in mouse neural progenitors resulted in glioblastoma formation [22], although neither oncogene alone led to tumor development.

In an effort to understand the key events in brain tumor development involving the PI3K pathway, we targeted the PI3K pathway in mouse NSPCs by conditional activation of an oncogenic mutation in *Pik3ca*, the gene encoding the PI3K catalytic p110α catalytic subunit of PI3K [29], in combination with the deletion of the PI3K pathway negative regulator, PTEN. To investigate the downstream transcriptional programs regulated by the PI3K pathway in our mouse model, we deleted CREB in *Pik3ca-Pten* mutant NSPCs and show that upon CREB loss tumor growth is attenuated via inhibition of mutant cell proliferation and subsequent conversion into a less aggressive tumor type.

RESULTS

Activation of *Pik3ca*^{H1047R} expression in NSPCs is sufficient for tumor initiation but simultaneous deletion of *Pten* is necessary for the development of invasive tumors.

The *Nestin-CreER^{T2}* transgene used restricts Cre-recombinase expression to the sub-ventricular zone (SVZ) and the recombination only occurs following tamoxifen administration [25]. First, mice heterozygous for a latent Cre recombinase (Cre)-inducible knock-in of the *Pik3ca*^{H1047R} mutation (*Pik3ca$^{H1047R\text{-}lox}$*) [29] and/or two Cre-inducible *Pten* deletion alleles (*Pten$^{loxP/loxP}$*) [20] were crossed with mice expressing a single (heterozygous) *Nestin-CreER^{T2}* transgene. Further F1 crosses generated mice which were heterozygous for mutant *Pik3ca^{H1047R}* (*Pik3ca$^{H1047R\text{-}lox}$-Nestin-CreER^{T2}*) and homozygous *Pten* deletion (*Pten$^{loxP/loxP}$-Nestin-CreER^{T2}*) (*Pten$^{\Delta}$*).

Control *Pik3ca$^{H1047R\text{-}lox}$-Pten$^{loxP/loxP}$* mice without the *Nestin-CreER^{T2}* transgene but treated with tamoxifen, did not develop neurological symptoms, nor show evidence of tumor growth over the experimental time window of 200 days (Fig. 1A). Single mutant *Pten$^{\Delta}$* mice showed normal brain size with no overt abnormalities but did exhibit increased SVZ cellularity and proliferation compared to controls (Fig. 1A). Examination of single mutant heterozygous *Pik3ca^{H1047R}* mouse brains between 50 to 150 days post-tamoxifen administration revealed the presence of tumors in the lateral ventricles (Fig. 1A).

Tamoxifen-treated double mutant *Pik3ca$^{H1047R\text{-}lox}$-Pten$^{loxP/loxP}$-Nestin-CreER^{T2}* (hereafter referred to as *Pik3ca^{H1047R}-Pten$^{\Delta}$*) 6-8-week-old mice, resulted in a completely penetrant (100%; 30 from 30 mice) neurological phenotype, apparent 55-90 days after tamoxifen administration. An early sign of ill health was a decline in body weight, compared to controls, in both male and female mice (Fig. 1B), followed by the appearance of progressively more severe neurological symptoms. The first neurological manifestation was ataxia, followed by sporadic seizures and a gradual increase in seizure frequency and length. Mice were culled when weight loss was more than 15% of the experiment start weight and/or when seizures occurred more than three times per day and at least one seizure lasted more than one minute. These criteria were deemed as the

experimental endpoint. All tamoxifen-treated mice mutant mice reached the experimental endpoint between 55 and 90 days (Fig. 1C) and were subsequently culled. Furthermore, single mutant *Pik3ca*^{H1047R} expression or *Pten* mice showed no body weight decrease, signs of brain dysfunction, nor reduced survival over 200 days (Fig 1B, C). When *Pik3ca*^{H1047R}-*Pten*$^{\Delta}$ mutations were activated in one day old newborn mice (P1) via tamoxifen treatment of the mother and transmission of the tamoxifen to pups via the mother's milk, the pups began exhibiting severe neurological symptoms between 28 and 43 days (Fig. 1C), earlier than in adult mice treated with tamoxifen. P1 tamoxifen-treated mouse brains showed the presence of tumors, consistent with those seen in adult mice.

Histological examination of brains demonstrated that compared to control mouse brains, *Pik3ca*^{H1047R}-*Pten*$^{\Delta}$ mouse brains showed hypercellularity of the SVZ, with multiple tumor nodules protruding into the lateral ventricles (Fig. 1D, upper panel) and tumors completely filling the anterior lateral ventricles (Fig. 1D, lower panels). Further examination showed the presence of multiple hypercellular clusters lining the SVZ and tumor cell migration into the developing tumor nodules (Fig. 2A, B). Away from the lateral ventricles, tumor cells invaded the brain parenchyma and white matter tracts, including the corpus callosum (Fig. 2C). Apoptotic cells were scattered within tumors (not shown), lying amongst atypical, irregularly arranged tumor cells and blood vessels (Fig. 2D).

Immunohistochemical analysis of *Pik3ca*^{H1047R}-*Pten*$^{\Delta}$ brains showed that tumors expressed glial fibrillary acidic protein (GFAP) and β-III-tubulin (Tuj1) (Fig. 2E) showing that the NSPCs from which the tumors developed could differentiate into glial-like and neuronal-like cells. pAKT (S473) and pRps6 expression were highly expressed in all tumor cells (Fig. 2F), evidence that the PI3K pathway was activated by the mutations. Activation of additional oncogenic signaling

and transcriptional pathways was observed by examining phospho-ERK1/2 (pERK1/2) and phospho-CREB (pCREB) expression (Fig. 2F). Proliferating cell nuclear antigen (PCNA), Ki67 and nestin expression demonstrated that tumors also harbored proliferating, immature cells (Supplemental Fig.S1).

Overall, the histopathological analysis of the mouse brain tumors demonstrated heterogeneous features overlapping with both lower (II) and higher (III) grade astrocytic tumors. Specifically, the presence of atypical cells, evidence of cells undergoing apoptosis and tumor cell invasion into white matter tracts is consistent with low grade / WHO grade II astrocytoma, while the presence of blood vessels within tumors, suggests the presence of tumor phenotypes consistent with high-grade astrocytoma / WHO grade III.

Mutant NSPCs exhibit enhanced proliferation and migration

Since mutant mice succumbed due to neurological complications associated with tumor growth, prior to broad dissemination of the disease, we assessed the invasive and functional characteristics of mutant cells in vitro. To obtain pure mutant NSPCs, SVZ tissue was used to isolate and propagate NSPCs from *Pik3ca*^{H1047R}-*Pten*$^{lox/lox}$-*UBC-Cre*^{ERT2} mice [30] and Cre-mediated recombination was induced, in vitro, by the addition of 4-OH-T to the medium for 24h. Recombination in 4-OH-T treated cells was confirmed by PCR (data not shown) and loss of Pten protein (Supplemental Fig.S2), compared to untreated parental NSPCs and PTEN+ human GBM T98G cells. Mutant *Pik3ca*^{H1047R}-*Pten*$^{\Delta}$ neurospheres formed loosely aggregated rough-edged spheres (Fig. 3A) compared with parental vehicle treated control neurospheres. Moreover, mutant neurosphere cells showed the presence of more filopodia, compared to controls (Fig. 3A, B), a feature associated with a more invasive, malignant phenotype in GBM and some cancer

cell lines [41]. Incorporation of the thymidine analog, 5-ethynyl-2′-deoxyuridine (EdU) and flow cytometry analysis showed that *Pik3ca*^{H1047R}-*Pten*$^{\Delta}$ cells had a higher proliferation rate compared to parental Pik3ca-Pten wild-type cells (Fig. 3C). Mutant cells showed enhanced pAKT expression, in the presence or absence of EGF and bFGF (Fig. 3D). Correlating with enhanced proliferation, mutant cells exhibited increased expression of cyclins B1 and D1. Both control and mutant cells exhibited similar proportions of nestin-expressing cells (~97%) (Supplemental Fig. S2).

Seeding single neurospheres into a gel matrix showed that *Pik3ca*^{H1047R}-*Pten*$^{\Delta}$ NSPCs migrated to cover more than three times the area compared to control NSPCs at 48h (Fig. 3E,F), demonstrating that mutant cells have increased migratory capacity. Seeding cells at high density for 72h showed that mutant NSPCs detached and migrated away from spheres, unlike control NSPCs, which did not exhibit this behavior under the same seeding conditions (Supplemental Fig.S4).

Mutant NSPCs exhibit enhanced sphere-forming capacity, persistent nestin expression and Wnt pathway activition

To determine the long-term proliferation differences between mutant and control NSPCs, cumulative growth was measured over 8 passages (8 weeks). *Pik3ca*^{H1047R}-*Pten*$^{\Delta}$ cells showed significantly higher cell number from week two onward and almost four times more cells by eight weeks (Fig. 4A). To elucidate the differences seen in cumulative growth, we next investigated the neurosphere-forming efficiency (a correlate of neural stem cell potential) differences between mutant and control NSPCs. Use of extreme-limiting dilution analysis (ELDA) [24] to measure neurosphere-forming efficiency, showed that in neurosphere culture

conditions, the sphere-forming capacity of *Pik3ca*^{H1047R}-*Pten*$^{\Delta}$ cells (1 NSFU (neurosphere forming unit) / 1.55 cells seeded) was lower than control cells (1 NSFU / 2.01 cells seeded) (Fig. 4B). To test the inherent neurosphere forming stability of the NSPCs, we subjected the cells to alternating rounds of growth in neurosphere medium, serum-containing medium and a return to neurosphere medium to evaluate the ability of the cells in maintaining their neurosphere forming capacity under conditions which promote differentiation (Fig 4C). Flow cytometry analysis demonstrated that the NSPC marker, nestin, was still expressed in 70% of *Pik3ca*^{H1047R};*Pten*$^{\Delta}$ differentiated cells compared with 52% of control cells after seven days (Fig. 4D). Returning differentiated cells to serum-free neurosphere conditions, revealed a significantly higher sphere-forming capacity in mutant cells (1 NSFU / 15.4 cells seeded), compared to control cells (1 NSFU / 36.0 cells seeded) (Fig 4E). Independent assessment by measuring nestin+, GFAP+ and Tuj-1+ cells grown on laminin for five days, supported the flow cytometric analysis with respect to an enhanced nestin+ cell stability under differentiating conditions. Mutant cells also exhibited higher GFAP+ cell numbers at day one but similar a number by day five, compared to parental wild-type NSPCs (Supplemental Fig. S5).

Analysis of a panel of PI3K/AKT pathway-associated phosphoproteins in NSPCs grown in vitro, showed an upregulation of activation of numerous factors compared to parental control cells, including the factors: Akt, ribosomal protein S6 (rpS6), mTOR, GSK3α, GSK3β, p70S6 kinase, RSK1 and ERK1/2 (Fig. 5A). To further investigate the possible biological basis of the enhanced neurosphere forming capacity observed in *Pik3ca*^{H1047R}-*Pten*$^{\Delta}$ NSPCs, we postulated that Wnt signaling was upregulated in mutant cells, as cross-talk between PI3K and Wnt signaling is common in stem cells [23]. Analysis of NSPCs showed that β-catenin was expressed at higher levels in mutant cell nuclei, compared to wild-type cells (Fig. 5B), indicating activation of Wnt

signaling. Moreover, qRT-PCR demonstrated that the mRNA of Wnt pathway stem cell factors and targets was overexpressed in mutant NSPCs, compared to wild-type controls (Fig 5C). Further analysis demonstrated that neurosphere forming potential could be modulated by chemical inhibitors which modulate the Wnt pathway (Fig. 5E). CHIR99021 ('CHIR'), a potent GSK3 inhibitor, and Wnt pathway activator, increased neurosphere forming potential of mutant NSPCs, where sphere per cells seeded capacity ratio, was 1:1 for CHIR-treated NSPCs, compared to 1:2.6 for vehicle (DMSO) treated cells. Upstream inhibition of the Wnt pathway, using IWP-2, which targets the membrane-bound protein, porcupine, and inhibits Wnt protein secretion, did not have a significant effect on sphere forming capacity, compared to vehicle treated mutant NSPCs, suggesting that the PI3K modulates Wnt signals downstream from porcupine and receptor activation.

Creb1 deletion suppresses malignancy of *Pik3ca*^{H1047R}-*Pten*$^{\Delta}$ tumors

Most cells in *Pik3ca*^{H1047R}-*Pten*$^{\Delta}$ tumors expressed pCREB (Fig. 2F) and this expression overlapped with nestin and GFAP expressing SVZ cells (Fig. 6A). We previously showed that mouse SVZ cells express activated pCREB [15] and human glioma tissue express high levels of both total CREB and pCREB [12]. To determine the contribution of CREB in brain tumor development and growth, we used *CREB*$^{lox/lox}$ mice[39] to generate triple mutant *Pik3ca*$^{H1047R\text{-}lox}$-*Pten*$^{lox/lox}$-*CREB*$^{lox/lox}$-*Nestin-CreER*^{T2} mice, resulting in deletion of CREB in addition to the *Pik3ca* and *Pten* mutations in NSPCs (*Pik3ca*^{H1047R}-*Pten*$^{\Delta}$-*CREB*$^{\Delta}$, hereafter referred to as 'triple mutant').

Triple mutant *CREB*$^{\Delta}$ brain tumors exhibited the presence of large cells (Fig. 6B) and circumscribed growth with little or no invasion into non-tumor brain parenchyma (Supplemental

Fig. 6A). We also observed a reduction in cell density in triple mutant *CREB*$^{\Delta}$ tumors, compared to double mutant CREB wild-type tumors (Fig. 6B), which was confirmed by counting cells in DAPI stained sections (Fig. 6C), with triple mutant *CREB*$^{\Delta}$ tumors exhibiting 65% cell density of *Pik3ca*^{H1047R}-*Pten*$^{\Delta}$ tumor cellularity. Notably, triple mutant *CREB*$^{\Delta}$ mice were symptom-free for longer (median 125 days) following tamoxifen treatment, compared with double mutant *Pik3ca*^{H1047R}-*Pten*$^{\Delta}$ *mice* (median 70 days) (Fig. 6D).

To explore the proliferative potential of *CREB*$^{\Delta}$ NSPCs, in vitro proliferation assays were performed and showed that triple mutant *CREB*$^{\Delta}$ NSPC proliferation was reduced compared with *Pik3ca*^{H1047R}-*Pten*$^{\Delta}$ (Supplemental Fig. 6B).

Consistent with the proliferation defect, cell cycle analysis showed that triple mutant *CREB*$^{\Delta}$ NSPCs had fewer (5.9%) S-phase cells and more (80.2%) G0/G1 phase cells, compared to *Pik3ca*^{H1047R}-*Pten*$^{\Delta}$ (12.8% S-phase; 70% G0/G1-phase) NSPCs (Supplemental Fig. 6C). However, the sphere-forming capacity of *CREB*$^{\Delta}$ NSPCs did not differ compared to *Pik3ca*^{H1047R}-*Pten*$^{\Delta}$ NSPCs (data not shown).

DISCUSSION

The role of the PI3K pathway in driving malignant astrocytic brain tumors comes from murine models in which activation of retroviral vector-encoded AKT needs to be coexpressed with a second potent oncogene, such as Ras or BRAF, to trigger tumor development and growth [22, 49]. To our knowledge, no studies have demonstrated a direct involvement of PI3K subunit mutations. Recent large-scale cancer sequencing data suggest that *PIK3CA* may be a key driver of malignant astrocytic brain cancer [52]. Our study is the first to directly test the role of *Pik3ca* in

brain tumor development and we demonstrate that expression of constitutive catalytically active Pik3ca^{H1047R} can initiate tumor growth when targeted to NSPCs, although simultaneous deletion of tumor suppressor Pten was necessary for the development of invasive malignant tumors, similar to that reported in other murine brain cancer models, where a second driver gene/tumor suppressor loss is necessary to trigger development of malignant tumors [10, 26, 37]. In our model, homozygous loss of Pten only, did not lead to tumor development, although increased SVZ cellularity was observed, similar to the hyperproliferative neurogenic phenotype previously reported in *Pten$^{loxP/lox}$-Nestin-Cre* mice [3, 20].

The NSPC tumors in the mice presented with highly variable, heterogeneous histopathological features, a characteristic of high-grade astrocytic tumors/GBM in young adult patients [32]. The *Pik3ca^{H1047R}-Pten$^{\Delta}$* tumors resemble some features commonly seen in patients with tuberous sclerosis, where mutations in the *TSC1* and *TSC2* genes, which encode factors downstream from the PI3K pathway, cause cortical layering defects, epilepsy, as well as the development of benign nodular subependymal tumors of the lateral ventricles [11]. However, a *Tsc1* mutant mouse targeting NSPCS using a *nestin*-driven Tet-conditional transgene exhibits cortical disruption but no SVZ/ependymal tumors [18]. Moreover, the data we present demonstrate the inherent invasiveness of the *Pik3ca^{H1047R}-Pten$^{\Delta}$* tumor cells, where prominent tumor cell migration/invasion into the white matter occurred, an important feature of malignant astrocytomas and GBM. Furthermore, coexpression of both the glial marker GFAP and neuronal marker TuJ1 revealed in our model is significant, since this coexpression pattern in patient astrocytic tumors is associated with aggressive astrocytic tumors [28]. Interestingly, tumors also exhibited rosette-like tumor cell arrangements tumors, which are features of both pediatric and young adult GBM [32].

One of the major roadblocks toward effective treatment of patients with high grade malignant brain cancers is the invasiveness of tumor cells into healthy brain tissue, which renders tumor removal by surgery almost impossible. Our data also shows that *Pik3ca*^{H1047R}-*Pten*$^{\Delta}$ NSPCs exhibit enhanced migratory properties and sphere-forming/stem cell-associated characteristics, consistent with previous studies demonstrating that PI3K pathway activation promotes GBM cell migration [34], neurosphere-formation and tumorigenicity of glioma stem cells (GSCs) [54].

Using extreme limiting dilution analysis, we found that *Pik3ca*^{H1047R}-*Pten*$^{\Delta}$ NSPCs were able to efficiently maintain nestin expression and sphere-forming capacity, even after forced differentiation. This implies that the *Pik3ca*^{H1047R}-*Pten*$^{\Delta}$ mutations stabilize stem cell properties, and, in a clinical setting, these mutations may impart stable, therapy tumor cell resistant characteristics and the capacity for tumor recurrence/relapse. Phospho-protein analysis of PI3K/AKT downstream targets revealed an array of upregulated factors. Notably, GSK3β, a key factor in the PI3K/AKT pathway, exhibited increased phosphorylation in mutant NSPCs, compared with wild-type control cells. GSK3β is also integral for activation of the Wnt pathway [40]. Wnt and PI3K signaling are commonly co-activated in stem cells, which could explain the enhanced neurosphere forming capacity in *Pik3ca*^{H1047R}-*Pten*$^{\Delta}$ mutant NSPCs. Wnt signaling is a critical pathway for maintaining efficient self-renewal of NSPCs [27, 55] and is also implicated in maintenance of GSC self-renewal [47, 57]. The clinical importance of Wnt signaling in patient gliomas is highlighted by the correlation of Wnt factors with independent markers of poor prognosis [36]. Our data shows that *Pik3ca*^{H1047R}-*Pten*$^{\Delta}$ mutant NSPCs express high levels of all canonical Wnt pathway factors examined, except for the Wnt pathway receptor, Fzd7. Most of these genes examined have been reported to regulate NSPC and/or glioma cell biology. For example, the Leucine-rich repeat-containing G-protein-coupled receptor 5 (LGR5), plays a role

in the maintenance and survival of patient-derived GSCs [42]; Sox9 has a role in NSPC self-renewal capacity [50]; Myc inhibition disrupts mouse and human GSC self-renewal [4]. Notably, cooperation between the PI3K and WNT pathways plays a key role in hematopoietic stem cell self-renewal [46], which may be similar to the cooperativity at play in NSPCs.

Cooperativity between the PI3K and MAPK pathways is suggested to be a requirement for GBM pathogenesis, explored in GBM in vitro and in vivo, using primary astrocytes with mutations in Kras and/or Pten [53]. The authors observed that each individual mutation caused upregulation of both the PI3K and MAPK pathway and that inhibition of one of the pathways inhibited tumorigenic potential.

Although the oncogenic roles and mechanisms involving cytoplasmic signaling pathways, such as the PI3K and MAPK pathways are still being deciphered, the transcriptional programs activated by oncogenic mutations are less well understood. We and others have shown that the kinase-inducible transcription factor CREB and its activated form, pCREB are expressed in human astrocytic tumors, including the most deadly form, GBM [5, 12], and that CREB has a role in glioma cell proliferation [12]. Analysis of *Pik3ca*^{H1047R}-*Pten*$^{\Delta}$ tumor brain tissue and NSPC lysates, showed that aside from the expected upregulation of the PI3K/AKT pathway factors, the MAPK pathway was also upregulated. Our previous work shows that a transcriptional convergence point of the PI3K and MAPK pathways is CREB [12]. To explore the oncogenic role of CREB in vivo, we deleted CREB in *Pik3ca*^{H1047R}-*Pten*$^{\Delta}$ NSPCs. Strikingly, triple mutant *Pik3ca*^{H1047R}-*Pten*$^{\Delta}$-*CREB*$^{\Delta}$ mice were symptom-free for a longer period, compared with double mutant *Pik3ca*^{H1047R}-*Pten*$^{\Delta}$ mice. CREB deletion resulted in reduced tumor cellularity and a phenotypic shift of tumor cells toward a less malignant state, reminiscent of giant-cell GBM, which has a

better prognosis compared with GBM [33]. Moreover, no invasion into white matter tracts was observed in triple mutant *CREB*$^{\Delta}$ brains. To our knowledge, this is the first in vivo data demonstrating that genetically targeted loss of CREB in tumor cells suppresses tumor growth and is consistent with studies correlating elevated CREB expression and activation with poor prognosis in many neoplasms including those in lung [38] and breast [9].

Overall, our data lead us to propose a model in which the PI3K pathway is critical and sufficient for reprograming normal NSPCs into tumor-initiating cells, in which the Wnt pathway is hyperactivated and contributes to NSPC self-renewal. As the resulting mutant tumor cells mature, the PI3K pathway activates a CREB-dependent transcriptome which contributes to tumor growth. MAPK signaling is also co-activated which probably contributes to CREB activation, to further fuel tumor cell proliferation. The putative efficacy of targeting CREB has led to the design of several experimental compounds which target CREB and can inhibit tumor cell proliferation in vitro and in vivo [56]. Indeed, co-targeting archetypal oncogenic pathways, including PI3K, MAPK and WNT, as well as transcription factors such as CREB, may prove to be effective therapeutic approaches for difficult to treat cancers, including HGGs, since transcription factors are less prone to direct mutations, thus circumventing the development of drug resistance [17].

Materials and Methods

Ethics statement

Experiments in mice were carried out with the approval of The University of Melbourne, School of Biomedical Sciences (AEC No 1112336.1) and Peter MacCallum Cancer Center (AEEC No. E406) Animal Ethics Committees.

Mouse maintenance and husbandry

Mice were housed at the Biomedical Sciences University of Melbourne animal house in a pathogen-free environment with food and water freely accessible. Environmental supplementation of the cages was limited to necessary bedding materials to standardize conditions between cages and mice. *Pten*$^{lox/lox}$ (c;129S4-Ptentm1Hwu/J) were from The Jackson Laboratory. *Pik3ca*$^{H1047R\text{-}lox}$ [29], *CREB*$^{lox/lox}$ [39], and *Nestin-CreER*^{T2} [25] mice were generated, as previously described. All mice were on a C57BL/6 background.

In vivo tumor induction

Control (*Pik3ca*$^{H1047R\text{-}lox}$-*PTEN*$^{lox/lox}$), double mutant (*Pik3ca*$^{H1047R\text{-}lox}$-*PTEN*$^{lox/lox}$-*Nestin-CreER*^{T2}) or triple mutant (*Pik3ca*$^{H1047R\text{-}lox}$-*PTEN*$^{lox/lox}$-*CREB*$^{lox/lox}$-*Nestin-CreER*^{T2}) mice were treated with tamoxifen at 6-8 weeks of age, as described previously [7].

NSPC isolation and culture

Adult (6-10 week) control (*Pik3ca*$^{H1047R\text{-}lox}$-*PTEN*$^{lox/lox}$), double mutant (*Pik3ca*$^{H1047R\text{-}lox}$-*PTEN*$^{lox/lox}$-*Nestin-CreER*^{T2}) or triple mutant (*Pik3ca*$^{H1047R\text{-}lox}$-*PTEN*$^{lox/lox}$-*CREB*$^{lox/lox}$-*Nestin-CreER*^{T2}) mice were culled immediately before harvesting. Brains were placed in ice cold PBS before dissection of the SVZs and NSPCs were isolated as previously described [15]. NSPCs were grown in Dulbecco's modified eagle medium (DMEM) (Invitrogen, USA) with the addition of 2% B27 supplement (Invitrogen), 20 ng/mL basic fibroblast growth factor (b-FGF, Sigma,

USA), and 40 ng/mL epidermal growth factor (EGF, Sigma). NSPC maintenance and passaging was performed as previously described [15].

In vitro controls

For experiments involving NSPCs, mutant NSPCs were generated by transient (24h) treatment with 0.02mg/ml 4-OH-T (in methanol) to induce Cre-mediated recombination of floxed alleles, while control cells were derived from the same genotype but treated with vehicle only (methanol). 4-OH-T was removed after 24h and never included in the medium in further experiments / assays.

Cell cycle analysis

Cells were dissociated and then resuspended in PBS. Cells were then fixed by adding cell solution dropwise into ice cold 100% ethanol. Fixed cells were kept at -20°C until day of analysis where they were washed 3x with PBS and then incubated with DAPI staining solution (5µg/mL; Thermo Fisher Scientific, MA USA) for 15 minutes on ice. Following incubation, cells were washed, resuspended in PBS and immediately run on a LSR Fortessa using the UV laser (405nm). Cells were first gated with forward scatter width (FSW) vs DAPI (405nm) to exclude doublets and debris. A histogram of DAPI vs count was generated and analyzed on the flow cytometry analysis software FlowLogic (version 6) to identify the population (%) of cells in each of the cell cycle phases.

Proliferation assays

Cells were plated onto a 96 well plate and grown under required treatment conditions. On the day of analysis, Resazurin solution (Sigma, MO, USA) was diluted in appropriate media and

added to wells to obtain a 10% v/v solution before incubation for at least 3 hours at 37°C. Plates were analyzed using the EnSpire Plate Reader (PerkinElmer).

Migration assay

Single neurospheres grown in DMEM-F12 with growth factors and supplements (see above) for 48h were placed into a 96-well plate (1 sphere/well) and assayed using the Trevigen 96-well 3D spheroid BME cell invasion assay kit (Bio Scientific, Australia), according to the manufacturer's protocol. Briefly, neurospheres were incubated either with (test) or without (control) addition of invasion matrix for 48h. Spheres were photographed on an inverted microscope and invasion area was calculated by measuring the area of invasion by subtracting the control neurosphere area using Image J (http://rsb.info.nih.gov/ij/index.html).

Extreme Limiting Dilution Analysis (ELDA)

Neurospheres were dissociated and plated in suspension media at decreasing cellular densities (20, 10, 5, 1 cell) using 24 wells per cell density condition. Wells were imaged 7 days after plating and the number of wells with one or more sphere, greater than ~20µm diameter, were scored. Data was analyzed as previously reported [24] using the online ELDA software hosted by WEHI (http://bioinf.wehi.edu.au/software/elda/). Cells were plated at 200,000 cells/9.61cm^2 in DMEM-F12 with 10%FCS and cultured for 7 days before subsequent analysis.

Flow cytometry analysis

Cells were harvested to single cell suspension as described above and resuspended in PBS. Cells were then fixed by adding cell solution dropwise into ice cold 100% ethanol. Fixed cells were kept at -20°C until day of analysis when they were washed 3x with PBS and then incubated for

30 minutes in blocking solution (PBS supplemented with 2% (v/v) normal goat serum and 0.1% (v/v) Tween-20). Cells were spun down and supernatant discarded before nestin antibody (Millipore) diluted in blocking solution (1:200) was added to cells. The primary antibody was left on for 60 minutes before a wash in PBS and staining cells with an anti-mouse Alexa-Fluor 568 secondary antibody (1:500) (ThermoFisher) for 10 minutes. DAPI staining solution was added to cells after the 10-minute incubation had elapsed and left to incubate for a further 5 minutes on ice. Following a final wash in PBS, cells were resuspended in 100µl of PBS and immediately run on a LSR Fortessa. Cells were gated with forward scatter width (FSW) vs DAPI (405nm) to exclude doublets and debris. Flow data was analyzed using the analysis software FlowLogic (version 6) to identify the population (%) of cells in each of the cell cycle phases.

Statistical analysis. Data were analyzed using the Student's t-test and were presented as mean ± standard deviation (SD) or standard error of the mean (SEM), as indicated in relevant data/sections. $P<0.05$ (*) was considered as significant.

CONFLICT OF INTEREST

The authors declare no conflict of interest.

ACKNOWLEDGMENTS

We thank Rob Ramsay, Frederic Hollande, Andrew Allen, Daniel Gough, Jason Cain, Ryan Hutchinson for helpful scientific discussions. We thank Tina Isaakidis for proofreading. Special thanks to Sarah Louise Taverner for dedicated animal care and monitoring throughout this

project, as well as to Teresa Drever, Jessica Sturrock, Michelle Williams and Marica Kesar for running and managing the excellent animal facility. Daniel Blashki and Vanta Jameson for flow cytometry assistance. We thank the Department of Pathology and The CASS Foundation Science & Medicine Grant #6236 for financial support. WAP was supported, in part, by project grant #1080491 from the National Health and Medical Research Council (NHMRC) of Australia. We would also like to acknowledge the donors of the tumor-derived sample data within the TCGA, Rembrandt GBM Datasets.

Supplementary Information accompanies the paper on the *Oncogene* website (http://www.nature.com/onc)

REFERENCES

1 Alcantara Llaguno S, Chen J, Kwon CH, Jackson EL, Li Y, Burns DK *et al*. Malignant astrocytomas originate from neural stem/progenitor cells in a somatic tumor suppressor mouse model. Cancer cell 2009; 15: 45-56.

2 Alcantara Llaguno SR, Wang Z, Sun D, Chen J, Xu J, Kim E *et al*. Adult Lineage-Restricted CNS Progenitors Specify Distinct Glioblastoma Subtypes. Cancer Cell 2015; 28: 429-440.

3 Amiri A, Cho W, Zhou J, Birnbaum SG, Sinton CM, McKay RM *et al*. Pten deletion in adult hippocampal neural stem/progenitor cells causes cellular abnormalities and alters neurogenesis. J Neurosci 2012; 32: 5880-5890.

4 Annibali D, Whitfield JR, Favuzzi E, Jauset T, Serrano E, Cuartas I *et al*. Myc inhibition is effective against glioma and reveals a role for Myc in proficient mitosis. Nature communications 2014; 5: 4632.

5 Barresi V, Mondello S, Branca G, Rajan TS, Vitarelli E, Tuccari G. p-CREB expression in human gliomas: potential use in the differential diagnosis between astrocytoma and oligodendroglioma. Human pathology 2015; 46: 231-238.

6 Bermudez Brito M, Goulielmaki E, Papakonstanti EA. Focus on PTEN Regulation. Front Oncol 2015; 5: 166.

7 Casanova E, Fehsenfeld S, Lemberger T, Shimshek DR, Sprengel R, Mantamadiotis T. ER-based double iCre fusion protein allows partial recombination in forebrain. Genesis 2002; 34: 208-214.

8 Chalhoub N, Baker SJ. PTEN and the PI3-kinase pathway in cancer. Annu Rev Pathol 2009; 4: 127-150.

9 Chhabra A, Fernando H, Watkins G, Mansel RE, Jiang WG. Expression of transcription factor CREB1 in human breast cancer and its correlation with prognosis. Oncol Rep 2007; 18: 953-958.

10 Chow LM, Endersby R, Zhu X, Rankin S, Qu C, Zhang J *et al*. Cooperativity within and among Pten, p53, and Rb pathways induces high-grade astrocytoma in adult brain. Cancer cell 2011; 19: 305-316.

11 Crino PB, Nathanson KL, Henske EP. The tuberous sclerosis complex. The New England journal of medicine 2006; 355: 1345-1356.

12 Daniel P, Filiz G, Brown DV, Hollande F, Gonzales M, D'Abaco G *et al*. Selective CREB-dependent cyclin expression mediated by the PI3K and MAPK pathways supports glioma cell proliferation. Oncogenesis 2014; 3: e108.

13 Danks RA, Orian JM, Gonzales MF, Tan SS, Alexander B, Mikoshiba K *et al*. Transformation of astrocytes in transgenic mice expressing SV40 T antigen under the transcriptional control of the glial fibrillary acidic protein promoter. Cancer Res 1995; 55: 4302-4310.

14 Di Cristofano A, Pandolfi PP. The multiple roles of PTEN in tumor suppression. Cell 2000; 100: 387-390.

15 Dworkin S, Malaterre J, Hollande F, Darcy PK, Ramsay RG, Mantamadiotis T. cAMP response element binding protein is required for mouse neural progenitor cell survival and expansion. Stem Cells 2009; 27: 1347-1357.

16 Friedmann-Morvinski D, Bushong EA, Ke E, Soda Y, Marumoto T, Singer O *et al*. Dedifferentiation of neurons and astrocytes by oncogenes can induce gliomas in mice. Science 2012; 338: 1080-1084.

17 Gonda TJ, Ramsay RG. Directly targeting transcriptional dysregulation in cancer. Nat Rev Cancer 2015; 15: 686-694.

18 Goto J, Talos DM, Klein P, Qin W, Chekaluk YI, Anderl S *et al*. Regulable neural progenitor-specific Tsc1 loss yields giant cells with organellar dysfunction in a model of tuberous sclerosis complex. Proc Natl Acad Sci U S A 2011; 108: E1070-1079.

19 Gregorian C, Nakashima J, Le Belle J, Ohab J, Kim R, Liu A *et al*. Pten deletion in adult neural stem/progenitor cells enhances constitutive neurogenesis. J Neurosci 2009; 29: 1874-1886.

20 Groszer M, Erickson R, Scripture-Adams DD, Lesche R, Trumpp A, Zack JA *et al*. Negative regulation of neural stem/progenitor cell proliferation by the Pten tumor suppressor gene in vivo. Science 2001; 294: 2186-2189.

21 Holland EC, Hively WP, DePinho RA, Varmus HE. A constitutively active epidermal growth factor receptor cooperates with disruption of G1 cell-cycle arrest pathways to induce glioma-like lesions in mice. Genes Dev 1998; 12: 3675-3685.

22 Holland EC, Celestino J, Dai C, Schaefer L, Sawaya RE, Fuller GN. Combined activation of Ras and Akt in neural progenitors induces glioblastoma formation in mice. Nat Genet 2000; 25: 55-57.

23 Holland JD, Klaus A, Garratt AN, Birchmeier W. Wnt signaling in stem and cancer stem cells. Current opinion in cell biology 2013; 25: 254-264.

24 Hu Y, Smyth GK. ELDA: extreme limiting dilution analysis for comparing depleted and enriched populations in stem cell and other assays. Journal of immunological methods 2009; 347: 70-78.

25 Imayoshi I, Ohtsuka T, Metzger D, Chambon P, Kageyama R. Temporal regulation of Cre recombinase activity in neural stem cells. Genesis 2006; 44: 233-238.

26 Jacques TS, Swales A, Brzozowski MJ, Henriquez NV, Linehan JM, Mirzadeh Z *et al*. Combinations of genetic mutations in the adult neural stem cell compartment determine brain tumour phenotypes. The EMBO journal 2010; 29: 222-235.

27 Kalani MY, Cheshier SH, Cord BJ, Bababeygy SR, Vogel H, Weissman IL *et al*. Wnt-mediated self-renewal of neural stem/progenitor cells. Proc Natl Acad Sci U S A 2008; 105: 16970-16975.

28 Katsetos CD, Del Valle L, Geddes JF, Assimakopoulou M, Legido A, Boyd JC *et al*. Aberrant localization of the neuronal class III beta-tubulin in astrocytomas. Archives of pathology & laboratory medicine 2001; 125: 613-624.

29 Kinross KM, Montgomery KG, Kleinschmidt M, Waring P, Ivetac I, Tikoo A *et al*. An activating Pik3ca mutation coupled with Pten loss is sufficient to initiate ovarian tumorigenesis in mice. J Clin Invest 2012; 122: 553-557.

30 Kinross KM, Montgomery KG, Mangiafico SP, Hare LM, Kleinschmidt M, Bywater MJ *et al*. Ubiquitous expression of the Pik3caH1047R mutation promotes hypoglycemia, hypoinsulinemia, and organomegaly. FASEB journal : official publication of the Federation of American Societies for Experimental Biology 2015; 29: 1426-1434.

31 Kita D, Yonekawa Y, Weller M, Ohgaki H. PIK3CA alterations in primary (de novo) and secondary glioblastomas. Acta Neuropathol 2007; 113: 295-302.

32 Kleinschmidt-DeMasters BK, Meltesen L, McGavran L, Lillehei KO. Characterization of glioblastomas in young adults. Brain pathology 2006; 16: 273-286.

33 Kozak KR, Moody JS. Giant cell glioblastoma: a glioblastoma subtype with distinct epidemiology and superior prognosis. Neuro-oncology 2009; 11: 833-841.

34 Kubiatowski T, Jang T, Lachyankar MB, Salmonsen R, Nabi RR, Quesenberry PJ *et al*. Association of increased phosphatidylinositol 3-kinase signaling with increased invasiveness and gelatinase activity in malignant gliomas. Journal of neurosurgery 2001; 95: 480-488.

35 Liu C, Sage JC, Miller MR, Verhaak RG, Hippenmeyer S, Vogel H *et al*. Mosaic analysis with double markers reveals tumor cell of origin in glioma. Cell 2011; 146: 209-221.

36 Liu C, Tu Y, Sun X, Jiang J, Jin X, Bo X *et al*. Wnt/beta-Catenin pathway in human glioma: expression pattern and clinical/prognostic correlations. Clinical and experimental medicine 2011; 11: 105-112.

37 Liu HK, Wang Y, Belz T, Bock D, Takacs A, Radlwimmer B *et al*. The nuclear receptor tailless induces long-term neural stem cell expansion and brain tumor initiation. Genes Dev 2010; 24: 683-695.

38 Liu W, Wu Y, Wang L, Gao L, Wang Y, Liu X *et al*. Protein signature for non-small cell lung cancer prognosis. American journal of cancer research 2014; 4: 256-269.

39 Mantamadiotis T, Lemberger T, Bleckmann SC, Kern H, Kretz O, Martin Villalba A *et al*. Disruption of CREB function in brain leads to neurodegeneration. Nat Genet 2002; 31: 47-54.

40 McManus EJ, Sakamoto K, Armit LJ, Ronaldson L, Shpiro N, Marquez R *et al*. Role that phosphorylation of GSK3 plays in insulin and Wnt signalling defined by knockin analysis. The EMBO journal 2005; 24: 1571-1583.

41 Memmel S, Sukhorukov VL, Horing M, Westerling K, Fiedler V, Katzer A *et al*. Cell surface area and membrane folding in glioblastoma cell lines differing in PTEN and p53 status. PLoS One 2014; 9: e87052.

42 Nakata S, Campos B, Bageritz J, Bermejo JL, Becker N, Engel F *et al*. LGR5 is a marker of poor prognosis in glioblastoma and is required for survival of brain cancer stem-like cells. Brain pathology 2013; 23: 60-72.

43 Ozawa T, Riester M, Cheng YK, Huse JT, Squatrito M, Helmy K *et al*. Most human non-GCIMP glioblastoma subtypes evolve from a common proneural-like precursor glioma. Cancer Cell 2014; 26: 288-300.

44 Padala RR, Karnawat R, Viswanathan SB, Thakkar AV, Das AB. Cancerous perturbations within the ERK, PI3K/Akt, and Wnt/beta-catenin signaling network constitutively activate inter-pathway positive feedback loops. Mol Biosyst 2017.

45 Peltier J, O'Neill A, Schaffer DV. PI3K/Akt and CREB regulate adult neural hippocampal progenitor proliferation and differentiation. Developmental neurobiology 2007; 67: 1348-1361.

46 Perry JM, He XC, Sugimura R, Grindley JC, Haug JS, Ding S *et al*. Cooperation between both Wnt/{beta}-catenin and PTEN/PI3K/Akt signaling promotes primitive hematopoietic stem cell self-renewal and expansion. Genes Dev 2011; 25: 1928-1942.

47 Pulvirenti T, Van Der Heijden M, Droms LA, Huse JT, Tabar V, Hall A. Dishevelled 2 signaling promotes self-renewal and tumorigenicity in human gliomas. Cancer Res 2011; 71: 7280-7290.

48 Rheinbay E, Suva ML, Gillespie SM, Wakimoto H, Patel AP, Shahid M *et al*. An aberrant transcription factor network essential for Wnt signaling and stem cell maintenance in glioblastoma. Cell Rep 2013; 3: 1567-1579.

49 Robinson JP, VanBrocklin MW, Guilbeault AR, Signorelli DL, Brandner S, Holmen SL. Activated BRAF induces gliomas in mice when combined with Ink4a/Arf loss or Akt activation. Oncogene 2010; 29: 335-344.

50 Scott CE, Wynn SL, Sesay A, Cruz C, Cheung M, Gomez Gaviro MV *et al*. SOX9 induces and maintains neural stem cells. Nature neuroscience 2010; 13: 1181-1189.

51 Song MS, Salmena L, Pandolfi PP. The functions and regulation of the PTEN tumour suppressor. Nat Rev Mol Cell Biol 2012; 13: 283-296.

52 Tamborero D, Gonzalez-Perez A, Perez-Llamas C, Deu-Pons J, Kandoth C, Reimand J *et al*. Comprehensive identification of mutational cancer driver genes across 12 tumor types. Scientific reports 2013; 3: 2650.

53 Vitucci M, Karpinich NO, Bash RE, Werneke AM, Schmid RS, White KK *et al*. Cooperativity between MAPK and PI3K signaling activation is required for glioblastoma pathogenesis. Neuro-oncology 2013; 15: 1317-1329.

54 Wei Y, Jiang Y, Zou F, Liu Y, Wang S, Xu N *et al*. Activation of PI3K/Akt pathway by CD133-p85 interaction promotes tumorigenic capacity of glioma stem cells. Proc Natl Acad Sci U S A 2013; 110: 6829-6834.

55 Wexler EM, Paucer A, Kornblum HI, Palmer TD, Geschwind DH. Endogenous Wnt signaling maintains neural progenitor cell potency. Stem Cells 2009; 27: 1130-1141.

56 Xie F, Li BX, Kassenbrock A, Xue C, Wang X, Qian DZ *et al*. Identification of a Potent Inhibitor of CREB-Mediated Gene Transcription with Efficacious in Vivo Anticancer Activity. Journal of medicinal chemistry 2015; 58: 5075-5087.

57 Zhang N, Wei P, Gong A, Chiu WT, Lee HT, Colman H *et al*. FoxM1 promotes beta-catenin nuclear localization and controls Wnt target-gene expression and glioma tumorigenesis. Cancer cell 2011; 20: 427-442.

58 Zhu Y, Harada T, Liu L, Lush ME, Guignard F, Harada C *et al*. Inactivation of NF1 in CNS causes increased glial progenitor proliferation and optic glioma formation. Development 2005; 132: 5577-5588.

59 Zhu Z, Khan MA, Weiler M, Blaes J, Jestaedt L, Geibert M *et al*. Targeting self-renewal in high-grade brain tumors leads to loss of brain tumor stem cells and prolonged survival. Cell stem cell 2014; 15: 185-198.

FIGURE LEGENDS

Figure 1. Combined *Pik3ca^{H1047R}* oncogene activation and *Pten* deletion in neural stem/progenitor cells leads to the development of SVZ tumors.

(**A**) H&E staining of brains from control mice (tamoxifen-treated *Pik3ca^{H1047R}-Pten$^{lox/lox}$* without *Nestin-CreER^{T2}*) showing the SVZ layer (arrow) harboring NSPCs. Single mutant homozygous *Pten$^{\Delta}$* mice showed thickening of the SVZ layer (arrow). Single mutant heterozygous *Pik3ca^{H1047R}* mice exhibited a normal SVZ (arrow) and a single tumor nodule (*) extending into the lateral ventricular space. Scale bar is 250μm. (**B**) Body weight of a representative cohort of adult mice (6 weeks of age) which received tamoxifen (Tam) at day 0. (**C**) Kaplan-Meier survival analysis shows that only tamoxifen-treated double mutant *Pik3ca^{H1047R}-Pten$^{\Delta}$* adult (n=10) and newborn (P1) mouse (n=3) cohorts, compared to the control cohort (n=12). (**D**) H&E staining of a double mutant *Pik3ca^{H1047R}-Pten$^{\Delta}$* brain shows the development of multiple tumors (*) along a single ventricular zone, each tumor at an apparent different stage of growth, which grow out from the neurogenic zone (arrows) into the lateral ventricles (LV) (Upper panel). Scale bar is 200 μm. Anterior brain sections (lower panels) demonstrate almost complete occlusion of the ventricular space by the tumor tissue. Scale bar is 1mm.

Figure 2. Mutant *Pik3ca^{H1047R}-Pten$^{\Delta}$* NSPC initiated tumors exhibit features consistent with malignant astrocytoma.

(**A**) A prominent tumor nodule (*) and hyperplastic germinal zones (arrows) (**A, B**). Tumor cell invasion (arrows) into the brain parenchyma and corpus callosum white matter tract (demarcated

by the dotted lines) (**C**) ; (**D**) tumor vascularization was observed in tumors. (**E**) Tumors expressed astrocytoma markers including GFAP and Tuj1. (**F**) Tumors exhibited elevated expression of pAKT(Ser473), pRpS6, pMAPK and pCREB. The dotted lines represent the SVZ-tumor interface, with tumors lying above the dotted line. Scale bars are: 200μm for (A), (E), (F); 100μm for (B); 500μm for (C); 20μm for (D).

Figure 3. *Pik3ca^{H1047R}-Pten$^{\Delta}$* mutations enhance the in vitro growth and migratory capacity of NSPCs

(**A**) Control and double mutant *Pik3ca^{H1047R}-Pten$^{\Delta}$* NSPCs were grown in non-adherent neurosphere culture conditions. Control NSPCs form neurospheres with smooth circumscribed borders, while mutant NSPCs are larger forming mutant neurospheres exhibiting irregular edges. The inset, above right highlights part of a neurosphere with filopodia. Scale bar for the main images is 20μm. (**B**) Mutant neurospheres (NS) showed the presence of more filopodia per cell, (mean ±SD, n=5; ***P<0.001, Student's t-test). (**C**) *Pik3ca^{H1047R}-Pten$^{\Delta}$* NSPCs exhibited enhanced proliferation, measured by EdU incorporation over 24h. ****P<0.00001. (**D**) Western blot analysis showing that *Pik3ca^{H1047R}-Pten$^{\Delta}$* NSPCs express increased pAKT, cyclin D1 and cyclin D1, with or without EGF and bFGF-supplemented neurosphere medium. (**E**) Neurospheres seeded into a 96-well plate with or without invasion matrix for 48h show that in the presence of invasion matrix mutant NSPCs exhibit a higher invasive capacity compared to control NSPCs. The lower panels are "threshold" converted images (of the central (+ matrix) images) to enhance the contrast to show the extent of cell migration. Scale bar in top left panel of

(c) is 50μm and applies to all images in the panel. (**F**) Quantitation of invasion expressed as area of spread (mean ±SD, n=5; ***P<0.001, Student's t-test).

Figure 4. *Pik3ca*^{H1047R}-*Pten*$^{\Delta}$ mutant NSPCs exhibit enhanced sphere forming potential and maintenance of sphere forming potential under conditions promoting differentiation

(**A**) Cumulative cell number of control and *Pik3ca*^{H1047R}-*Pten*$^{\Delta}$ NSPCs over 8 passages (1,000 cells/ml seeded/1 passage/7 days). Cell counts were performed in triplicate from separate wells. (**B**) NSPCs seeded at low densities showed a selective advantage in forming a neurosphere compared to control cells. n=3, Student's t-test, **P<0.01. (**C**) The protocol flow used to test the maintenance of nestin expression and neurosphere forming capacity following differentiation. (**D**) Analysis of nestin expression by flow cytometry after differentiation for 7 days. After 7 days in differentiation conditions cells were returned to neurosphere medium and sphere-forming efficiency determined by extreme limiting dilution analysis (ELDA) (**E**), n=3, ****P<0.0001. See Materials and Methods for details.

Figure 5. *Pik3ca*^{H1047R}-*Pten*$^{\Delta}$ mutant NSPCs exhibit enhanced PI3K downstream activity, MAPK activation, WNT pathway activation and WNT pathway-dependent sel-renewal capacity. (**A**) A PathScan® Akt Signaling Antibody Array was used to measure the phosphorylation of a panel of PI3K/AKT-dependent factors in lysates of *Pik3ca*^{H1047R}-*Pten*$^{\Delta}$ mutant and control NSPCs. (**B**) Western blot showing increased nuclear β-catenin expression in *Pik3ca*^{H1047R}-*Pten*$^{\Delta}$ mutant NSPCs. Nuclear proteins, CREB and Histone-H3 were used as

loading controls (**C**) qRT-PCR analysis of a panel of WNT pathway factors showing upregulation of the WNT pathway in nuclei from *Pik3ca*^{H1047R}-*Pten*$^{\Delta}$ mutant cells. (**D**) Extreme limiting dilution analysis of NSPCs showing that WNT pathway activation by pharmacological inhibition of GSK3β using CHIR99021 increases neurosphere forming capacity of mutant NSPCs while WNT inhibition using IWP-2 reduces neurosphere forming capacity to wild-type levels. All error bars are S.E.M. from n=3. *p<0.05 or as indicated in.

Figure 6. *CREB* deletion in *Pik3ca*^{H1047R}-*Pten*$^{\Delta}$ NSPCs increases survival by slowing tumor growth.

(**A**) Immunofluorescence analysis of *Pik3ca*^{H1047R}-*Pten*$^{\Delta}$ tumors for expression of pCREB, the neural stem-cell marker, nestin, and glial-marker, GFAP. The SVZ-tumor boundary is demarcated by the dotted lines, with tumors lying below the line. Scale bars=100μm. (**B**) H&E analysis showing differences in the cellularity of tumors derived from double mutant (*Pik3ca*^{H1047R}-*Pten*$^{\Delta}$) (DM) and triple mutant (*Pik3ca*^{H1047R}-*Pten*$^{\Delta}$-*CREB*$^{\Delta}$) mice. Triple mutant *CREB*$^{\Delta}$ tumors demonstrated the presence of large cells (arrow); absent in DM tumors. The SVZ non-tumor-tumor boundary is demarcated by the dotted lines; T=tumor, N=non-tumor. Scale bars = 100μm. (**C**) Quantitative analysis of tumor cellularity between DM and triple mutant (DM+CREB$^{\Delta}$) (Mean ±SD, n=3; ** P<0.01, Student's t-test). (**D**) Kaplan-Meier survival analysis of DM mice (n=10), compared to triple mutant *CREB*$^{\Delta}$ mice (n=11) and control mice.

Fig 1

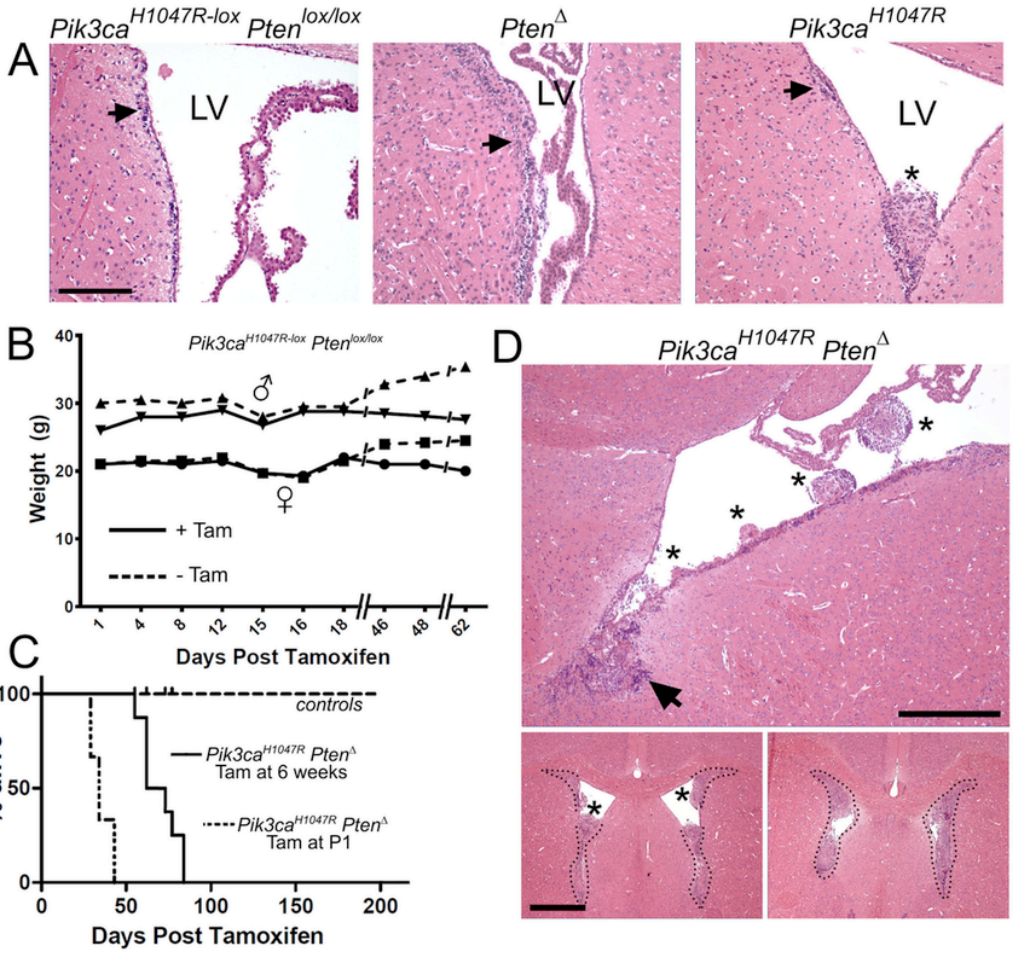

Fig. 2

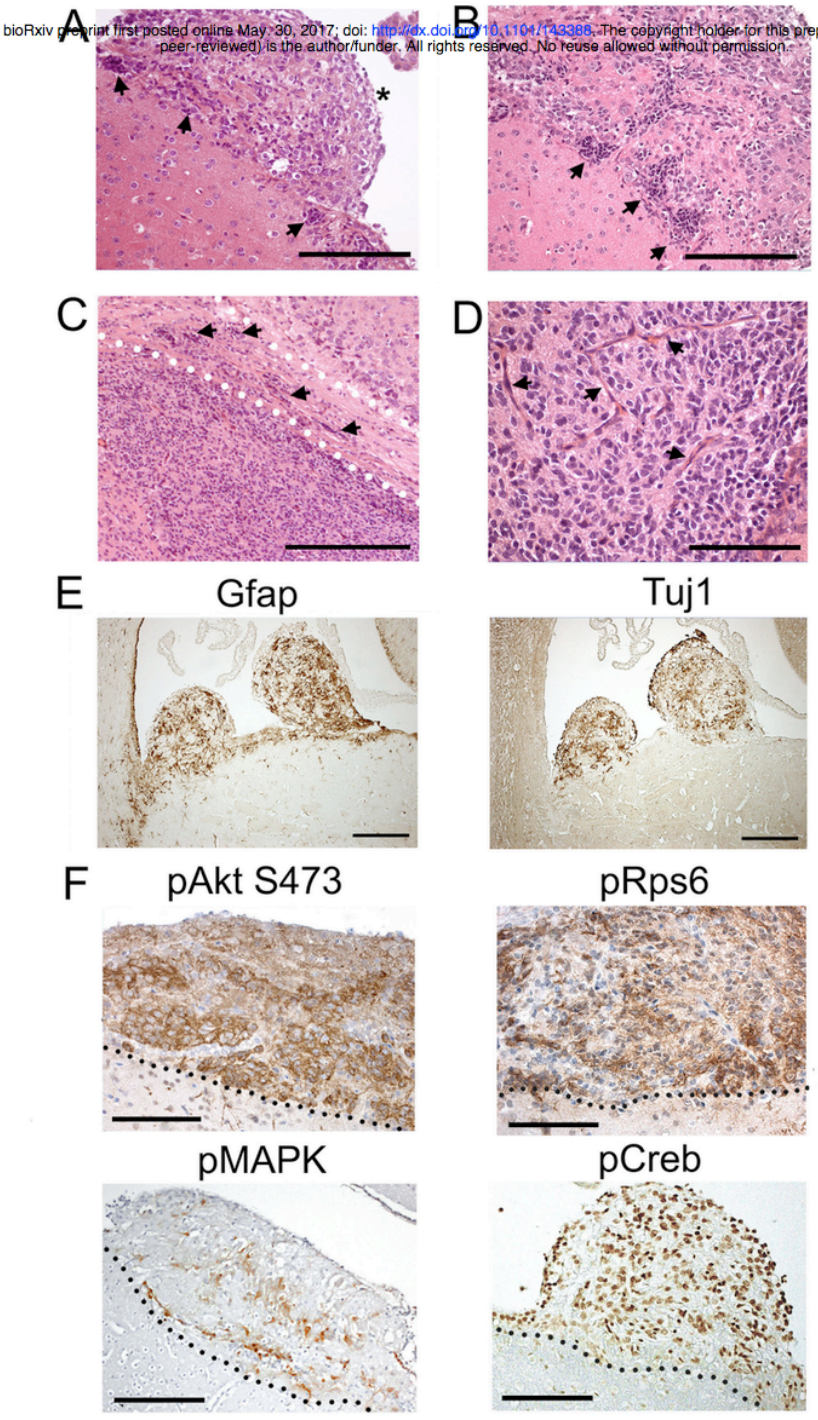

Fig. 3

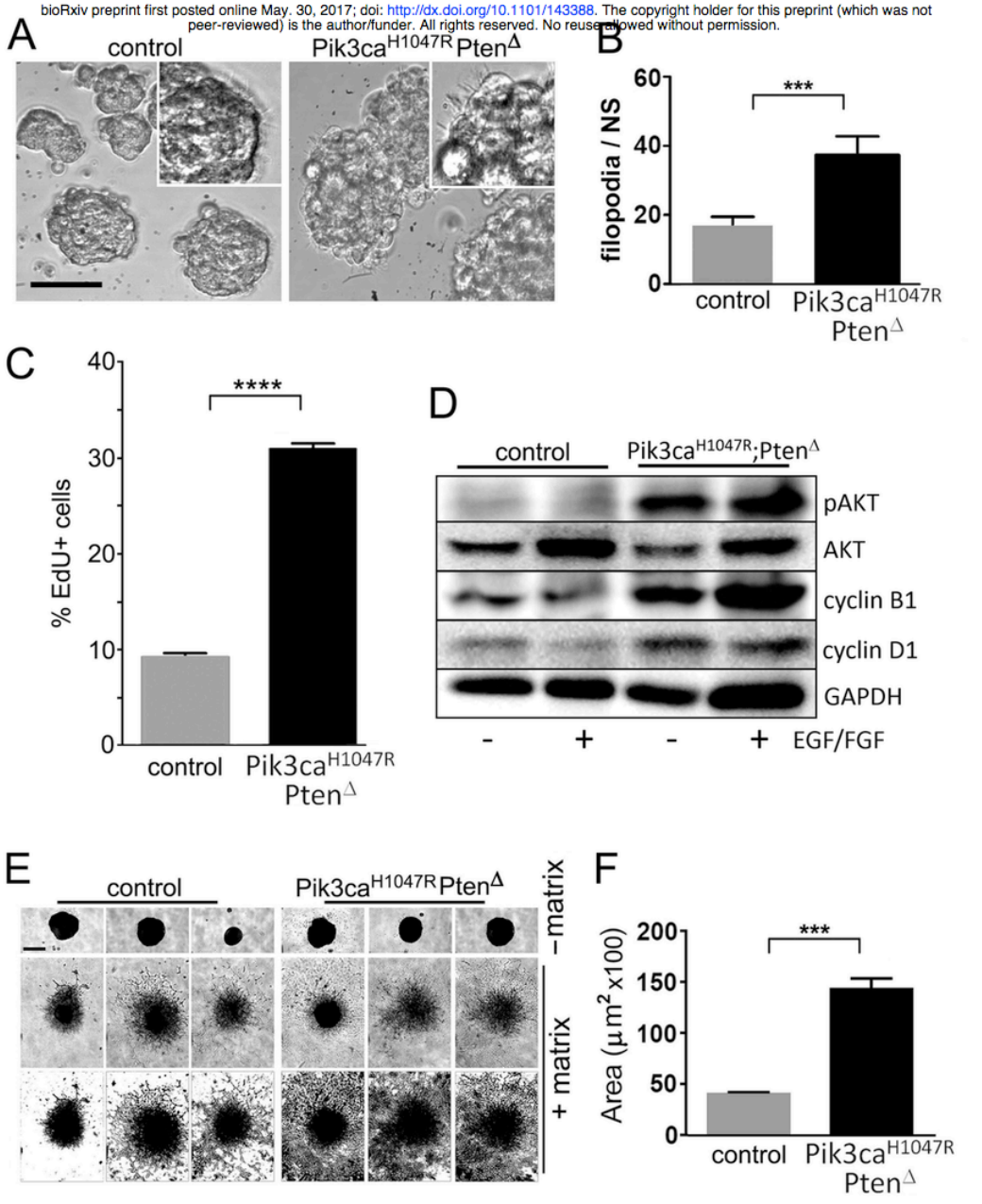

Fig. 4

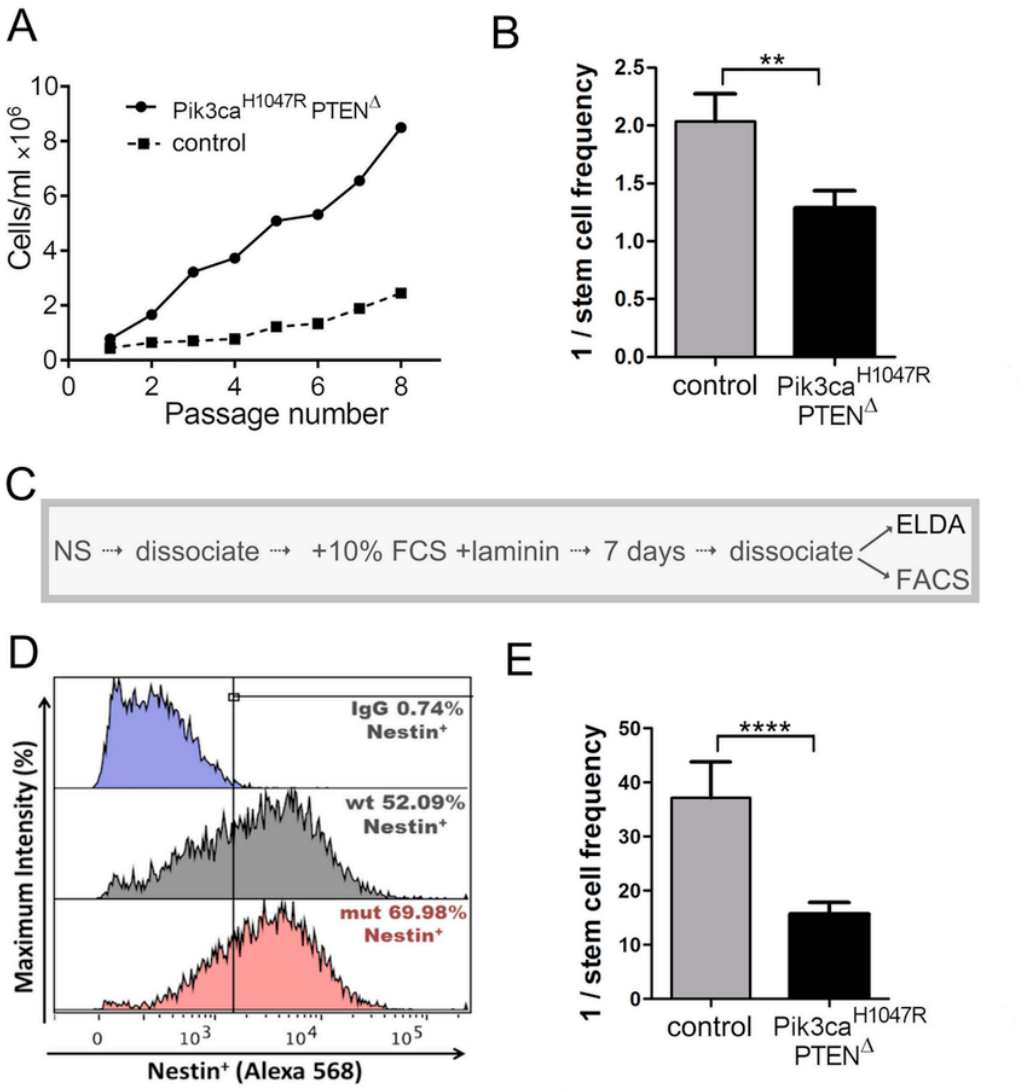

Fig. 5

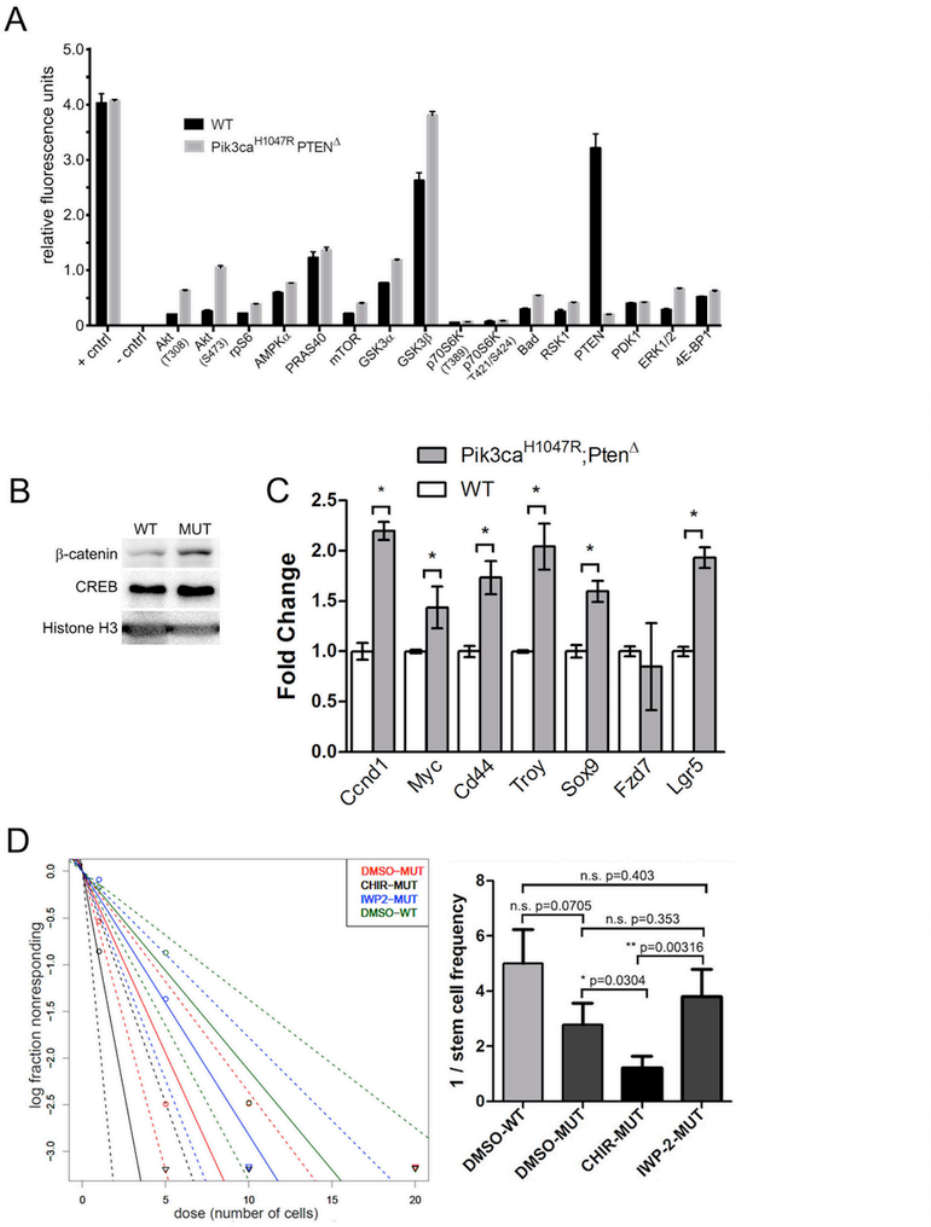

Fig. 6